January 2017

Design And Manufacture Of A Negative Index Metamaterial Using A Magnetized Photonic Crystal

Mohamed Zein Radwan

DESIGN AND MANUFACTURE OF A NEGATIVE INDEX METAMATERIAL USING A MAGNETIZED PHOTONIC CRYSTAL

by

Mohamed Z. Radwan

Master of Science, Pittsburg State University, 2009

Bachelor of Science, Cairo University, 2000

A Dissertation

Submitted to the Graduate Faculty

of the

University of North Dakota

in partial fulfillment of the requirements

for the degree of

Doctor of Philosophy

Grand Forks, North Dakota

December

2017

This dissertation, submitted by Mohamed Radwan in partial fulfillment of the requirements for the Degree of Doctor of Philosophy from the University of North Dakota, has been read by the Faculty Advisory Committee under whom the work has been done and is hereby approved.

_____
Dr. Graeme Dewar

_____
Dr. Kanishka Marasinghe

_____
Dr. Nuri Oncel

_____
Dr. Yen Lee Loh

_____
Dr. Sima Noghanian

This dissertation is being submitted by the appointed advisory committee as having met all of the requirements of the School of Graduate Studies at the University of North Dakota and is hereby approved.

_____
Dr. Grant McGimpsey
Dean of the School of Graduate Studies

_____
Date

PERMISSION

Title Design and Manufacture of a Negative Index Metamaterial using a Magnetized Photonic Crystal

Department Physics & Astrophysics

Degree Doctor of Philosophy

In presenting this dissertation in partial fulfillment of the requirements for a graduate degree from the University of North Dakota, I agree that the library of this University shall make it freely available for inspection. I further agree that permission for extensive copying for scholarly purposes may be granted by the professor who supervised my dissertation work or, in his absence, by the Chairperson of the department or the dean of the School of Graduate Studies. It is understood that any copying or publication or other use of this dissertation or part thereof for financial gain shall not be allowed without my written permission. It is also understood that due recognition shall be given to me and to the University of North Dakota in any scholarly use which may be made of any material in my Dissertation.

Mohamed Z. Radwan

Signature 

Date 12/6/2017

TABLE OF CONTENTS

LIST OF FIGURES

LIST OF TABLES

ACKNOWLEDGMENT

The author wishes to express his gratitude to Dr. Graeme Dewar, Chairperson of the committee, for his intelligent guidance, encouragement and patience. I also would like to thank Dr. Mizuho Schwalm for her support and advising, and Dr. William Schwalm for teaching me some useful mathematical techniques I used. Finally, I want to express my grateful to my Graduate Committee for giving so generously of their time and effort in the evaluation of my dissertation.

ABSTRACT

Negative index materials (NIM) are artificial structures in which the refractive index for light has a negative value over some frequency range. This does not occur in any known natural materials, and thus is only achievable with engineered structures known as metamaterials. Metamaterials demonstrating a negative refractive index for light usually consist of arrays of wires and cut-ring structures: such media are characterized by both the electrical permittivity and magnetic permeability being negative. My method for obtaining a NIM is different from previous attempts. I get the negative magnetic permeability from a ferrite material which is the host medium for the wire array. The ferrite plus wires array creates a NIM in the microwave frequency range. One important consideration involves decoupling the ferrite and wire array's response to incident microwaves. Experiments involving transmission and reflection of microwaves through, and from, a ferrite / wire array metamaterial inside a waveguide demonstrates that $n < 0$ over a frequency range tunable by adjusting an externally imposed static magnetic field.

CHAPTER I

INTRODUCTION

Negative index materials (NIM) are artificial structures in which the refractive index for light has a negative value over some frequency range. This does not occur in any known natural material, and thus is only achievable with engineered structures known as metamaterials.

The NIM idea originated in 1968 when Viktor Veselago predicted the existence of such materials [1] but no experiments checking his prediction were attempted at that time. Modern day interest in negative refraction was sparked by Smith et al. [2], [3] when they showed in 2000 that it was possible to construct a structure that can exhibit a negative index of refraction in the microwave frequency range.

Metamaterials demonstrating a negative refractive index for light usually consist of arrays of wires (to achieve a negative electric permittivity) and split - ring structures (to achieve a negative magnetic permeability) as shown in Fig 1.1.1. Such media are characterized by both the electrical permittivity and magnetic permeability being simultaneously negative.

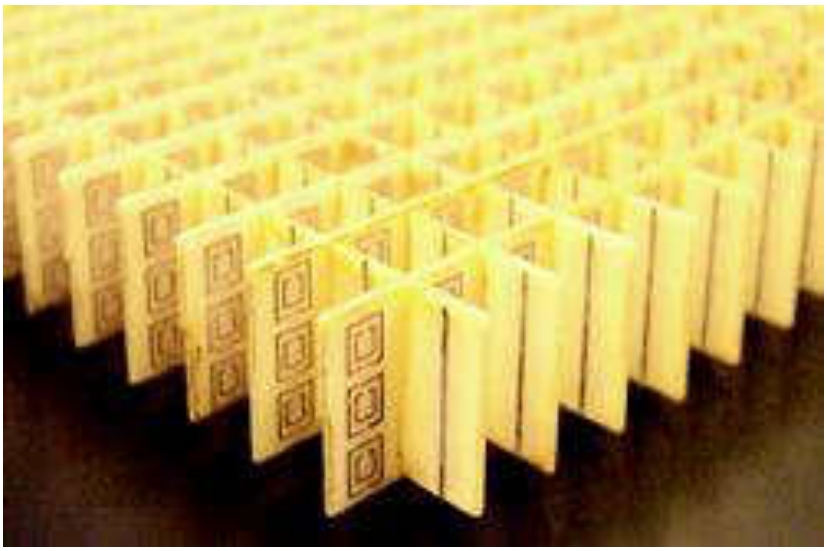

Fig. 1.1.1 A wire arrays imbedded in an array of split – ring resonators. [4]

My aim is to obtain the negative magnetic permeability with a ferrite material which is the host material surrounding the wire array. A static magnetic field is used to control the magnetic permeability of the ferrite material. The expectation is to have both the magnetic permeability and electric permittivity negative in some range of microwave frequency below the structure's plasma frequency. In order for the ferrite not to destroy the negative permittivity of the wire array, the wires must be cladded in a nonmagnetic dielectric material.

For an electromagnetic wave incident on a material, Snell's law connecting the incident angle of the wave with propagation direction θ_i with respect to the interfere normal and the refracted angle of the wave inside the medium θ_r is

$$n_0 \, \mathrm{Sin}\theta_i = n \, \mathrm{Sin}\theta_r \ , \qquad (1.1.1)$$

here n_0 is the refractive index of the wave in the incident medium and n is the refractive index in the refraction medium.

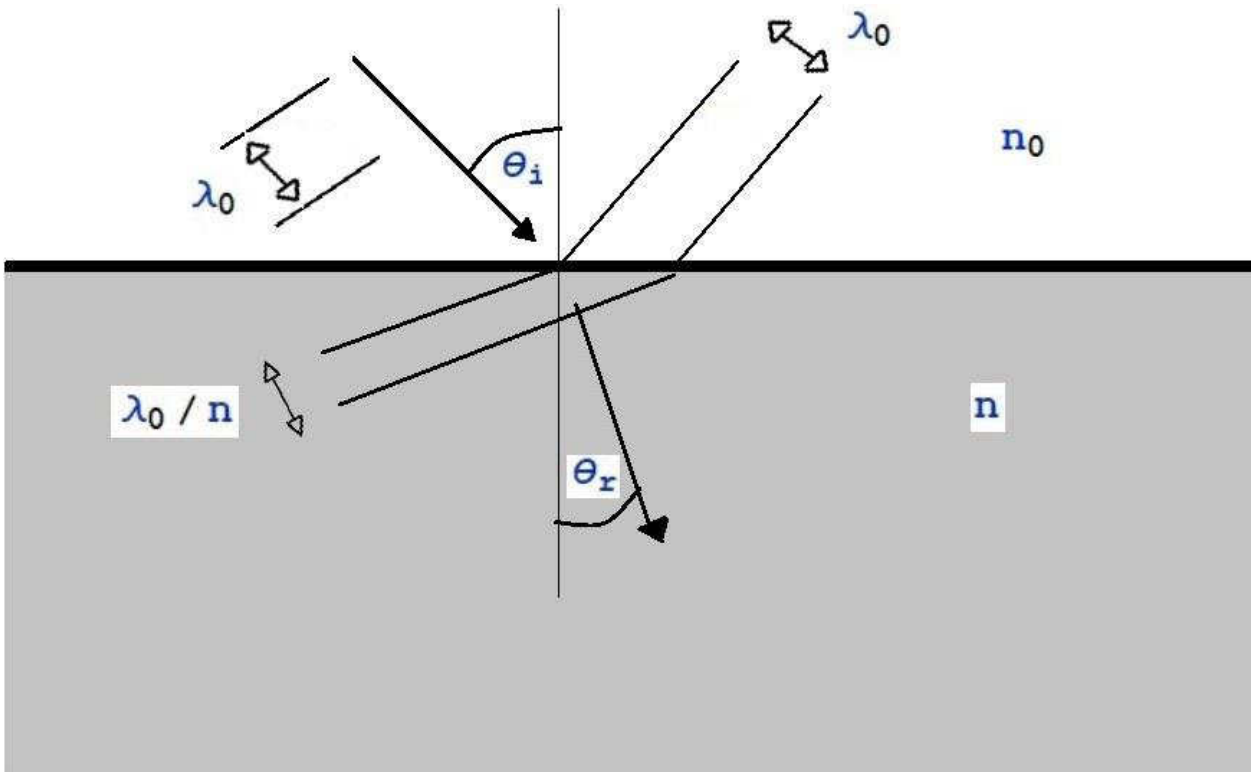

Figure 1.1.2 Snell's law of refraction based on wave propagation with positive *n*.

This assures the wavelength changes by a factor of "*n* " in passing from vacuum to the medium.

The refractive index is given by,

$$n = \frac{c}{v} \quad , \tag{1.1.2}$$

where $c = \frac{1}{\sqrt{\epsilon_0 \mu_0}}$ is the vacuum speed of light and $v = \frac{1}{\sqrt{\epsilon\, \mu}}$ is the speed of light in the medium. Here μ_0 and ϵ_0 are the permeability and permittivity of free space, respectively. The relation between the refractive index "*n* " and the permittivity ε and permeability μ of the medium for specific frequencies is

$$n = \pm \left(\frac{\epsilon\mu}{\epsilon_0 \mu_0}\right)^{1/2} \quad . \tag{1.1.3}$$

The amplitude of the electric field of a plane wave of angular frequency ω propagating along the z-direction in the medium is given by the real part of

$$\vec{E} = \vec{E_0}\, e^{i(kz-\omega t)}, \qquad (1.1.4)$$

where $k = \frac{n\,\omega}{c}$ is the wave number.

To describe the relationship between ε and the frequency ω , I use the Lorentz–Drude model to find the dispersion relation

$$\epsilon(\omega) = \epsilon_0\left(1 + \frac{{\omega_p}^2}{{\omega_0}^2-\omega^2-i\Gamma\omega}\right), \qquad (1.1.5)$$

where ω_0 is the single resonance frequency for bound electrons (which is equal to zero for the electrons in conductors) and Γ is the damping rate per unit mass and

$${\omega_p}^2 = \frac{Ne^2}{m\epsilon_0}\ .$$

A plot of μ versus f is illustrated in Fig.1.1.3 and a plot of ϵ versus ω/ω_p is illustrated in Fig.1.1.4.

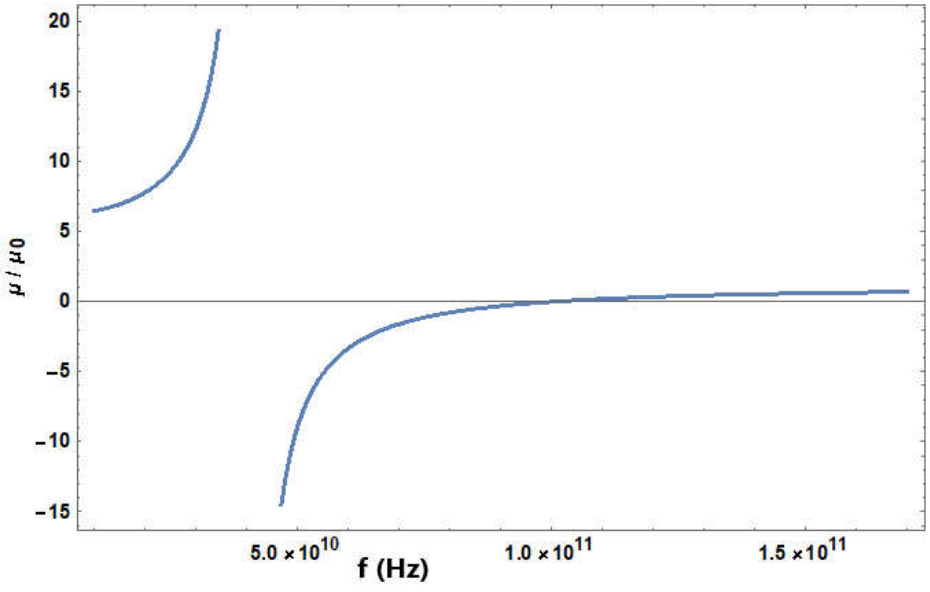

Fig. 1.1.3 Magnetic permeability vs. frequency for a ferrite.

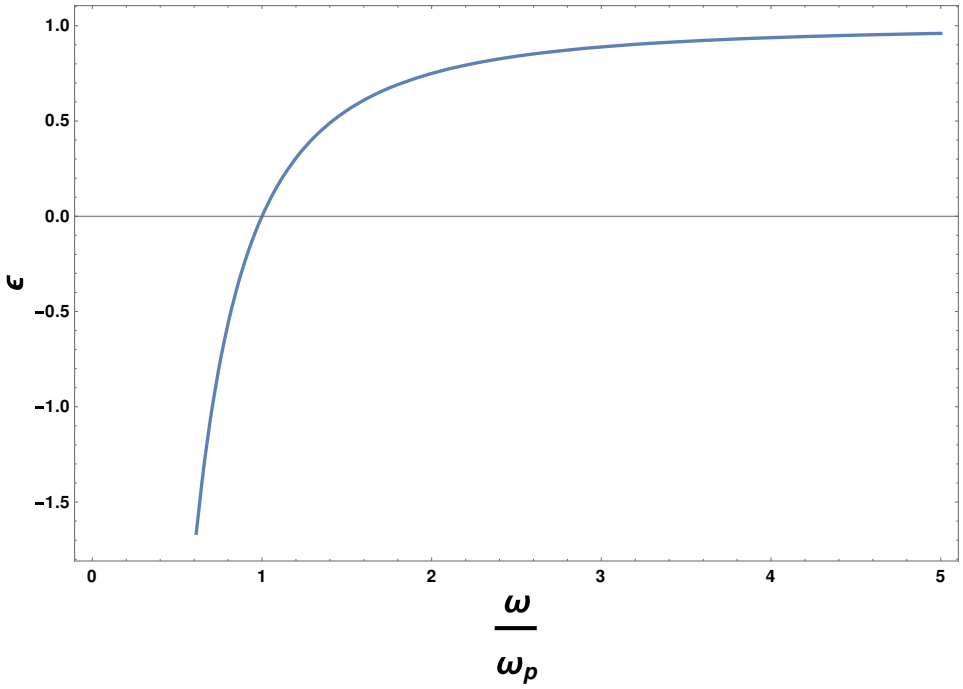

Fig. 1.1.4 Electrical permittivity vs. frequency.

At frequencies below the plasma frequency but above the resonance frequency, Re (ϵ) is negative. Similarly, Re (μ) is negative below the anti-resonance and above the resonance frequency.

Since "n " can be positive or negative in Eq. 1.1.3, the question is which sign is appropriate for both ϵ and μ negative. I show here that k is negative for both ϵ and μ negative. Thus, since $k = \frac{n\,\omega}{c}$, n is negative.

For an electromagnetic wave propagating in a medium, the electric field $\vec{E}(\vec{r},t)$ can in general be written as a Fourier expansion of plane waves

$$\vec{E}\left(\vec{r},t\right) = \int \vec{E}\left(\vec{k},\omega\right) e^{i\left(\vec{k}.\vec{r}-\omega t\right)} d^3k \; \mathrm{d}\omega \; . \qquad (1.1.6)$$

From Maxwell's equation

$$\nabla \times \vec{E}\left(\vec{r},t\right) = -\frac{\partial \vec{B}}{\partial t} \tag{1.1.7}$$

we obtain,

$$\vec{k} \times \vec{E}(\vec{k},\omega) = \omega \vec{B}\,(\vec{k},\omega)\ . \tag{1.1.8}$$

Similarly, in the absence of free charges,

$$\nabla \times \vec{H}\left(\vec{r},t\right) = \frac{\partial \vec{D}}{\partial t} \tag{1.1.9}$$

leads to

$$\vec{k} \times \vec{H}\left(\vec{k},\omega\right) = -\omega\, \vec{D}\,(\vec{k},\omega)\ . \tag{1.1.10}$$

But since,

$$\vec{B} = \mu(\omega)\, \vec{H}\ , \tag{1.1.11}$$

we find

$$\vec{k} \times \vec{E} = \omega\, \vec{B} = \mu\, \vec{H}\ , \tag{1.1.12}$$

$$\vec{k} \times \vec{H} = -\omega\, \vec{D} = -\omega\, \epsilon\, \vec{E}\ . \tag{1.1.13}$$

If ϵ and μ are both negative, the disposition of the vectors $\vec{k}, \vec{E}, \vec{B}$ and $\vec{H}$ must be as shown in the Fig. 1.1.5.

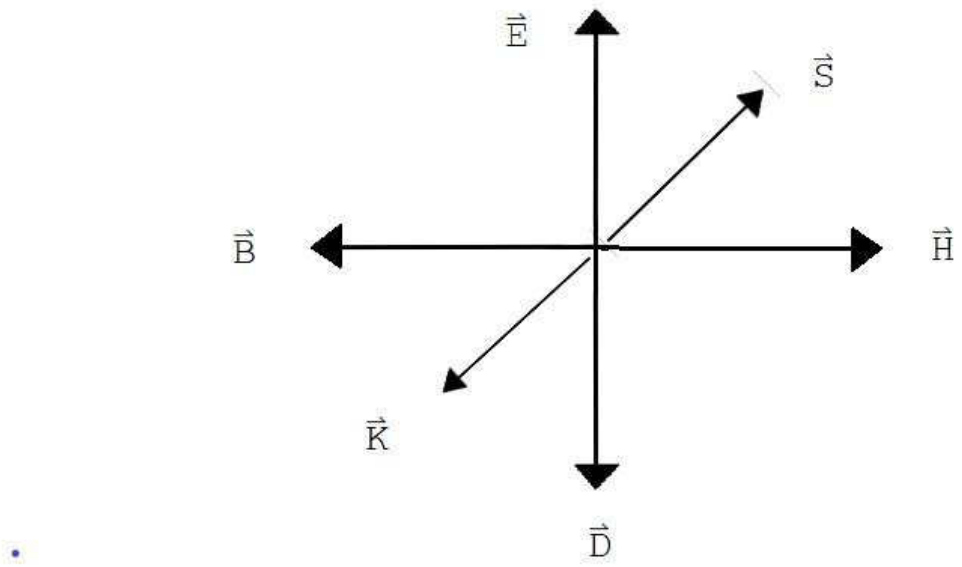

Fig. 1.1.5 Electromagnetic wave parameters for negative ϵ and μ.

In particular, we note that Eq.1.1.12 implies that the vectors $\vec{k}, \vec{E}$ and $\vec{H}$ must form a left-handed triad if $\mu < 0$. The power flow is given by the conventional expression for the Poynting vector:

$$\vec{S} = \frac{1}{2}\mathrm{Re}(\vec{E} \times \vec{H}) \,. \qquad (1.1.14)$$

From the Fig.1.1.5, we see that $\vec{S}$ is anti-parallel to $\vec{k}$ or $\vec{S} \cdot \vec{k} < 0$, but from equations (1.1.7) and (1.1.9), we see that

$$k^2 = \epsilon\, \mu\, \omega^2. \qquad (1.1.15)$$

Since $\vec{k}$ is in the opposite direction to $\vec{S}$, we must take the negative square root for n .

This is what is meant by a negative phase velocity, we get $k = -\sqrt{\epsilon\, \mu}\, \omega = \frac{n\, \omega}{c}$,

Thus,

$$n = -\sqrt{\frac{\epsilon\,\mu}{\epsilon_0\,\mu_0}}. \qquad (1.1.16)$$

Potential Applications of a NIM

There are many applications for a NIM in the microwave range, and the whole frequency spectrum in general. I mention here a few of them:

1- Non-Attenuation Medium.

If only one of ϵ and μ is negative, electromagnetic waves are heavily attenuated. However, if both ϵ and μ are negative, the attenuation of electromagnetic waves in a medium occurs due to the imaginary parts of the complex electric permittivity and magnetic permeability. In a NIM, the electric permittivity is close to a pure negative real value as is the permeability, so there is little attenuation in it [5].

2- The Perfect Lens.

The imaging process which uses ordinary lenses suffers from many problems: for example, the resolution of the image can't be less than the wavelength of the light used. If we used a lens made of a NIM, the resolution of the image can be less than the wavelength of light [6].

Another defect in ordinary lenses that the NIM can fix is spherical aberration. It is easy for a lens which is made of a NIM to focus the light in two foci, one inside the lens and one outside. The image created exhibits no spherical aberration, and depending on the

losses within the lens, can have a resolution much less than a wavelength of light (Fig.1.1.6) [6].

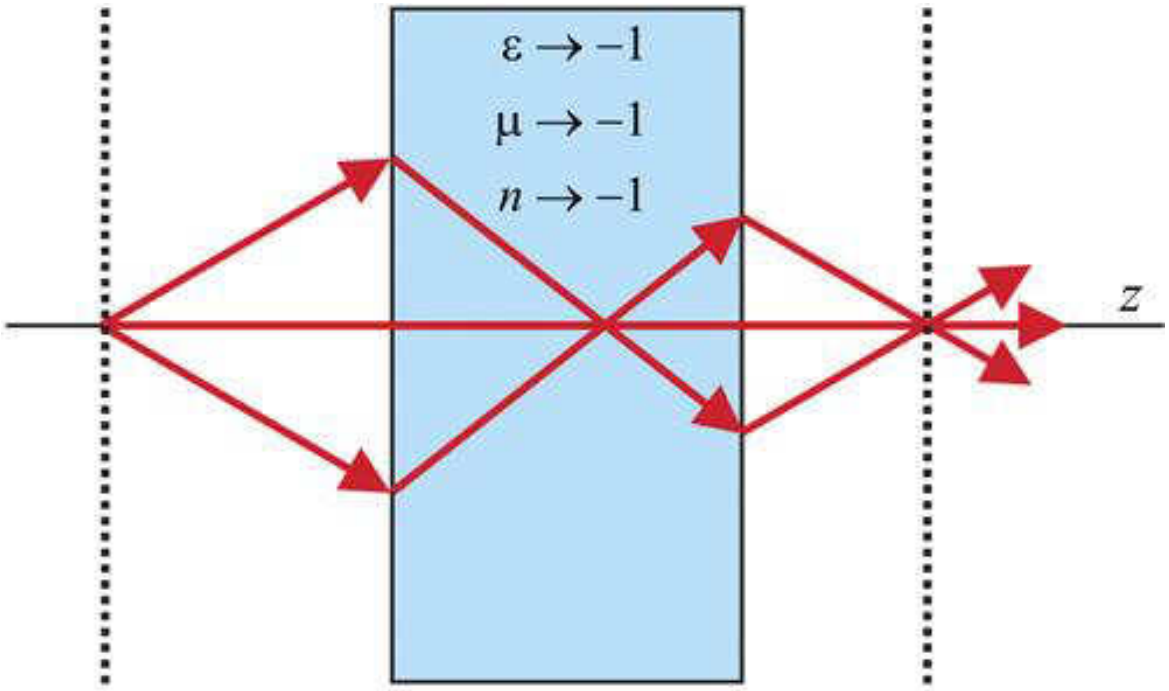

Fig. 1.1.6 Near-field lens made from a slab of negatively refracting medium [7]

CHAPTER II

THEORY

2.1 The Magnetic Properties of the Ferrite Host Material

The target of my research is to achieve a negative refractive index material by adjusting the electric permittivity and magnetic permeability of a metamaterial to have simultaneously negative values.

The magnetic permeability of a material placed in a static magnetic field or radio frequency (RF) magnetic field (electromagnetic waves) is a function of multiple parameters such as the strength of the magnetic field (static or variable), frequency of the electromagnetic waves, magnetization of the material, and the direction of the fields with respect to each other. The magnetic permeability can vary between positive and negative values.

To calculate the limits of the region where the permeability is negative I had to measure some intrinsic properties of the host ferrite material, specifically the magnetization and the g-factor. The magnetization and g-factor of the ferrite are a function of the procedures used in the sintering process which creates the ferrite, so I could not depend on the tabulated values supplied by the material manufacturer [17] and I had to measure these

myself. These measurements can be done by several of methods but the most accurate and reliable method is based on ferromagnetic resonance.

To calculate the magnetic permeability and g-factor of the magnetic host ferrite material under the influence of a steady magnetic field H_0 and RF alternating magnetic field h_{RF}, I executed ferromagnetic resonance measurements on several samples of the ferrite.

To perform a good measurement for ferromagnetic resonance, the size of the sample must be much smaller than the wavelength used in the experiment. I used samples in the shape of cylindrical rods, as sketched in Fig. 2.1.1, with the magnetic field applied along the long axis of the sample and the microwave field perpendicular to it. The theory behind these measurements follows.

Let $\vec{H}_0$ be a steady magnetic field in the $\hat{z}$ direction applied to the ferrite, $\vec{M}_0$ be the steady magnetization of the material, $\vec{m}$ be the amplitude of the RF magnetization, $\vec{M}$ be the total magnetization, $\vec{h}_{\mathrm{RF}}$ be the RF magnetic field, $\bar{\bar{D}}$ be the steady state demagnetization tensor due to $\vec{H}$, $\bar{\bar{d}}$ be the RF demagnetization tensor, $\vec{k}$ be the wave vector and ω be the angular frequency of the wave which is traveling in $\vec{r}$ direction.

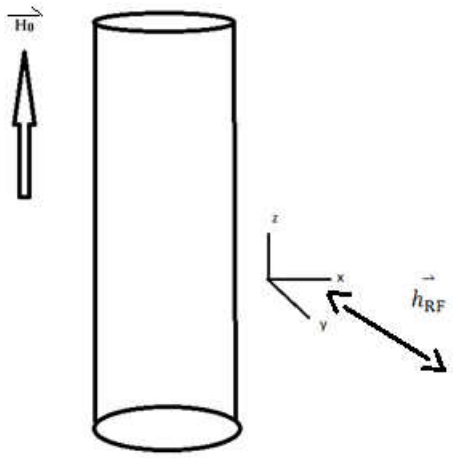

Fig. 2.1.1 Ferrite rod placed in a steady magnetic field.

The RF magnetic field in this case is

$$\vec{h}_{\mathrm{RF}} = (h_x \hat{x} + h_y \hat{y}) e^{i(\vec{k}.\vec{r} - \omega t)} \qquad (2.1.1)$$

and the total magnetization is

$$\vec{M} = M_0 \hat{z} + \vec{m} \ , \qquad \vec{m} \perp \vec{M}_0 \qquad , \qquad (2.1.2)$$

where the RF magnetization is

$$\vec{m} = (m_x \hat{x} + m_y \hat{y}) e^{i(\vec{k}.\vec{r} - \omega t)} \ . \qquad (2.1.3)$$

For a small sample size, the wavelength is very large compared to the sample diameter, therfore we can assume that $\vec{k}.\vec{r} \to 0$ and $e^{i\vec{k}.\vec{r}} \to 1$

The total RF magnetic field due to the microwaves is

$$\vec{h_{\text{tot}}} = \vec{h_{\text{RF}}} - \bar{\bar{d}}\,\vec{m} \ , \qquad (2.1.4)$$

and

$$\vec{H} = \vec{H_0} - \bar{\bar{D}}\vec{M_0} + \vec{h_{\text{tot}}} \ . \qquad (2.1.5)$$

For a cylindrical sample the RF demagnetization tensor is [8],[9]

$$\bar{\bar{d}} = \begin{pmatrix} d_{\text{xx}} & 0 & 0 \\ 0 & d_{\text{yy}} & 0 \\ 0 & 0 & d_{\text{zz}} \end{pmatrix}, \qquad (2.1.6)$$

$$d_{\text{xx}} = d_{\text{yy}} = \frac{1}{2} \quad , \qquad (2.1.7)$$

$$d_{\text{zz}} = 0 \quad . \qquad (2.1.8)$$

The total magnetic field inside the material is

$$\vec{H} = (H_0 - D_{\text{zz}} M_0)\hat{z} + \vec{h_{\text{tot}}} \ . \qquad (2.1.9)$$

I used the Gilbert form of dissipation in the equation of motion for the magnetization:

$$\left(\frac{-1}{\gamma}\right)\frac{\mathrm{d}\vec{M}}{\mathrm{dt}} = \mu_0\vec{M} \times \vec{H} + \frac{\lambda}{\mu_0\gamma^2{M_0}^2}\left(\vec{M} \times \frac{\mathrm{d}\vec{M}}{\mathrm{dt}}\right) \ , \qquad (2.1.10)$$

where $$\gamma = \frac{ge}{2m_e}$$

is the gyro-magnetic factor, λ is the phenomenological damping rate, and g is the g-factor. The equation equates the torque on the magnetization to rate of change of angular momentum.

By substituting $\vec{M}, \vec{H}, \frac{\mathrm{d}\vec{M}}{\mathrm{dt}}$ values into the equation of motion and equating the components in the $\hat{x}, \hat{y}$ and $\hat{z}$ we get the following equations:

$$\frac{i\omega m_x}{\gamma} = \mu_0\left(m_y H_0 - D_{zz}M_0 m_y - M_0 h_y + \frac{M_0 m_y}{2}\right) + \frac{i\lambda\omega m_y}{\mu_0\gamma^2 M_0}, \qquad (2.1.11)$$

$$\frac{i\omega m_y}{\gamma} = \mu_0\left(-m_x H_0 + D_{zz}M_0 m_x + M_0 h_x - \frac{M_0 m_x}{2}\right) - \frac{i\lambda\omega m_x}{\mu_0\gamma^2 M_0}, \qquad (2.1.12)$$

$$0 = m_x h_y - m_y h_x. \qquad (2.1.13)$$

By defining $\tilde{H}$ as

$$\tilde{H} = H_0 - D_{zz}M_0 + \frac{M_0}{2} + \frac{i\lambda\omega}{{\mu_0}^2\gamma^2 M_0} \ , \qquad (2.1.14)$$

the equations (2.1.11) and (2.1.12) become

$$\left(\frac{i\omega}{\mu_0\gamma}\right)m_x = m_y\tilde{H} - M_0 h_y \quad , \tag{2.1.15}$$

$$\left(\frac{i\omega}{\mu_0\gamma}\right)m_y = -m_x\tilde{H} + M_0 h_x \, . \tag{2.1.16}$$

After using Cramer's rule, I find m_x and m_y:

$$m_x = \frac{h_x M_0 \tilde{H} - \frac{iM_0\omega h_y}{\gamma\mu_0}}{(\tilde{H})^2 - (\frac{\omega}{\gamma\mu_0})^2} \, , \tag{2.1.17}$$

$$m_y = \frac{h_y M_0 \tilde{H} + \frac{iM_0\omega h_x}{\gamma\mu_0}}{(\tilde{H})^2 - (\frac{\omega}{\gamma\mu_0})^2} \quad . \tag{2.1.18}$$

The alternating component of the magnetic induction is

$$\vec{b} = \mu_0(\vec{h_{tot}} + \vec{m}) \, . \tag{2.1.19}$$

After substitute for $\vec{h_{\mathrm{tot}}}$ and $\vec{m}$ and equating the components of $\vec{b}$ in the $\hat{x}$ and $\hat{y}$ directions, we obtain

$$\frac{1}{\mu_0}b_x = \left(1 + \frac{\tilde{H}M_0}{2\left(\left(\tilde{H}\right)^2 - \left(\frac{\omega}{\gamma\mu_0}\right)^2\right)}\right)h_x + \left(\frac{-i\omega M_0}{2\gamma\mu_0\left(\left(\tilde{H}\right)^2 - \left(\frac{\omega}{\gamma\mu_0}\right)^2\right)}\right)h_y \, . \tag{2.1.20}$$

$$\frac{1}{\mu_0}b_y = \left(\frac{i\omega M_0}{2\gamma\mu_0\left(\left(\tilde{H}\right)^2 - \left(\frac{\omega}{\gamma\mu_0}\right)^2\right)}\right)h_x + \left(1 + \frac{\tilde{H}M_0}{2\left(\left(\tilde{H}\right)^2 - \left(\frac{\omega}{\gamma\mu_0}\right)^2\right)}\right)h_y \, . \tag{2.1.21}$$

After rearranging, the last two equations become

$$\frac{1}{\mu_0}\begin{pmatrix} b_x \\ b_y \end{pmatrix} = \begin{pmatrix} \left(1 + \frac{\tilde{H}M_0}{2\left(\left(\tilde{H}\right)^2 - \left(\frac{\omega}{\gamma\mu_0}\right)^2\right)}\right) & \left(\frac{-i\omega M_0}{2\gamma\mu_0\left(\left(\tilde{H}\right)^2 - \left(\frac{\omega}{\gamma\mu_0}\right)^2\right)}\right) \\ \left(\frac{i\omega M_0}{2\gamma\mu_0\left(\left(\tilde{H}\right)^2 - \left(\frac{\omega}{\gamma\mu_0}\right)^2\right)}\right) & \left(1 + \frac{\tilde{H}M_0}{2\left(\left(\tilde{H}\right)^2 - \left(\frac{\omega}{\gamma\mu_0}\right)^2\right)}\right) \end{pmatrix} \begin{pmatrix} h_x \\ h_y \end{pmatrix}. \quad (2.1.22)$$

We know that

$$\vec{b} = \mu\vec{h_{\text{tot}}}\,, \quad (2.1.23)$$

Therefore

$$\mu = \mu_0 \begin{pmatrix} \left(1 + \frac{\tilde{H}M_0}{2\left(\left(\tilde{H}\right)^2 - \left(\frac{\omega}{\gamma\mu_0}\right)^2\right)}\right) & \left(\frac{-i\omega M_0}{2\gamma\mu_0\left(\left(\tilde{H}\right)^2 - \left(\frac{\omega}{\gamma\mu_0}\right)^2\right)}\right) \\ \left(\frac{i\omega M_0}{2\gamma\mu_0\left(\left(\tilde{H}\right)^2 - \left(\frac{\omega}{\gamma\mu_0}\right)^2\right)}\right) & \left(1 + \frac{\tilde{H}M_0}{2\left(\left(\tilde{H}\right)^2 - \left(\frac{\omega}{\gamma\mu_0}\right)^2\right)}\right) \end{pmatrix}. \quad (2.1.24)$$

We find the determinant of μ is

$$\det(\mu) = {\mu_0}^2\left[\left(1 + \frac{\tilde{H}M_0}{2\left(\left(\tilde{H}\right)^2 - \left(\frac{\omega}{\gamma\mu_0}\right)^2\right)}\right)^2 - \left(\frac{\omega M_0}{2\gamma\mu_0\left(\left(\tilde{H}\right)^2 - \left(\frac{\omega}{\gamma\mu_0}\right)^2\right)}\right)^2\right]. \quad (2.1.25)$$

For the case of ferromagnetic resonance, the determinant of $\to \infty$, resulting in a large $\vec{b}$ in response to the incident microwaves. This occurs for

$$\tilde{H} = \frac{\omega}{\gamma\mu_0}. \quad (2.1.26)$$

After substituting for $\tilde{H}$ from equation (2.1.26) into (2.1.14) and neglecting dissipation, we get

$$H_0 = \frac{\omega}{\mu_0\gamma} + (D_{zz} - \tfrac{1}{2})M_0. \quad (2.1.27)$$

By plotting H_0 versus ω at resonance, the slope of the straight line is $\frac{1}{\mu_0\gamma}$, and the intercept is $(D_{zz}-\frac{1}{2})M_0$, which allows me to calculate magnetization and g-factor. I found the resonance field H_0 for various frequencies and constructed such a straight line plot.

The above derivation of the equation for ferromagnetic applied to a small cylindrically shaped sample. I also need the equation for the magnetic permeability of the ferrite host which is large and shaped as a rectangular parallelepiped. I use this equation for the metamaterial structure which has dimensions comparable to the microwave wavelength ($\lambda \approx 3$ cm). I treat the sample as an infinite half plane. The relevant $\bar{\bar{d}}$ or $\bar{\bar{D}}$ are different than for the cylinder. Equations (2.1.1), (2.1.2) and (2.1.3) are still valid and here the total magnetic field inside the material is

$$\vec{H} = (H_0 - D_{zz}M_0)\hat{z} + \vec{h_{RF}} \,. \tag{2.1.28}$$

The alternating component of the magnetic induction is again

$$\vec{b} = \mu_0(\vec{h_{RF}} + \vec{m}) \,. \tag{2.1.29}$$

By substituting $\vec{M}, \vec{H}, \frac{d\vec{M}}{dt}$ values into the equation of motion (2.1.10) and equating the components in the $\hat{x}, \hat{y}$ and $\hat{z}$ directions, we get the following equations:

$$\frac{i\omega m_x}{\gamma} = \mu_0\left(m_y H_0 - D_{zz}M_0 m_y - M_0 h_y\right) + \frac{i\lambda\omega m_y}{\mu_0\gamma^2 M_0} \,, \tag{2.1.30}$$

$$\frac{i\omega m_y}{\gamma} = \mu_0(-m_x H_0 - (1 - D_{zz})M_0 m_x) - \frac{i\lambda\omega m_x}{\mu_0\gamma^2 M_0} \,. \tag{2.1.31}$$

The Maxwell equations applied at the boundary of the sample require the normal component of $\vec{b}$ to be continuous, so $b_x(\text{outside sample}) = b_x(\text{inside sample})$ at the surface normal to $\hat{x}$. But we know that in the free space outside the sample there is no magnetic induction for normally incident microwaves, so we obtain

$$b_x = 0 = \mu_0(m_x + h_x) \quad , \tag{2.1.32}$$

which can be treated as $h_x = -m_x$ and which implies $d_{xx} = -1$, $d_{zz} = d_{yy} = 0$.

By defining H'' as

$$H'' = H_0 - D_{zz}M_0 + \frac{i\lambda\omega}{{\mu_0}^2\gamma^2 M_0} \quad , \tag{2.1.33}$$

and using equations (2.1.32) and (2.1.33) , the equations (2.1.30) and (2.1.31) become

$$\left(\frac{i\omega}{\mu_0\gamma}\right)m_x = m_y H'' - M_0 h_y \tag{2.1.34}$$

$$\left(\frac{i\omega}{\mu_0\gamma}\right)m_y = -m_x\left(H'' + M_0\right). \tag{2.1.35}$$

Using Cramer's rule to find m_y , I get

$$\left(H''\left(H'' + M_0\right) - \left(\frac{\omega}{\mu_0\gamma}\right)^2\right)m_y = \left(H'' + M_0\right)M_0 h_y \, . \tag{2.1.36}$$

By comparing equation (2.1. 36) to the equation (2.1.37) below,

$$m_y = \chi h_y \, , \tag{2.1.37}$$

we find that the magnetic susceptibility of the ferrite is

$$\chi = \frac{(H^{"}+M_0)M_0}{\left(H^{"}(H^{"}+M_0)-\left(\frac{\omega}{\mu_0\gamma}\right)^2\right)} \quad . \tag{2.1.38}$$

Since

$$b_y = \mu h_y = \mu_0\left(h_y + m_y\right) = \mu_0(1+\chi)h_y \quad , \tag{2.1.39}$$

the magnetic permeability becomes

$$\frac{\mu}{\mu_0} = \frac{\left((H^{"}+M_0)^2-\left(\frac{\omega}{\mu_0\gamma}\right)^2\right)}{\left(H^{"}(H^{"}+M_0)-\left(\frac{\omega}{\mu_0\gamma}\right)^2\right)} \quad . \tag{2.1.40}$$

From equation (2.1.40), we note that μ can be positive, negative or zero. When μ is equal to zero or approaches infinity, we call it the anti-resonance or the resonance condition, respectively.

2.2 Theory of the Model

In order to have a negative refractive index we must have negative permittivity and permeability at the same time. How can that be arranged? Smith et al. [2], [3] showed in 2000 that one could construct a metamaterial having a negative phase velocity (NPV) or negative index of refraction. Their material used an array of conducting rods which had a negative permittivity at frequencies below the structure's plasma frequency, and a cut-ring array which had a negative permeability in the same frequency range.

My objective is to find a metamaterial with a negative index of refraction (for some specific frequency range) by constructing a conducting wire array (to create negative permittivity) embedded in a ferrite host (to create negative permeability) in the presence

of a static magnetic field. This will be the first time a magnetic material has been used to achieve a negative refractive index in a low loss medium.

In order that the ferrite not destroy the negative permittivity of the wire array, the wires must be cladded in a nonmagnetic dielectric material as shown in Fig. 2.2.1.

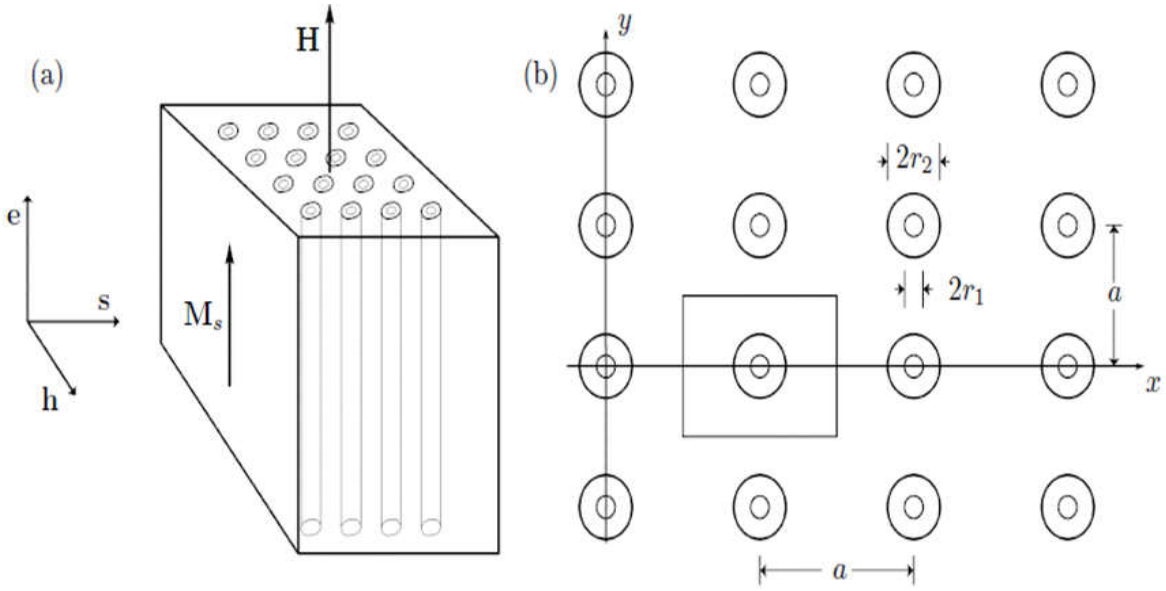

Fig. 2.2.1 Wire array imbedded in magnetic material [10]

The wires lie within the plane of the slab, are all parallel to one another, are infinitely long in theory, and form a square array of lattice constant "a". The wires have a radius r_1 and are cladded with a nonmagnetic insulator out to a radius r_2. The space surrounding the wires is filled with nonconducting magnetic material that is magnetized parallel to the wires by an externally imposed a magnetic field. We choose $r_1 << r_2 << a$. Electromagnetic waves propagating perpendicular to the plane of the slab with the

electric field parallel to the wires can exhibit a negative refractive index in the material [19].

To explain the effect of the electromagnetic wave on the wires and vice versa, I begin by numbering the wires in x and y direction by n_x and n_y, respectively, so the distance in x-direction will be ($a\ n_x$) and distance in y-direction is ($a\ n_y$). The effect will be the following, with each item indicating a step in the calculations to follow.

1-The electrical field of the electromagnetic wave will drive a current in the wires.

2-Current in each wire will create its own electric field outside the cladding at r_2, representing a scattered wave.

3- Each wire will experience a scattered electric field from the other wires of same depth (same n_x).

4-Every wire will also experience a scattered electric field from all the wires of different depth (different n_x and all n_y).

Thus, the electric field outside the cladding at r_2 of a specific wire is consists of four parts,

$$E_{\text{tot}}(x,t) = plain\ wave\ coming\ from\ RF\ source + electric\ field\ scattered\ from\ the\ wire\ itself + electric\ field\ scattered\ from\ wires\ at\ same\ depth + electric\ field\ scattered\ from\ wires\ at\ different\ depth\ . \quad (2.2.1)$$

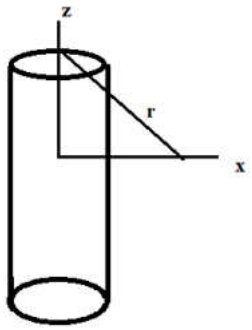

Fig. 2.2.2 Co-ordinate system for calculating the vector potential due to a current in a long wire.

I determine first the self-scattered field of one wire, then I sum this field over wires of the same depth, then wires of different depth. The time dependence of the electric field goes as

$$E_{\text{tot}} \propto e^{-i\omega t} . \tag{2.2.2}$$

Initially, I consider the wire to be infinitely thin.

The RF current in the wire is

$$\vec{J} = j_0 e^{-i\omega t}\delta(x)\delta(y)\hat{z} . \tag{2.2.3}$$

The magnetic vector potential due to the electric current in the wire is

$$\vec{A} = \frac{\mu_0}{4\pi}\int_0^{\infty} \frac{\vec{J}(x,y,z)e^{i\,k_h r}}{r}\,\text{dx dy dz} . \tag{2.2.4}$$

Where the distance r is the radial distance between the wire and the point under examination, and k_h is the wave vector in the ferrite host

The magnetic potential in the *z*-direction is

$$A_z = \frac{\mu_0}{2\pi} e^{-i\omega t} \int_0^{\infty} \frac{j_0 e^{i\, k_h \sqrt{x^2+z^2}}}{\sqrt{x^2+z^2}} \mathrm{dz} = \frac{i\mu_0 j_0 e^{-i\omega t}}{4} H_0^{(1)}(\, k_h x) \ , \tag{2.2.5}$$

where $H_0^{(1)}(\, k_h x)$ is the Hankel function of the first order with argument $k_h x$.

The electric field in the *z*-direction is

$$E_z = \frac{-\partial A_z}{\partial t} = \frac{-\mu_0 \omega j_0 e^{-i\omega t}}{4} H_0^{(1)}(\, k_h x) \ . \tag{2.2.6}$$

My method to calculate the total electric field at the wire at position $x = n_{x'}\, a$ ($n_{x'}$ is an integer) is to sum the electric field coming from different wires at constant (x) but different (y) then sum the electric field coming from different wires at different (x).

The total field coming from wires at a different n_y is

$$E_{\mathrm{other}(y)}(x = n_{x'} a) = 2 \sum_{n_y=1}^{\infty} \frac{-\mu_0 \omega j_0 e^{-i\omega t}}{4} H_0^{(1)}\big(\, k_h\, n_y\, a\big) \ . \tag{2.2.7}$$

Let

$$S_{\mathrm{sd}} = 2 \sum_{n_y=1}^{\infty} H_0^{(1)}\big(\, k_h\, n_y\, a\big) \ , \tag{2.2.8}$$

then

$$E_{\text{other(y)}}(x = n_{x'}a) = \frac{-\mu_0 \omega j_0 e^{-i\omega t}}{4} S_{\text{sd}} \ . \tag{2.2.9}$$

Where "sd" means same depth. Then evaluate to [11]

$$S_{\text{sd}} = -1 + \frac{2}{k_h a} - \frac{2i}{\pi}\left\{\log\left(\frac{k_h a}{2\pi}\right) + \gamma + 2\pi \sum_{m=1}^{\infty}\left(\frac{1}{\sqrt{(2\pi m)^2 - (k_h a)^2}} - \frac{1}{2\pi m}\right)\right\}. \tag{2.2.10}$$

The total field coming from different (y) and different (x) is

$$E_{\text{other}(x,y)}(x = n_{x'}a) = \sum_{(n_x=0, n_x \neq n_{x'})}^{\infty} \sum_{n_y=-\infty}^{\infty} \frac{-\mu_0 \omega e^{-i\omega t}}{4} j_0 H_0^{(1)}\left(k_h a \sqrt{n_x^2 + n_y^2}\right). \tag{2.2.11}$$

Let

$$S_{\text{dd}} = \sum_{n_y=-\infty}^{\infty} H_0^{(1)}\left(k_h a \sqrt{n_x^2 + n_y^2}\right). \tag{2.2.12}$$

Then

$$E_{\text{other}(x,y)}(x = n_{x'}a) = \sum_{(n_x=0, n_x \neq n_{x'})}^{\infty} \frac{-\mu_0 \omega e^{-i\omega t}}{4} j_0 \ S_{\text{dd}} \ , \tag{2.2.13}$$

where "dd" means different depth. Then evaluate to [11]

$$S_{\text{dd}}(n_{x'}, n_x) = \frac{2}{k_h a} e^{i|n_{x'} - n_x| \, k_h a} + \sum_{m=0}^{\infty} \frac{4e^{i|n_{x'} - n_x|\sqrt{(k_h a)^2 - (2\pi m)^2}}}{\sqrt{(k_h a)^2 - (2\pi m)^2}} \ . \tag{2.2.14}$$

Next, I discuss what constitutes the scattered electric field in equation 2.2.1. The scattered waves outside the wires can be phase shifted with respect to the incident field, plus the time dependence of equation (2.2.2) allows me to introduce the initial amplitude of the scattered electric field $E^{I}_{z\_sca}$ outside the cladding at r_2 due to one wire. It will be included in all the summation terms (same depth or different depth) and the response of wires in different phase will allow the wave inside the ferrite-wire model to propagate in different modes. Analogous to the orders of a diffraction grating. I use $E^{I}_{z\_sca}$ later in section (2.3) and (2.4) to solve the boundary value problem of the wire and to calculate the electromagnetic modes.

Using equations (2.2.1), (2.2.2), (2.2.6), (2.2.9) and (2.2.13), I can write the expression for the total electric field as

$$E^{I}_{z\_total}(n_x,t) = E^{\mathrm{pw}} e^{i(n_x k_h a - \omega t)} + E^{I}_{z\_sca}(n_x) H_0^{(1)}(k_h r_2) e^{-i\omega t} + E^{I}_{z\_sca}(n_x) S_{\mathrm{sd}} e^{-i\omega t} + \sum_{n_{x'}=0}^{\infty} E^{I}_{z\_sca}(n_{x'}) S_{\mathrm{dd}}(n_x, n_{x'}) e^{-i\omega t} \quad , \tag{2.2.15}$$

where E^{pw} is the amplitude of the plane wave incident on a wire.

2.3 Boundary Value Problem for the Electromagnetic Field at Wire

In order to calculate the scattered field at a wire, I recapitulate the main points of our model. The model consists of a conducting wire array (to create negative permittivity) embedded in a ferrite host (to create negative permeability) in the presence of strong magnetic field parallel to wires.

In order that the ferrite not destroy the negative permittivity of the wire array, the wires must be cladded in a nonmagnetic dielectric material such as Teflon.

The wires array scatters any incident microwaves and since in the sequel I use superposition of fields scattered by each wire, I initially discuss the scattering by only one wire.

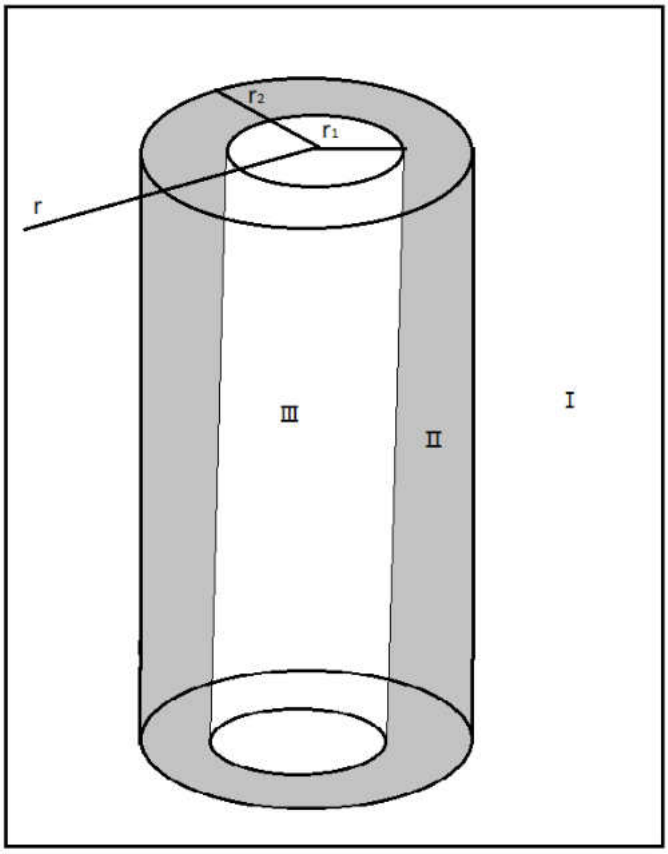

Fig. 2.3.1 Conducting wire cladded with dielectric material and imbedded in ferrite host.

The neighborhood of the wire shown in Fig. 2.3.1 is made of the ferrite medium (medium I) plus the cladding dielectric material (medium II) and the wire itself which is made of metallic conductor (medium III). The radius of the wire and the dielectric are r_1, r_2 respectively, and the coordinate r is the radial distance between the center of the wire to a point under consideration in the ferrite medium.

The electromagnetic field for waves propagating in the *x-y* plane for the polarization of interest is completely specified by a scaler (E_z) where the z-axis is parallel to wires. For the harmonic time variations $e^{-i\omega t}$ in homogenous isotropic media $E_z(\alpha r)$ obeys the wave equation in cylindrical coordinates [12]

$$\frac{1}{r}\frac{\partial}{\partial r}\left(r\frac{\partial E_z}{\partial r}\right)+\frac{1}{r^2}\frac{\partial^2 E_z}{\partial \phi^2}+\alpha_p^2 E_z=0\,, \qquad (2.3.1)$$

with $$\alpha_p = k_p n_p\,, \quad p = I, II \text{ or } III.$$

k_p , n_p are the wave vector and refractive index in the medium p respectively:

$$k_p=\frac{n_p\omega}{c}\ ,\ n_p=\sqrt{\frac{\epsilon_p\mu_p}{\epsilon_0\mu_0}}\ .$$

To solve equation (2.3.1) for each medium, I make two assumptions,

1- $E_z \to 0$ as $r \to \infty$,

2- $k_p r_p \ll 1$.

The electromagnetic field E_z consists of two terms, the incident field $E^p_{z\_inc}$ and the scattered field $E^p_{z\_sca}$ for $p = I, II \text{ or } III$.

To simplify the problem, I deal with the normalized electromagnetic fields by dividing all fields in the three media by $E^I_{z_{sca}}$ at $r = r_2$, the electromagnetic field scattered into the ferrite medium.

The solution of the field in the medium I (ferrite) at $r = r_2^+$ is

$$E^I_{z\_total} = E^I_{z\_inc} + E^I_{z\_sca} \ , \tag{2.3.2}$$

Or

$$\frac{E^I_{z\_total}}{E^I_{z_{sca}}(r=r_2)} = \frac{E^I_{z\_inc}}{E^I_{z_{sca}}(r=r_2)} + \frac{E^I_{z\_sca}}{E^I_{z_{sca}}(r=r_2)} \ , \tag{2.3.3}$$

where

$$\frac{E^I_{z\_inc}}{E^I_{z_{sca}}(r=r_2)} = \sum_{m=-\infty}^{\infty} b_m J_m(\alpha_1 r) e^{\mathrm{im}(\phi - \frac{\pi}{2})} \ , \tag{2.3.4}$$

$$\frac{E^I_{z\_sca}}{E^I_{z_{sca}}(r=r_2)} = \sum_{m=-\infty}^{\infty} a_m H_m^{(2)}(\alpha_1 r) e^{\mathrm{im}(\phi - \frac{\pi}{2})} \ . \tag{2.3.5}$$

$J_m(\alpha_p r)$ is a Bessel function and $H_m^{(2)}(\alpha_p r)$ is a Henkel function of degree m and $\alpha_p r$ is the argument.

By using the $k_p r_p \ll 1$ assumption, the first term of the sum ($m = 0$) dominates the solution and I can neglect the other terms which will be small compared to first term. Thus

$$\frac{E^I_{z\_inc}}{E^I_{z\_sca}(r=r_2)} = \sum_{m=-\infty}^{\infty} b_m J_m(\alpha_1 r) e^{\mathrm{im}\left(\phi-\frac{\pi}{2}\right)} \rightarrow b_0 J_0(\alpha_1 r) \ , \qquad (2.3.6)$$

$$\frac{E^I_{z\_sca}}{E^I_{z_{sca}}(r=r_2)} = \sum_{m=-\infty}^{\infty} a_m H_m^{(2)}(\alpha_1 r) e^{\mathrm{im}(\phi-\frac{\pi}{2})} \rightarrow a_0 H_0^{(2)}(\alpha_1 r) \ , \qquad (2.3.7)$$

The waves in the dielectric medium, i.e. for $r_1 \le r \le r_2$, are

$$E^{II}_{z\_total} = E^{II}_{z\_inc} + E^{II}_{z\_sca} \ , \qquad (2.38)$$

$$\frac{E^{II}_{z\_total}}{E^I_{z\_sca}(r=r_2)} = \frac{E^{II}_{z\_inc}}{E^I_{z\_sca}(r=r_2)} + \frac{E^{II}_{z\_sca}}{E^I_{z\_sca}(r=r_2)}, \qquad (2.3.9)$$

$$\frac{E^{II}_{z\_inc}}{E^I_{z\_sca}(r=r_2)} = \sum_{m=-\infty}^{\infty} c_m H_m^{(1)}(\alpha_2 r) e^{\mathrm{im}(\phi-\frac{\pi}{2})} \rightarrow c_0 H_0^{(1)}(\alpha_2 r), \qquad (2.3.10)$$

$$\frac{E^{II}_{z\_sca}}{E^I_{z\_sca}(r=r_2)} = \sum_{m=-\infty}^{\infty} d_m H_m^{(2)}(\alpha_2 r) e^{\mathrm{im}(\phi-\frac{\pi}{2})} \rightarrow d_0 H_0^{(2)}(\alpha_2 r) \ . \qquad (2.3.11)$$

In the last medium (conductor), there is a standing wave inside the wire with α_3 complex due to the non-zero electrical conductivity of the wire. The wave is represented by

$$E^{III}_{z\_total} = E^{III}_{z\_ins} \ , \qquad (2.3.12)$$

$$\frac{E^{III}_{z\_ins}}{E^I_{z\_sca}(r=r_2)} = \sum_{m=-\infty}^{\infty} f_m J_m(\alpha_3 r) e^{\mathrm{im}(\phi-\frac{\pi}{2})} \rightarrow f_0 J_0(\alpha_3 r) \ . \qquad (2.3.13)$$

In order to assign the field constants b_0, c_0, d_0 and f_0 I use the boundary conditions for continuity of tangential $\vec{E}$ and tangential $\vec{H}$, resulting in $E^p_{z\_total}$ and $\frac{1}{\mu}\frac{\partial E^p_{z\_total}}{\partial r}$ being continuous at r_1 and r_2.

Let

$$\tau^p = \frac{1}{\mu_p} \ .$$

At $r = r_2$ by equating (2.3.3) to (2.3.9) (remembering to normalize with respect to $E^I_{z\_sca}(r = r_2^+)$),

$$1 + b_0 J_0(\alpha_1 r_2) = c_0 H_0^{(1)}(\alpha_2 r_2) + d_0 H_0^{(2)}(\alpha_2 r_2) \ , \qquad (2.3.14)$$

$$\tau_1 \alpha_1 \left(\frac{H_0^{`(2)}(\alpha_1 r_2)}{H_0^{(2)}(\alpha_1 r_2)} + b_0 J_0^{`}(\alpha_1 r_2) \right) = \tau_2 \alpha_2 \left(c_0 H_0^{`(1)}(\alpha_2 r_2) + d_0 H_0^{`(2)}(\alpha_2 r_2) \right) \ , (2.3.15)$$

at $r = r_1$, by equating (2.3.12) to (2.3.9), I obtain

$$f_0 J_0(\alpha_3 r_1) = c_0 H_0^{(1)}(\alpha_2 r_1) + d_0 H_0^{(2)}(\alpha_2 r_1) \ , \qquad (2.3.16)$$

and $$\tau_3 \alpha_3 f_0 J_0^{`}(\alpha_3 r_1) = \tau_2 \alpha_2 \left( c_0 H_0^{`(1)}(\alpha_2 r_1) + d_0 H_0^{`(2)}(\alpha_2 r_1) \right) \ . \qquad (2.3.17)$$

After solving equations (2.3.14), (2.3.15), (2.3.16) and (2.3.17) for field constants b_0, c_0, d_0 and f_0 I obtain

$$
\begin{aligned}
b_0 \to \Big(& H^{`(2)}(\alpha_1\ r_2)\ \alpha_1\ \tau_1 \\
& \Big(J_0(\alpha_3\ r_1)\ \Big(-H^{(1)}(\alpha_2\ r_2)\ H^{`(2)}(\alpha_2\ r_1) + H^{`(1)}(\alpha_2\ r_1)\ H^{(2)}(\alpha_2\ r_2)\Big) \\
& \quad \alpha_2\ \tau_2 + \Big(H^{(1)}(\alpha_2\ r_2)\ H^{(2)}(\alpha_2\ r_1) - H^{(1)}(\alpha_2\ r_1)\ H^{(2)}(\alpha_2\ r_2)\Big) \\
& \quad J_0^{`}(\alpha_3\ r_1)\ \alpha_3\ \tau_3\Big) + H^{(2)}(\alpha_1\ r_2)\ \alpha_2\ \tau_2 \\
& \Big(J_0(\alpha_3\ r_1)\ \Big(H^{`(1)}(\alpha_2\ r_2)\ H^{`(2)}(\alpha_2\ r_1) - H^{`(1)}(\alpha_2\ r_1)\ H^{`(2)}(\alpha_2\ r_2)\Big) \\
& \quad \alpha_2\ \tau_2 + \Big(-H^{`(1)}(\alpha_2\ r_2)\ H^{(2)}(\alpha_2\ r_1) + H^{(1)}(\alpha_2\ r_1)\ H^{`(2)}(\alpha_2\ r_2)\Big) \\
& \quad J_0^{`}(\alpha_3\ r_1)\ \alpha_3\ \tau_3\Big)\Big) \Big/ \Big(H^{(2)}(\alpha_1\ r_2)\ J_0^{`}(\alpha_1\ r_2)\ \alpha_1\ \tau_1 \\
& \Big(J_0(\alpha_3\ r_1)\ \Big(H^{(1)}(\alpha_2\ r_2)\ H^{`(2)}(\alpha_2\ r_1) - H^{`(1)}(\alpha_2\ r_1)\ H^{(2)}(\alpha_2\ r_2)\Big) \\
& \quad \alpha_2\ \tau_2 + \Big(-H^{(1)}(\alpha_2\ r_2)\ H^{(2)}(\alpha_2\ r_1) + H^{(1)}(\alpha_2\ r_1)\ H^{(2)}(\alpha_2\ r_2)\Big) \\
& \quad J_0^{`}(\alpha_3\ r_1)\ \alpha_3\ \tau_3\Big) + J_0(\alpha_1 r_2)\ H^{(2)}(\alpha_1\ r_2)\ \alpha_2\ \tau_2 \\
& \Big(J_0(\alpha_3\ r_1)\ \Big(-H^{`(1)}(\alpha_2\ r_2)\ H^{`(2)}(\alpha_2\ r_1) + H^{`(1)}(\alpha_2\ r_1)\ H^{`(2)}(\alpha_2\ r_2)\Big) \\
& \quad \alpha_2\ \tau_2 + \Big(H^{`(1)}(\alpha_2\ r_2)\ H^{(2)}(\alpha_2\ r_1) - H^{(1)}(\alpha_2\ r_1)\ H^{`(2)}(\alpha_2\ r_2)\Big) \\
& \quad J_0^{`}(\alpha_3\ r_1)\ \alpha_3\ \tau_3\Big)\Big),
\end{aligned}
$$

$$
\begin{aligned}
c_0 \to \Big(& \Big(-J_0(\alpha_1 r_2)\ H^{`(2)}(\alpha_1\ r_2) + H^{(2)}(\alpha_1\ r_2)\ J_0^{`}(\alpha_1\ r_2)\Big)\ \alpha_1\ \tau_1 \\
& \Big(J_0(\alpha_3\ r_1)\ H^{`(2)}(\alpha_2\ r_1)\ \alpha_2\ \tau_2 - H^{(2)}(\alpha_2\ r_1)\ J_0^{`}(\alpha_3\ r_1)\ \alpha_3\ \tau_3\Big)\Big) \Big/ \\
& \Big(H^{(2)}(\alpha_1\ r_2)\ J_0^{`}(\alpha_1\ r_2)\ \alpha_1\ \tau_1 \\
& \quad \Big(J_0(\alpha_3\ r_1)\ \Big(H^{(1)}(\alpha_2\ r_2)\ H^{`(2)}(\alpha_2\ r_1) - H^{`(1)}(\alpha_2\ r_1)\ H^{(2)}(\alpha_2\ r_2)\Big) \\
& \quad\quad \alpha_2\ \tau_2 + \Big(-H^{(1)}(\alpha_2\ r_2)\ H^{(2)}(\alpha_2\ r_1) + H^{(1)}(\alpha_2\ r_1)\ H^{(2)}(\alpha_2\ r_2)\Big) \\
& \quad\quad J_0^{`}(\alpha_3\ r_1)\ \alpha_3\ \tau_3\Big) + J_0(\alpha_1 r_2)\ H^{(2)}(\alpha_1\ r_2)\ \alpha_2\ \tau_2 \\
& \quad \Big(J_0(\alpha_3\ r_1)\ \Big(-H^{`(1)}(\alpha_2\ r_2)\ H^{`(2)}(\alpha_2\ r_1) + H^{`(1)}(\alpha_2\ r_1)\ H^{`(2)}(\alpha_2\ r_2)\Big) \\
& \quad\quad \alpha_2\ \tau_2 + \Big(H^{`(1)}(\alpha_2\ r_2)\ H^{(2)}(\alpha_2\ r_1) - H^{(1)}(\alpha_2\ r_1)\ H^{`(2)}(\alpha_2\ r_2)\Big) \\
& \quad\quad J_0^{`}(\alpha_3\ r_1)\ \alpha_3\ \tau_3\Big)\Big),
\end{aligned}
$$

$$
\begin{aligned}
d_0 \to & \Big(\big(J_0(\alpha_1 r_2)\, H^{(2)\prime}(\alpha_1\, r_2) - H^{(2)}(\alpha_1\, r_2)\, J_0{}'(\alpha_1\, r_2) \big)\, \alpha_1 \tau_1 \\
& \big(J_0(\alpha_3\, r_1)\, H^{(1)\prime}(\alpha_2\, r_1)\, \alpha_2 \tau_2 - H^{(1)}(\alpha_2\, r_1)\, J_0{}'(\alpha_3\, r_1)\, \alpha_3 \tau_3 \big) \Big) / \\
& \Big(H^{(2)}(\alpha_1\, r_2)\, J_0{}'(\alpha_1\, r_2)\, \alpha_1 \tau_1 \\
& \quad \big(J_0(\alpha_3\, r_1) \big(H^{(1)}(\alpha_2\, r_2)\, H^{(2)\prime}(\alpha_2\, r_1) - H^{(1)\prime}(\alpha_2\, r_1)\, H^{(2)}(\alpha_2\, r_2) \big) \\
& \qquad \alpha_2 \tau_2 + \big(-H^{(1)}(\alpha_2\, r_2)\, H^{(2)}(\alpha_2\, r_1) + H^{(1)}(\alpha_2\, r_1)\, H^{(2)}(\alpha_2\, r_2) \big) \\
& \qquad J_0{}'(\alpha_3\, r_1)\, \alpha_3 \tau_3 \big) + J_0(\alpha_1 r_2)\, H^{(2)}(\alpha_1\, r_2)\, \alpha_2 \tau_2 \\
& \quad \big(J_0(\alpha_3\, r_1) \big(-H^{(1)\prime}(\alpha_2\, r_2)\, H^{(2)\prime}(\alpha_2\, r_1) + H^{(1)\prime}(\alpha_2\, r_1)\, H^{(2)\prime}(\alpha_2\, r_2) \big) \\
& \qquad \alpha_2 \tau_2 + \big(H^{(1)\prime}(\alpha_2\, r_2)\, H^{(2)}(\alpha_2\, r_1) - H^{(1)}(\alpha_2\, r_1)\, H^{(2)\prime}(\alpha_2\, r_2) \big) \\
& \qquad J_0{}'(\alpha_3\, r_1)\, \alpha_3 \tau_3 \big) \Big),
\end{aligned}
$$

$$
\begin{aligned}
f_0 \to & \Big(\big(H^{(1)\prime}(\alpha_2\, r_1)\, H^{(2)}(\alpha_2\, r_1) - H^{(1)}(\alpha_2\, r_1)\, H^{(2)\prime}(\alpha_2\, r_1) \big) \\
& \big(J_0(\alpha_1 r_2)\, H^{(2)\prime}(\alpha_1\, r_2) - H^{(2)}(\alpha_1\, r_2)\, J_0{}'(\alpha_1\, r_2) \big)\, \alpha_1 \alpha_2 \tau_1 \tau_2 \big) / \\
& \Big(H^{(2)}(\alpha_1\, r_2)\, J_0{}'(\alpha_1\, r_2)\, \alpha_1 \tau_1 \\
& \quad \big(J_0(\alpha_3\, r_1) \big(H^{(1)}(\alpha_2\, r_2)\, H^{(2)\prime}(\alpha_2\, r_1) - H^{(1)\prime}(\alpha_2\, r_1)\, H^{(2)}(\alpha_2\, r_2) \big) \\
& \qquad \alpha_2 \tau_2 + \big(-H^{(1)}(\alpha_2\, r_2)\, H^{(2)}(\alpha_2\, r_1) + H^{(1)}(\alpha_2\, r_1)\, H^{(2)}(\alpha_2\, r_2) \big) \\
& \qquad J_0{}'(\alpha_3\, r_1)\, \alpha_3 \tau_3 \big) + J_0(\alpha_1 r_2)\, H^{(2)}(\alpha_1\, r_2)\, \alpha_2 \tau_2 \\
& \quad \big(J_0(\alpha_3\, r_1) \big(-H^{(1)\prime}(\alpha_2\, r_2)\, H^{(2)\prime}(\alpha_2\, r_1) + H^{(1)\prime}(\alpha_2\, r_1)\, H^{(2)\prime}(\alpha_2\, r_2) \big) \\
& \qquad \alpha_2 \tau_2 + \big(H^{(1)\prime}(\alpha_2\, r_2)\, H^{(2)}(\alpha_2\, r_1) - H^{(1)}(\alpha_2\, r_1)\, H^{(2)\prime}(\alpha_2\, r_2) \big) \\
& \qquad J_0{}'(\alpha_3\, r_1)\, \alpha_3 \tau_3 \big) \Big)
\end{aligned}
$$

The four constants b_0, c_0, d_0 and f_0 depend on $\alpha_p = k_p n_p$ and $\tau^p = \frac{1}{\mu_p}$ which can be determined for each medium $p = I, II\ or\ III$.

The purpose of the previous calculation is to calculate $\frac{E^I_{z\_total}}{E^I_{z\_sca}} = b_0\, J_0(\alpha_1 r_2) \ + 1$ at $r = r_2$ which I use later to calculate the electromagnetic modes of wire lattice consisting of a number of wires like the wire just considered in this section.

2.4 Calculation of the Amplitude of each Electromagnetic Mode in the Photonic Lattice

After determining the equation for the normalized total electric field due to the wire lattice embedded into the ferrite host $\frac{E^I_{z\_total}}{E^I_{z\_sca}}$, it remains to determine $E^I_{z\_sca}$ and to use it to obtain the total electric field $E^I_{z\_total}$.

I use the expression for the total electric field $E^I_{z\_total}$ found in section 2.2 .

$$E^I_{z\_total}(n_x,t) = E^{\mathrm{pw}} e^{i(n_x k_h a - \omega t)} + E^I_{z\_sca}(n_x) H_0^{(1)}(k_h r_2) e^{-i\omega t} + E^I_{z\_sca}(n_x) S_{\mathrm{sd}} e^{-i\omega t} + \sum_{n_{x'}=0}^{\infty} E^I_{z\_sca}(n_{x'}) S_{\mathrm{dd}}(n_x, n_{x'}) e^{-i\omega t} \quad , \qquad (2.4.1)$$

where E^{pw} is the amplitude of the plane wave incident on a wire and $E^I_{z\_sca}$ the amplitude of the wave scattered off a wire and k_h is the same as k_I I used section 2.3

As explained in section 2.2, the total electric field consists of different modes of different amplitudes and propagation constants.

To find the parameters describing these different modes, one can assert that the total field can be related to the amplitude of the incident field:

$$E^I_{z\_total}(n_x,t) = \sum_{l=0}^{\infty} f_l e^{i\bar{k}_l x} \, E^{\mathrm{pw}} \, e^{i(n_x k_h a - \omega t)} \quad , \qquad (2.4.2)$$

where f_l is the amplitude of the lth mode, $\bar{k}_l$ is an augmentation of k_h for the lth mode and $x = n_x a$, $y = 0$. We can choose $y = 0$ because there is translational symmetry in the *y*- direction

Setting the relation between the total field and the scattered field at a wire as

$$E^I_{z\_sca}(n_x,t) = RE^I_{z\_total}(n_x,t) \quad , \tag{2.4.3}$$

with R as the scattering factor which I determined in equation (2.3.3), I obtain

$\frac{E^I_{z\_total}}{E^I_{z\_sca}} = b_0\, J_0(\alpha_1 r_2) \; + 1 = \frac{1}{R}$ at $r = r_2$ where b_0 , α_1 , r_2 are determined in section 2.3 .

Substituting equation (2.4.2) into (2.4.1) and using (2.4.3) to eliminate $E^I_{z\_sca}(n_x,t)$ and dividing both sides by $E^{\mathrm{pw}}\, e^{-\mathrm{i}\omega \mathrm{t}}$, I get

$$\sum_{l=0}^{\infty} f_l e^{i\bar{k}_l n_x a} e^{\mathrm{i}k_h n_x a} = e^{ik_h n_x a} + \sum_{l=0}^{\infty} Rf_l\, e^{i\bar{k}_l n_x a}\, e^{ik_h n_x a}\, H_0^{(1)}(k_h r_2) +$$

$$\sum_{l=0}^{\infty} Rf_l\, e^{i\bar{k}_l n_x a}\, e^{\mathrm{i}k_h n_x a}\, S_{\mathrm{sd}} +$$

$$\sum_{n_{x'}=0}^{\infty} \sum_{l=0}^{\infty} Rf_l e^{i\bar{k}_l n_{x'}\, a}\, e^{\mathrm{i}k_h n_{x'} a}\, S_{\mathrm{dd}}(n_{x'}, n_x) \quad , \tag{2.4.4}$$

where the sum over $n_{x'}$ excludes $n_{x'} = n_x$.

Substitute $\bar{k}_l + k_h = k_l$, for equation (2.4.4) I obtain

$$\sum_{l=0}^{\infty} f_l e^{\mathrm{i}k_l n_x a} = e^{ik_h n_x a} + \sum_{l=0}^{\infty} Rf_l\, e^{ik_l n_x a}\, H_0^{(1)}(k_h r_2) +$$

$$\sum_{l=0}^{\infty} Rf_l\, e^{\mathrm{i}k_l n_x a}\, S_{\mathrm{sd}} + \cdots$$

$$\ldots\ldots \sum_{n_{x'}=0}^{\infty} \sum_{l=0}^{\infty} Rf_l \, e^{\mathrm{i}k_l n_{x'} a} \, S_{\mathrm{dd}}(n_{x'}, n_x) \quad . \qquad (2.4.5)$$

I evaluated S_{sd} in (2.2.10) to be,

$$S_{\mathrm{sd}} = -1 + \frac{2}{k_h a} - \frac{2i}{\pi}\left\{\log\left(\frac{k_h a}{2\pi}\right) + \gamma + 2\pi \sum_{M=1}^{\infty}\left(\frac{1}{\sqrt{(2\pi M)^2 - (k_h a)^2}} - \frac{1}{2\pi M}\right)\right\}.$$

Next I carry out the summation in $\Phi = \sum_{n_{x'}=0}^{\infty} e^{\mathrm{i}k_l n_{x'} a} S_{\mathrm{dd}}(n_{x'}, n_x)$ where the function $S_{\mathrm{dd}}(n_{x'}, n_x)$ is equal to

$$S_{\mathrm{dd}}(n_{x'}, n_x) = \frac{2}{k_h a} e^{i|n_{x'} - n_x| \, k_h a} + \sum_{m=0}^{\infty} \frac{4e^{i|n_{x'} - n_x|\sqrt{(k_h a)^2 - (2\pi m)^2}}}{\sqrt{(k_h a)^2 - (2\pi m)^2}} \quad .$$

I split the summation Φ into two parts. The first part is

$$I_1 = \sum_{n_{x'}=0}^{\infty} \frac{2}{k_h a} e^{\mathrm{i}k_l n_{x'} a} e^{i|n_{x'} - n_x| \, k_h a}$$

We see in the summation I_1 that $n_{x'}$ starts from zero and goes to infinity so $n_{x'}$ can be bigger or smaller than n_x . Thus the sign under the absolute magnitude of the difference changes and I evaluate I_1 in two parts, $I_{1>}$ for $n_x > n_{x'}$ and $I_{1<}$ for $n_x < n_{x'}$.Thus

$$I_{1>} = \sum_{n_{x'}=0}^{n_x-1} \frac{2}{k_h a} e^{\mathrm{ia}\left((k_l-k_h)n_{x'}+k_h n_x\right)} = \frac{2}{k_h a} \frac{e^{\mathrm{ik}_l n_x a} - e^{\mathrm{ik}_h n_x a}}{e^{i\bar{k}_l a} - 1}$$

and

$$I_{1<} = \sum_{n_{x'}=n_x+1}^{\infty} \frac{2}{k_h a} e^{\mathrm{ia}\left((k_l+k_h)n_{x'}-k_h n_x\right)} = \frac{-2}{k_h a} \frac{e^{\mathrm{ik}_l n_x a}}{1 - e^{-ia(k_l+k_h)}} \quad .$$

Here $I_1 = I_{1>} + I_{1<}$ becomes

$$I_1 = \frac{2}{k_h a}\left[\frac{e^{\mathrm{ik}_l n_x a} - e^{\mathrm{ik}_h n_x a}}{e^{i\bar{k}_l a} - 1} + \frac{e^{\mathrm{ik}_l n_x a}}{e^{-ia(k_l+k_h)} - 1}\right] \quad .$$

Next I deal with the second part of the summation Φ which is

$$I_2 = \sum_{n_{x'}=0}^{\infty} e^{\mathrm{ik}_l n_{x'} a} \frac{4e^{i|n_{x'} - n_x|\sqrt{(k_h a)^2 - (2\pi m)^2}}}{\sqrt{(k_h a)^2 - (2\pi m)^2}} \quad .$$

Again, I split the summation into two parts, $I_{2>}$ for $n_x > n_{x'}$ and $I_{2<}$ for $n_x < n_{x'}$. Thus

$$I_{2>} = \sum_{n_{x'}=0}^{n_x-1} e^{\mathrm{i}k_l n_{x'} a} \frac{4e^{i(n_x - n_{x'})\sqrt{(k_h a)^2-(2\pi m)^2}}}{\sqrt{(k_h a)^2-(2\pi m)^2}}$$

$$= \frac{4}{\sqrt{(k_h a)^2-(2\pi m)^2}} \left(\frac{e^{in_x\sqrt{(k_h a)^2-(2\pi m)^2}} - e^{in_x k_l a}}{1 - e^{i\left(ak_l - \sqrt{(k_h a)^2-(2\pi m)^2}\right)}} \right)$$

and $$I_{2<} = \sum_{n_{x'}=n_x+1}^{\infty} e^{\mathrm{i}k_l n_{x'} a} \frac{4e^{i\left(n_{x'} - n_x\right)\sqrt{(k_h a)^2-(2\pi m)^2}}}{\sqrt{(k_h a)^2-(2\pi m)^2}}$$

$$= \frac{-4}{\sqrt{(k_h a)^2-(2\pi m)^2}} \left(\frac{e^{\mathrm{i}k_l n_x a}}{1-e^{-i\left(k_l a + \sqrt{(k_h a)^2-(2\pi m)^2}\right)}} \right) \quad .$$

Here $I_2 = I_{2>} + I_{2<}$ becomes

$$I_2 = \frac{4}{\sqrt{(k_h a)^2-(2\pi m)^2}} \left(\frac{e^{in_x\sqrt{(k_h a)^2-(2\pi m)^2}} - e^{in_x k_l a}}{1-e^{i\left(ak_l - \sqrt{(k_h a)^2-(2\pi m)^2}\right)}} - \frac{e^{\mathrm{i}k_l n_x a}}{1-e^{-i\left(k_l a + \sqrt{(k_h a)^2-(2\pi m)^2}\right)}} \right) \quad ,$$

hence $$\Phi = \sum_{n_{x'}=0}^{\infty} e^{\mathrm{i}k_l n_{x'} a} S_{\mathrm{dd}}(n_{x'}, n_x) = I_1 + I_2 \quad . \qquad (2.4.6)$$

After substituting equation (2.4.6) into equation (2.4.5) and then dividing by $e^{ik_h n_x a}$ I obtain

$$\sum_{l=0}^{\infty} f_l [e^{i\bar{k}_l a n_x} - Re^{i\bar{k}_l a n_x} H_0^{(1)}(k_h r_2) - Re^{i\bar{k}_l a n_x} S_{\mathrm{sd}} -$$

$$\frac{2R}{ak_h}\left(\frac{e^{i\bar{k}_l a n_x}-1}{e^{i\bar{k}_l a}-1}+\frac{e^{i\bar{k}_l a n_x}}{e^{-ia\left(\bar{k}_l+2k_h\right)}-1}\right)-\sum_{m=1}^{\infty}\frac{4R}{\sqrt{(k_h a)^2-(2\pi m)^2}}*$$

$$\left(\frac{e^{i\bar{k}_l a n_x}}{e^{-i\left(\bar{k}_l a+k_h a+\sqrt{(k_h a)^2-(2\pi m)^2}\right)}-1}+\frac{e^{in_x\left(\sqrt{(k_h a)^2-(2\pi m)^2}-k_h a\right)}-e^{i\bar{k}_l a n_x}}{1-e^{i\left(\bar{k}_l a+k_h a-\sqrt{(k_h a)^2-(2\pi m)^2}\right)}}\right)] = 1 \qquad (2.4.7)$$

To find the roots of the equation, I define new variables:

$$\zeta = e^{\mathrm{i}k_l a} = e^{ia\left(\bar{k}_l+k_h\right)} \qquad (2.4.8)$$

$$P_m = e^{-i\sqrt{(k_h a)^2-(2\pi m)^2}} \qquad (2.4.9)$$

$$P_0 = e^{-ik_h a} \ . \qquad (2.4.10)$$

Next I rewrite equation (2.4.7) as

$$\sum_{l=0}^{\infty} f_l e^{ia\bar{k}_l n_x} G = 1 \ . \qquad (2.4.11)$$

After substituting equations (2.4.8), (2.4.9) and (2.4.10) into equation (2.4.11), the coefficient of $f_l e^{ia\bar{k}_l n_x}$ is

$$G = 1 - RH_0^{(1)}(k_h r_2) - RS_{\mathrm{sd}} - \frac{2R}{ak_h}\left(\frac{1 - e^{-i\bar{k}_l a n_x}}{P_0\zeta - 1} + \frac{1}{\frac{P_0}{\zeta} - 1}\right) + \sum_{m=1}^{\infty} \frac{4R}{\sqrt{(k_h a)^2 - (2\pi m)^2}}\left(\frac{1}{\frac{-P_m}{\zeta} + 1} + \frac{e^{\mathrm{in}_x\left(\sqrt{(k_h a)^2 - (2\pi m)^2} - a\left(k_h + \bar{k}_l\right)\right)} - 1}{P_m\zeta - 1}\right) . \quad (2.4.12)$$

After rearranging equation (2.4.12) ,

$$G = 1 - RH_0^{(1)}(k_h r_2) - RS_{\mathrm{sd}} - \frac{2\,R/k_h\,a}{P_0\zeta - 1} - \frac{2\,R/k_h\,a}{\frac{P_0}{\zeta} - 1} + \sum_{m=1}^{\infty} \frac{4R}{\sqrt{(k_h a)^2 - (2\pi m)^2}}\left(\frac{1}{\frac{-P_m}{\zeta} + 1} - \frac{1}{P_m\zeta - 1}\right) + \frac{(2\,R/k_h\,a)e^{-i\bar{k}_l a n_x}}{P_0\zeta - 1} + \sum_{m=1}^{\infty} \frac{4R}{\sqrt{(k_h a)^2 - (2\pi m)^2}} \frac{e^{\mathrm{in}_x\left(\sqrt{(k_h a)^2 - (2\pi m)^2} - k_l a\right)}}{P_m\zeta - 1} . \quad (2.4.13)$$

Make the substitutions

$$(P_0\zeta)^{n_x} = e^{\left(i\bar{k}_l a + ik_h a - ik_h a\right)n_x} = e^{i\bar{k}_l a n_x}, \tag{2.4.14}$$

$$(P_0\zeta)^{-n_x} = e^{-i\bar{k}_l a n_x}\ , \tag{2.4.15}$$

$$\text{and}\ \ (P_m\zeta)^{-n_x} = e^{\mathrm{i}n_x\sqrt{(k_h a)^2-(2\pi m)^2}} e^{-\mathrm{i}n_x\bar{k}_l a} e^{-\mathrm{i}n_x k_h a} =$$

$$e^{\mathrm{i}n_x\left(\sqrt{(k_h a)^2-(2\pi m)^2}-k_l a\right)}. \tag{2.4.16}$$

After substituting equations (2.4.13), (2.4.14), (2.4.15), (2.4.16) into (2.4.11), I obtain

$$\sum_{l=0}^{\infty} f_l (P_0\zeta)^{n_x} = 1 - \sum_{l=0}^{\infty} f_l \frac{(2\,R/k_h\,a)}{P_0\zeta - 1} - \sum_{m=1}^{\infty} f_l \frac{4R}{\sqrt{(k_h a)^2 - (2\pi m)^2}} *$$

$$\frac{(P_0/P_m)^{n_x}}{P_m\zeta - 1} + \sum_{l=0}^{\infty} f_l (P_0\zeta)^{n_x} [R H_0^{(1)}(k_h r_2) + R S_{\mathrm{sd}} + \frac{(2\,R/k_h\,a)}{P_0\zeta - 1} +$$

$$\frac{(2\,R/k_h\,a)}{\frac{P_0}{\zeta} - 1} - \sum_{m=1}^{\infty} \frac{4R}{\sqrt{(k_h a)^2 - (2\pi m)^2}} \left(\frac{1}{\frac{-P_m}{\zeta} + 1} - \frac{1}{P_m\zeta - 1} \right)] \quad . \tag{2.4.17}$$

After rearranging (2.4.17) ,

$$\sum_{l=0}^{\infty} f_l (P_0\zeta)^{n_x} (1 - [RH_0^{(1)}(k_h r_2) + RS_{sd} + \frac{(2\,R/k_h\,a)}{P_0\zeta - 1} +$$

$$\frac{(2\,R/k_h\,a)}{\frac{P_0}{\zeta} - 1} - \sum_{m=1}^{\infty} \frac{4R}{\sqrt{(k_h a)^2 - (2\pi m)^2}} \left(\frac{1}{\frac{-P_m}{\zeta} + 1} - \frac{1}{P_m\zeta - 1} \right)]) =$$

$$1 - \sum_{l=0}^{\infty} f_l \frac{(2\,R/k_h\,a)}{P_0\zeta - 1} - \sum_{m=1}^{\infty} f_l \frac{4R}{\sqrt{(k_h a)^2 - (2\pi m)^2}} \frac{(P_0/P_m)^{n_x}}{P_m\zeta - 1} \quad (2.4.18)$$

Equation (2.4.18) must be hold for all n_x . In particular, this requirement implies that the coefficient of $(P_0\zeta)^{n_x} = e^{i\bar{k}_l a n_x}$ must be zero. Hence

$$1 = RH_0^{(1)}(k_h r_2) + RS_{\mathrm{sd}} + \frac{(2\,R/k_h\,a)}{P_0\zeta - 1} + \frac{(2\,R/k_h\,a)}{\frac{P_0}{\zeta} - 1} -$$

$$\sum_{m=1}^{\infty} \frac{4R}{\sqrt{(k_h a)^2 - (2\pi m)^2}} \left(\frac{1}{\frac{-P_m}{\zeta} + 1} - \frac{1}{P_m\zeta - 1} \right) , \qquad (2.4.18)$$

and

$$1 = \sum_{l=0}^{\infty} f_l \frac{(2R/k_h a)}{P_0\zeta - 1} + \sum_{m=1}^{\infty} f_l \frac{4R}{\sqrt{(k_h a)^2 - (2\pi m)^2}} \frac{(P_0/P_m)^{n_x}}{P_m\zeta - 1} \ . \qquad (2.4.19)$$

From equations (2.4.18) and (2.4.19), I show how to solve it to obtain the amplitude f_l and the wave vector $(k_h + k_l)$ for each electromagnetic mode l. Let me first state which parameters in these two equations are known:

1) The (k-host) k_h is the wave vector of the microwave inside the ferrite host (no wires in the ferrite host) which can be calculated for specific frequency by $k_h = \omega\sqrt{\epsilon_h\mu_h/\epsilon_0\mu_0}$.
2) The lattice constant a and the cladding radius r_2 are measurable quantities.
3) $P_m = e^{-i\sqrt{(k_h a)^2-(2\pi m)^2}}$, $P_0 = e^{-ik_h a}$, for $k_h a \ll 2\pi m$ I can do the next approximation,

   $P_m = e^{-i\sqrt{(k_h a)^2-(2\pi m)^2}} = e^{-2i\pi m\sqrt{(\frac{k_h a}{2\pi m})^2-1}} \simeq e^{2\pi m(1-\frac{1}{2}(\frac{k_h a}{2\pi m})^2)}$, ${P_m}^{-1} \propto e^{-2\pi m}$

   so, the summation terms fall-off as $e^{-2\pi m}$ and $m_{\max} = 16$ is good enough to achieve accurate results for the total summation over m. The comparison between $k_h a$ and $2\pi m$ values in eq. (2.4.18) and (2.4.19) resembles the case of the diffraction grating. The diffracted light have maxima at angles θ_m given by $a\, k \sin(\theta_m) = 2\pi m$ which gives $ka \geqslant 2\pi m$, for the case of $ka < 2\pi m$, the wave can not constructively propagate except in the forward direction.

4) $S_{\mathrm{sd}} = -1 + \frac{2}{k_h a} - \frac{2i}{\pi}\left\{\log\left(\frac{k_h a}{2\pi}\right) + \gamma + 2\pi\sum_{M=1}^{\infty}\left(\frac{1}{\sqrt{(2\pi M)^2-(k_h a)^2}} - \frac{1}{2\pi M}\right)\right\}$ can be calculated after k_h and a determine an upper limit of $M = M_{\max}$, i.e. , for $k_h a \ll 2\pi M$. I make the next approximation,

   $\frac{1}{\sqrt{(2\pi M)^2-(k_h a)^2}} - \frac{1}{2\pi M} = \frac{1}{2\pi M}\left[\frac{1}{\sqrt{1-(\frac{k_h a}{2\pi M})^2}} - 1\right] \simeq \frac{1}{2\pi M}\left[1 + \frac{1}{2}(\frac{k_h a}{2\pi M})^2 - 1\right] \propto \frac{1}{M^3}$,

so the summation value will fall-off as $\frac{1}{M^3}$, in my numerical calculation I found that $M_{\max} = 2000$ is big enough to give accurate results. The terms beyond $M_{\max}$ can be approximated by an integral.

5- The scattering factor R can be calculated by $\frac{1}{R} = b_0 J_0(\alpha_1 r_2) + 1$ where b_0 is a constant I have determined in section 2.3.

Thus, we see that all the parameters are known except $\zeta = e^{\mathrm{i}k_l a} = e^{ia\left(\bar{k}_l + k_h\right)}$ and f_l . I start with (2.4.18) to solve for ζ and it is obvious that ζ and $\frac{1}{\zeta}$ both are roots to this equation. I get a root for each mode which propagates in the ferrite – wire block. After I solve for ζ values, I substitute it in (2.4.19) to solve for f_l corresponding to ζ values .

Finally, after I solve for ζ and f_l , I will substitute it back in (2.4.2) to obtain $\frac{E^I_{z\_total}}{E^{\mathrm{pw}}}$

2.5 Calculation of the Wave Vector using the Electromagnetic Mode Equation

After I obtained the equation (2.4.18) which can be solved for $\zeta = e^{\mathrm{i}k_l a}$, I solved equation (2.4.18) for ($k_l a$) for different values of frequency (0.0 GHz – 30.0 GHz) for the main mode TE_{10}, In the calculation I used the magnetic field $H_0 = 0.3$ kOe , magnetization $4\pi M = 4780.0\ G$, electric permittivity of the ferrite host $\epsilon = 5.0\ \epsilon_0$, and g-factor $g = 2.0062$.

I plotted $k_l a$ versus frequency for $l = 0$ in figure 2.5.1.

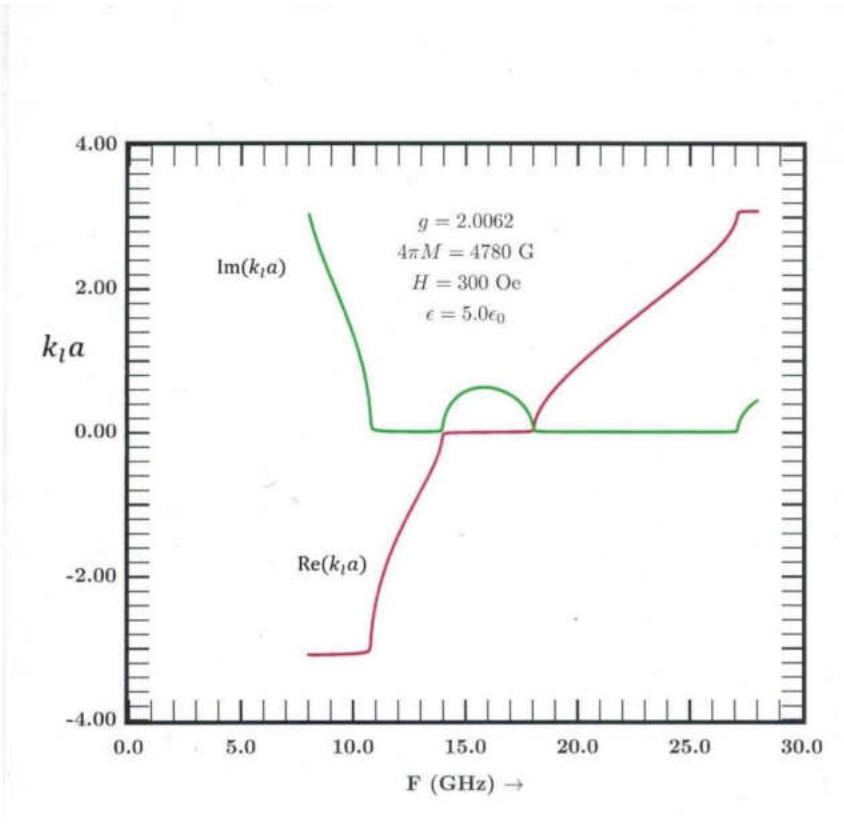

Figure 2.5.1 Plot of wave vector of negative (NIM) vs. frequency

As shown in figure 2.5.1 the wave vector has a negative real value in the frequency range 10.8 GHz to 14.0 GHz. This implies that the refractive index is negative in the same frequency range. The imaginary part of the wave vector close to zero when the real part is negative. The real part of the wave vector is equal to zero in the frequency range (14.0 GHz – 18.0 GHz) while the imaginary part is bigger than zero due to,

1) The wavelength being longer than twice the width of the waveguide.
2) The positive permeability of the region containing the Teflon dielectric dominating the small negative permeability of the ferrite.

CHAPTER III

APPARATUS

3.1 Mechanical and Heat Treatment

The ferrite material I selected to use in the research was a powder of unreacted precursor material. It was also not magnetic. I had to heat treat the powder to make a magnetic ferrite

In order to have rigid magnetized ferrite material I had to carry out several mechanical and heat treatment steps, including pressing, sintering and drilling [13]. These processes were

a- Pressing process: I pressed the powder into a cylindrical pellet under a force equal to 4.5 tons.

   I used in the pressing process the manual press "Carver Laboratory Press "[20], it gave me a disk shape with a 9.5 mm radius and 8 mm height.

b- Sintering process: To react the pressed ferrite disk, I heated the ferrite disk to 1200 °C ; unfortunately it was very hard and I could not drill any holes in it. I decided to reduce the heat treatment temperature in an attempt to make a more workable sample.

I placed the ferrite in the lab furnace for 25 hours following the following plan:

1- Heat the ferrite from room temperature to 1000°C at 100°C/hour

2- Maintain the temperature constant at 1000°C for 5 hours.

3- Cool down from 1000°C to room temperature at 100°C/hour.

The sample was placed in the center of the furnace chamber on a ceramic plate. I used in this process the " LINDBERG 1500ºC Heavy Duty Tube Furnace" operated by " Omega CN 3000 series dual input programmable controller"[21], [22].

c- After I sintered the ferrite disk, I had to drill the hole array and then cut it to a rectangular shape to fit the wave guide dimensions.

I drilled the array of holes using "South Bend Precision 14-inch Drill Press"[23], the distance between holes was 3 mm center to center and with each hole's diameter equal to 1.7 mm. Then I cut it using a hand wire saw into dimensions 30 x 15.7 x 8 mm^3.

Fig. 3.1.1 Sintered ferrite sample with holes drilled.

3.2 AC Capacitance Bridge

In order to make an estimate of the sample's electric permittivity at 15 GHz, I used an AC Capacitance Bridge to measure the permittivity of the material, at low frequency this set an upper limit to the permittivity in the GHz range.

I used the 1621 Precision Capacitance Measurement System GenRad [24] which consist of

a- 1316 Oscillation GenRad with specifications:

Frequency: 10 Hz to 100 kHz in 4 decade ranges.

Accuracy: ±1% of setting.

Power: 100 to 125 and 200 to 250 V, 50 to 60 Hz, 36 W.

b- 1238 Detector GenRad with specifications,

Frequency: 10 Hz to 100 kHz in 4 decade ranges.

Accuracy: ±5% of setting.

Power: 100 to 125 and 200 to 250 V, 50 to 60 Hz, 15 W.

c- 1616 Precision Capacitance Bridge GenRad with specifications,

Frequency: 10 Hz to 100 kHz.

Capacitance measurement, 3-terminal;

Decades: 12, Range: 0.1 aF to 1 μF , Accuracy: ±10 ppm, Capacitance measurement, 2-terminal: Same as above, except as follows. Range: One additional decade, to 10 μF.

Conductance measurement, 3-terminal;

Decades: 5 (virtually extended to 11 by G multiplier). RANGE; 100 aS to 100 μS , Accuracy: ±0.l

Conductance measurement, 2-terminal: Same as above, except as follows: Range: One additional decade, to 1000 μS,

Multipliers: for 3-Term: X1. X10; for 2-Term: X1, X10, X100; affect both C and G.

For conductance only: X1, $X10^{-1}$, . . . $X10^{-6}$ (7 positions).

3.3 Transmission and Reflection Instruments

In order to measure the transmission through, and reflection from the metamaterial I set up two guided microwave circuits: one circuit for transmission and the other for reflection. The equipment I used to set up these circuits is as follows,

a- Function Generator

The first element in the circuit is the function generator I used a Stanford Research Systems DS335 Function Generator to generate a sinusoidal reference for the phase sensitive detector and microwaves generator. Its specifications are,

Frequency Range for Sine-Wave: 3.1 MHz max. frequency with resolution 1 μHz.

Output: 50 Ω source impedance.

Amplitude: 50 mVpp to 10 Vpp (50 Ω) with accuracy 0.1 dB (sine output).

I set-up the function generator at 100 Hz and 2 Vpp through the whole measurements.

b- Microwave Generator

In order to generate microwaves, I used an hp 8620C Sweep Oscillator accompanied with a hp 86260A RF Plug In with Frequency range 12.4 to 18 GHz calibrated, 12 to 18 GHz usable.

c- Microwave Attenuator

I used PRD 158A attenuator to control the microwave power incident on the sample.

d- Waveguide

I used a rectangular waveguide with inner dimensions 16 x 8 mm.

e- Microwave Absorber

To absorb the microwaves at the terminal end of the waveguide I used a Microwave Associates 153-142-001 Absorber.

f- Micro-Voltmeters**.**

I used 3 different micro-voltmeters in my circuit.

(i) Kethley 199 DMM/Scanner with specifications

Range	Resolution	Input Resistance
300 mV	1 μV	>1GΩ
3 V	10 μV	>1GΩ
30 V	100 μV	11MΩ
300 V	1 mV	10MΩ

(ii) Kethley 197A Autoranging Microvolt DMM with specifications

Range	Resolution	Input Resistance
200 mV	1 μV	>1GΩ

2 V	10 μV	>1GΩ
20 V	100 μV	11MΩ
200 V	1 mV	10MΩ

(iii) Kethley 2000 Multimeter with specifications

Range	Resolution	Input Resistance
100 mV	0.1 μV	>10GΩ
1V	1 μV	>10GΩ
10 V	10 μV	>10GΩ
100 V	100 μV	10MΩ

g- Lock-in Amplifier

I used two different lock-in amplifiers to measure the transmitted/reflected signal produced by the microwave detector.

(i)-EG&G Princeton Applied Research PAR Lock-in Amplifier

Model 5104 with specifications

Sensitivity	100 μV- 3V
Frequency Range	5 Hz -20 kHz
Max. Input Voltage	±200V dc

(ii)- Princeton Applied Research PAR Precision Lock-in Amplifier Model HR-8 with specifications

Sensitivity	100 nV- 500 mV
Frequency Range	1.5 Hz -150 kHz

h- Microwave Detectors

I used two different detectors:

a HP Crystal Detector P424A and a Wave-Line type 714

i- Water cooled electromagnet

In order to produce the static magnetic field, I used a water cooled Varian V-HF 3401 electromagnet with VFR 2601 MK II Fieldial power supply. The DC electromagnet has a magnetic field range from 0 to 13 kOe.

To measure the magnetic field I used an F.W. Bell 9550 gaussmeter which had a hall probe placed between the magnetic poles and close to the sample.

3.4 Transmission and Reflection Circuits

To explain how I constructed the Transmission/Reflection Circuit (Fig. 3.4.1 and Fig.3.4.2), I number the instruments shown in Fig. 3.4.1 and Fig. 3.4.2 as follows:

1-Function generator (Stanford Research Systems DS335 Function Generator)

2-Microwave generator (hp 8620C Sweep Oscillator)

3-Microwave attenuator (PRD 158A)

4-Microwave absorber (Microwave Associates 153-142-001 Absorber)

5-Lock-in amplifier (PAR Precision Model HR-8)

6-Micro-voltmeter (Kethley 197A Autoranging Microvolt DMM)

7-Micro-voltmeter (Kethley 2000 Multimeter)

8-Micro-voltmeter (Kethley 199 DMM/Scanner)

9-Lock-in amplifier (PAR Model 5104)

10-Microwave detectors (HP Crystal Detector P424A)

11-Microwave detectors (Wave-Line type 714)

12- Ferrite –Wire array sample

13- Supporting ferrite material to homogenize the magnetic field.

14- Electromagnet poles

15- Gaussmeter F.W. Bell 9550

16- Micro computer (PC)

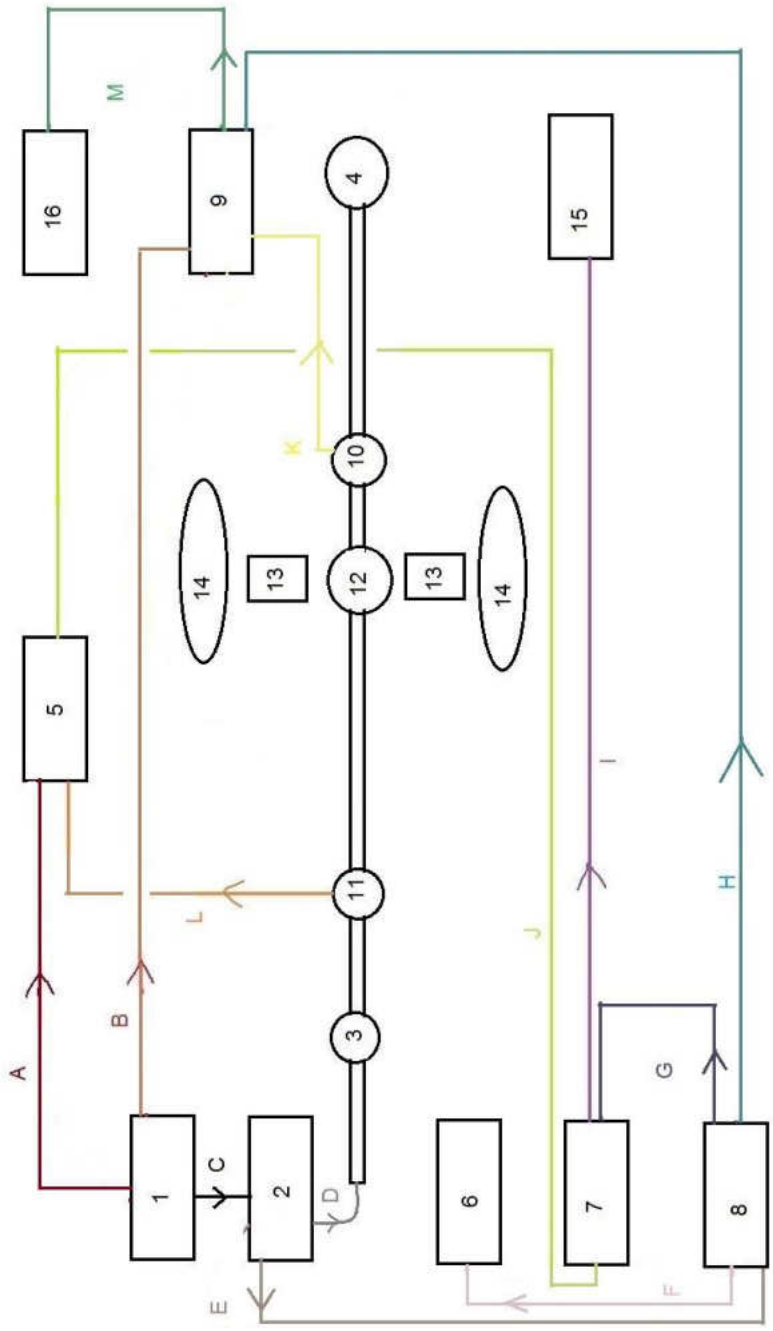

Fig.3.4.1 Transmission measurement circuit

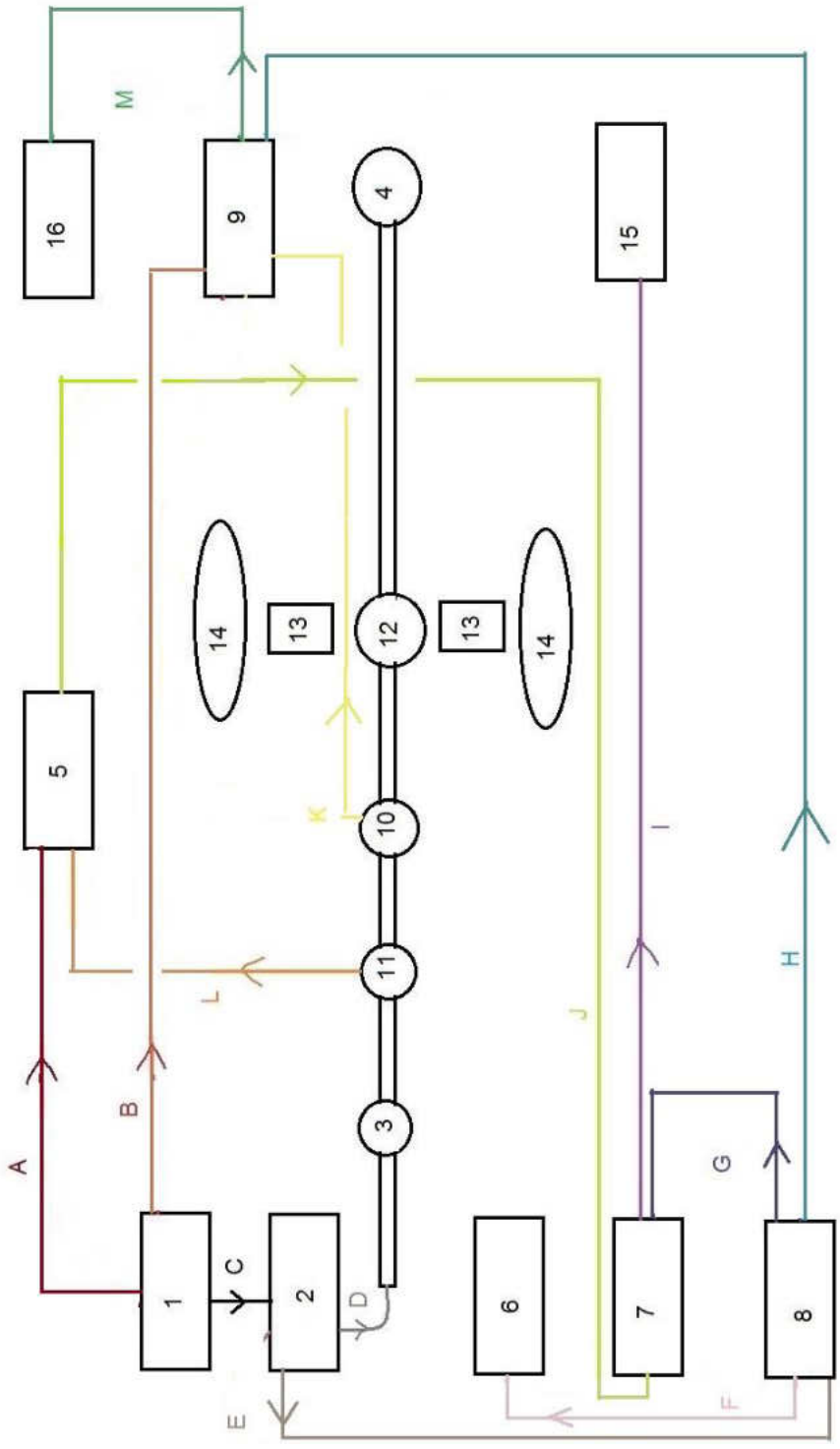

Fig.3.4.2 Reflection measurement circuit

The colored lines A, B, C, D, E, F, G, H, I, J, K, L and M are the connections between the different instruments. These are:

Line A: The function generator (#1) generates a $2V_{pp}$, 100 Hz sinusoidal voltage and sends it through line A to the lock-in amplifier (#5) to function it as a reference.

Line B: The function generator (#1) sends the reference through line B to the lock-in amplifier (#9) as TTL square wave synchronized to the main function output.

Line C: The function generator (#1) sends the sinusoidal signal to the microwave generator (#2) to modulate the microwave power.

Line D: The microwave generator (#2) generates microwaves with frequency 12-18 GHz and sends through line D to the waveguide.

Line E: The microwave generator (#2) connected to micro-voltmeter (#8) to enable (#8) to read the microwave frequency.

Line F: Micro-voltmeters (#8) connected to micro-voltmeter (#6) to enable (#6) to read the microwave frequency and provide a visual display to the operator.

Line G: An IEEE488 cable connects micro-voltmeter (#8) with micro-voltmeters (#7) to enable the PC (#16) to record the data from (#7) and (#15).

Line H: An IEEE488 cable connects micro-voltmeter (#8) to lock-in amplifier (#9) to enable the PC (#16) to record the data from (#7) and (#15) and (#8).

Line I: An IEEE488 cable connects Micro-Voltmeters (#7) to Gaussmeter (#15) to enable the PC (#16) to record the data from (#15).

Line J: This connection allowing the micro-voltmeters (#7) to display and then record the power generated by the sweep oscillator (#2), detected by detector (#11) and measured by the lock-in amplifier (#5) and recorded as the reference level.

Line K: This connection is between the microwave detector (#10) which detects the transmission/reflection signal and the lock-in amplifier (#9) to allow (#9) to display and record the transmission/reflection signal.

Line L: This connection is between microwave detector (#11) which detects the reference power level and the lock-in amplifier (#5) to allow (#5) to display the reference power level then pass it to (#7) through Line J.

Line M: This connection is between the lock-in amplifier (#9) and the PC which allows the PC to record all of the data (reference power level through lines L-J-G-H-M, transmission/reflection signal through lines K-M, microwave frequency through lines E-H-M and magnetic field strength through lines I-G-H-M).

The purpose of using microwave attenuator (#3) is to limit the microwave power level that enables the diodes to operate in the linear region and it absorbs the reflection from the sample. The microwave absorber (#4) absorbs any transmission so that no power is reflected back to the sample.

To solve the problem of the magnetic field inhomogeneity at the edge of the sample due to the demagnetizing field experienced near the sample edges, I placed two ferrite blocks similar to the sample material outside of the waveguide and between the ferrite –wire array sample (#12) [which was placed inside the waveguide] and the electromagnet poles (#14).

3.5 Ferromagnetic Resonance Circuit

To explain how I constructed the ferromagnetic resonance circuit (Fig. 3.5.1), I number the instruments which are shown in Fig.3.5.1 as follows:

1- Function generator (Stanford Research Systems DS335 Function Generator).

2- AC Transformer.

3- Electromagnet.

4- Oscilloscope Gold Star 9020G.

5- Lock-in amplifier (PAR Precision Model HR-8).

6- Lock-in amplifier (PAR Model 5104).

7- Lock-in amplifier (PAR 129A).

8- Voltage amplifier.

9- Power supply PASCO 8013.

10- Microwave generator (hp 8620C Sweep Oscillator).

11- Microwave resonant cavity.

12- Microwave detector (HP Crystal Detector P424A).

13- Micro computer (PC).

14- Gaussmeter F.W. Bell 9550.

The lines A, B, C, D, E, F, G, H, I, J, K, L, M, N, O are the connections between the different instruments. These are:

Line A: The function generator (#1) generates an oscillating voltage at 11 Hz with amplitude V_{OSC} and sends it to an AC step-down transformer (#2).

Line B: The AC step-down transformer (#2) sends an oscillating voltage at 11 Hz to the Oscilloscope (#4) for monitoring purpose.

Line C: The Oscilloscope (#4) generates an oscillating voltage at 8 kHz and sends it to lock-in amplifier (#7).

Line D: The lock-in amplifier (#7) sends a DC voltage with amplitude V_C to the Voltage amplifier.

Line E: The oscilloscope (#4) sends a voltage 11 Hz with amplitude V_{OSC} to the Voltage amplifier.

Line F: The AC step-down transformer (#2) sends a low-voltage/high-current 11 Hz signal to the electromagnet to generate AC-magnetic field at the position of the sample.

Line G: The function generator (#1) sends the signal V_{OSC} 11 Hz to the lock-in amplifier (#5) to read as a reference.

Line H: The power supply (#9) supplies the voltage amplifier with power to amplify the sum of the voltages coming from line E and line D.

Line I: The voltage amplifier (#8) sends a signal with amplitude V_{fm} to the microwave generator (#10). This signal is used to modulate the frequency of the microwaves.

Line J: The microwave generator (#10) generates microwaves and sends them to the microwave resonant cavity (#11) through the waveguide.

Line K: The microwave detector (#12) detects the reflected off the microwave resonant cavity (#11).

Line L: The microwave generator (#10) sends the reference frequency to PC (#13) to record it.

Line M: The microwave detector (#12) detects the signal reflected off the resonant cavity and sends a voltage to the lock-in amplifier (#6). The output represents the derivative with respect to magnetic field off the power absorbed by the sample.

Line N: Lock-in amplifier (#6) sends data to the PC (#13) to allow the PC to record it.

Line O: The Gaussmeter (#14) sends data to the PC (#13) to allow the PC to record it.

Line P: The microwave detector (#12) detects the signal reflected off the resonant cavity and sends a voltage to the lock-in amplifier (#7). This voltage has an AC component of amplitude V_D at 8 kHz.

Line Q: The micro computer (#13) records the reference power level has been measured by the lock-in amplifier (#5).

To explain how my FMR circuit works, I have to discuss first one of the major difficulties in the FMR experiment. During the FMR measurements, the RF frequency should be remain locked to the resonant frequency of the microwave cavity. As the magnetic permeability of the ferromagnetic sample changes with the imposed magnetic field (see section 2.1), the sample impedance, which is a function of the magnetic permeability, changes and the cavity resonance frequency changes with the sample

impedance. Due to that, we have to change the microwave frequency to stay locked to the cavity resonant frequency. This was accomplished with a locking circuit as follows:

1- The Oscilloscope (#4) sends an 8 kHz with amplitude V_{OSC} to the voltage amplifier.
2- The lock-in amplifier (#7) sends a DC voltage with amplitude V_C to the voltage amplifier.
3- The voltage amplifier (#8) sends a signal with amplitude V_{fm} to the microwave generator (#10), $V_{fm} = 10\ V_C + V_{OSC}$.
4- If the cavity resonance frequency increases, V_D and V_{OSC} are in-phase so the lock-in amplifier (#7) increases V_C and consequently V_{fm} is increased, the increasing the V_{fm} increases the microwave frequency generated by the microwave generator (#10) to maintain the frequency locked to the cavity. The gain of the amplifier chain was approximately 10^5, with 1 volt output corresponding to a 25 MHz shift of the microwave frequency.
5- If the cavity resonance frequency decreased, V_D and V_{OSC} are out of-phase, the lock-in amplifier (#7) will decrease V_C , and consequently V_{fm} is decreased. The decreased V_{fm} decreases the microwave frequency generated by the microwave generator (#10) to maintain the frequency again locked to the microwaves cavity's frequency.

To ensure the validity of the FMR measurement, I required the maximum voltage reflected from the microwave cavity, which signified the maximum resonant absorption occur within 50 Oe of static magnetic field for the "zero" recorded by

the lock- in – amplifier (#6). This latter measurement represented the derivative of the power reflected from the microwave cavity with respect to magnetic field. In this manner I was able to reject any measurements for which the microwave power generated by the microwave source changed with frequency as the locking circuitry followed the resonant frequency of the cavity.

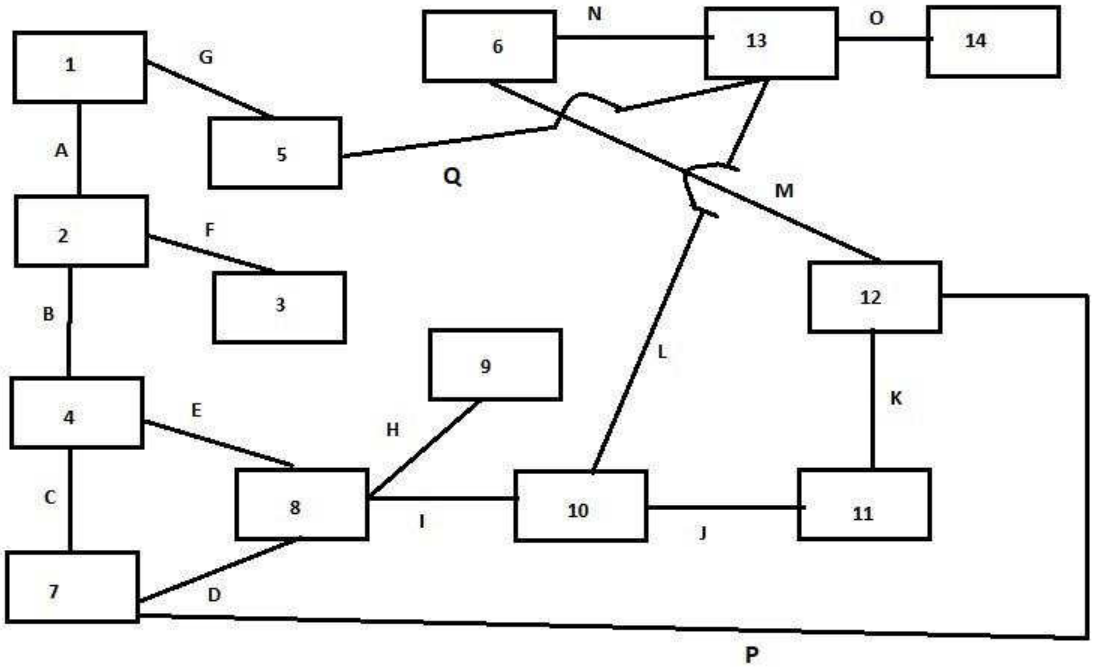

Fig.3.4.2 Ferromagnetic resonance circuit

CHAPTER IV
RESULTS

4.1 Electric Permittivity of the Ferrite

I did not sinter the ferrite material at 1200 °C as described in the article I used to prepare the ferrite sample [13]. The value of ϵ listed in the specification sheet accompanying the ferrite powder I bought was not likely to be the same as that of the partially sintered ferrite I used. Thus, I had to measure the electric permittivity of the partially sintered ferrite.

The electric permittivity depends on frequency and the only available tool I had to measure ϵ was a capacitance bridge. I measured ϵ through the capacitance bridge through the available frequency range of 10 kHz -1010 kHz. Since ϵ generally decreases with frequency, the ϵ I measured over the frequency range represents an upper limit to ϵ at the microwave frequencies of interest. Also, I wanted to compare its value at 1.0 MHz to the value listed on the specification sheet to know how the reduction in the sintering temperature affected its dielectric property.

I used one of the supporting ferrite blocks to measure ϵ. The dimensions of this block were 25 x 30 x 18 $(mm)^3$ and I connected it to the capacitance bridge terminals through copper plates with the same area as the block's biggest face

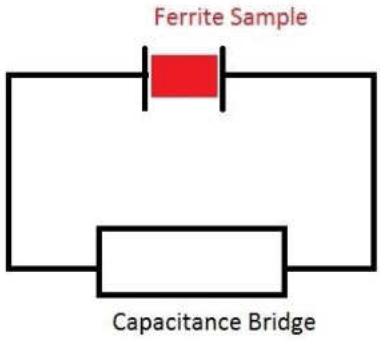

Fig. 4.1.1 The capacitance bridge circuit used to measure ϵ of the ferrite sample shown in the figure above.

I made capacitance measurements over the frequency range from 10 kHz to 1.01 MHz. I found ϵ from,

$$\epsilon = \frac{h\,C}{A}\ , \qquad (4.1.1)$$

where h is the sample thickness, A is sample area and C is sample capacitance. The table 4.1.1 displays my results.

Table 4.1.1 Capacitance measurements and results for ϵ for the ferrite sample using the capacitance bridge

Frequency (kHz)	Capacitance (pF)	ϵ/ϵ_0
10	15.20	41.20 ± 0.02
110	12.12	32.85± 0.01
210	10.67	28.92± 0.01
310	9.46	25.64± 0.02

410	7.31	19.81± 0.03
510	6.24	16.91± 0.02
610	6.70	18.15± 0.01
710	6.18	16.75± 0.02
810	5.90	15.99± 0.02
910	5.65	15.31± 0.03
1010	5.00	13.60± 0.01

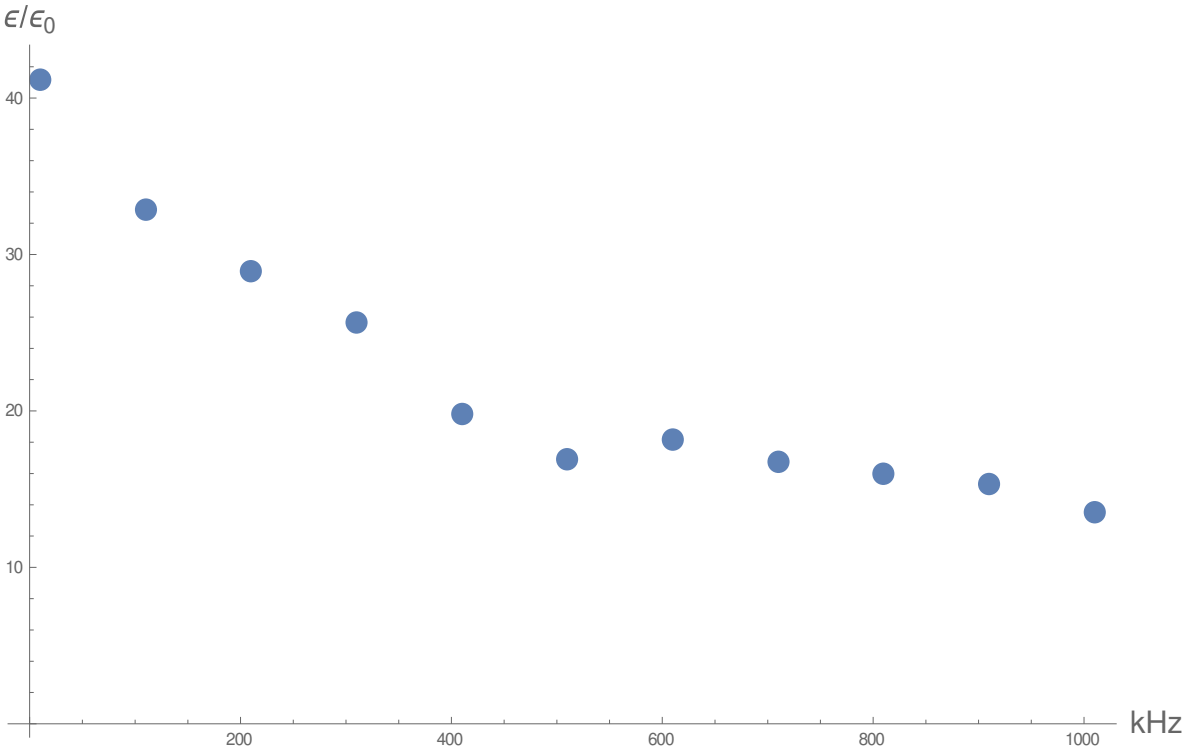

Fig. 4.1.2 Electric permittivity vs frequency for the ferrite sample using the capacitance bridge

The results show that the relative permittivity at 1.01 MHz is equal to 13.6± 0.01 which is close to the value from the specification sheet value of 12 @ 1.0 MHz . [17]

4.2 Ferromagnetic Resonance Measurements

I describe in this section the FMR results.

Because I didn't sinter the ferrite material at 1200 °C , I could not use the value for the magnetization listed on the manufacturer's specification sheet. I decided to measure the magnetization and g-factor using the ferromagnetic resonance at the ferrite material.

As stated before in section (2.1), the relation for FMR with a small cylindrically shaped rod implies that the magnetic field at resonance is,

$$H_{0/\text{resonance}} = \frac{\omega}{\mu_0 \gamma} + \left(D_{zz} - \frac{1}{2}\right) M_0. \tag{4.2.1}$$

where $H_{0/\text{resonance}}$ is the steady magnetic field applied, $M_0$is the static magnetization of the material, ω is the (angular) frequency, D_{zz} is the demagnetization factor in the direction parallel to H_0 , and the γ factor is

$$\gamma = \frac{ge}{2m_e} .$$

I calculated the demagnetization factor for a small cylindrically shape rod where the static magnetic field is parallel to the long axis and found the demagnetization factor,

$$D_{zz} = \left(\frac{\text{diameter of cylindrical sample}}{\text{length of cylindrical sample}}\right)^2 /2$$

$$= \left(\frac{0.75 \text{ mm}}{3.8 \text{ mm}}\right)^2 /2 = 0.020 . \tag{4.2.2}$$

The demagnetization factor I calculated is the demagnetization factor near the center of the cylindrically shape rod. For Eq. (4.2.2) to be consistent with the experimental results, I painted the ends of the ferrite rod with silver paint to shield the microwaves there, then

the only region exposed to the microwaves was the central section of the rod where the demagnetization factor was known.

I ran the FMR experiment to find the resonance for different frequencies and different magnetic field values. The results are listed in Table 4.2.1

Table 4.2.1 Resonance Frequency and Corresponding Magnetic Field

Frequency (GHz)	$H_{0/\text{resonance}}$ (kOe)
12.054±0.001	1.90±0.01
12.996±0.001	2.32±0.05
13.701 ±0.001	2.596±0.05
15.088±0.001	3.053±0.05
16.945 ±0.001	3.79±0.01
17.436±0.001	3.916±0.05
17.554±0.001	4.195±0.07

Using equation (4.2.1), a plot of H_0 vs ω has a slope of $\frac{1}{\mu_0\gamma}$ and the intercept is $(D_{zz} - \frac{1}{2})M_0$. The units of the magnetic field and magnetization in the Eq. (4.2.1) are A/m. I converted the magnetic field units of the data recorded in the experiment using 1 A/m = (1000/4 π) Oe. The relation between H_0 and ω is shown in Fig. 4.2.1.

The slope of the best linear fit was found to be = $\frac{1}{\mu_0\gamma}$ = $(4.5 \pm 0.1)\text{x}10^{-6}$.

The intercept of the best linear fit found to be = $(D_{zz} - \frac{1}{2})M_0 = -(1.826 \pm 0.110)\text{x}10^5$ A/m.

I found the g factor = 2.006 ± 0.049 and $M_0 = (3.804 \pm 0.228)\text{x}10^5$ A/m,

$4\pi M_0 = (4780 \pm 269)G$.

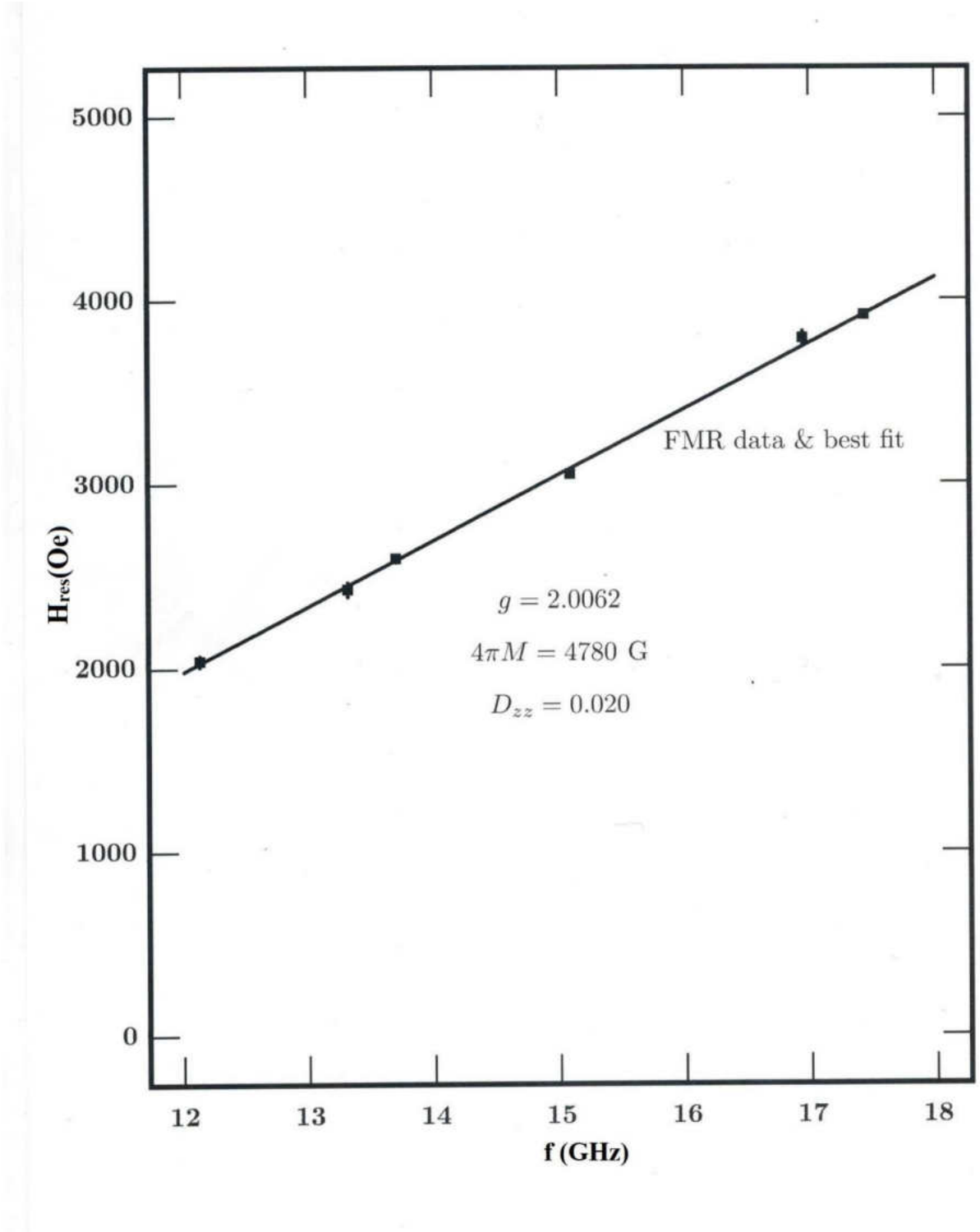

Fig. 4.2.1 Resonant magnetic field $H_{\mathrm{res}}(Oe)$ vs. frequency(GHz)

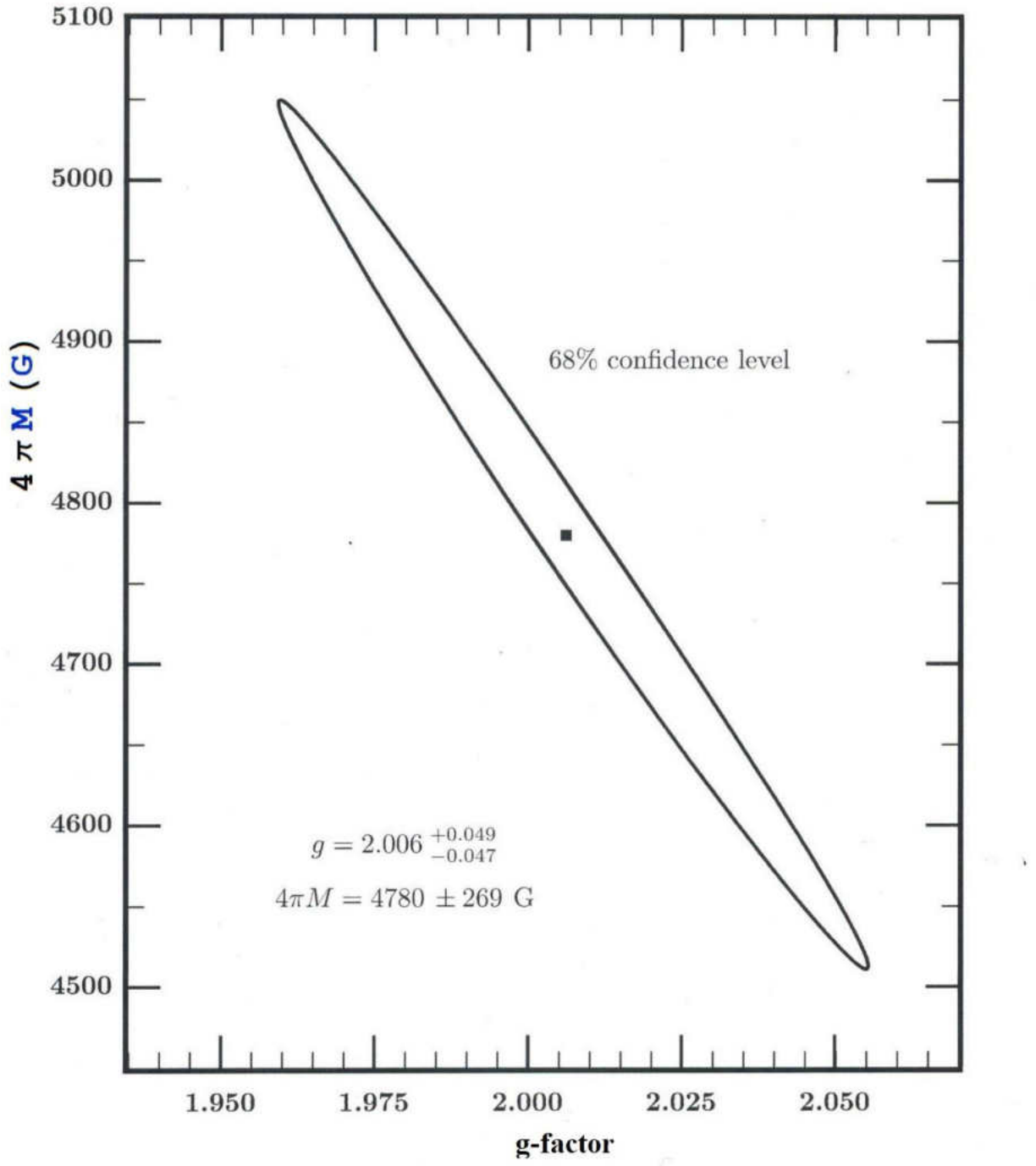

Fig. 4.2.2 *g*-Factor vs. magnetization (G)

4.3 Magnetic Field Homogenization

I noted in the apparatus chapter that I placed two ferrite blocks between the magnetic poles and the waveguide (adjacent to the wire-ferrite sample inside the waveguide) to create a homogeneous magnetic field. The two outer blocks (I call them supporting blocks) have the same transverse dimensions as the sample inside the waveguide.

In the case of the ferrite sample having no holes inside the waveguide, the magnetization inside the three blocks is depicted as Fig. 4.3.1. I used the (-) symbol to indicate a south magnetic pole and the (+) symbol to indicate a north magnetic pole.

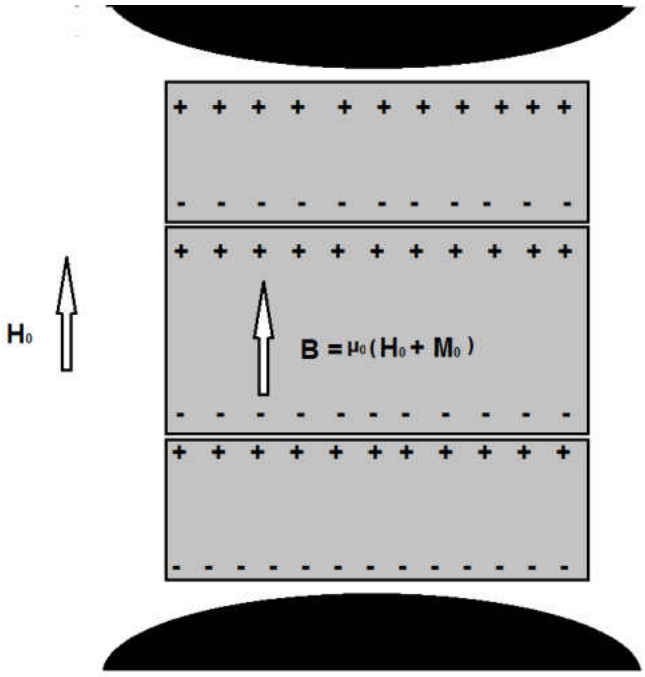

Fig. 4.3.1 Induced magnetic field inside non-holes ferrite blocks placed in uniform magnetic field.

As can be seen in the Fig. 4.3.1, the magnetic field inside the ferrite is due to magnetization plus the applied magnetic field, the edge effect at the borders between blocks is mostly canceled out by the other block; this causes the three blocks to behave like one continuous long ferrite block with a homogenous magnetic field in it. Also, the poles of the electro-magnet are not magnetically saturated and the sample supporting blocks see their "image charge" in the pole faces; they conspire to make the sample appear to be a long rod in the direction parallel to $\vec{H}_0$.

The situation for a ferrite block with holes is different; the induced magnetic field is affected by the holes in the block due to the non-symmetry between the supporting blocks and the wired block inside the waveguide. See Fig. 4.3.2.

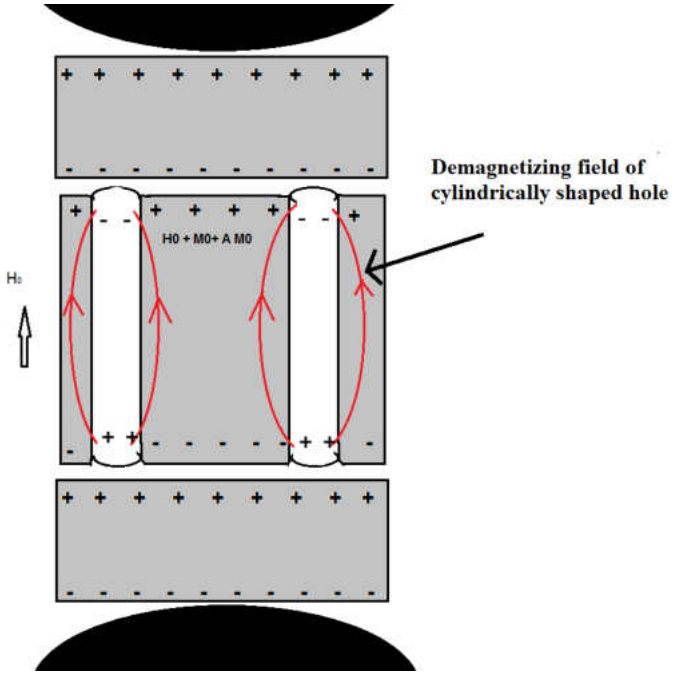

Fig. 4.3.2 Magnetic field augmentation in the ferrite sample due to drilled holes in it.

The edge effect is cancelled out at the boarders between blocks except in the area with holes. The lack of magnetic material in the holes behaves exactly as if we add a negative

magnetization in the holes (north-south poles direction in the hole opposite to the north-south poles in the ferrite).

The negative magnetization associated with the holes augments the magnetic field in the ferrite by an additional magnetic field which is represented by a negative demagnetization factor. This field is proportional to the magnetization and the ratio of the total holes' cross-section area to the total sample cross-section area. We can assume this field to be reasonably constant across the sample due to the symmetry in the holes' position.

I found the augmentation field for infinite medium to be on average

$$\text{Augmentation Field} = S\,M_0 \ , \tag{4.3.1}$$

$$S = \frac{N * \text{ Hole cross section area}}{\text{Sample cross section area}} \ , \tag{4.3.2}$$

$$N = \text{Number of holes in sample.} \tag{4.3.3}$$

the augmentation factor *S* is equal to 0.227 so the augmented magnetic field inside an infinite ferrite sample is

$$\vec{H_{\text{aug}}} = \vec{H_0} + (\vec{M_0} * \ 0.227). \tag{4.3.4}$$

Because I don't have an infinite ferrite sample, I calculated the augmented magnetic field in the midpoint of a ferrite sample with 5x9 holes array.

I used the boundary condition for the augmented induced field

$$\nabla \cdot \vec{B_{\text{aug}}} = 0 \ , \tag{4.3.5}$$

$$\vec{B_{\text{aug}}} = \vec{H_{\text{aug}}} + S_{\text{aug}} \vec{M_0}. \tag{4.3.6}$$

where S_{aug} is the augmentation factor for the finite medium. To calculate the augmented magnetic field $\vec{H_{\text{aug}}}$, I treat the hole as a dipole with magnetic charges placed at the two ends of the hole, the contribution to magnetic field of each monopole magnetic charge is,

$$\vec{H_1} = \frac{\mu_0}{4\pi} \ \frac{A\, M_0}{r^2} \ , \tag{4.3.7}$$

where *A* is the cross-section area of one hole and *r* is the radial distance from the magnetic charge $(A\, M_0)$ to the point of interest.

I calculated the field due to 5x9 holes and found the augmentation factor is, $S_{\text{aug}} = 0.163$, near the center of the ferrite slab.

Thus $$\vec{H_{\text{aug}}} = \vec{H_0} + (\vec{M_0} * 0.163). \tag{4.3.7}$$

4.4 Resonance & Anti-Resonance Frequencies

In this section I calculate the frequency of resonance and anti-resonance for different magnetic fields applied to our sample.

In section 4.2, I calculated the magnetization and g-factor for my material using the data I got from FMR experiments. Because I am interested in the range of magnetic field and

microwave frequency for which μ is negative, I determined the frequency range for negative μ. It extends from the resonance frequency to the anti-resonance frequency.

$$\frac{\mu}{\mu_0} = \left(\frac{(H+M_0)^2 - \left(\frac{\omega}{\mu 0 \gamma}\right)^2}{H(H+M_0) - \left(\frac{\omega}{\mu 0 \gamma}\right)^2} \right), \tag{4.4.1}$$

with $$H = H_0 + (M_0 * 0.163). \tag{4.4.2}$$

I used the magnetic permeability equation (4.4.1) to find the resonance frequency (where $\mu \to \infty$) and anti-resonance frequency (where $\mu = 0$) for different magnetic field values as shown in Fig 4.4.1

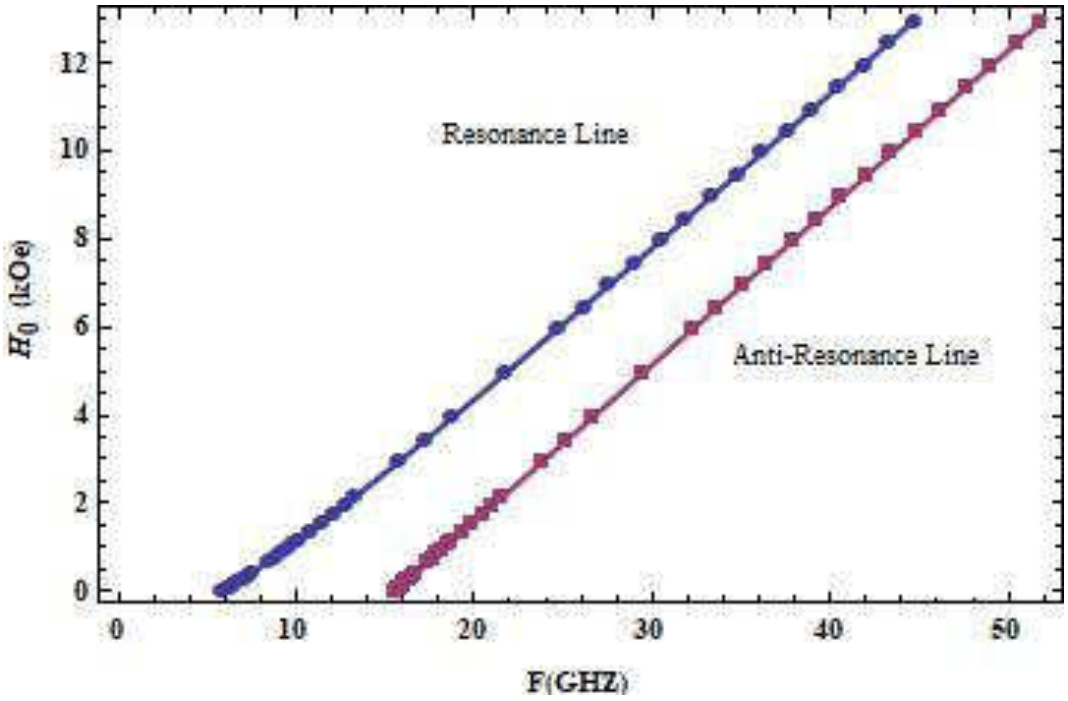

Fig 4.4.1 Resonance and anti-resonance frequency with respect to magnetic field. The region between the two lines in the figure is the region of negative .

The region between the two lines in Fig. 4.4.1 is the region of the negative magnetic permeability which can result in a negative refractive index if accompained by negative electric permittivity. The magnetic permeability is positive otherwise.

4.5 Spin Wave Manifold

According to R.W. Damon & J. R. Eshbach [14], the magnetostatic modes of a ferromagnetic slab can be divided into two branches: volume modes and surface modes. I studied these modes to evaluate what contribution these may have to my transmission measurements.

Each branch of these modes (volume or surface modes) can exist only in a specific frequency range. Following Damon & Eshbach, let me first assign the following parameters:

$$\Omega_H = \frac{H}{4\pi M_0}, \tag{4.5.1}$$

and

$$\Omega = \frac{\omega}{4\pi\gamma M_0} . \tag{4.5.2}$$

i) Volume Modes: The spin waves in the volume modes can exist in the frequency range $\Omega_H \leq \Omega \leq \sqrt{{\Omega_H}^2 + \Omega_H}$, for an infinite medium there are an infinite number of modes in this region, the density of these modes increasing as one approaches $\Omega = \sqrt{{\Omega_H}^2 + \Omega_H}$, and there is one mode

which emerges above $\Omega = \sqrt{{\Omega_H}^2 + \Omega_H}$ reaching $\Omega = \Omega_H + \frac{1}{2}$ as its highest frequency .

ii) Surface Modes: The spin waves on the surface can exist in the frequency range, $\Omega > \Omega_H + \frac{1}{2}$ and $\Omega < \Omega_H$.

I am not interested in surface spin waves because their amplitude is a maximum only at the surface of the slab and attenuates very fast toward the slab interior. These surface waves are weakly coupled to the microwaves incident on the sample.

I am interested in the volume modes, the long wave length spin waves which propagate through the body of my slab can contribute to the transmitted electromagnetic waves I measure. I calculated the frequency range for these spin waves with different magnetic fields values as shown in Fig. 4.5.1. (I calculated the frequency corresponding to $\Omega = \Omega_H$ and called it lower frequency, the frequency corresponding to $\Omega = \sqrt{{\Omega_H}^2 + \Omega_H}$ and called it higher frequency and the frequency corresponding to $\Omega = \Omega_H + \frac{1}{2}$ and called it up limit frequency).

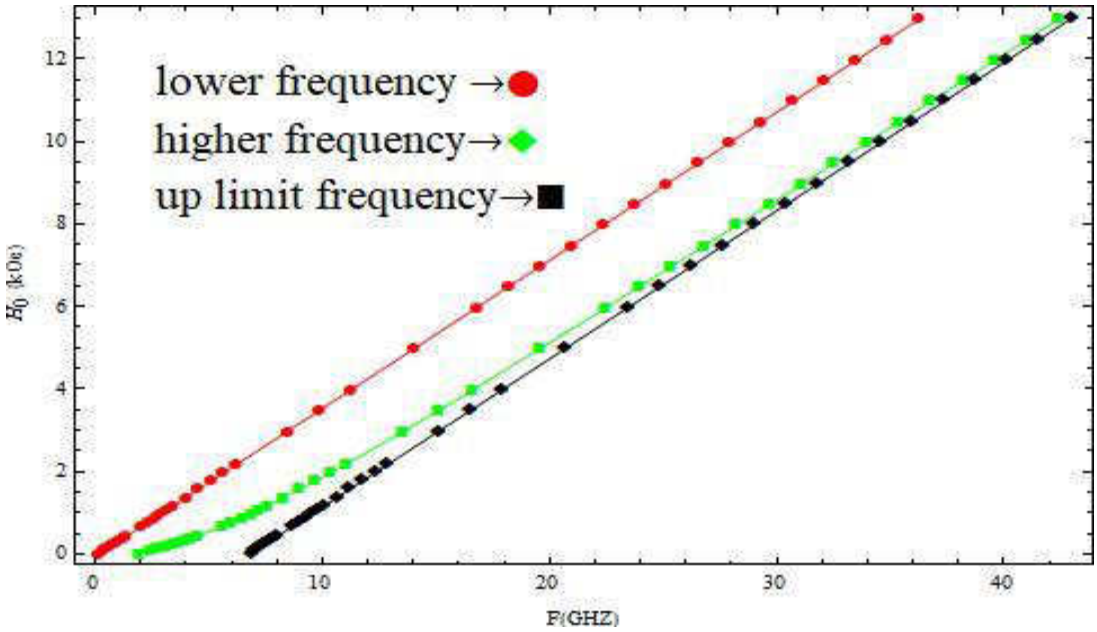

Fig. 4.5.1 Spin-wave frequency range for different magnetic fields. The three lines represent the limits for spin-wave propagation. They can propagate only between the highest and lowest limit lines shown.

4.6 Negative Permeability Range and Spin Wave Manifold Range Comparison

I calculated the negative magnetic permeability range, which extends from the resonance to the anti-resonance frequency, in section (4.4). I also calculated the frequency range over which the spin waves (volume modes) can exist and propagate in section (4.5).

In this section, I compare the intersection between these two regions in the microwave spectrum.

Fig.4.6.1 shows five lines. These represents:

1- Lowest frequency limit for which spin waves can propagate (I marked it in the graph with number "1").

2- Higher frequency for which most of the spin waves can propagate (I marked it in the graph with number "2").
3- The highest frequency limit for which no spin waves can propagate beyond this frequency limit (I marked it in the graph with number "3").
4- Resonance frequency (I marked it in the graph with number "4").
5- Anti-resonance frequency (I marked it in the graph with number "5").

As I noted in section (4.4), the existence of a negative refractive index must be in the same frequency range as that of negative magnetic permeability (the frequency above resonance and below anti-resonance). The region of negative magnetic permeability (region between line "4" and line "5") has no overlap with the spin waves frequency range (region between line "1" and line "3"). This means for any transmission modes observed in the negative magnetic permeability range cannot be spin wave volume modes but must be electromagnetic modes.

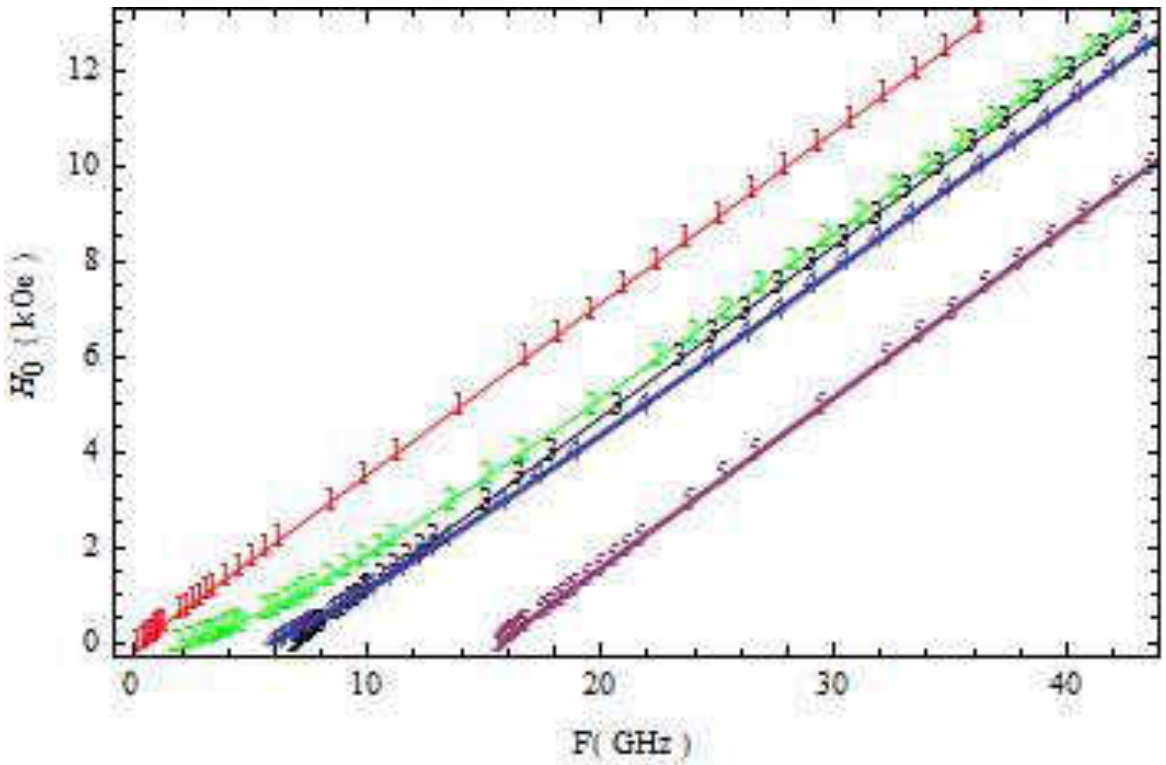

Fig. 4.6.1 Spin-wave frequency range and negative permeability frequency range for different magnetic fields

4.7 Transmission, Reflection, and Absorption Measurements

To search for evidence for the existence of negative refractive index in my ferrite sample at specific values of frequency and magnetic field, I made 39 measurements for the transmission through, and reflection from, the sample and then calculated the absorption which occurred.

Before I measured the transmission /reflection for the sample, I measured the transmission for an open waveguide (100% transmission) and reflection off an aluminum foil (100% reflection).

The treatment of the data was as follows,

1- Divide the signal diode data by the power level registered by the reference diode using a computer code.
2- Interpolate the ratio data to equally spaced (0.005 GHz) over the frequency range 12-18 GHz using computer code.
3- Divide the interpolated signal to reference ratio for the case of the sample in the waveguide by the signal to reference ratio of the case of (100% transmission) or (100% reflection).
4- I used data from 3rd point to plot transmission through and reflection off the sample.
5- I calculated the absorption data by subtracting the sum of transmission and reflection data from unity.

I calculated the resonance and anti-resonance frequency for the different value of the magnetic field H, ($H = H_0 + M_0 * 0.163$) . I did that to indicate the frequency range over which the permeability was negative.

I showed in section (4.6) that there was no overlap between spin waves (volume modes) and electromagnetic modes in the negative permeability frequency range.

I display in the next few pages the transmission, reflection and absorption measurements (percentage transmitted and reflected wave compared to reference power). Gaps in the data near 16 GHz are due to nulls in the diode detector's response. I also note the resonance and anti-resonance frequency.

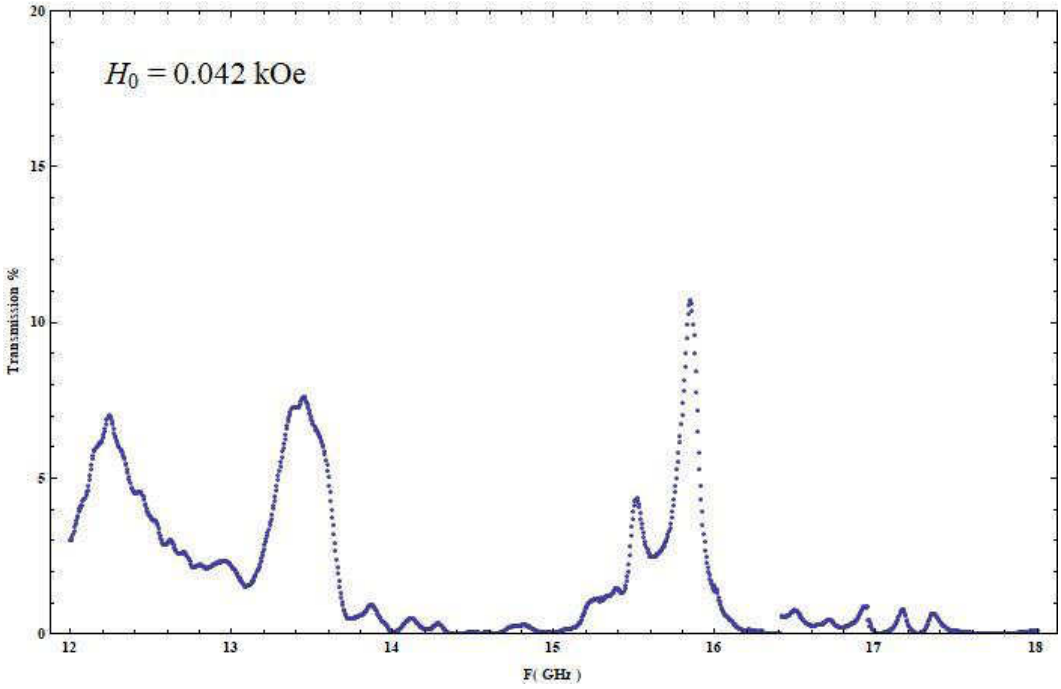

Fig. 4.7.1 Transmission vs. Frequency for $H_0 = 0.042$ kOe

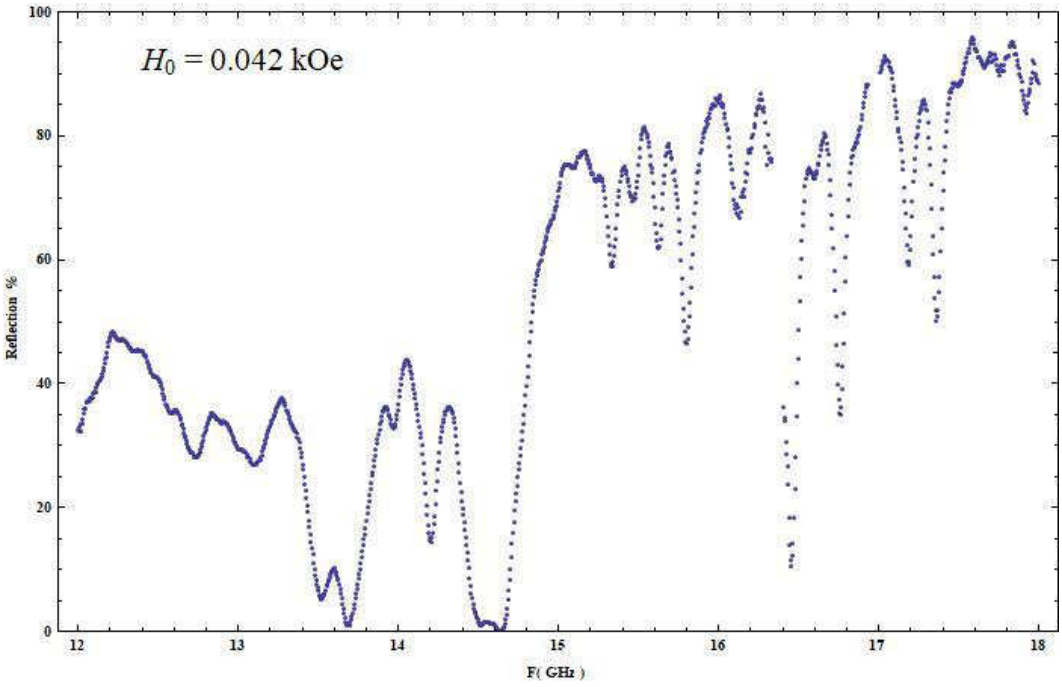

Fig. 4.7.2 Reflection vs. Frequency for $H_0 = 0.042$ kOe

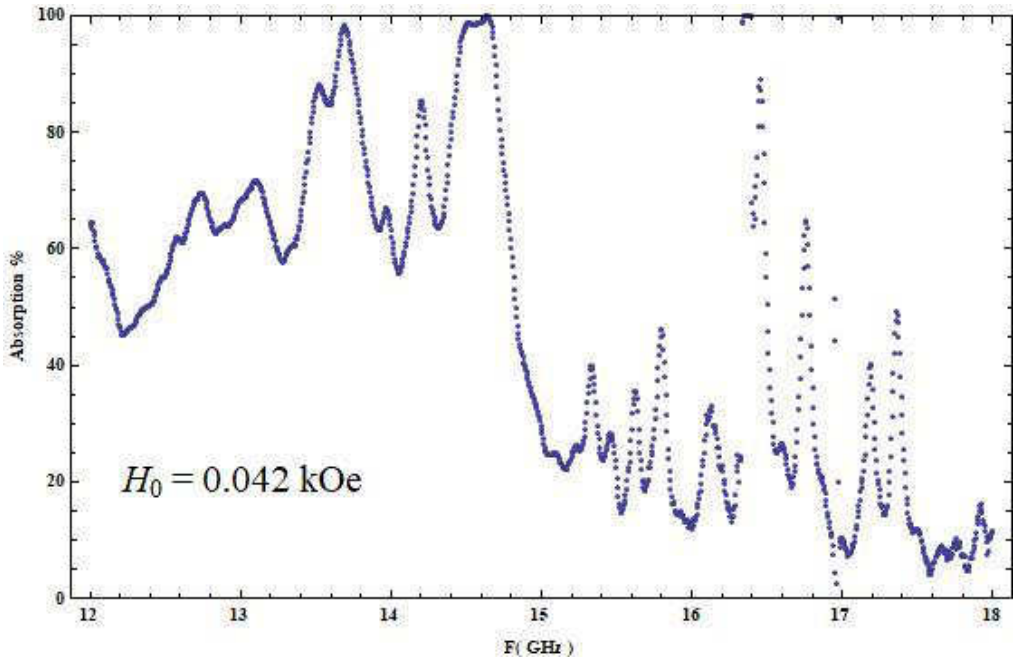

Fig. 4.7.3 Absorption vs. Frequency for $H_0 = 0.042$ kOe

Resonance-Anti-Resonance Frequency: 6.01→15.69 GHz

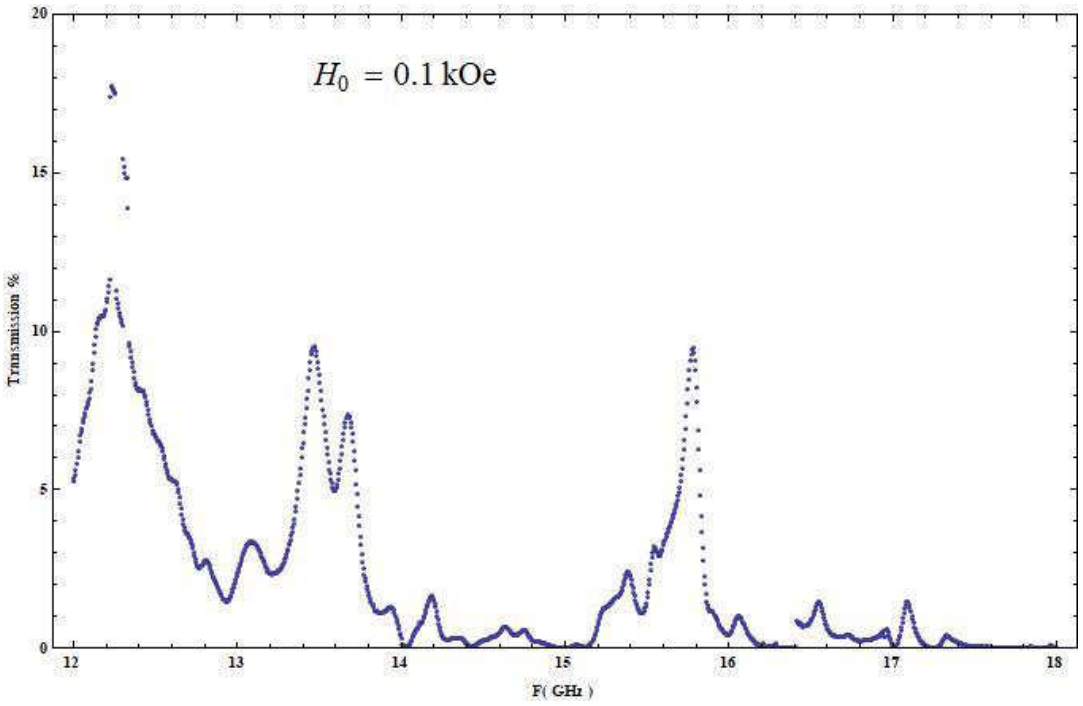

Fig. 4.7.4 Transmission vs. Frequency for $H_0 = 0.1$ kOe

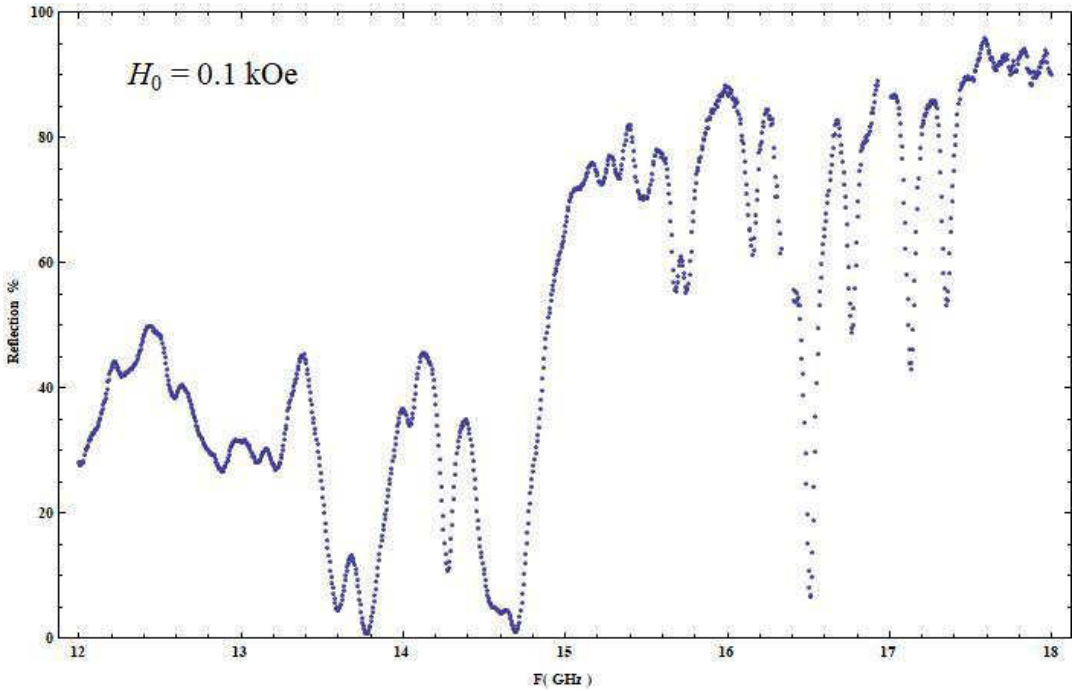

Fig. 4.7.5 Reflection vs. Frequency for $H_0 = 0.1$ kOe

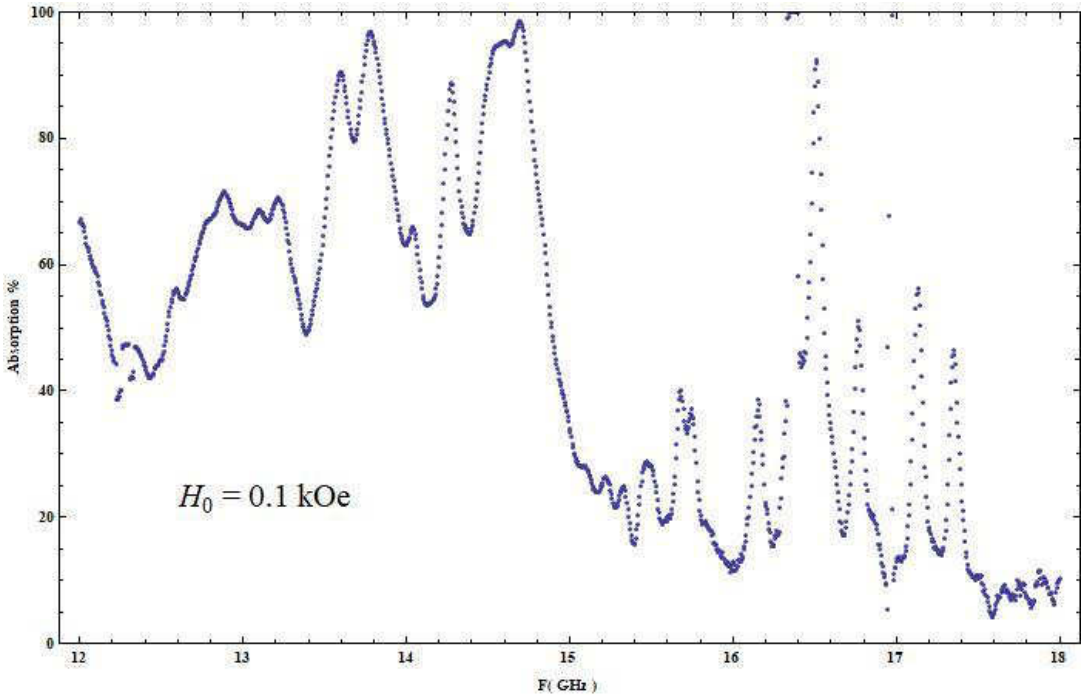

Fig. 4.7.6 Absorption vs. Frequency for $H_0 = 0.1$ kOe

Resonance-Anti-Resonance Frequency: 6.25→15.85 GHz

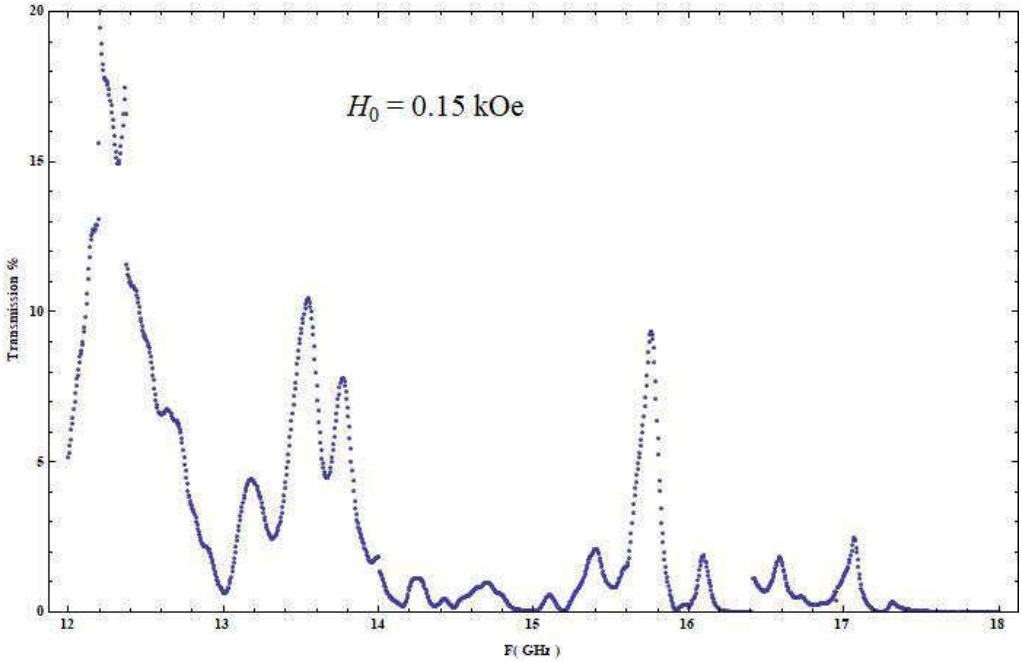

Fig. 4.7.7 Transmission vs. Frequency for $H_0 = 0.15$ kOe

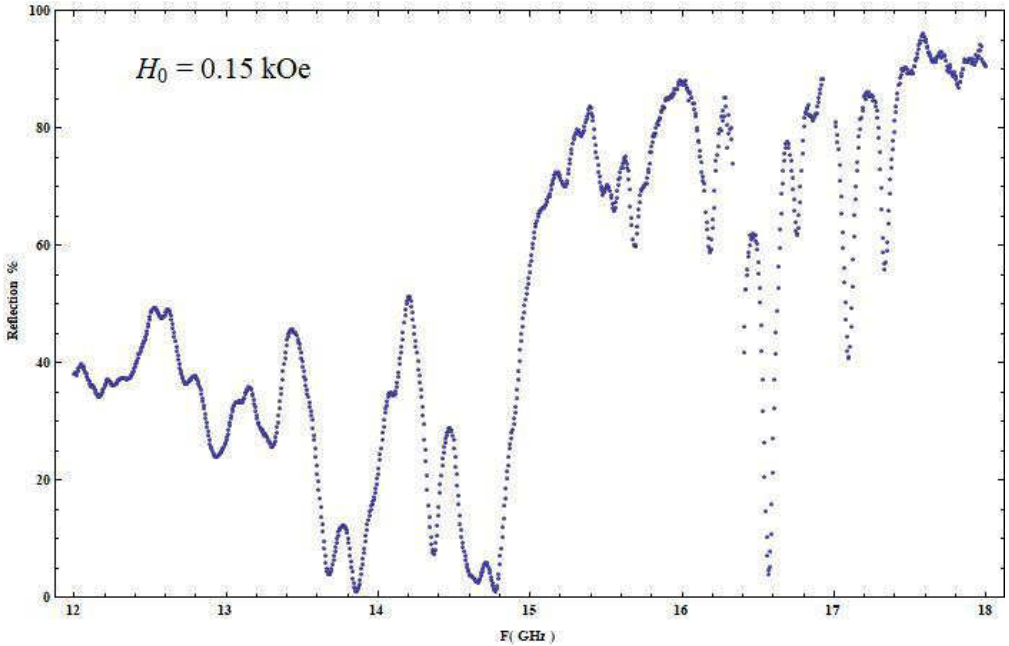

Fig. 4.7.8 Reflection vs. Frequency for $H_0 = 0.15$ kOe

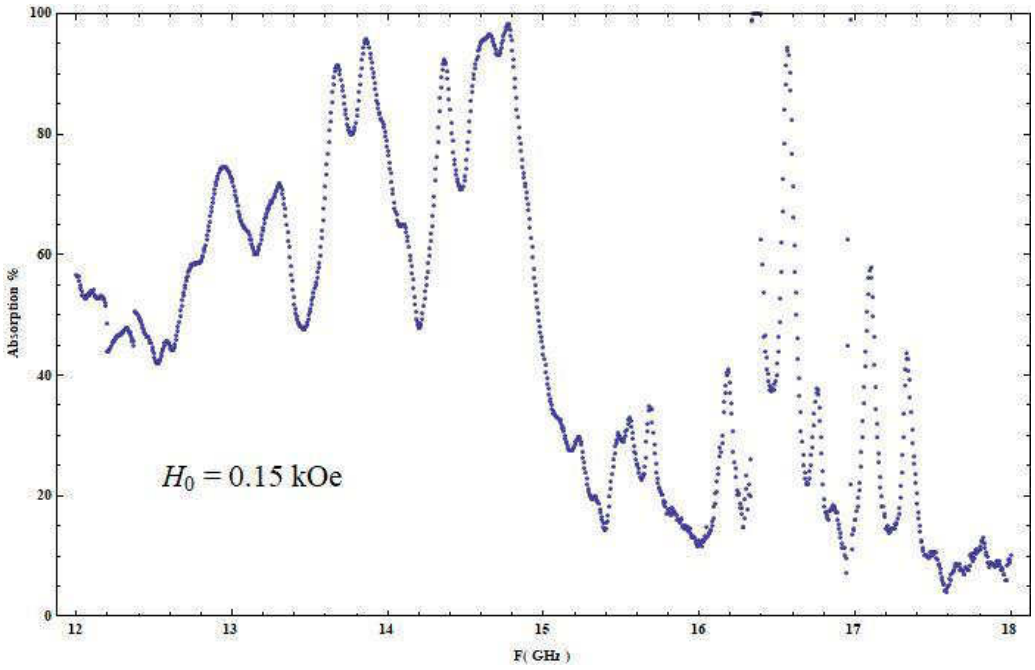

Fig. 4.7.9 Absorption vs. Frequency for $H_0 = 0.15$ kOe

Resonance-Anti-Resonance Frequency: 6.45→16.00 GHz

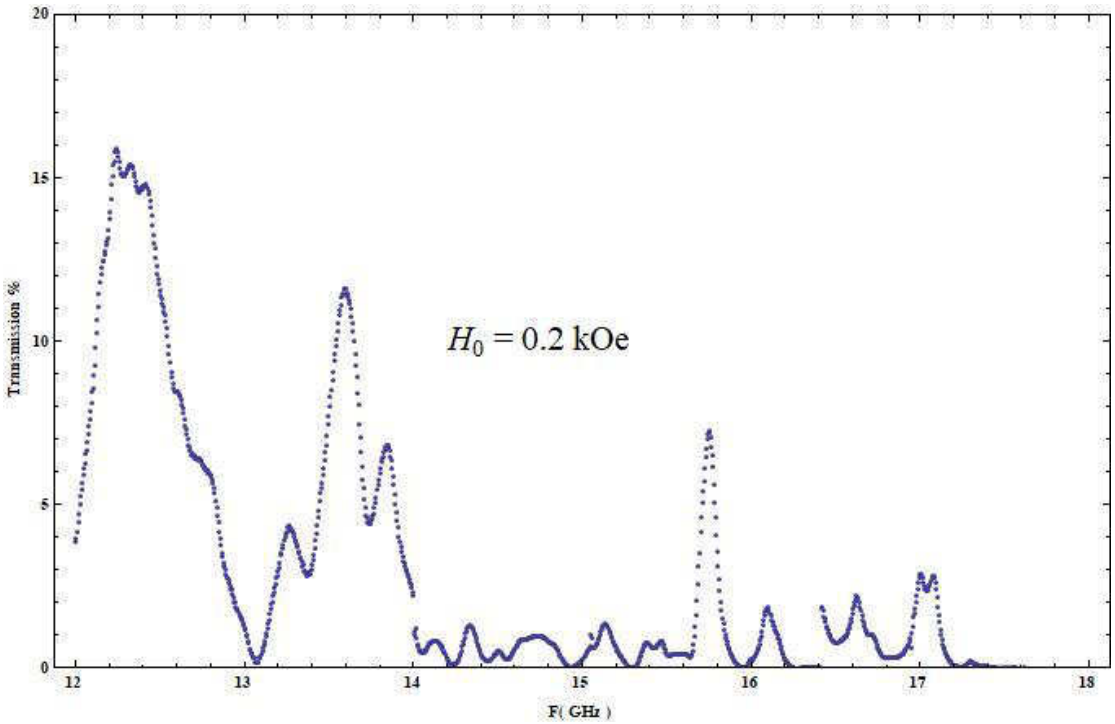

Fig. 4.7.10 Transmission vs. Frequency for $H_0 = 0.2$ kOe

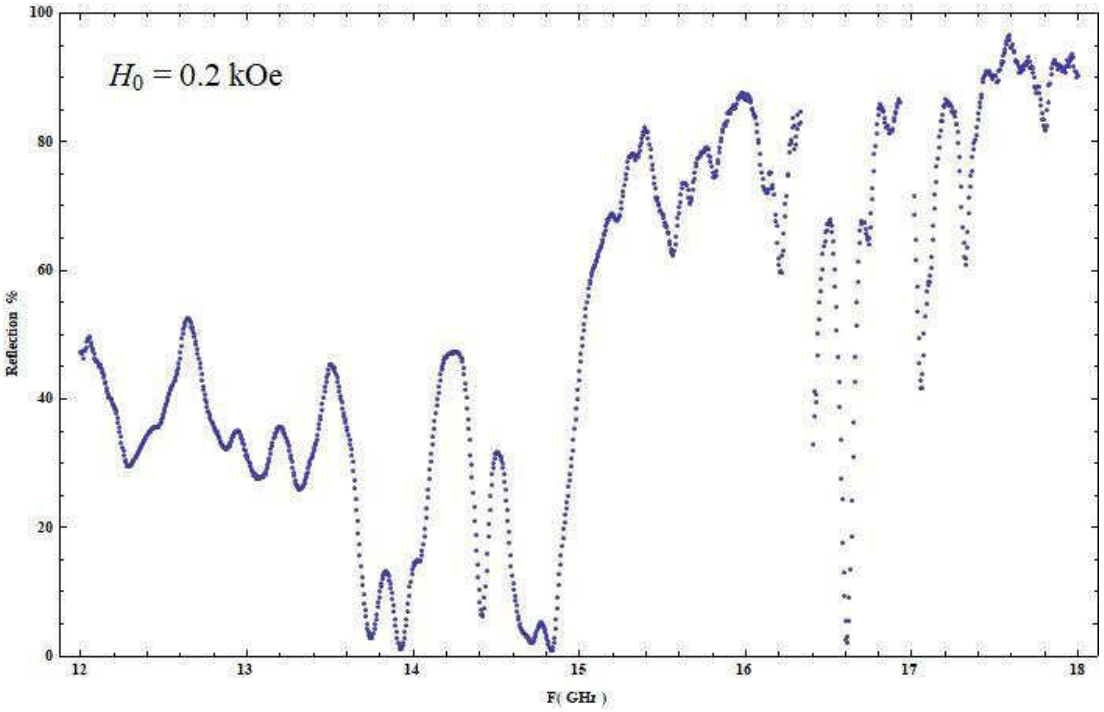

Fig. 4.7.11 Reflection vs. Frequency for $H_0 = 0.2$ kOe

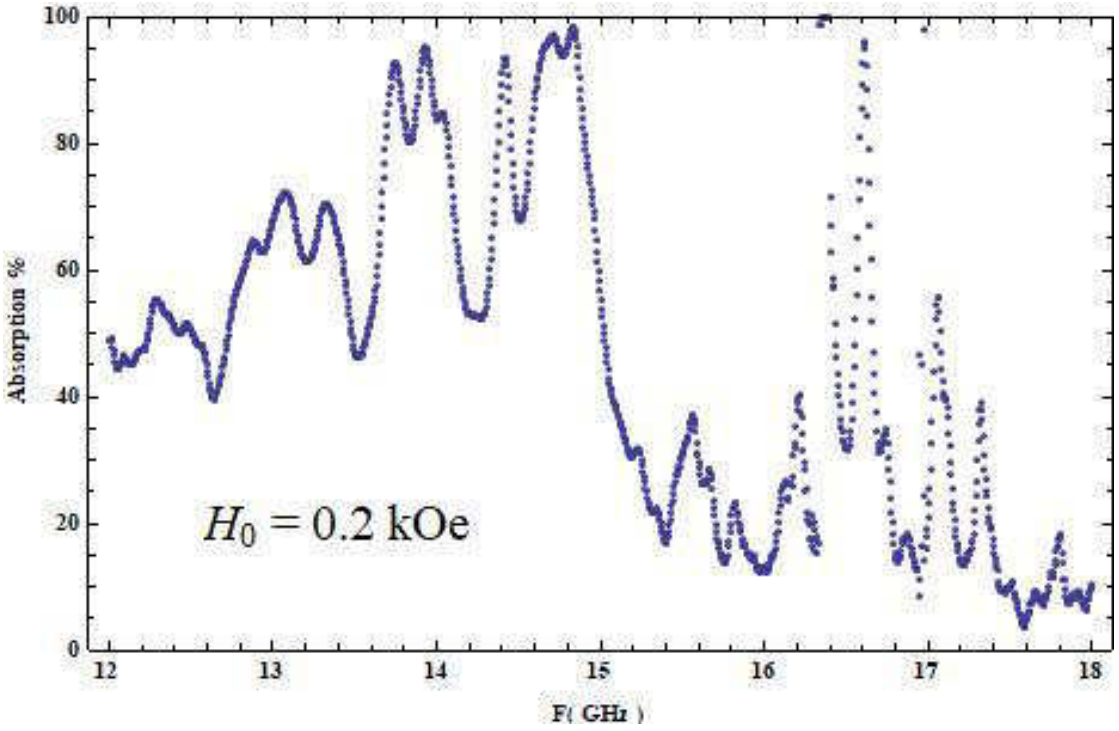

Fig. 4.7.12 Absorption vs. Frequency for $H_0 = 0.2$ kOe

Resonance-Anti-Resonance Frequency: 6.65→16.13 GHz

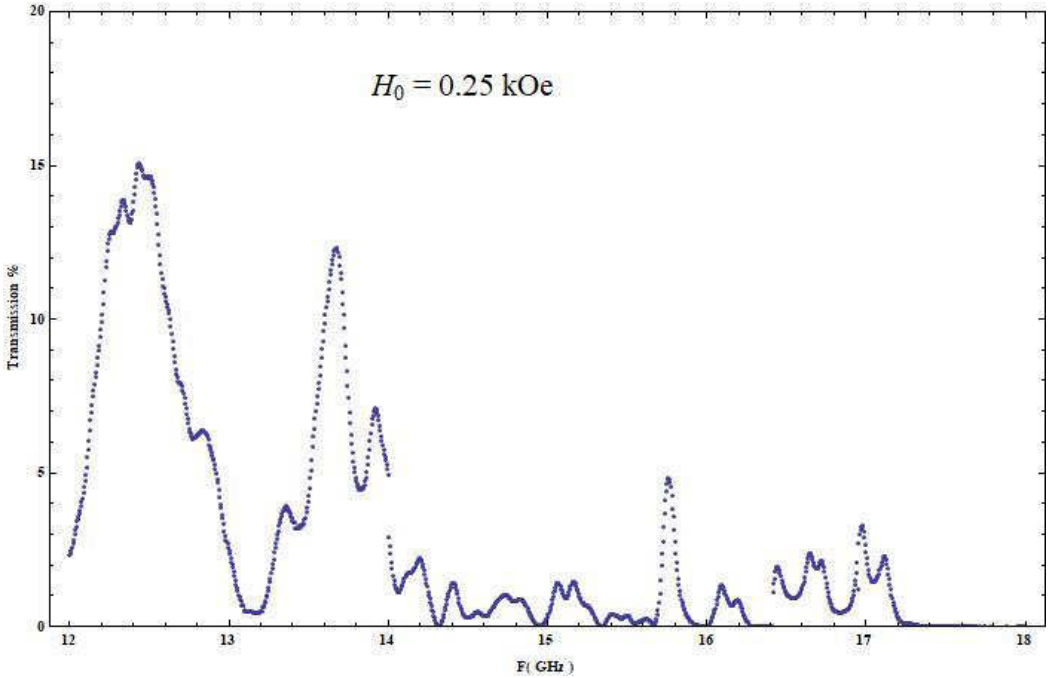

Fig. 4.7.13 Transmission vs. Frequency for $H_0 = 0.25$ kOe

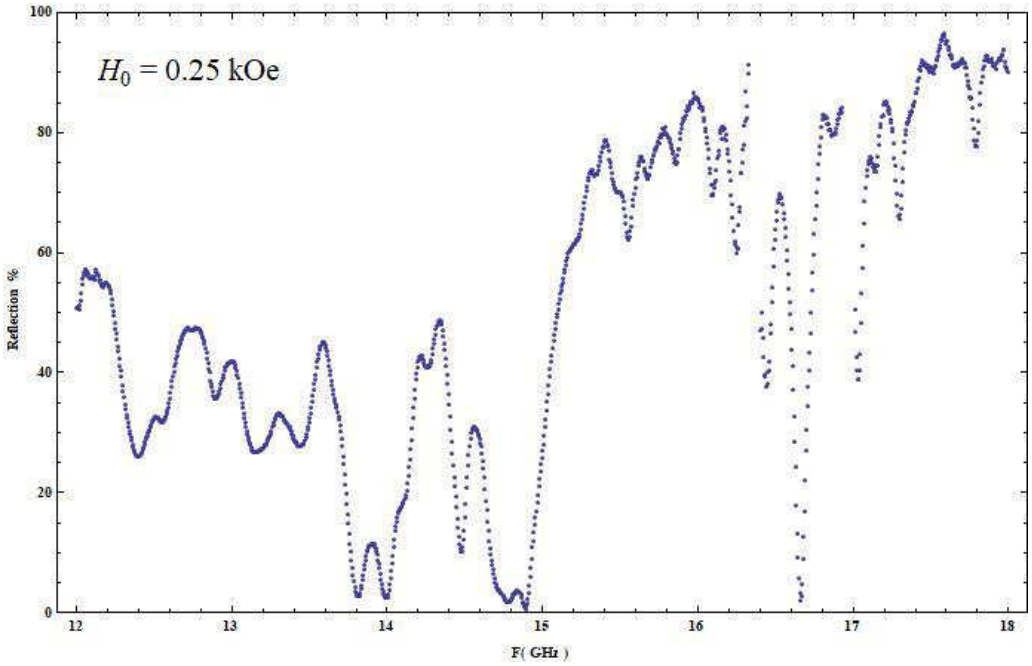

Fig. 4.7.14 Reflection vs. Frequency for $H_0 = 0.25$ kOe

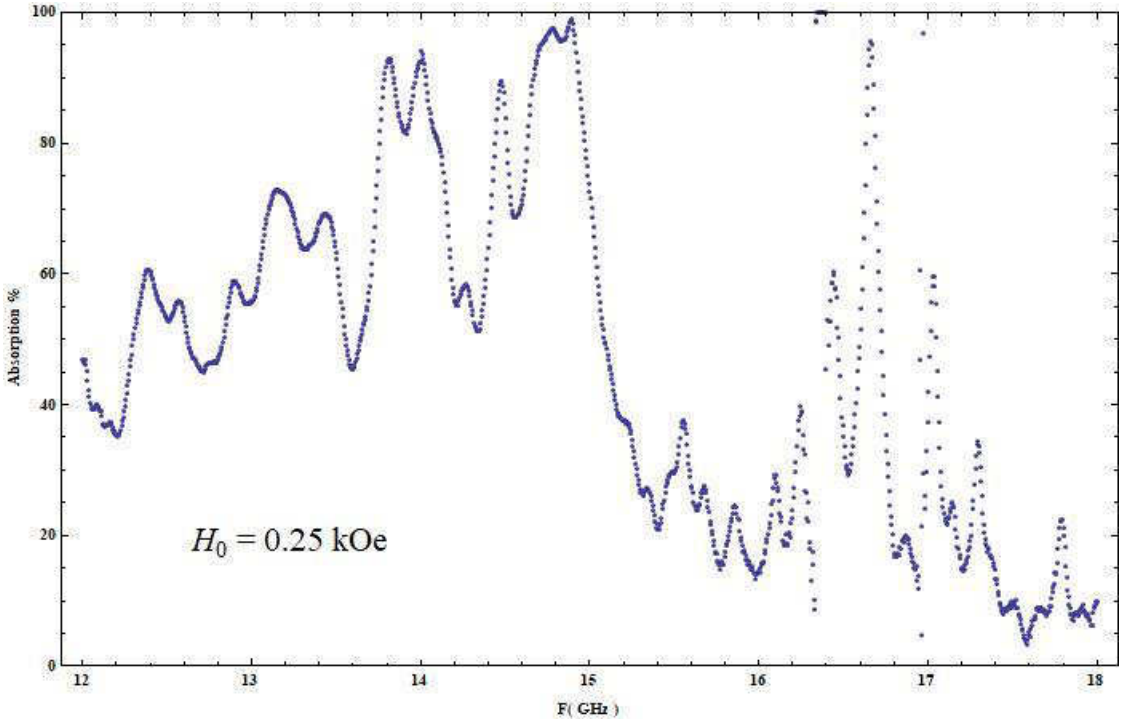

Fig. 4.7.15 Absorption vs. Frequency for $H_0 = 0.25$ kOe

Resonance-Anti-Resonance Frequency: 6.85→16.27 GHz

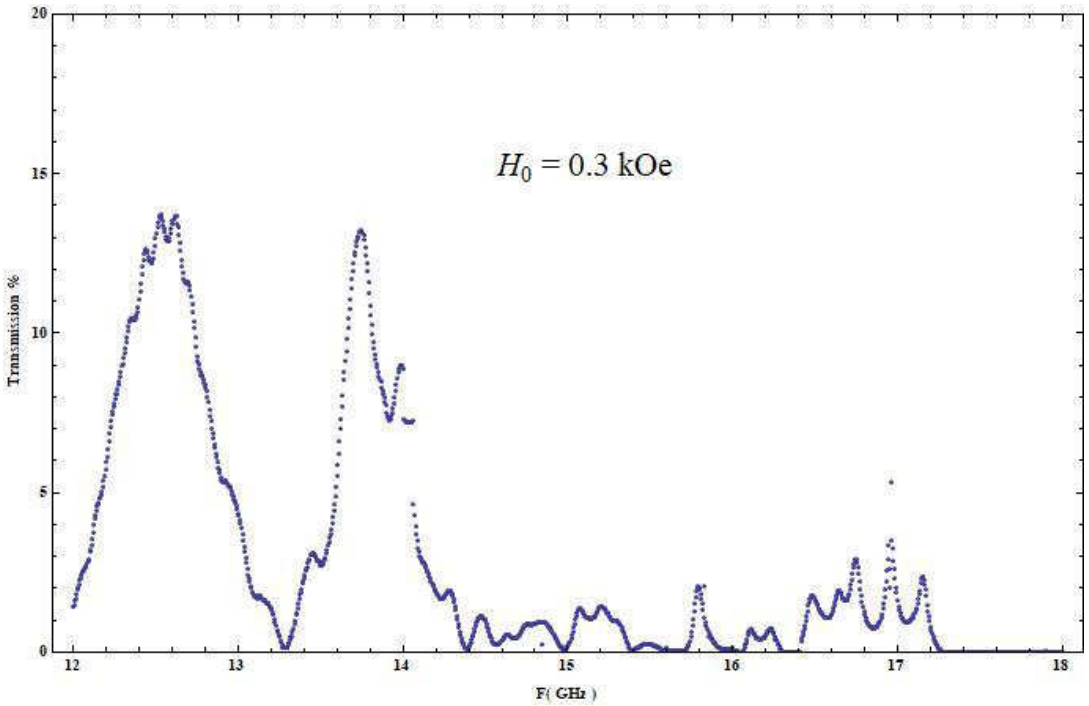

Fig. 4.7.16 Transmission vs. Frequency for $H_0 = 0.3$ kOe

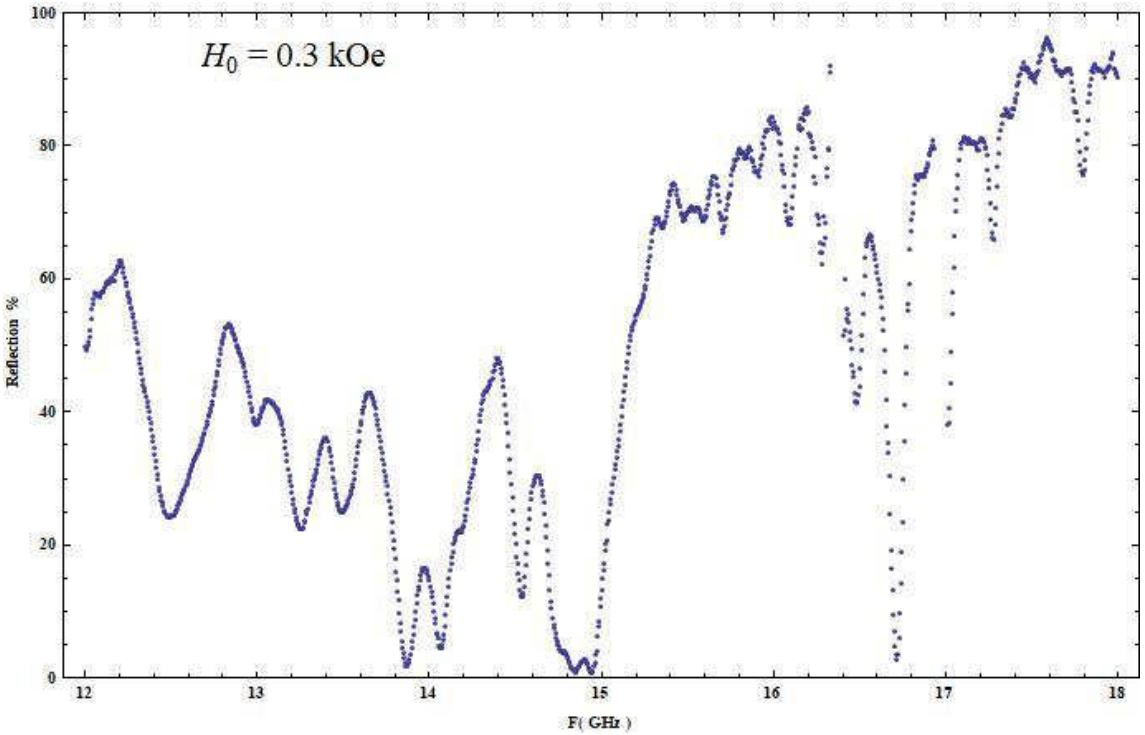

Fig. 4.7.17 Reflection vs. Frequency for $H_0 = 0.3$ kOe

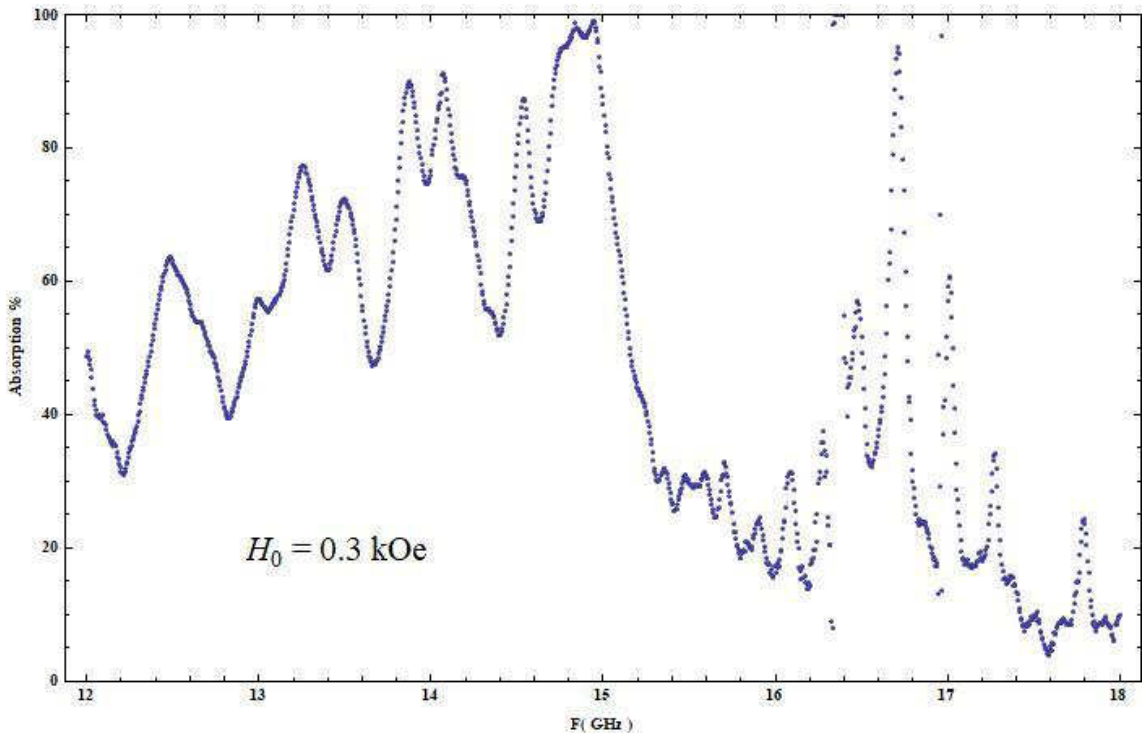

Fig. 4.7.18 Absorption vs. Frequency for $H_0 = 0.3$ kOe

Resonance-Anti-Resonance Frequency: 7.04→16.41 GHz

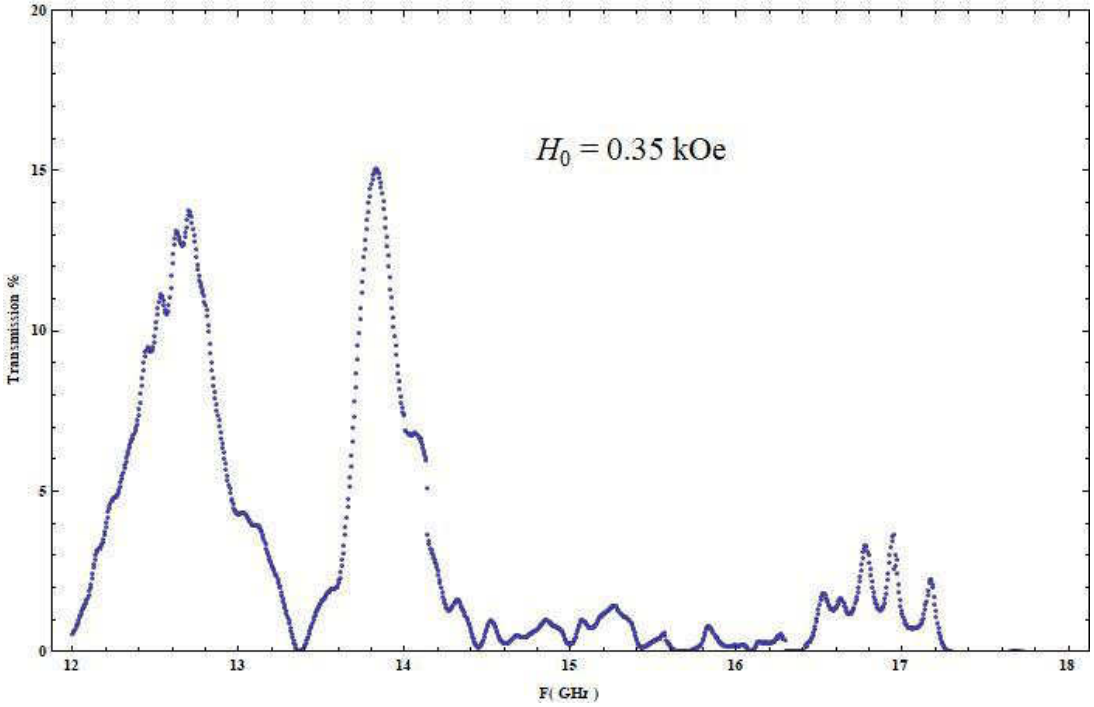

Fig. 4.7.19 Transmission vs. Frequency for $H_0 = 0.35$ kOe

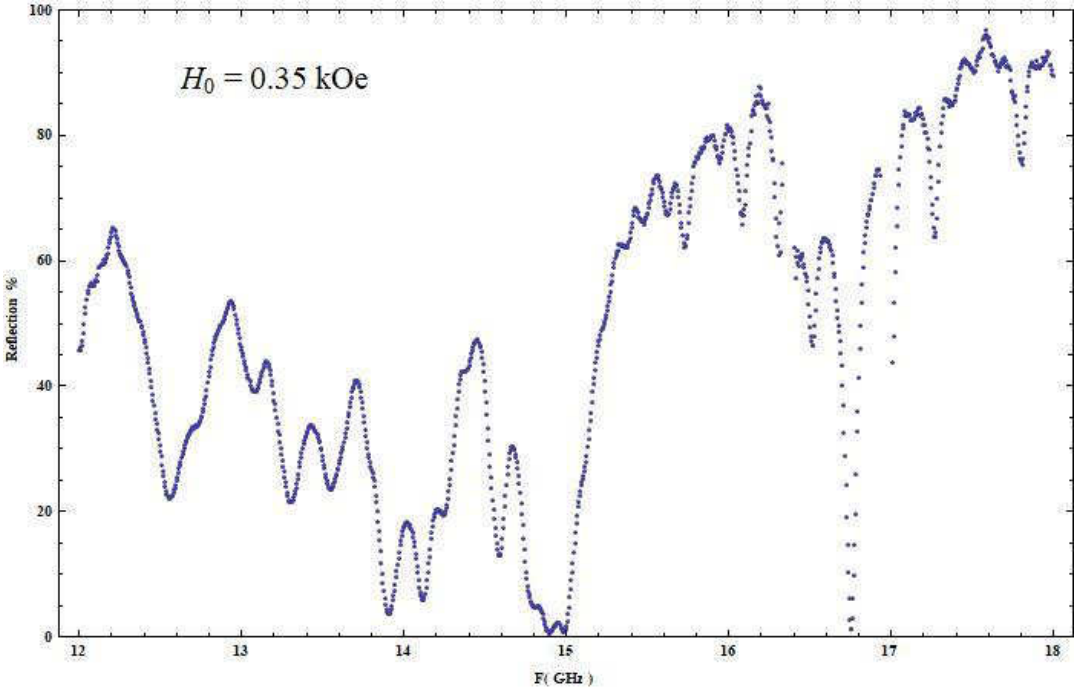

Fig. 4.7.20 Reflection vs. Frequency for $H_0 = 0.35$ kOe

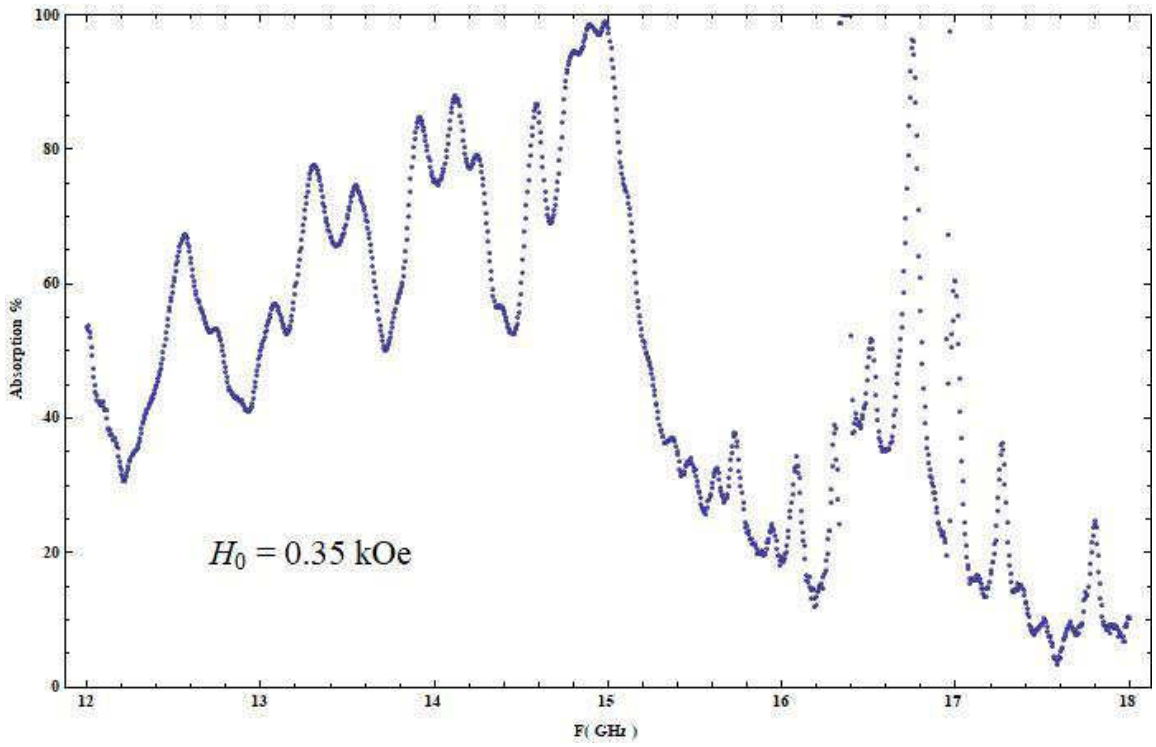

Fig. 4.7.21 Absorption vs. Frequency for $H_0 = 0.35$ kOe

Resonance-Anti-Resonance Frequency: 7.23→16.55 GHz

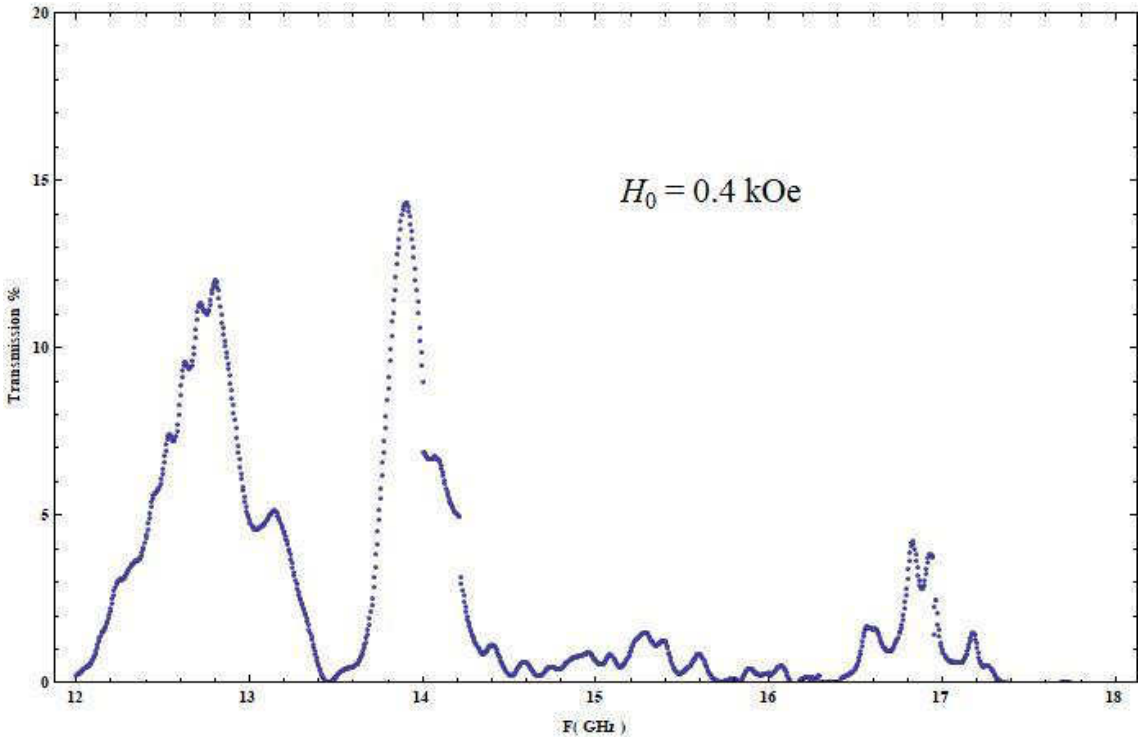

Fig. 4.7.22 Transmission vs. Frequency for $H_0 = 0.4$ kOe

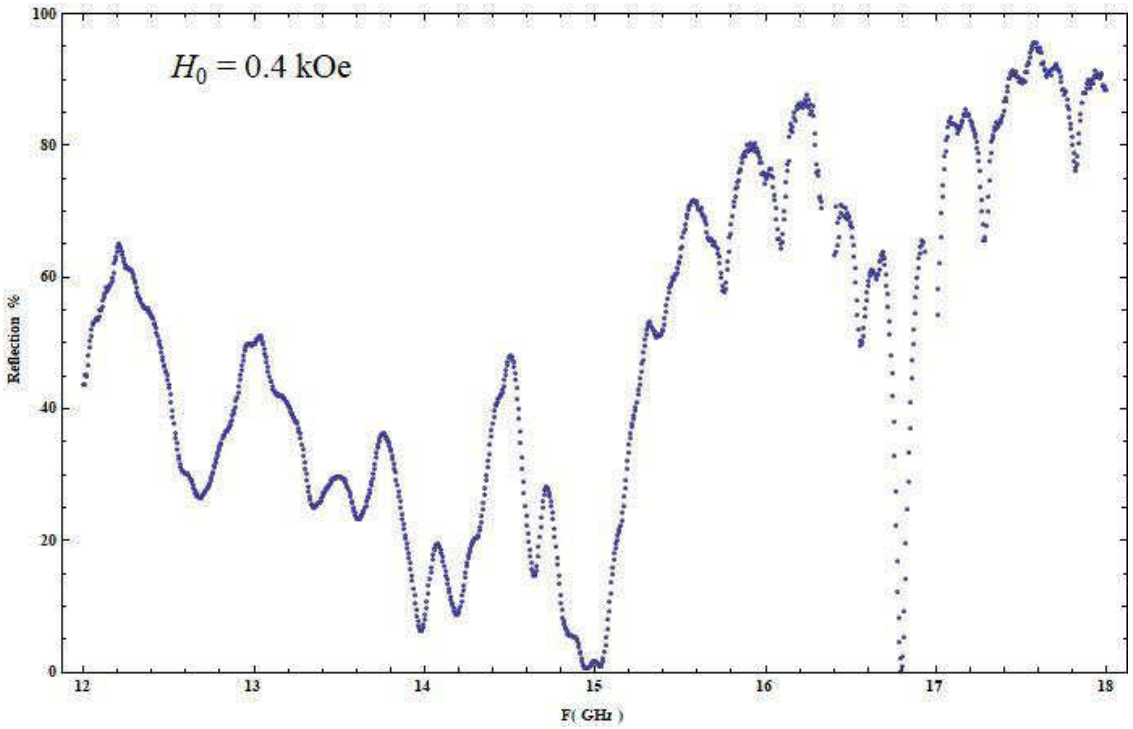

Fig. 4.7.23 Reflection vs. Frequency for $H_0 = 0.4$ kOe

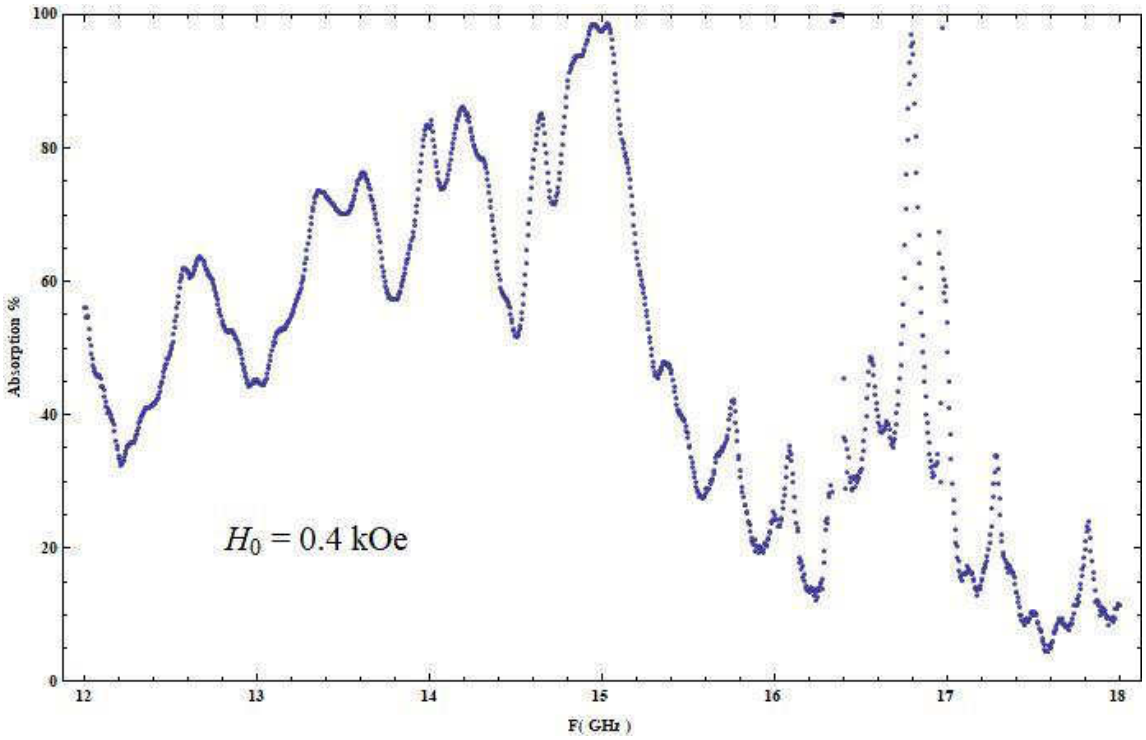

Fig. 4.7.24 Absorption vs. Frequency for $H_0 = 0.4$ kOe

Resonance-Anti-Resonance Frequency: 7.42→16.69 GHz

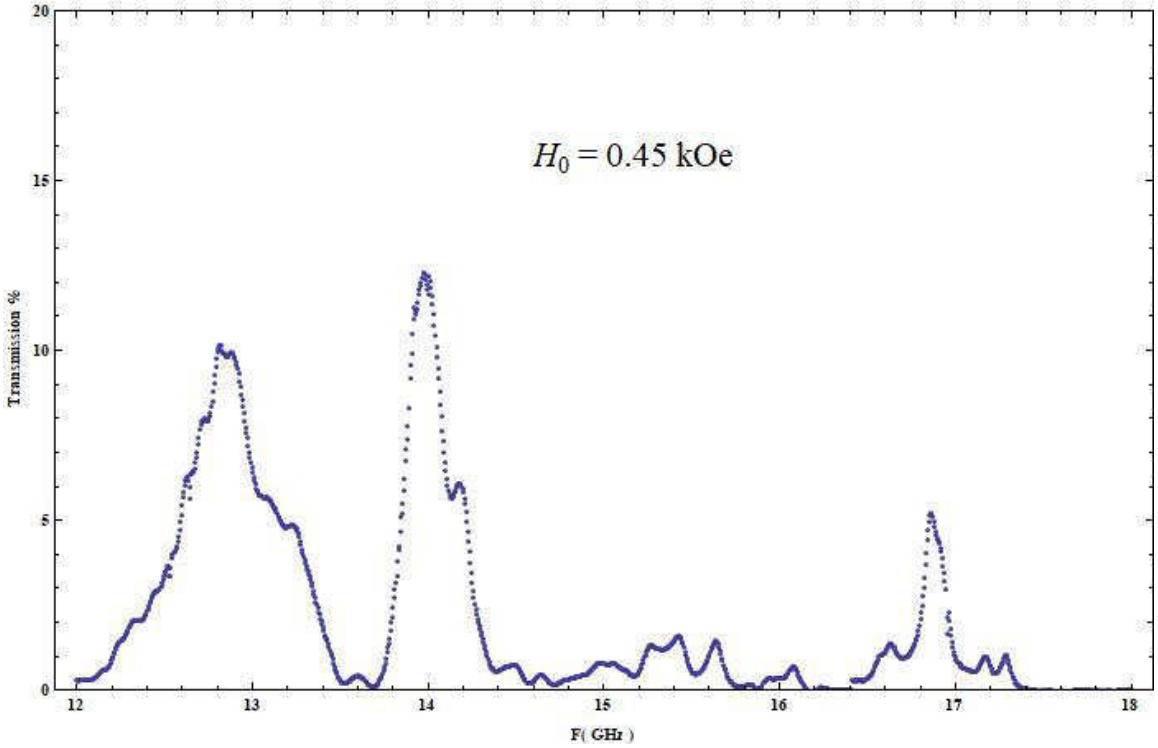

Fig. 4.7.25 Transmission vs. Frequency for $H_0 = 0.45$ kOe

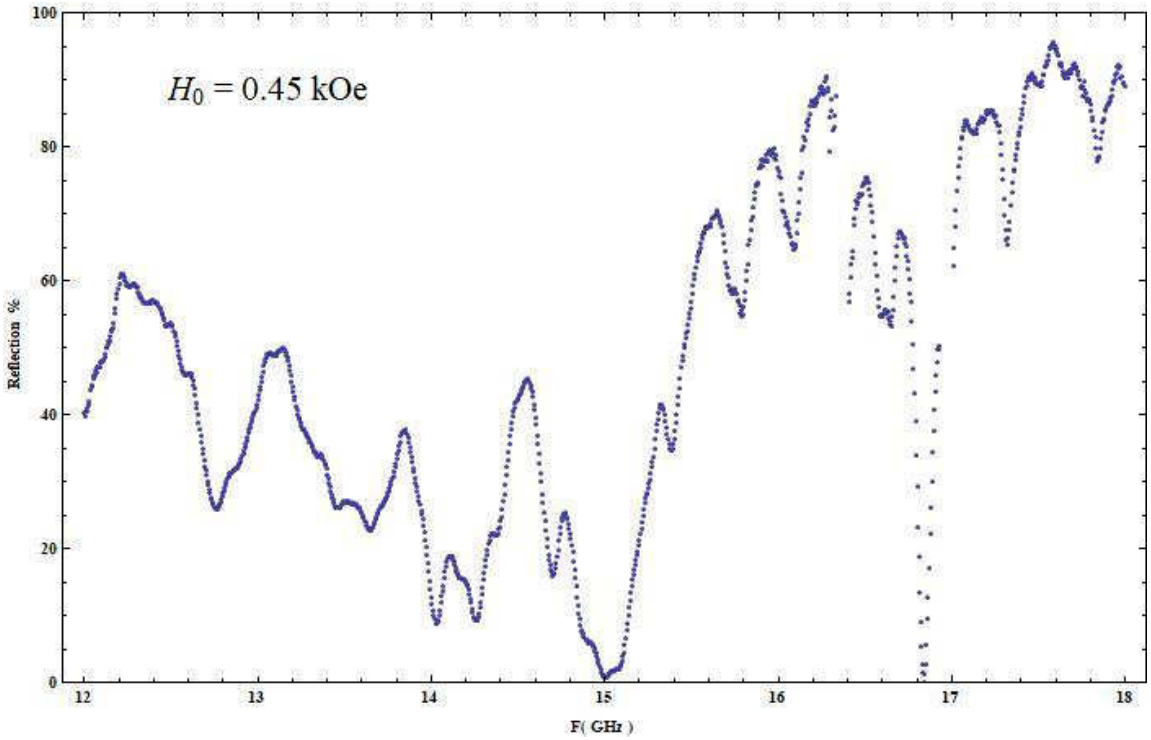

Fig. 4.7.26 Reflection vs. Frequency for $H_0 = 0.45$ kOe

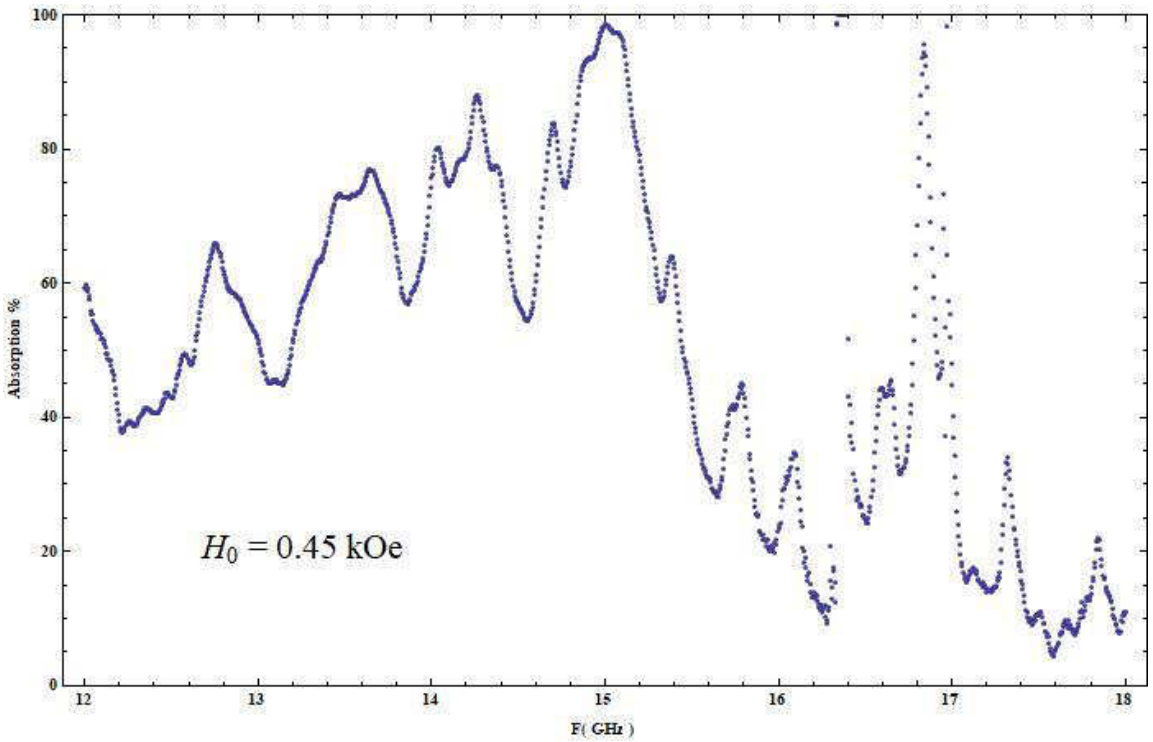

Fig. 4.7.27 Absorption vs. Frequency for $H_0 = 0.45$ kOe

Resonance-Anti-Resonance Frequency: 7.61→16.83 GHz

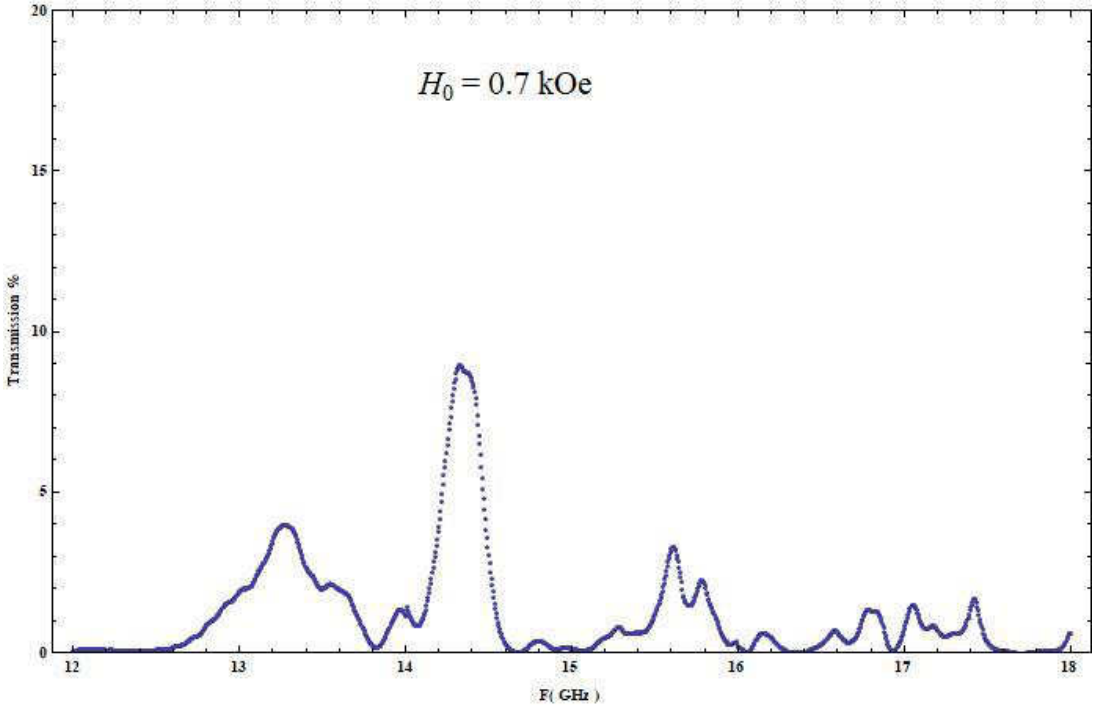

Fig. 4.7.28 Transmission vs. Frequency for $H_0 = 0.7$ kOe

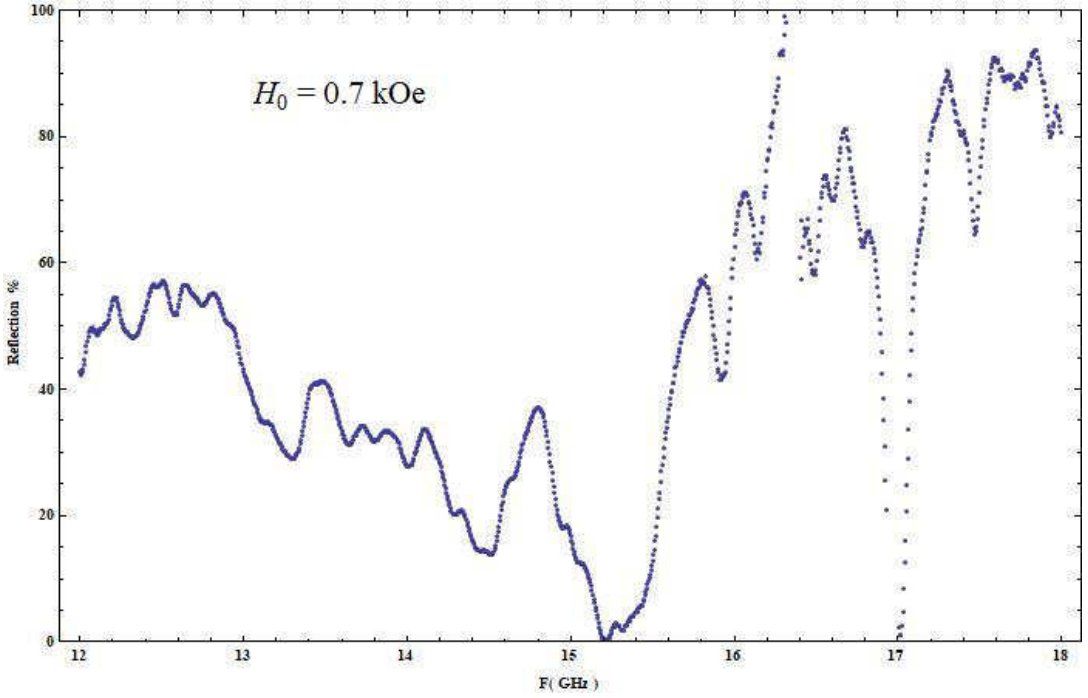

Fig. 4.7.29 Reflection vs. Frequency for $H_0 = 0.7$ kOe

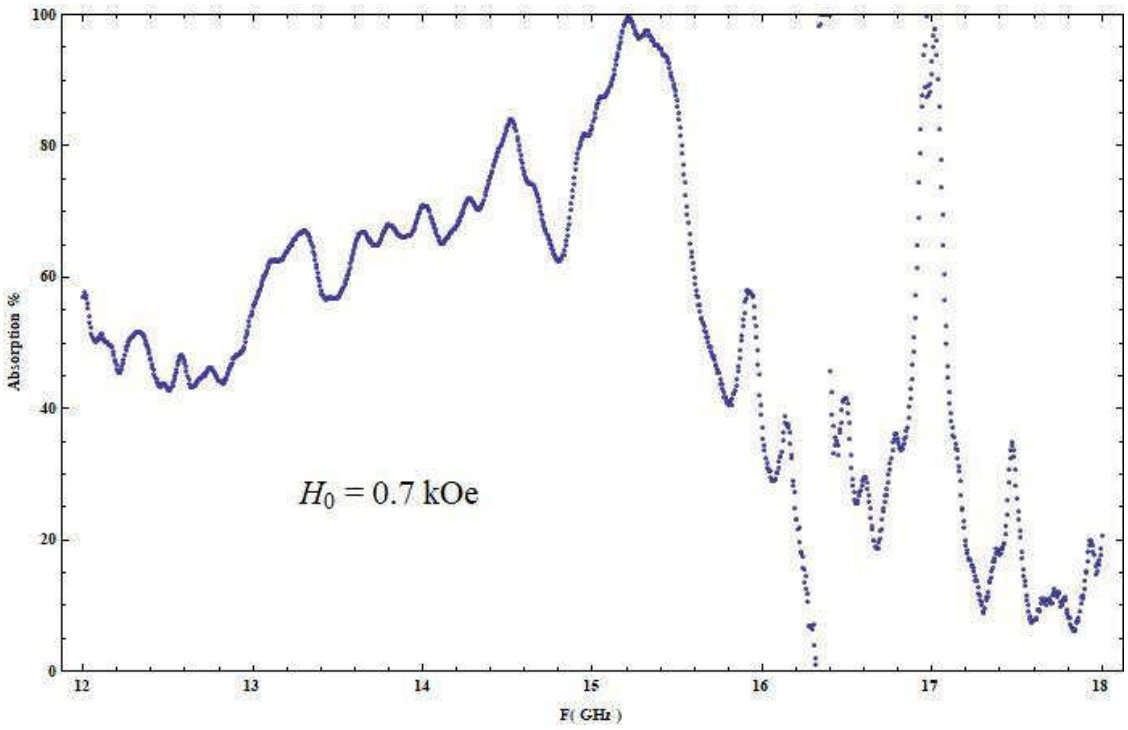

Fig. 4.7.30 Absorption vs. Frequency for $H_0 = 0.7$ kOe

Resonance-Anti-Resonance Frequency: 8.52→17.53 GHz

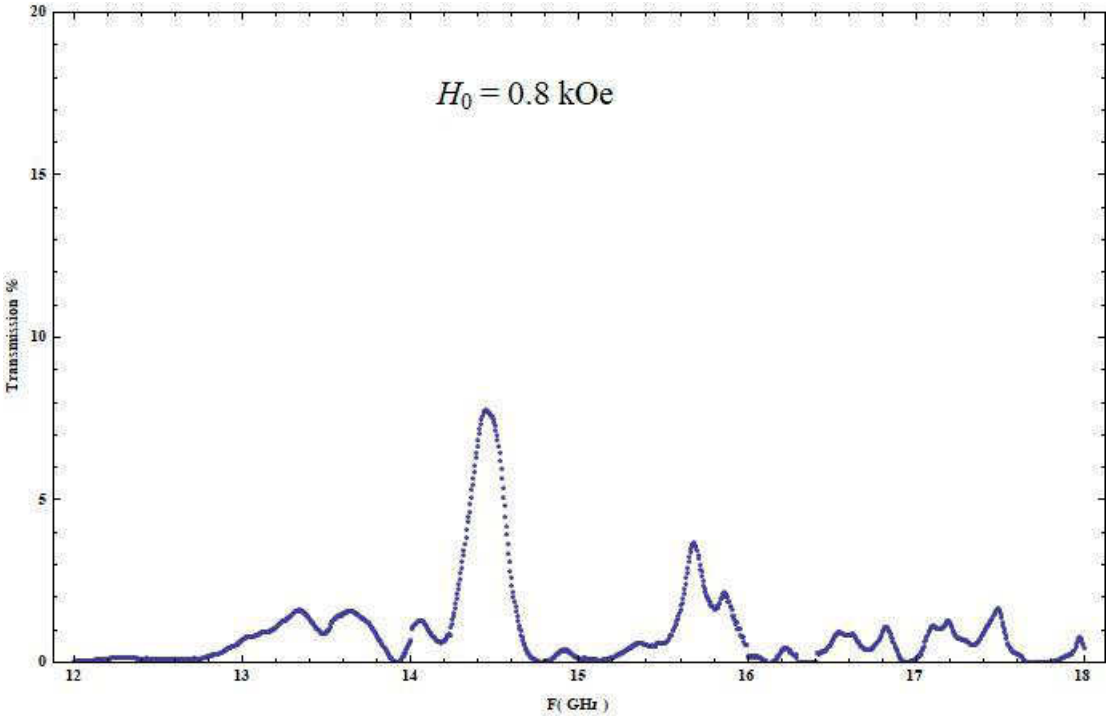

Fig. 4.7.31 Transmission vs. Frequency for $H_0 = 0.8$ kOe

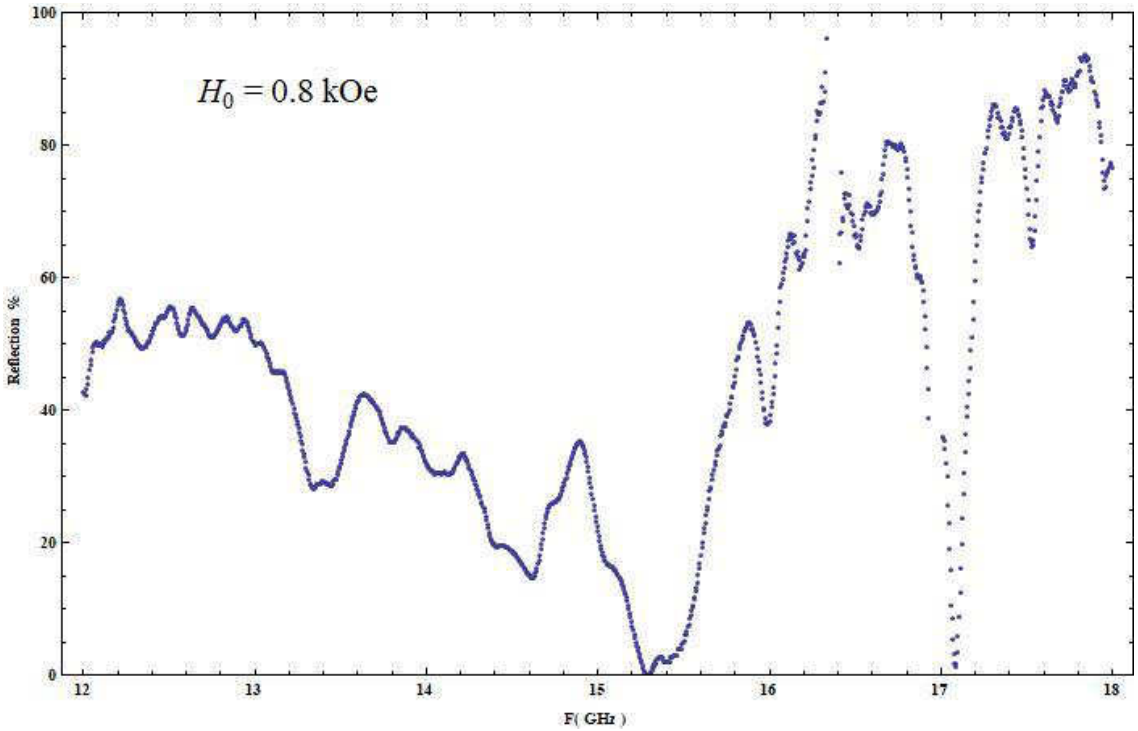

Fig. 4.7.32 Reflection vs. Frequency for $H_0 = 0.8$ kOe

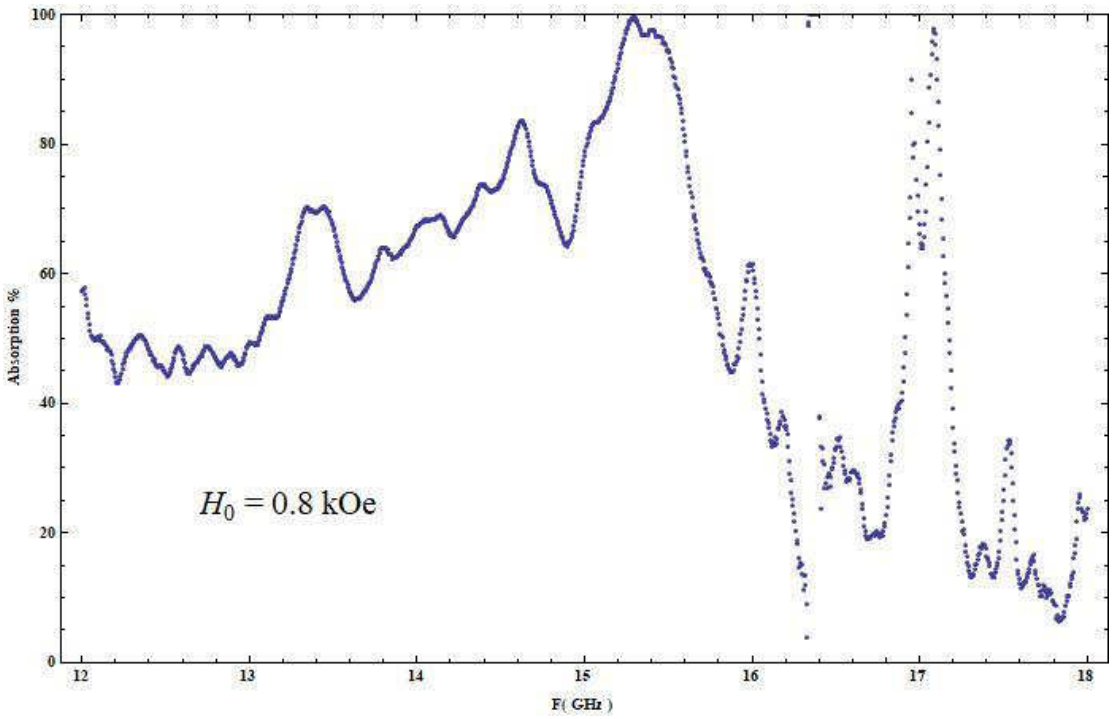

Fig. 4.7.33 Absorption vs. Frequency for $H_0 = 0.8$ kOe

Resonance-Anti-Resonance Frequency: 8.88→17.81 GHz

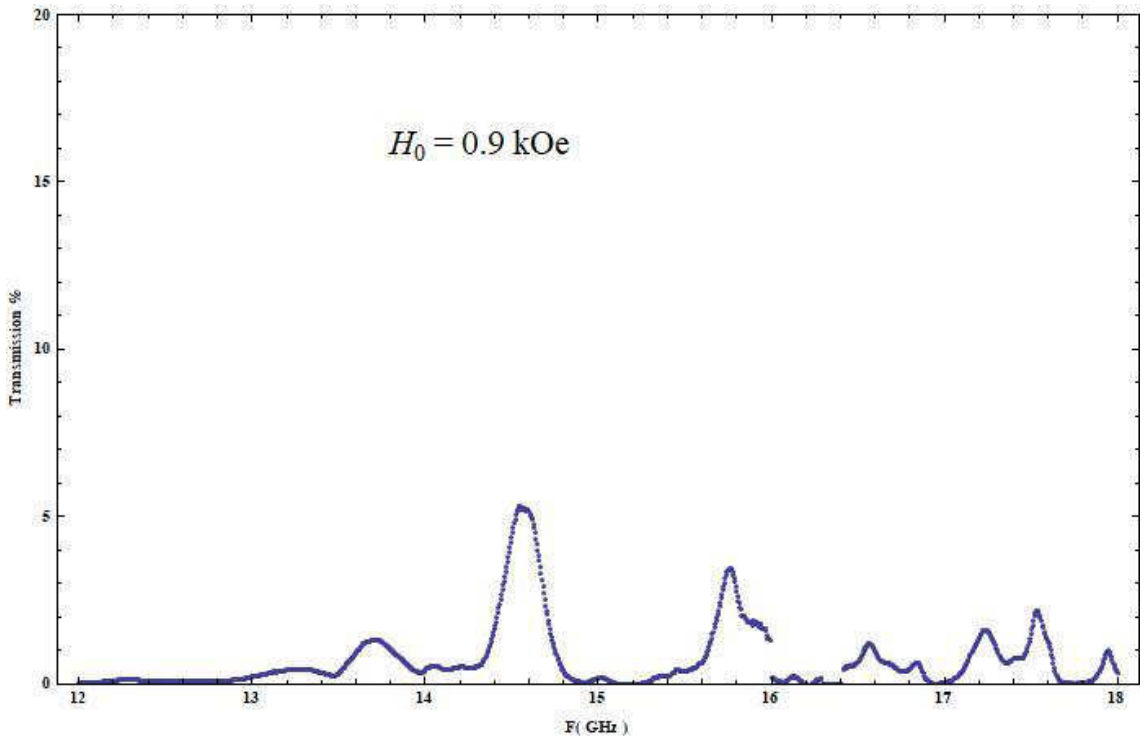

Fig. 4.7.34 Transmission vs. Frequency for $H_0 = 0.9$ kOe

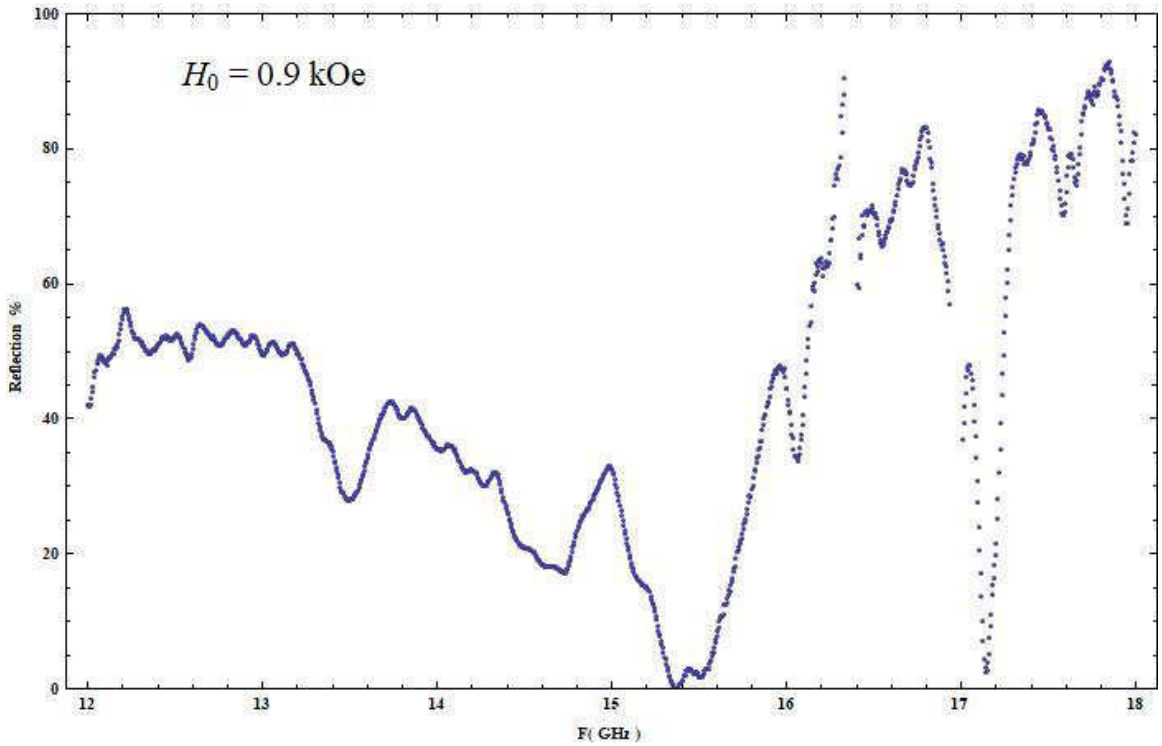

Fig. 4.7.35 Reflection vs. Frequency for $H_0 = 0.9$ kOe

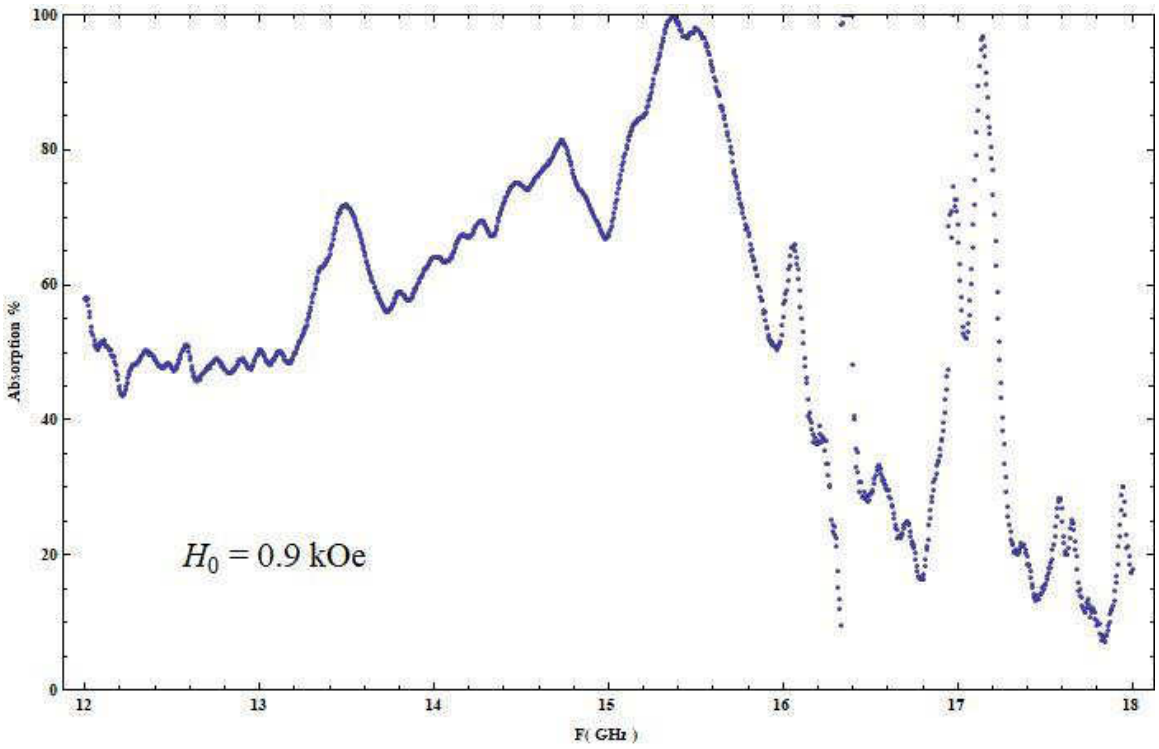

Fig. 4.7.36 Absorption vs. Frequency for $H_0 = 0.9$ kOe

Resonance-Anti-Resonance Frequency: 9.22 →18.10 GHz

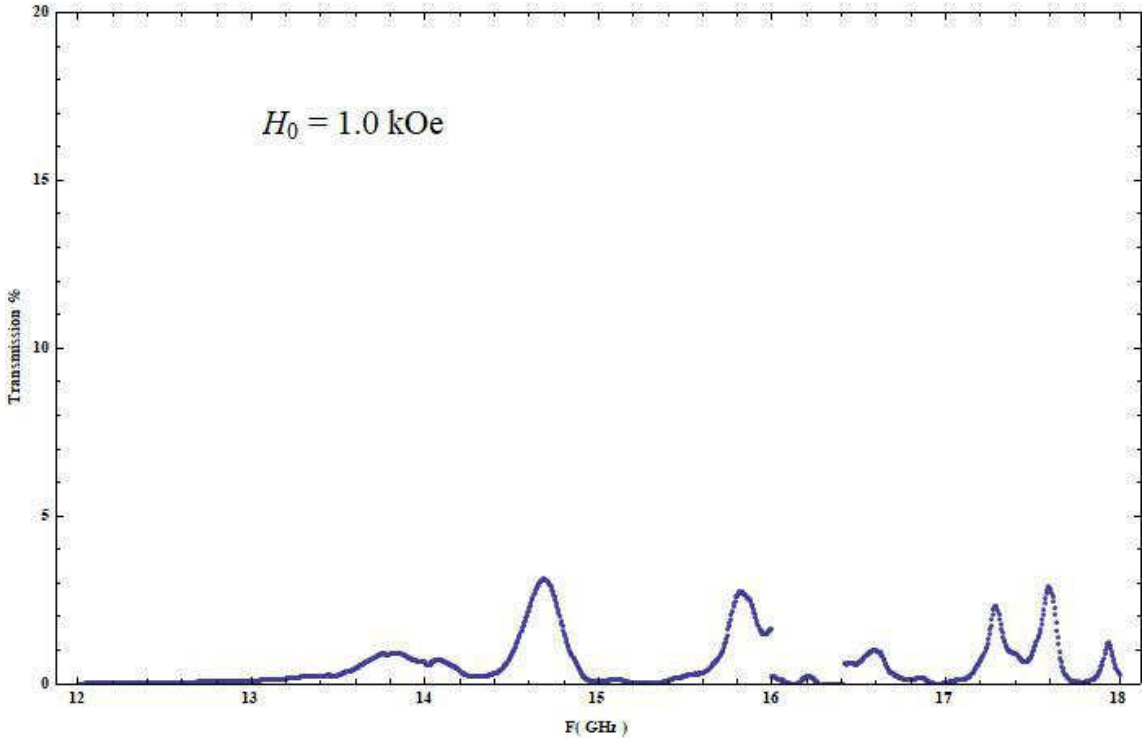

Fig. 4.7.37 Transmission vs. Frequency for $H_0 = 1.0$ kOe

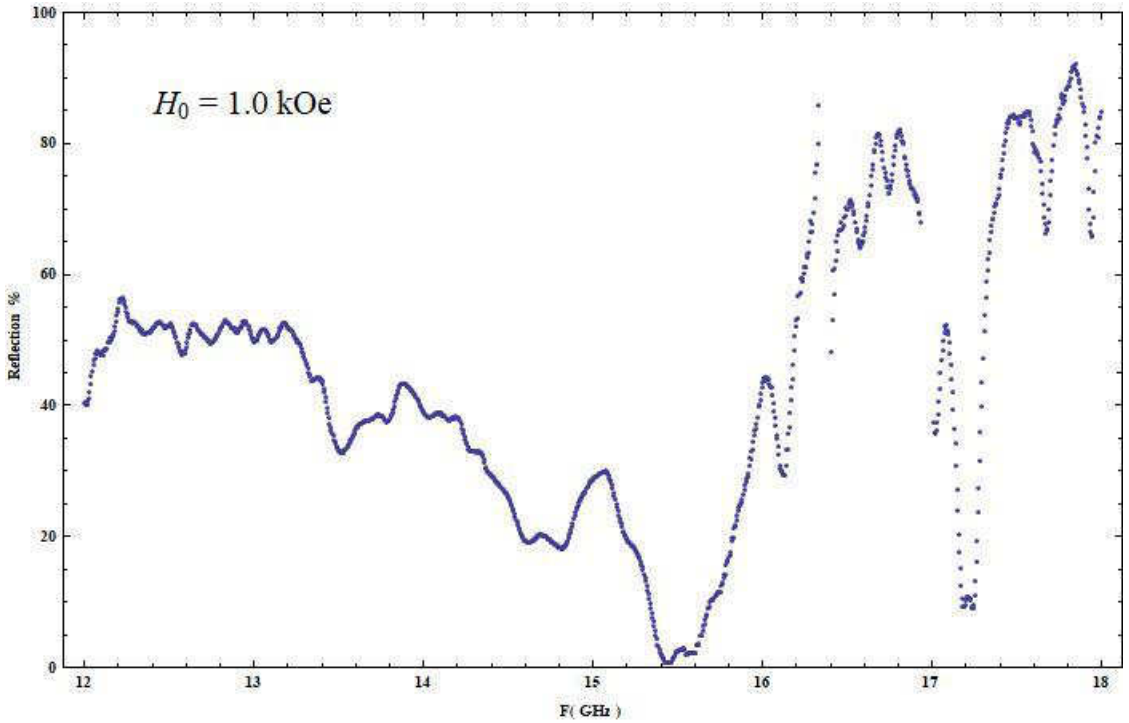

Fig. 4.7.38 Reflection vs. Frequency for $H_0 = 1.0$ kOe

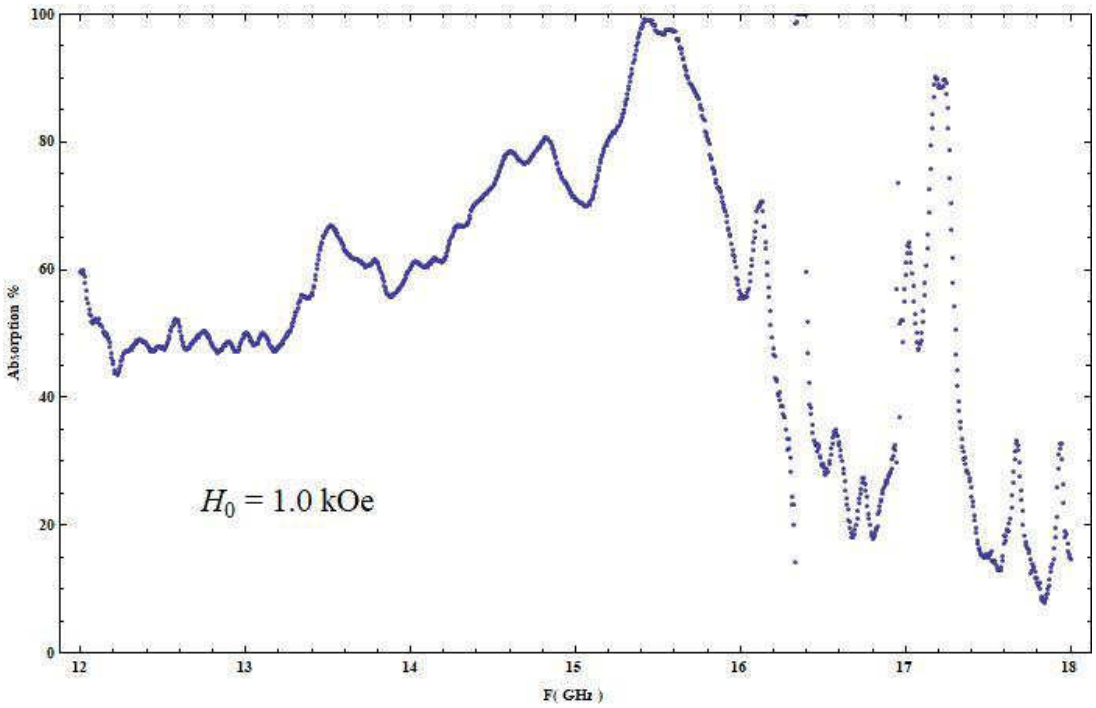

Fig. 4.7.39 Absorption vs. Frequency for $H_0 = 1.0$ kOe

Resonance-Anti-Resonance Frequency: 9.57→18.37 GHz

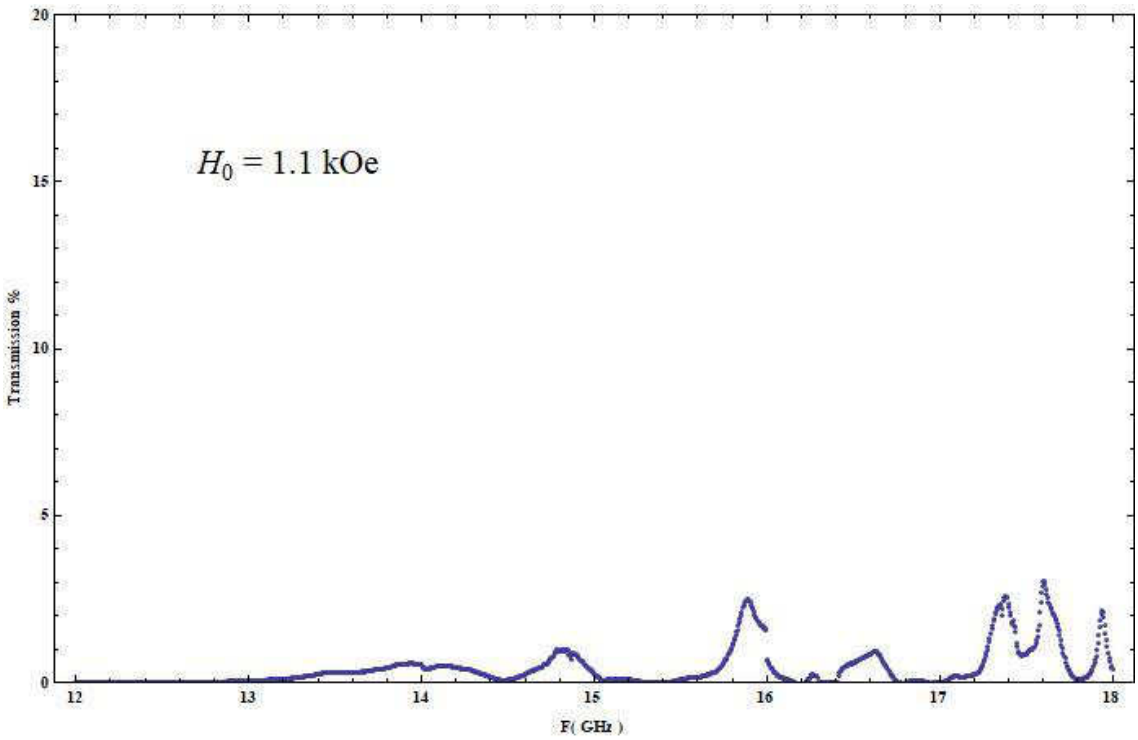

Fig. 4.7.40 Transmission vs. Frequency for $H_0 = 1.1$ kOe

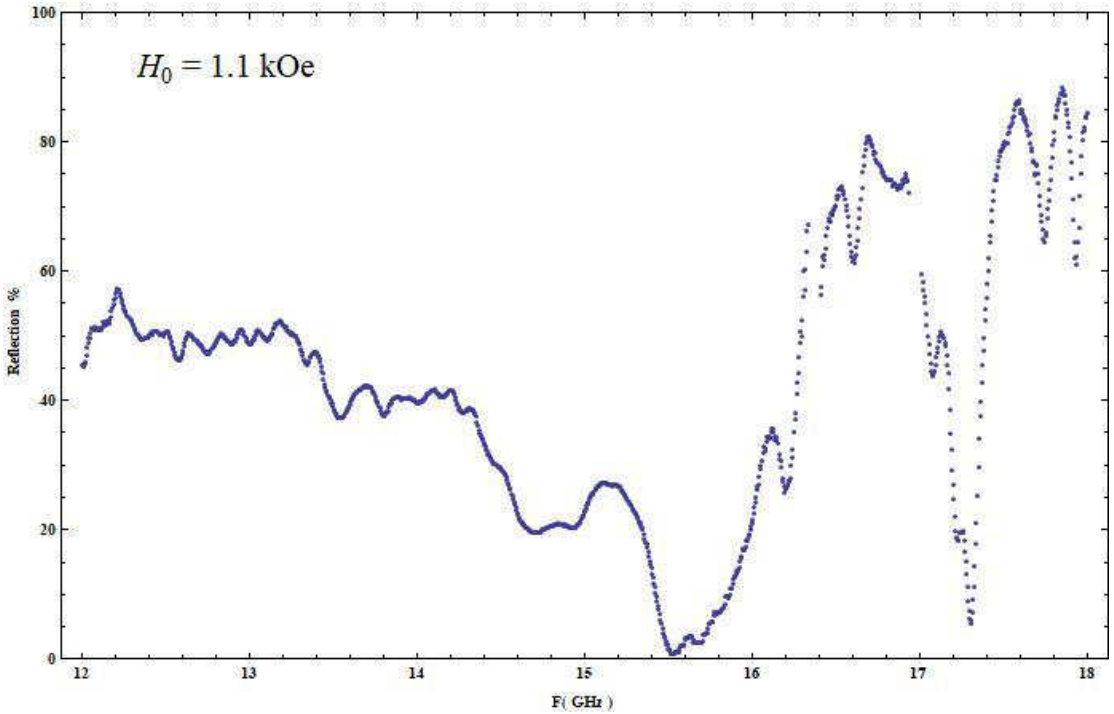

Fig. 4.7.41 Reflection vs. Frequency for $H_0 = 1.1$ kOe

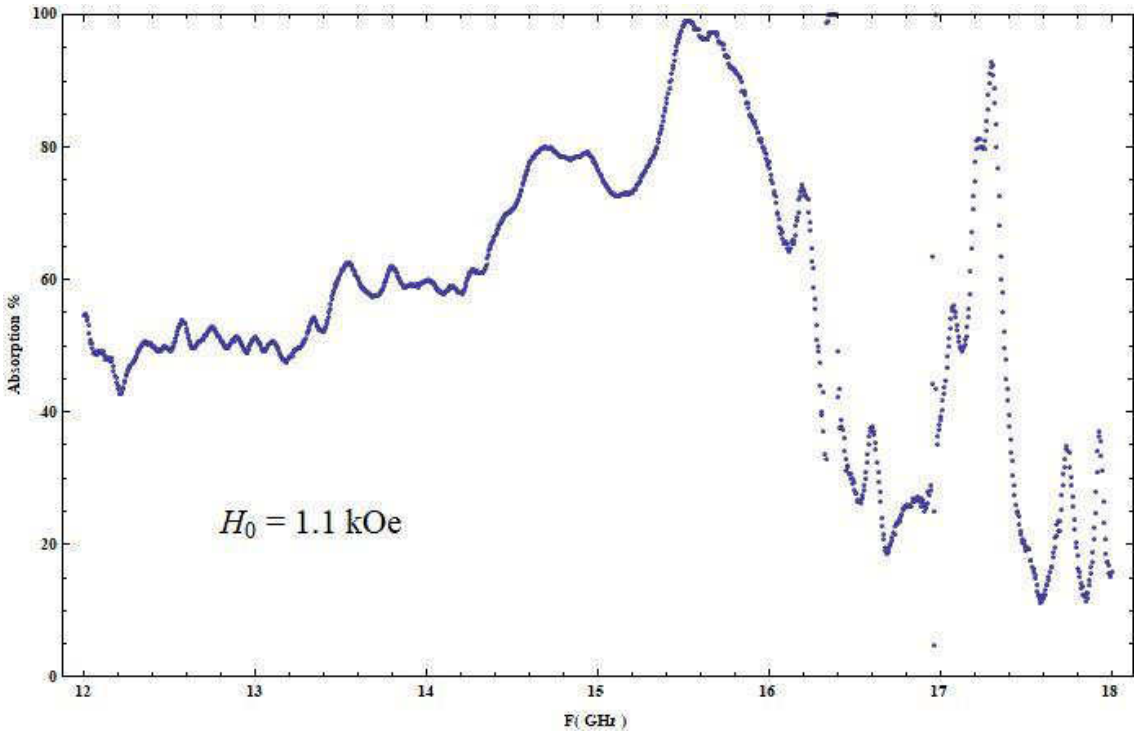

Fig. 4.7.42 Absorption vs. Frequency for $H_0 = 1.1$ kOe

Resonance-Anti-Resonance Frequency: 9.91→18.66 GHz

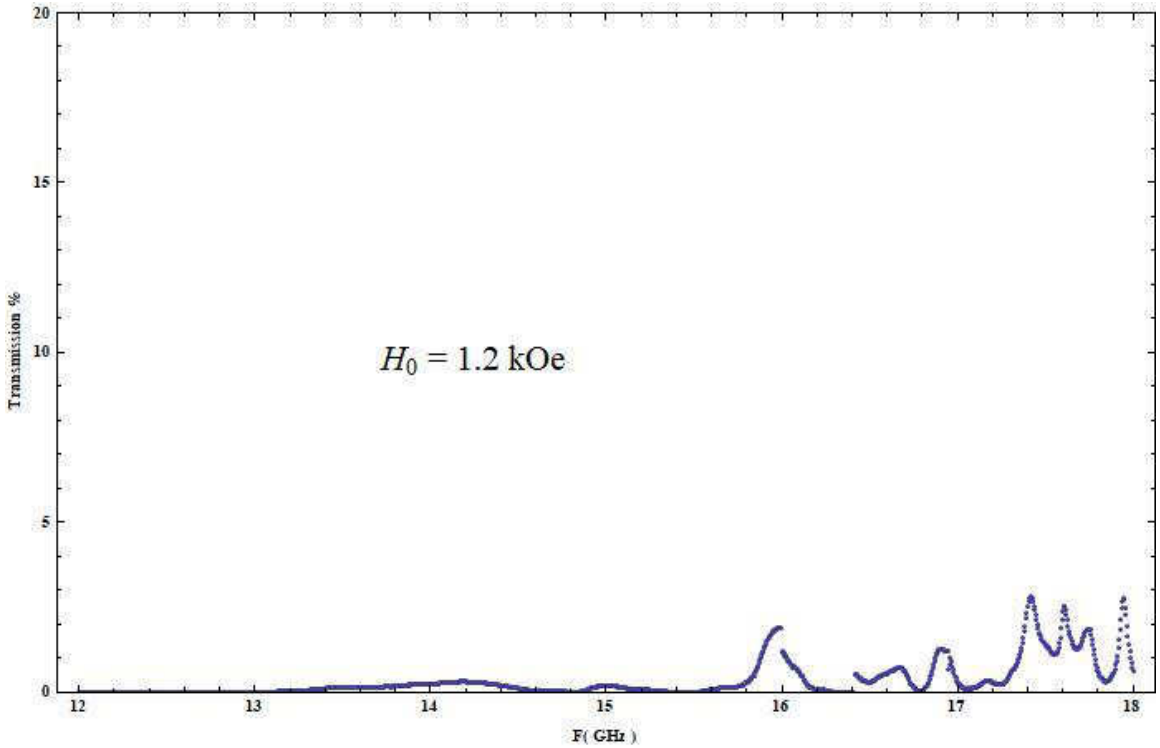

Fig. 4.7.43 Transmission vs. Frequency for $H_0 = 1.2$ kOe

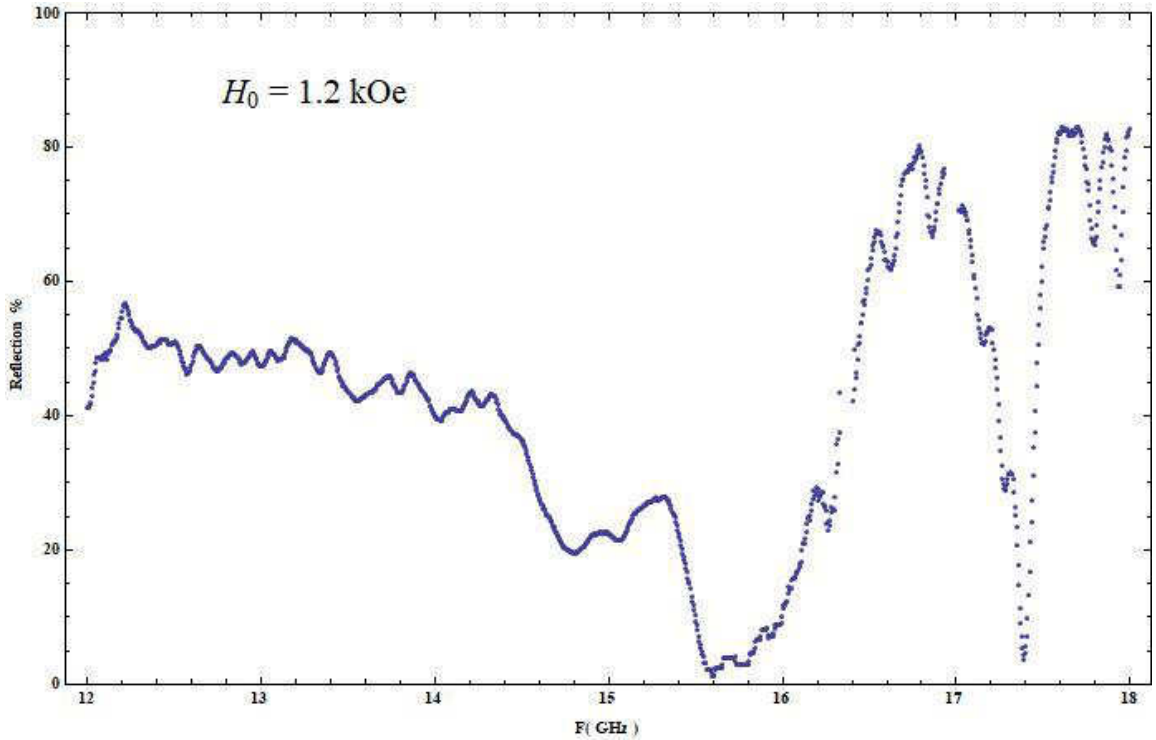

Fig. 4.7.44 Reflection vs. Frequency for $H_0 = 1.2$ kOe

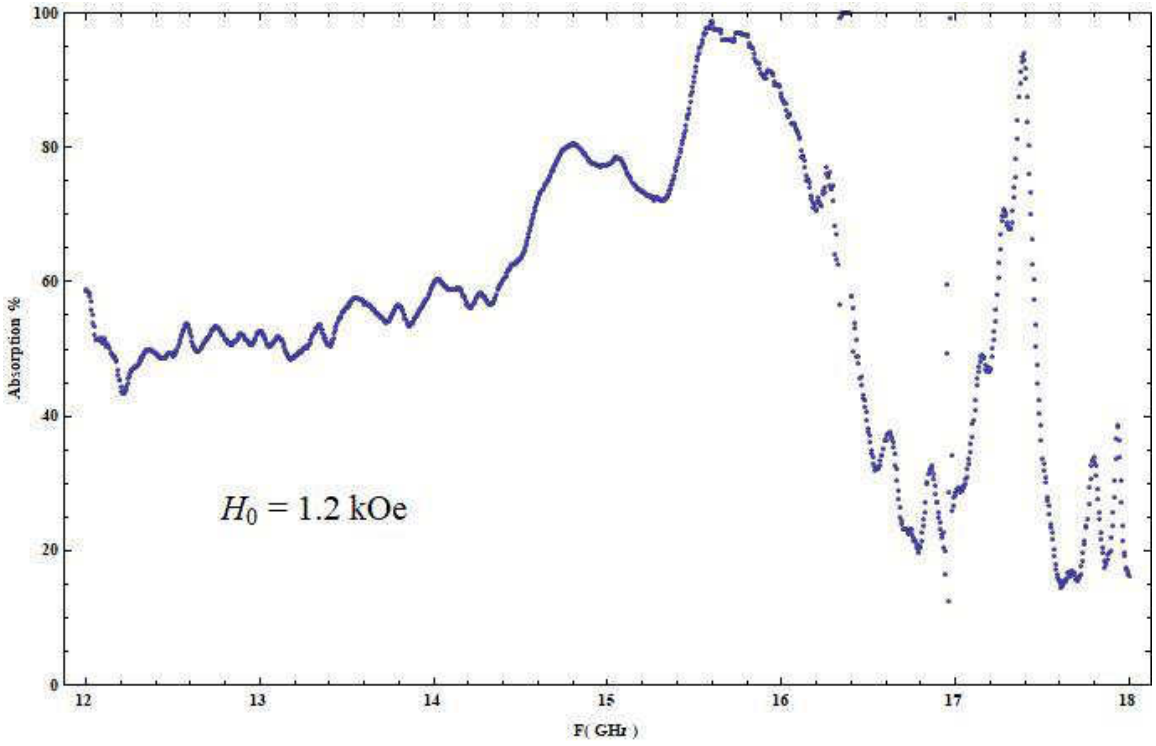

Fig. 4.7.45 Absorption vs. Frequency for $H_0 = 1.2$ kOe

Resonance-Anti-Resonance Frequency: 10.24→18.93 GHz

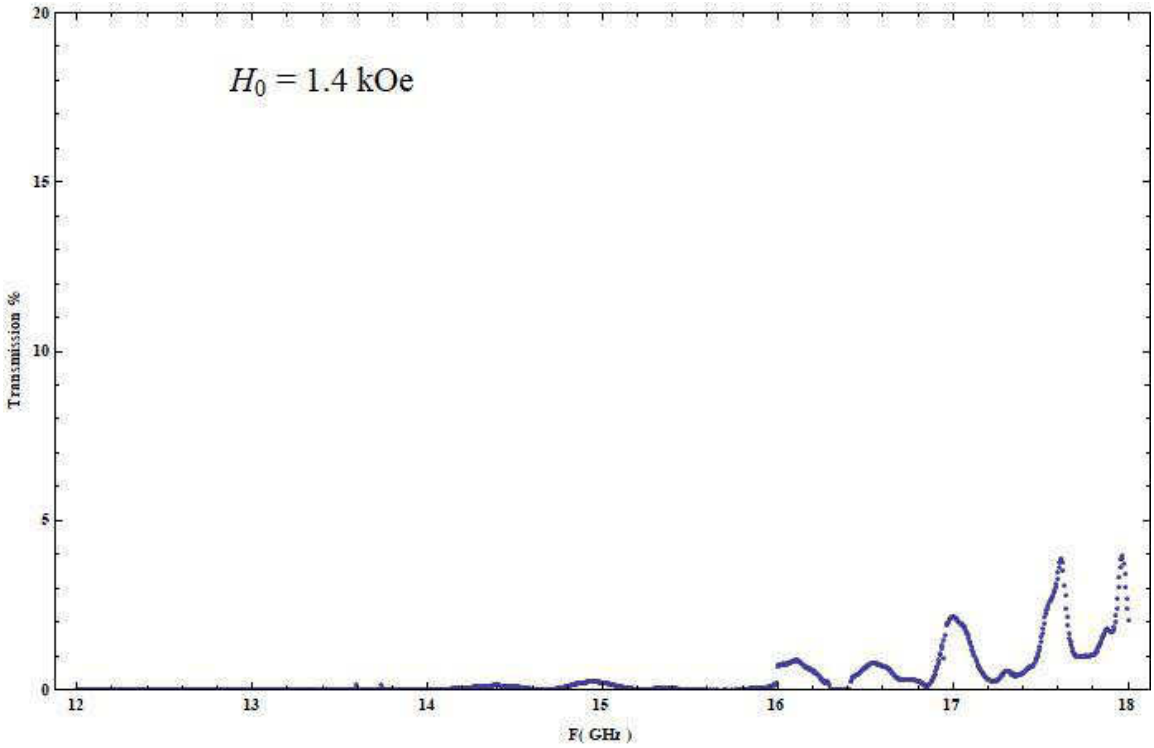

Fig. 4.7.46 Transmission vs. Frequency for $H_0 = 1.4$ kOe

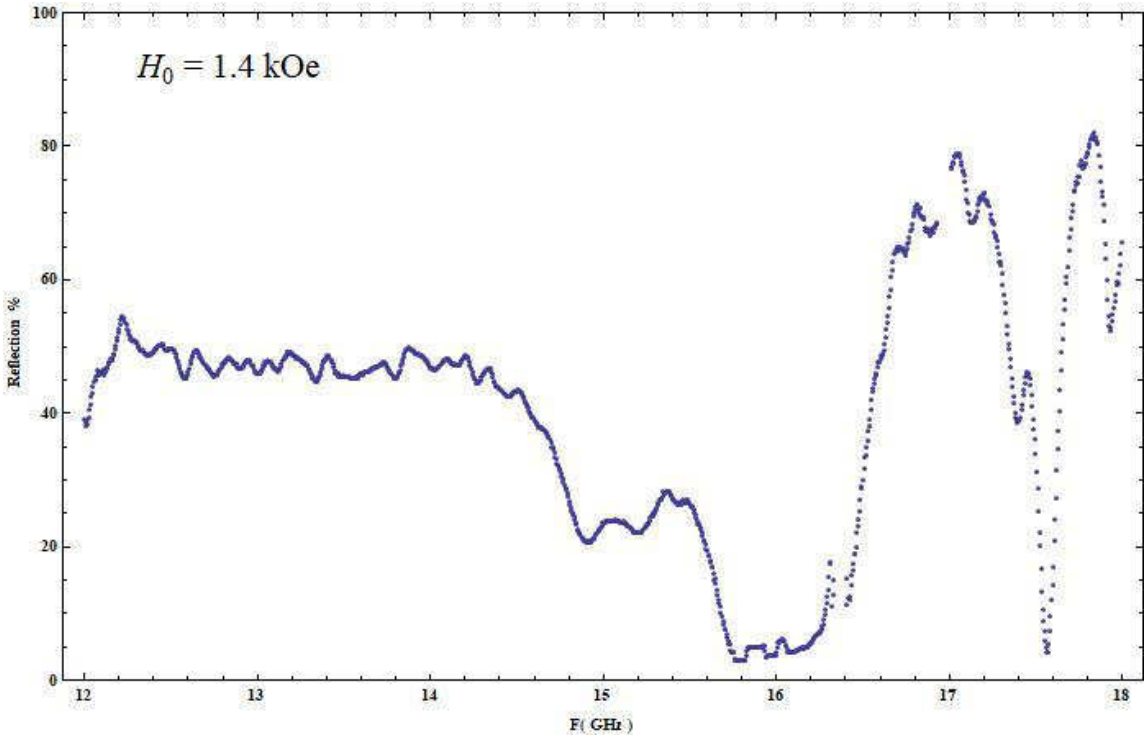

Fig. 4.7.47 Reflection vs. Frequency for $H_0 = 1.4$ kOe

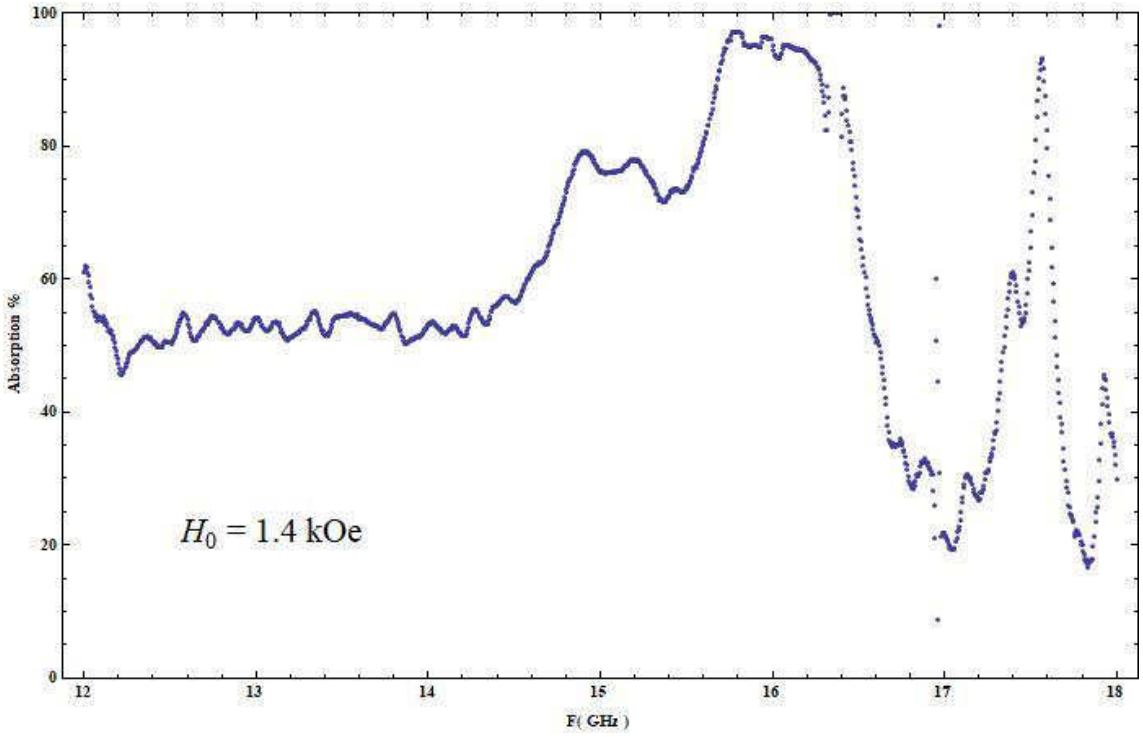

Fig. 4.7.48 Absorption vs. Frequency for $H_0 = 1.4$ kOe

Resonance-Anti-Resonance Frequency: 10.91→19.50 GHz

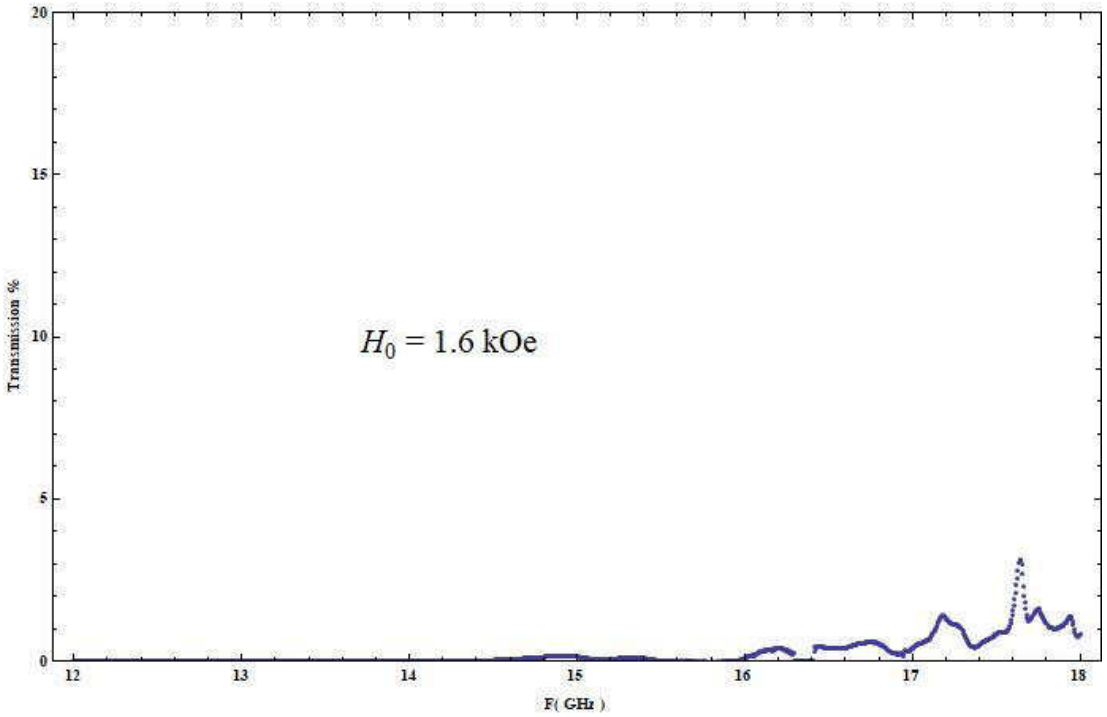

Fig. 4.7.49 Transmission vs. Frequency for $H_0 = 1.6$ kOe

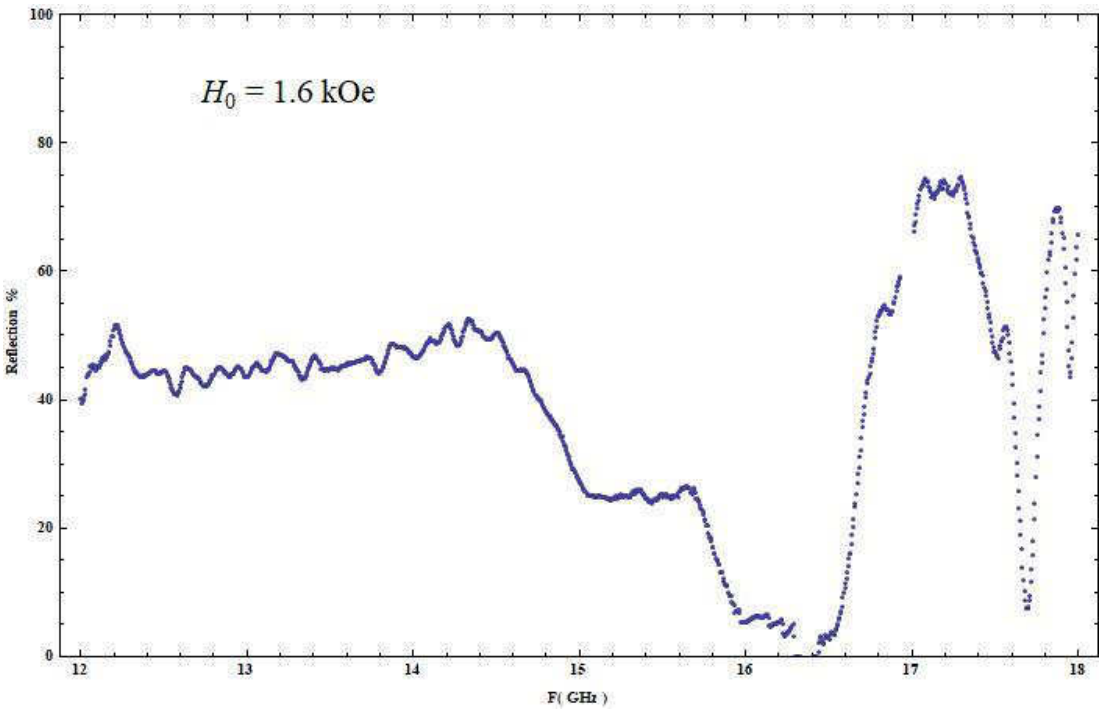

Fig. 4.7.50 Reflection vs. Frequency for $H_0 = 1.6$ kOe

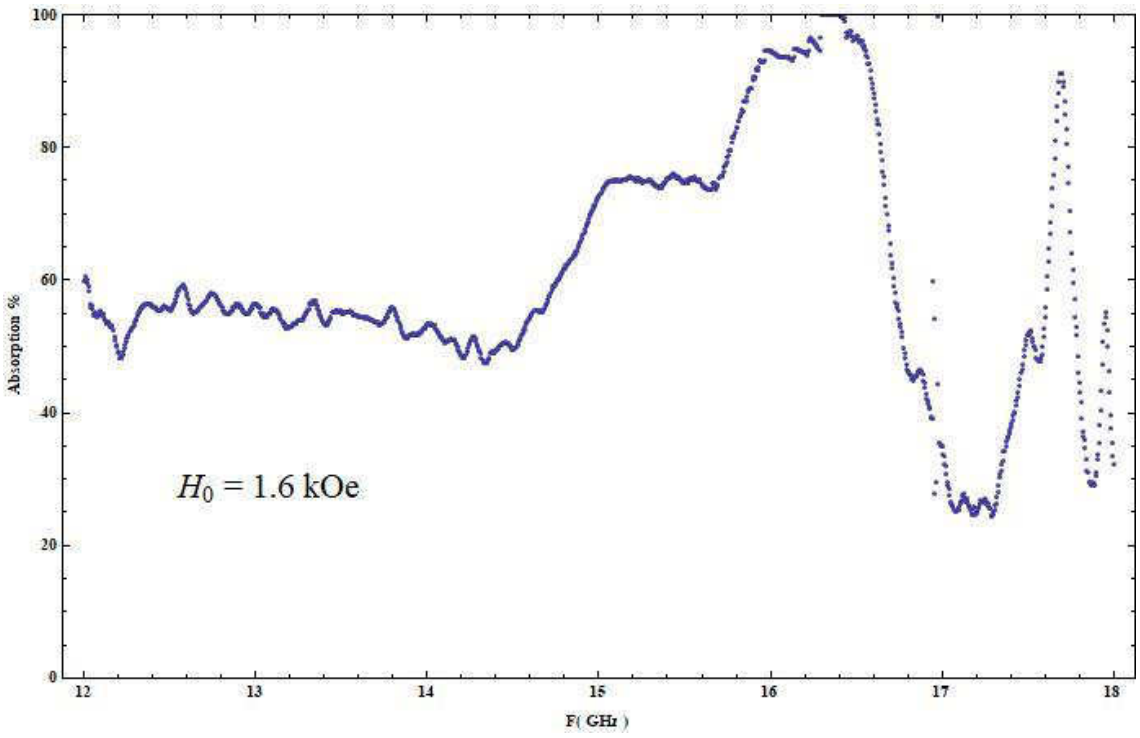

Fig. 4.7.51 Absorption vs. Frequency for $H_0 = 1.6$ kOe

Resonance-Anti-Resonance Frequency: 11.56→20.06 GHz

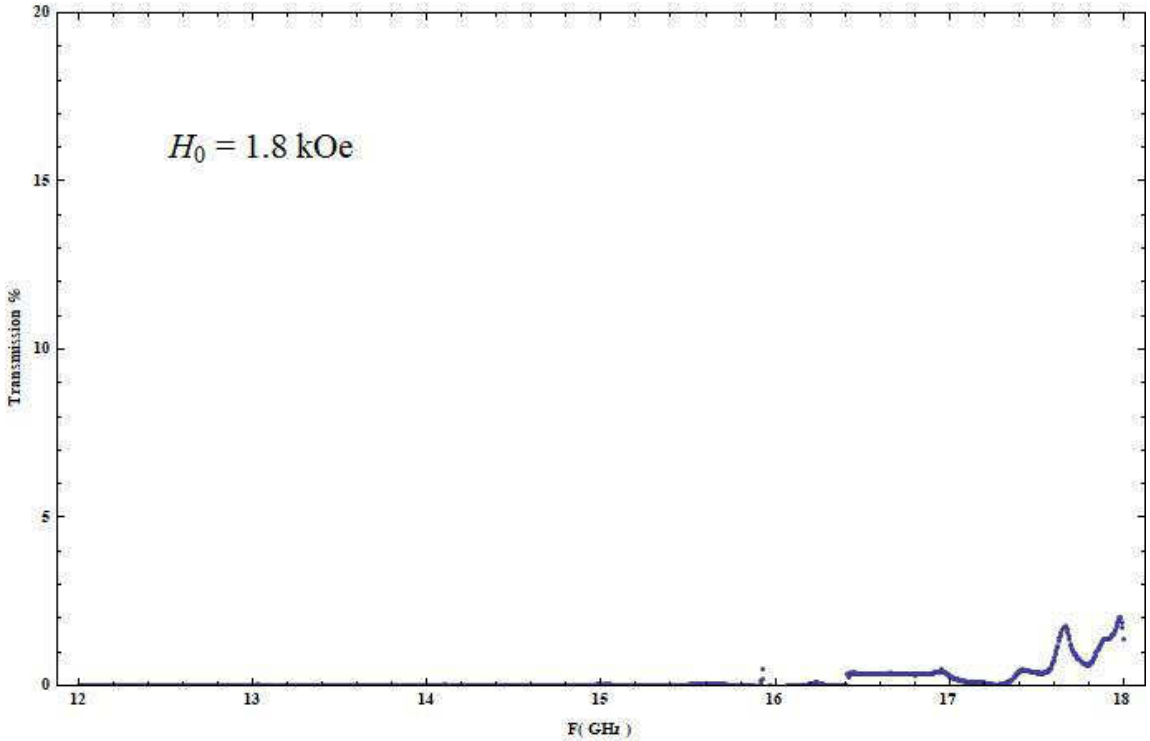

Fig. 4.7.52 Transmission vs. Frequency for $H_0 = 1.8$ kOe

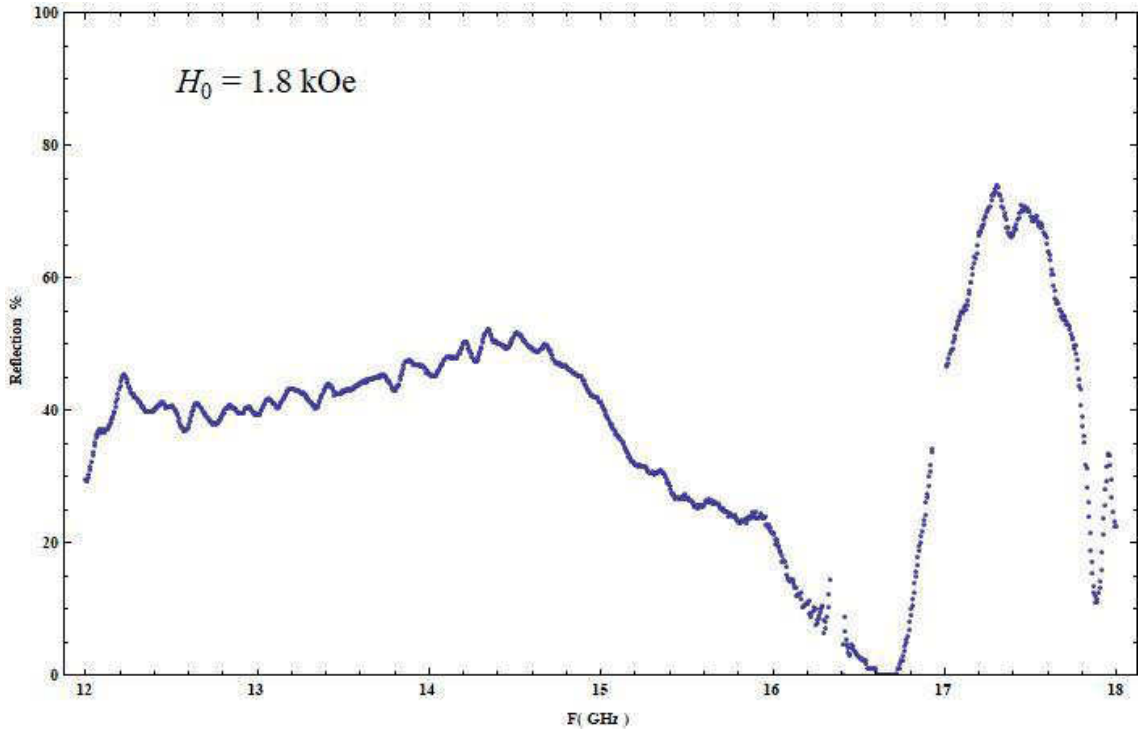

Fig. 4.7.53 Reflection vs. Frequency for $H_0 = 1.8$ kOe

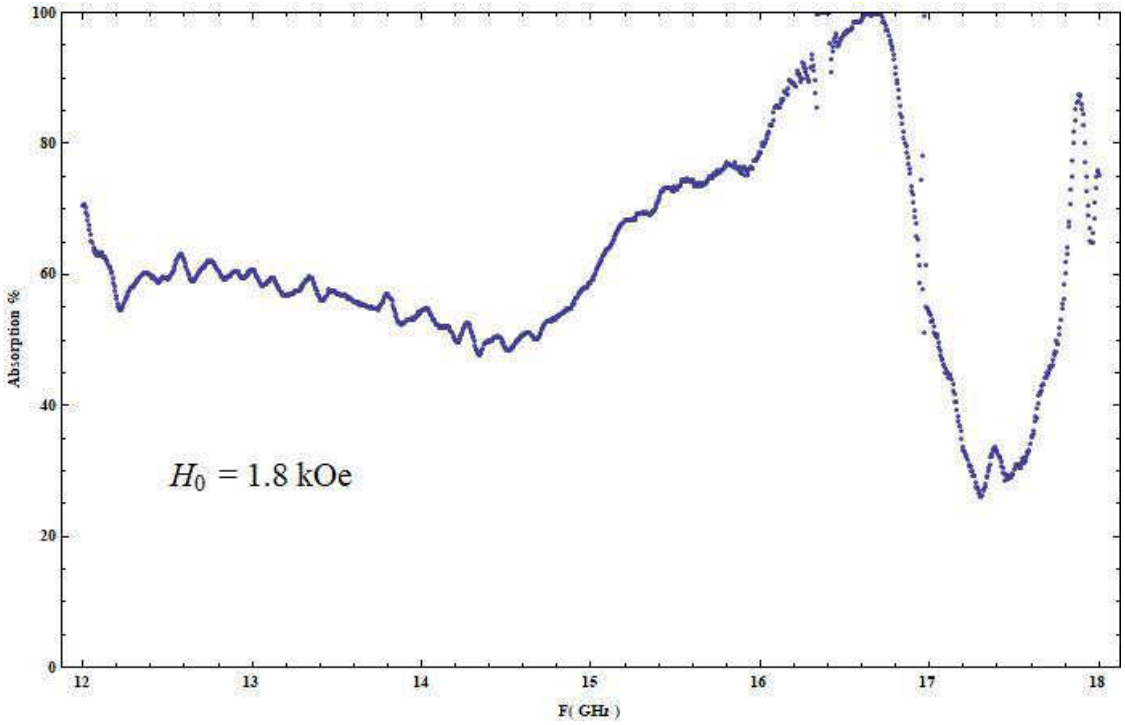

Fig. 4.7.54 Absorption vs. Frequency for $H_0 = 1.8$ kOe

Resonance-Anti-Resonance Frequency: 12.20→20.62 GHz

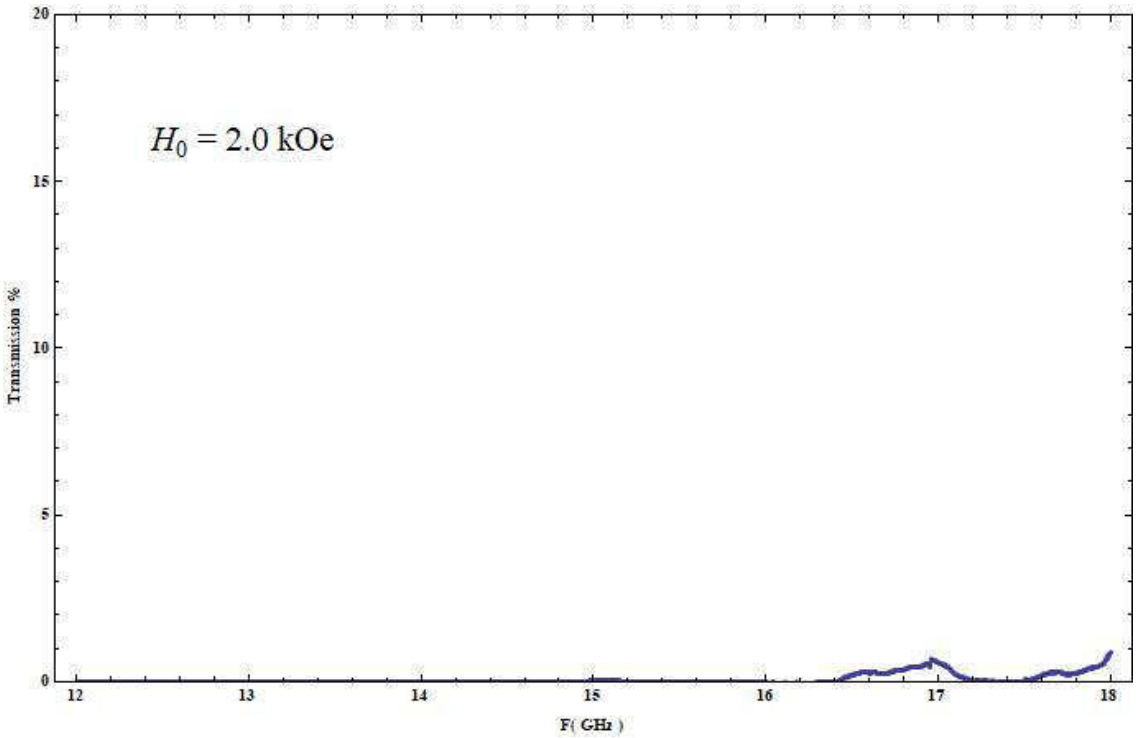

Fig. 4.7.55 Transmission vs. Frequency for $H_0 = 2.0$ kOe

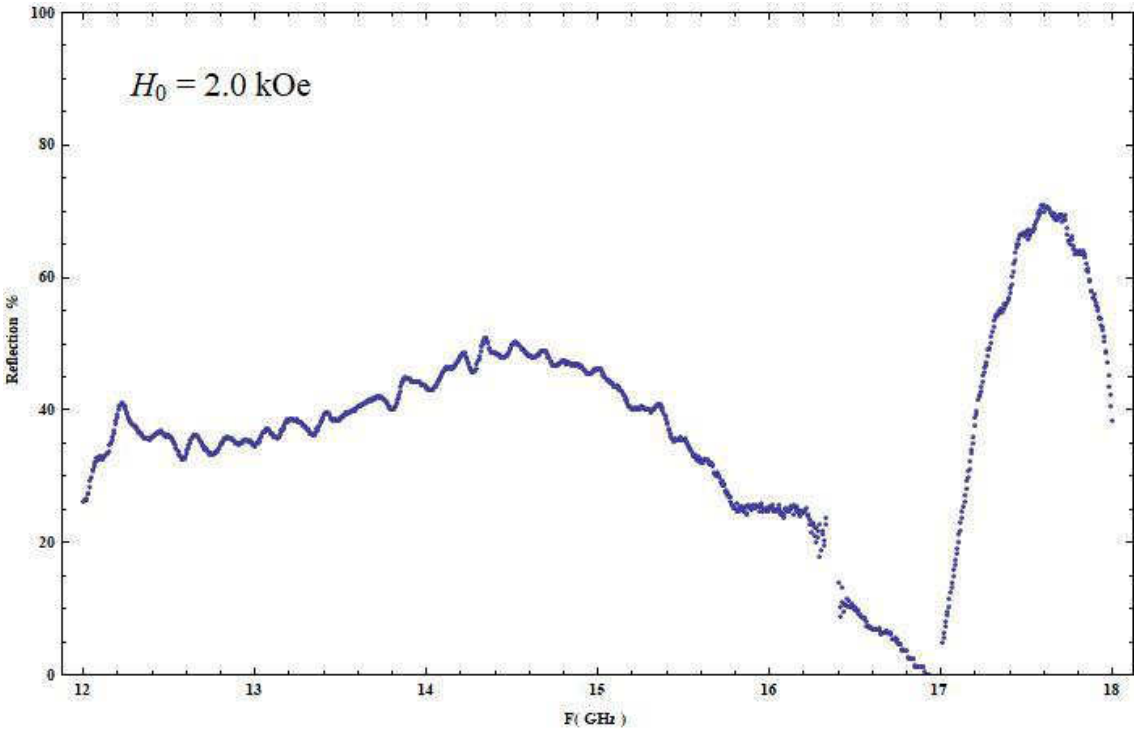

Fig. 4.7.56 Reflection vs. Frequency for $H_0 = 2.0$ kOe

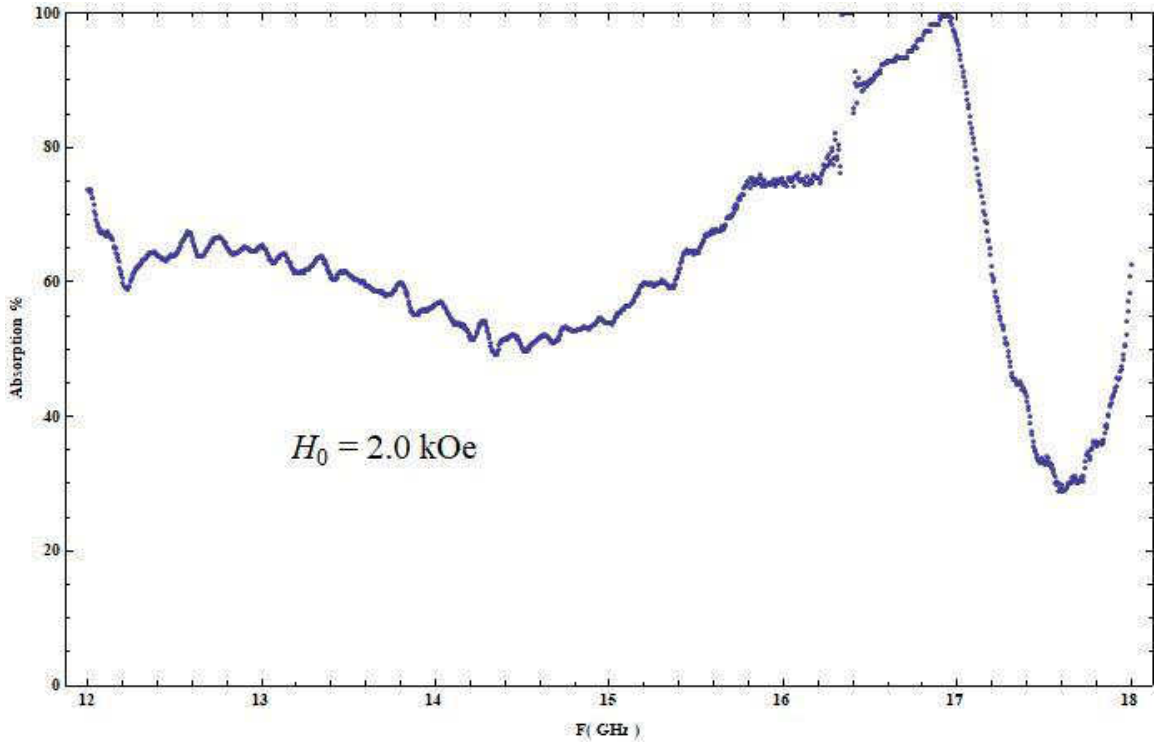

Fig. 4.7.57 Absorption vs. Frequency for $H_0 = 2.0$ kOe

Resonance-Anti-Resonance Frequency: 12.84→21.18 GHz

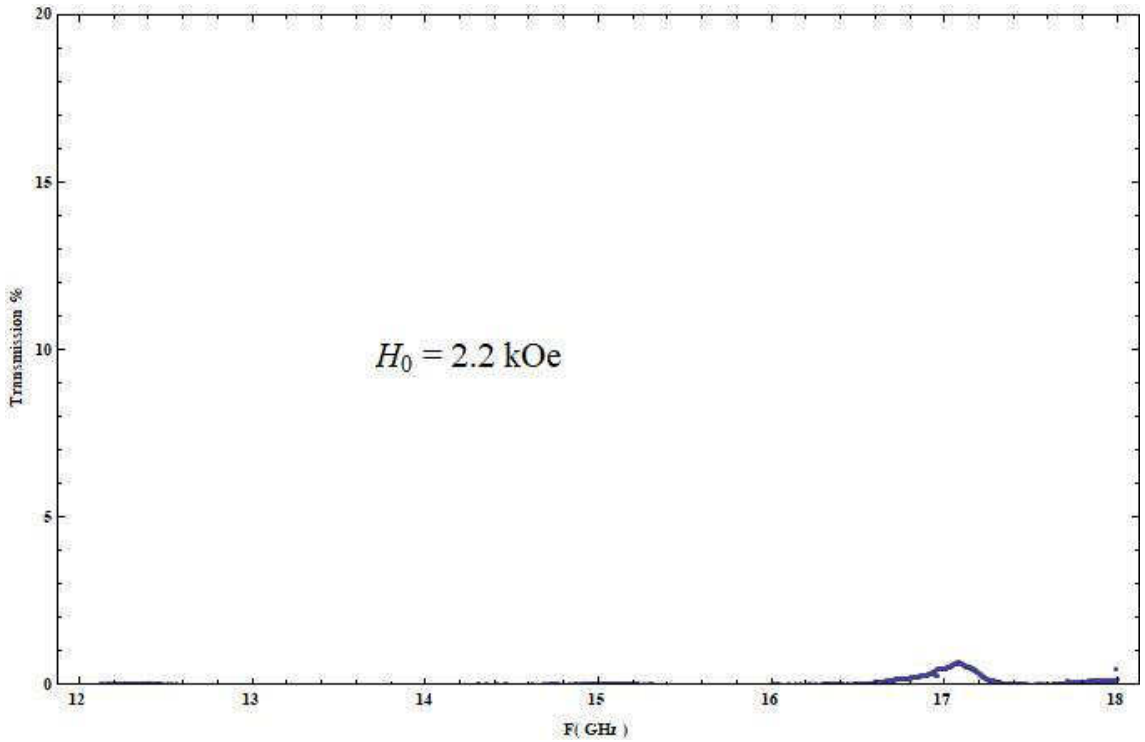

Fig. 4.7.58 Transmission vs. Frequency for $H_0 = 2.2$ kOe

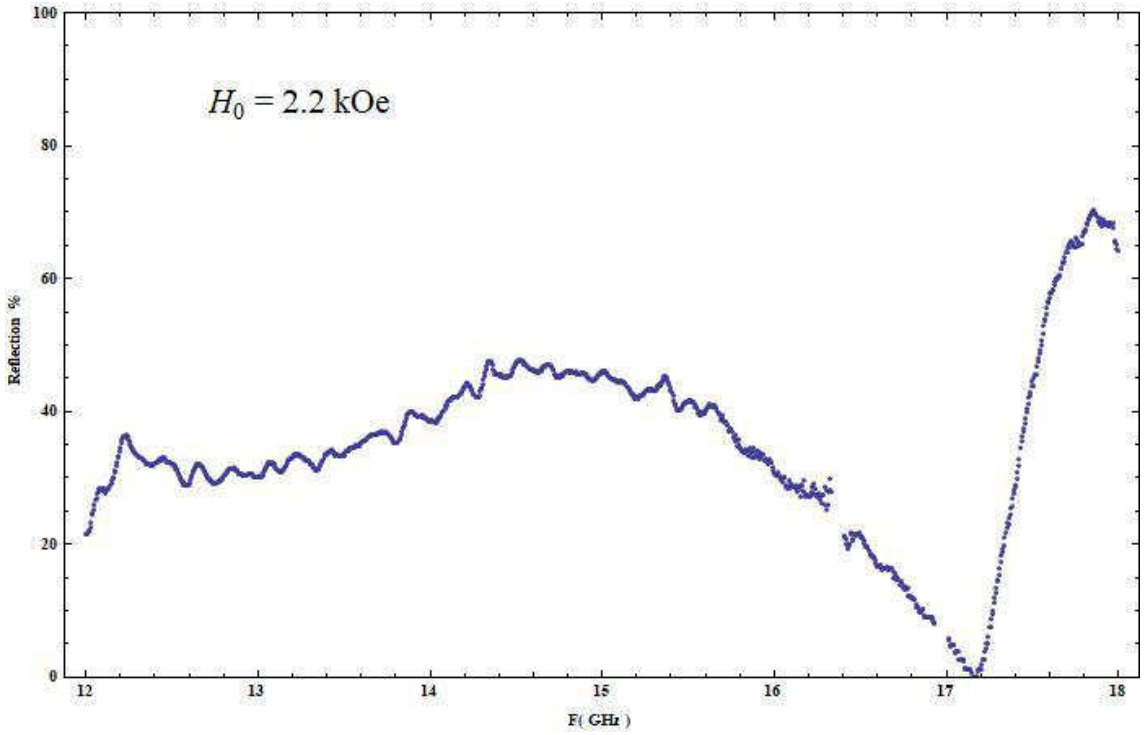

Fig. 4.7.59 Reflection vs. Frequency for $H_0 = 2.2$ kOe

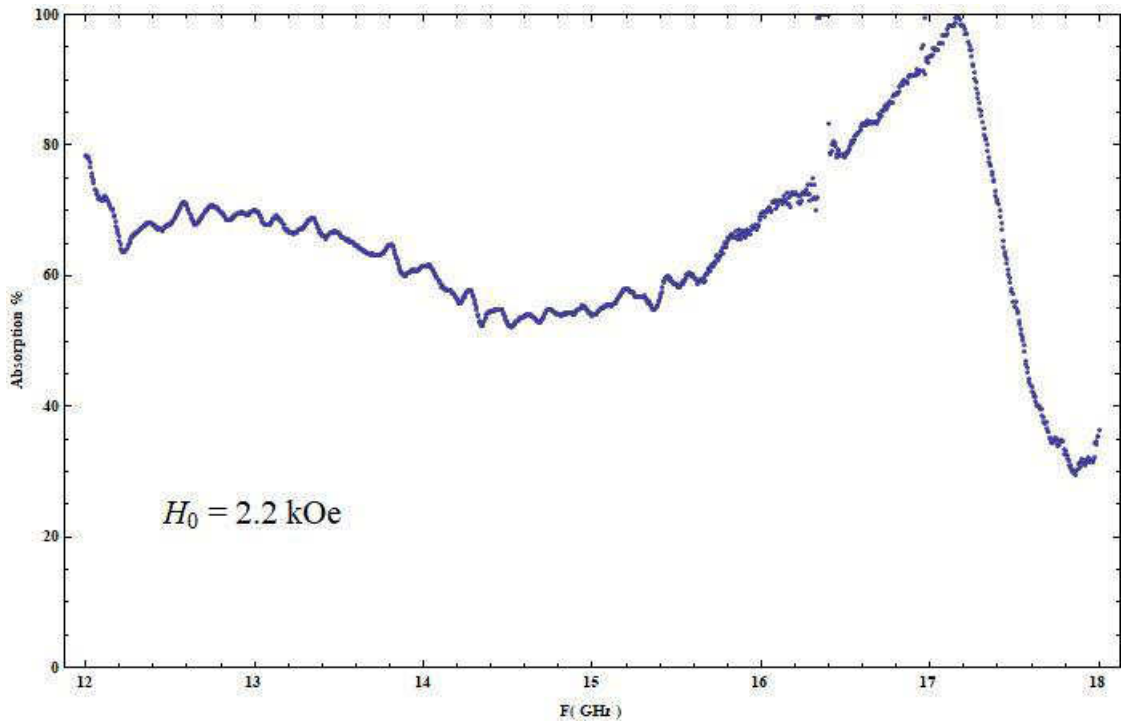

Fig. 4.7.60 Absorption vs. Frequency for $H_0 = 2.2$ kOe

Resonance-Anti-Resonance Frequency: 13.47→21.74 GHz

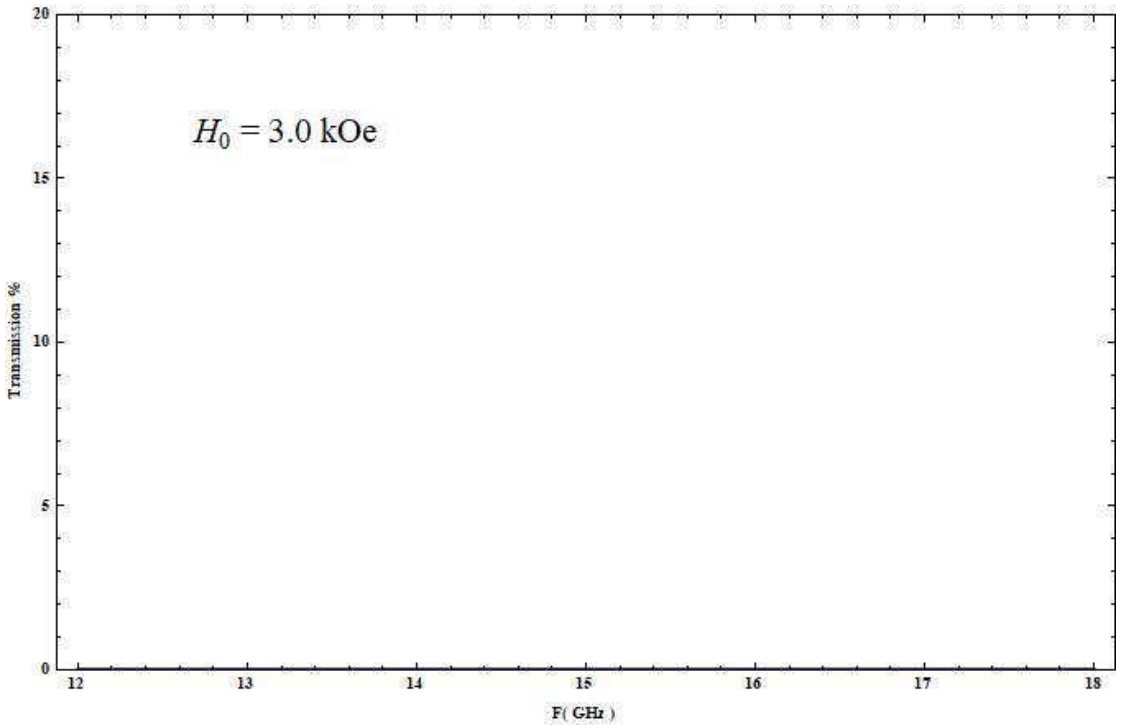

Fig. 4.7.61 Transmission vs. Frequency for $H_0 = 3.0$ kOe

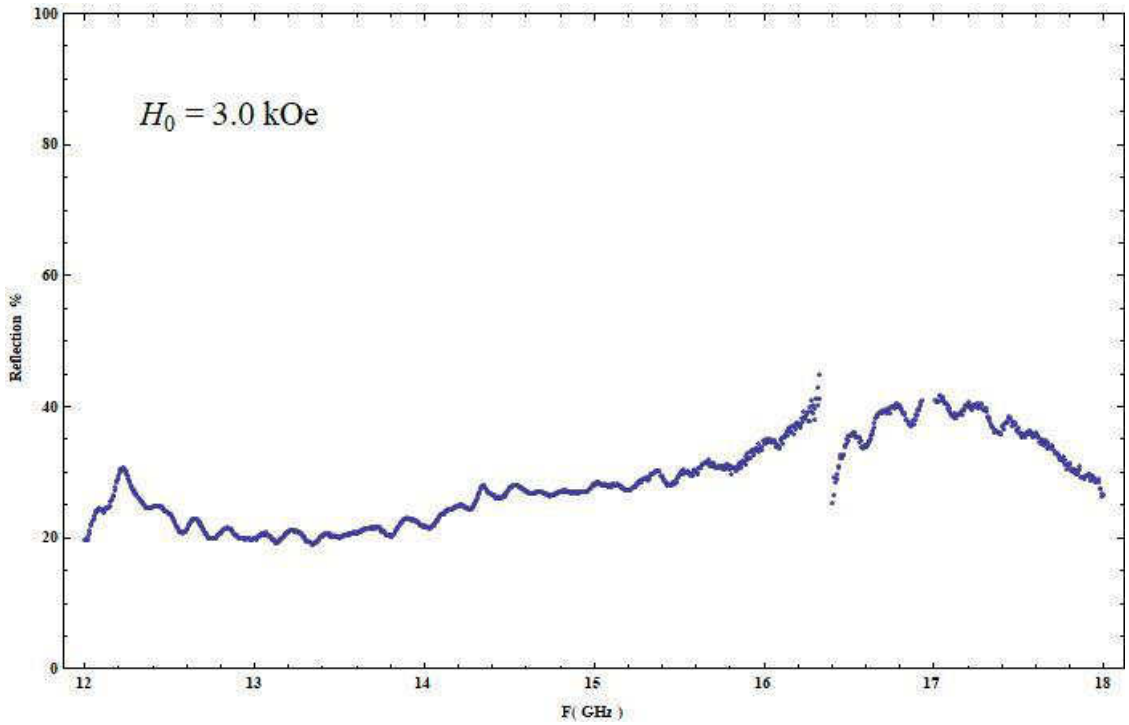

Fig. 4.7.62 Reflection vs. Frequency for $H_0 = 3.0$ kOe

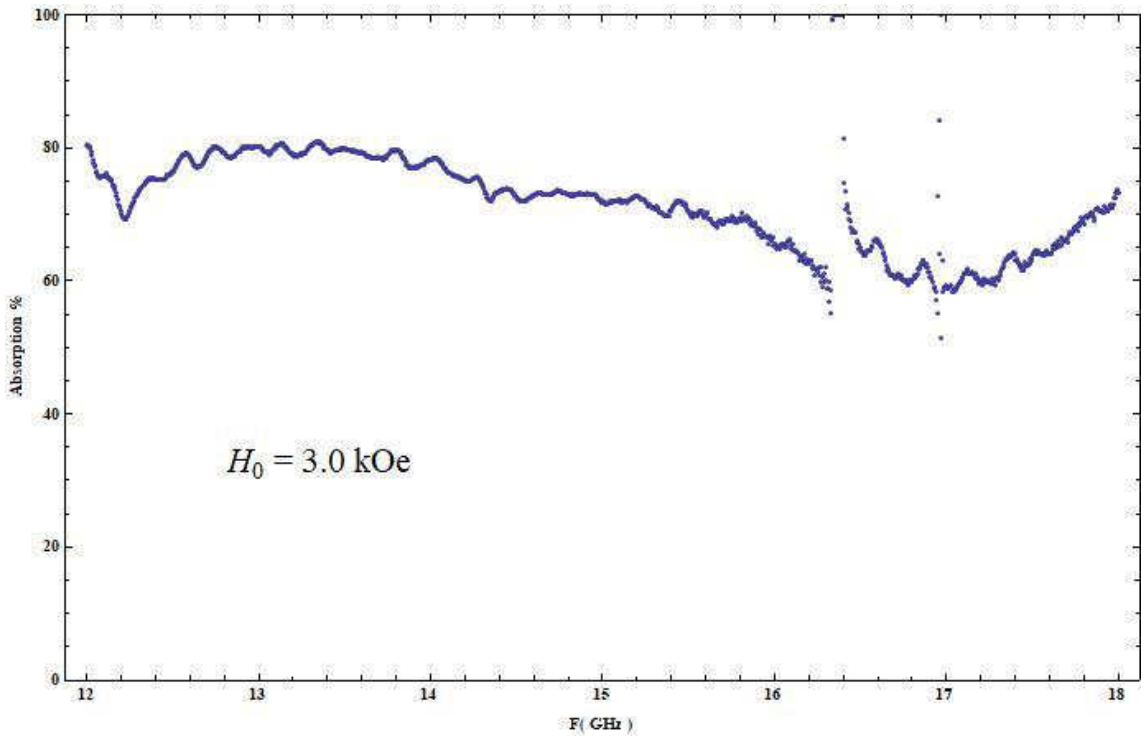

Fig. 4.7.63 Absorption vs. Frequency for $H_0 = 3.0$ kOe

Resonance-Anti-Resonance Frequency: 15.93→23.98 GHz

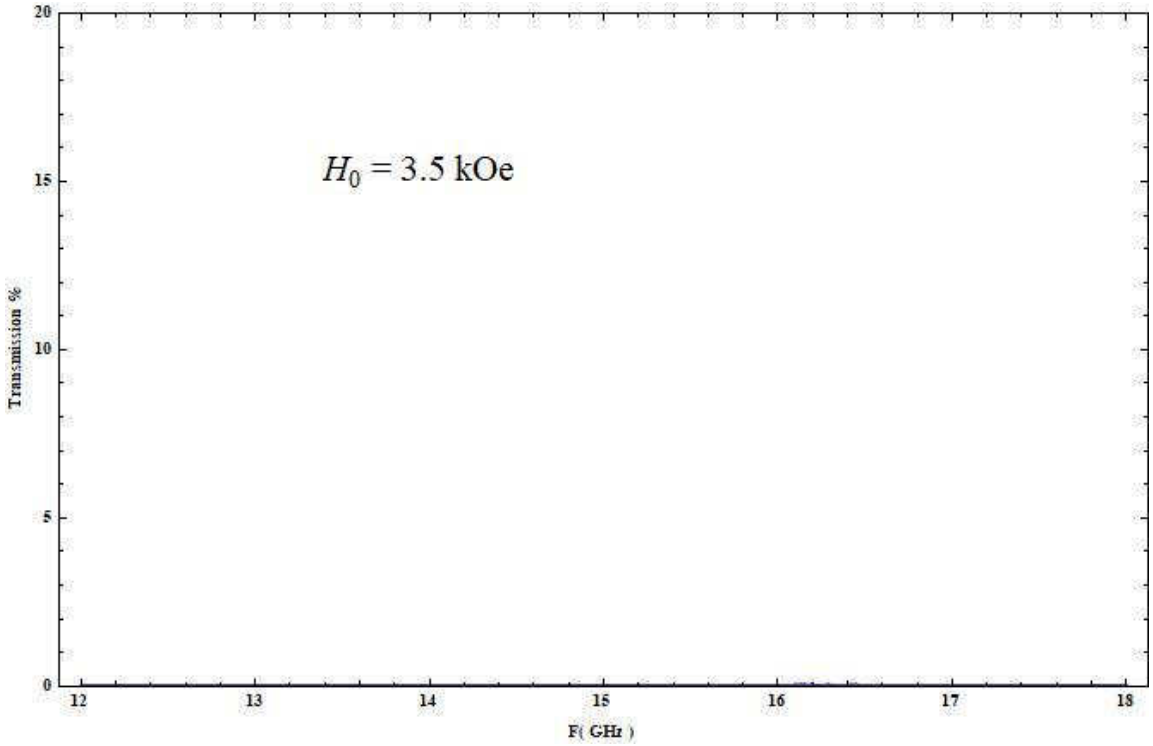

Fig. 4.7. 64 Transmission vs. Frequency for $H_0 = 3.5$ kOe

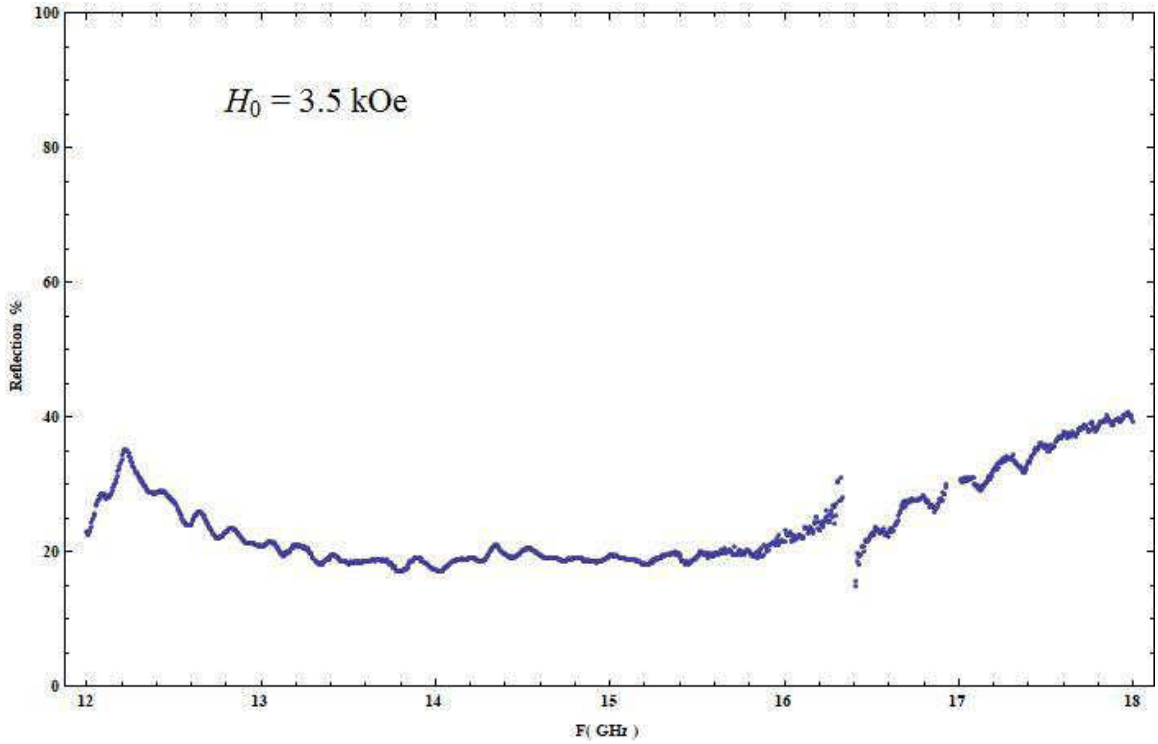

Fig. 4.7. 65 Reflection vs. Frequency for $H_0 = 3.5$ kOe

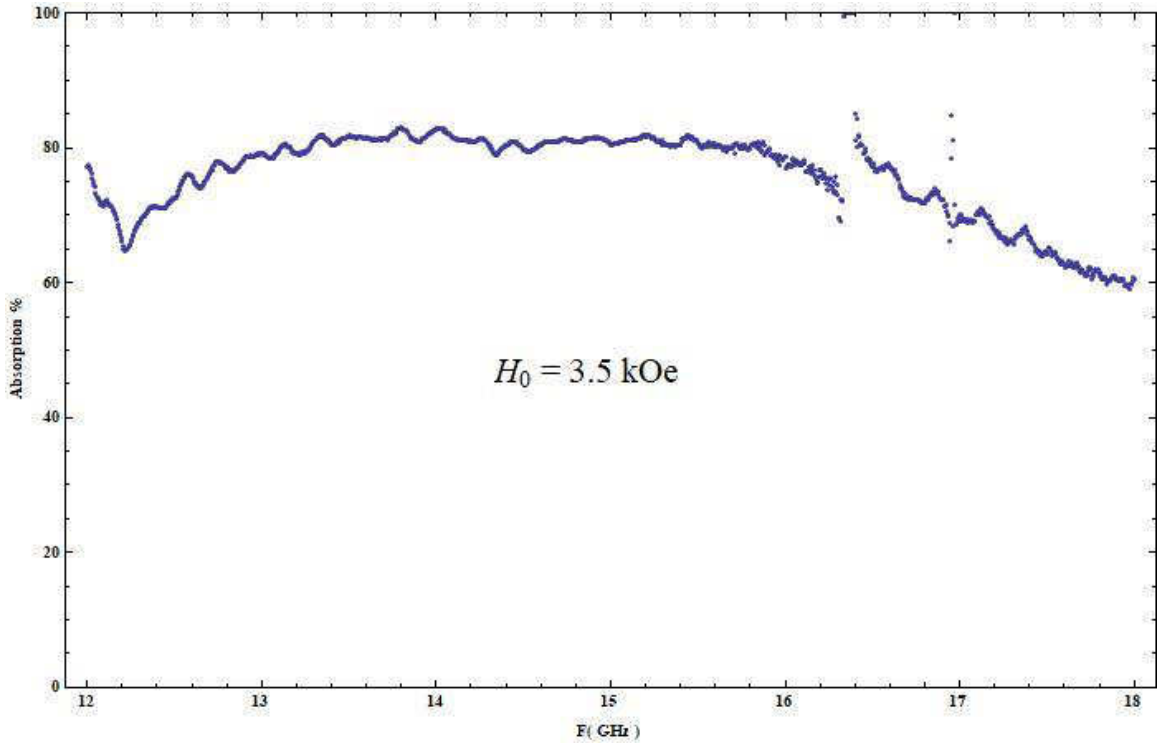

Fig. 4.7.66 Absorption vs. Frequency for $H_0 = 3.5$ kOe

Resonance-Anti-Resonance Frequency: 17.44→25.38 GHz

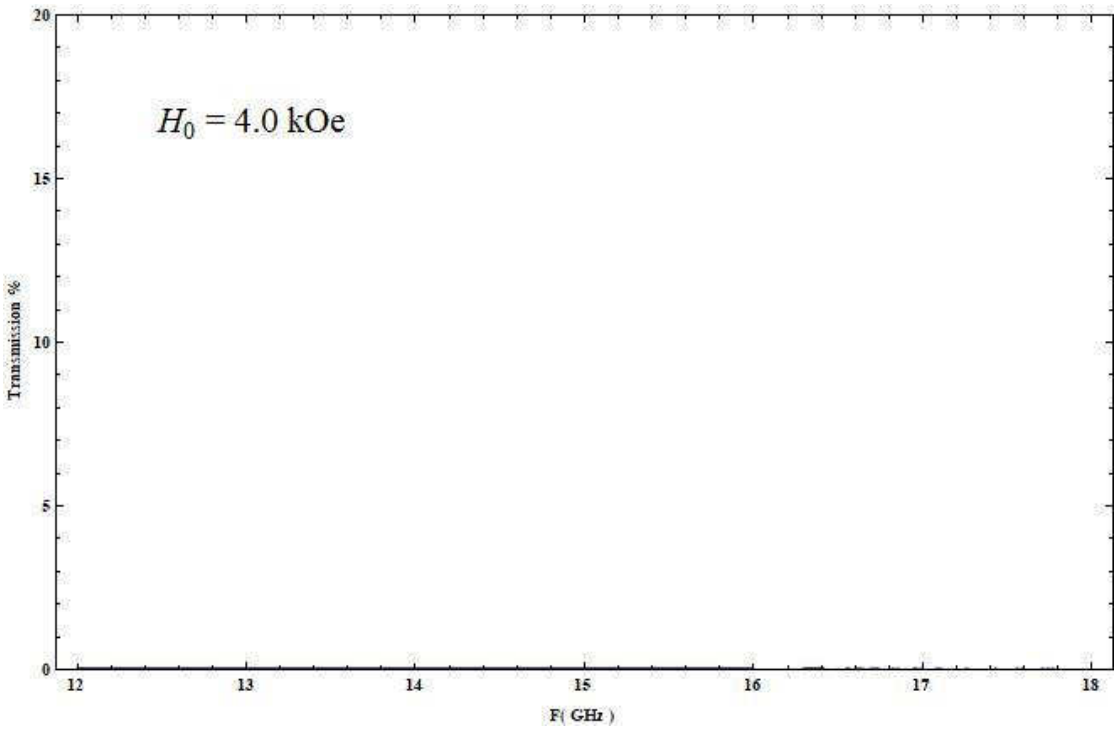

Fig. 4.7.67 Transmission vs. Frequency for $H_0 = 4.0$ kOe

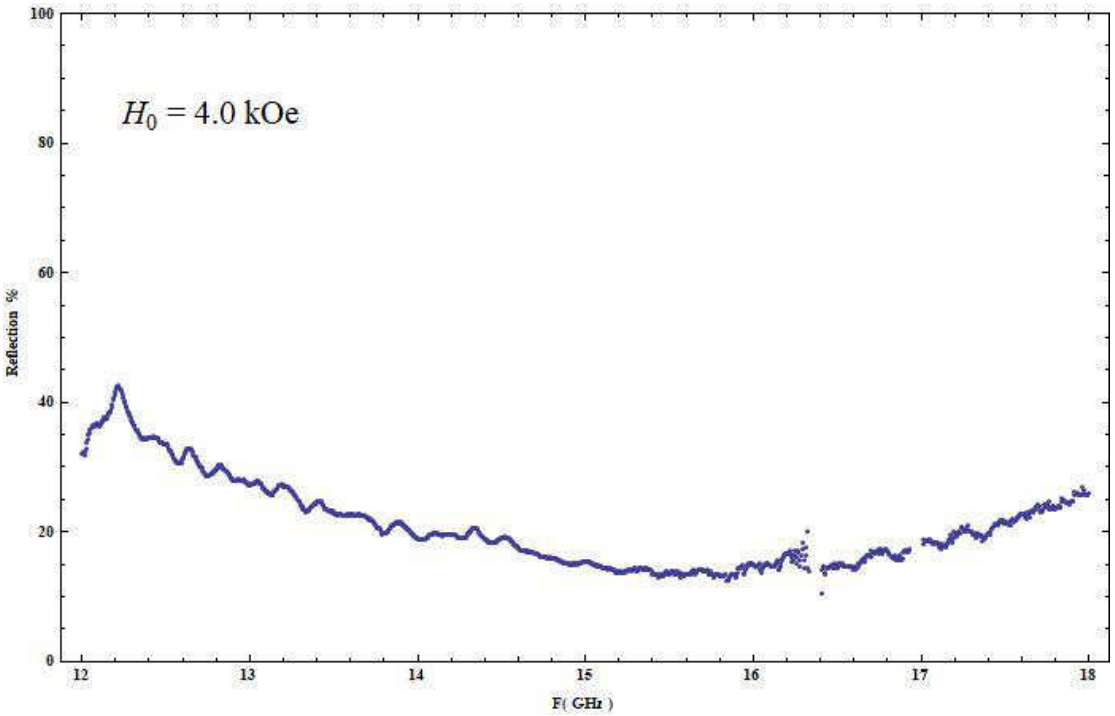

Fig. 4.7.68 Reflection vs. Frequency for $H_0 = 4.0$ kOe

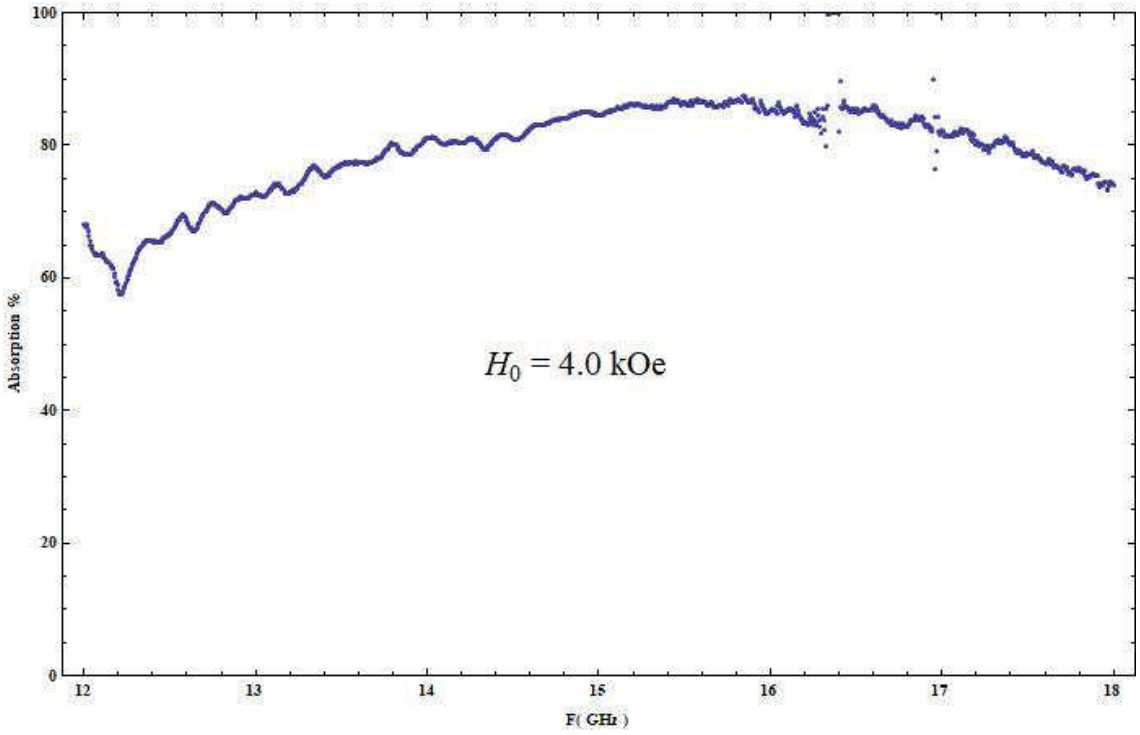

Fig. 4.7.69 Absorption vs. Frequency for $H_0 = 4.0$ kOe

Resonance-Anti-Resonance Frequency: 18.93→26.78 GHz

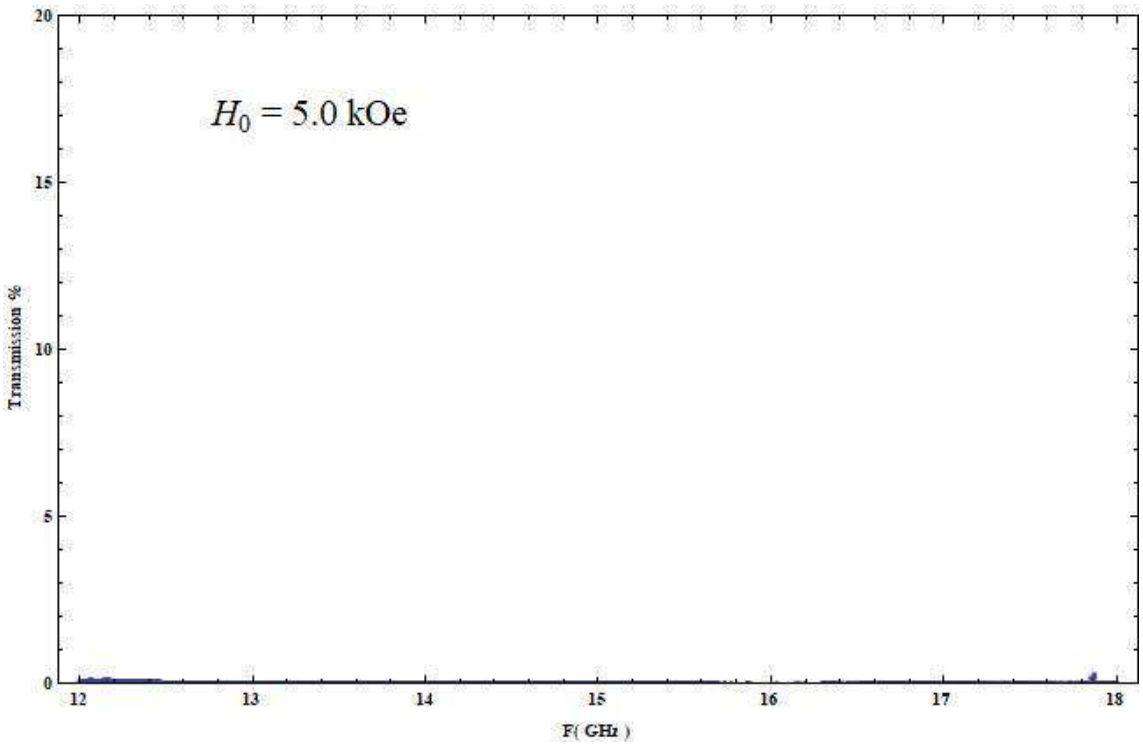

Fig. 4.7.70 Transmission vs. Frequency for $H_0 = 5.0$kOe

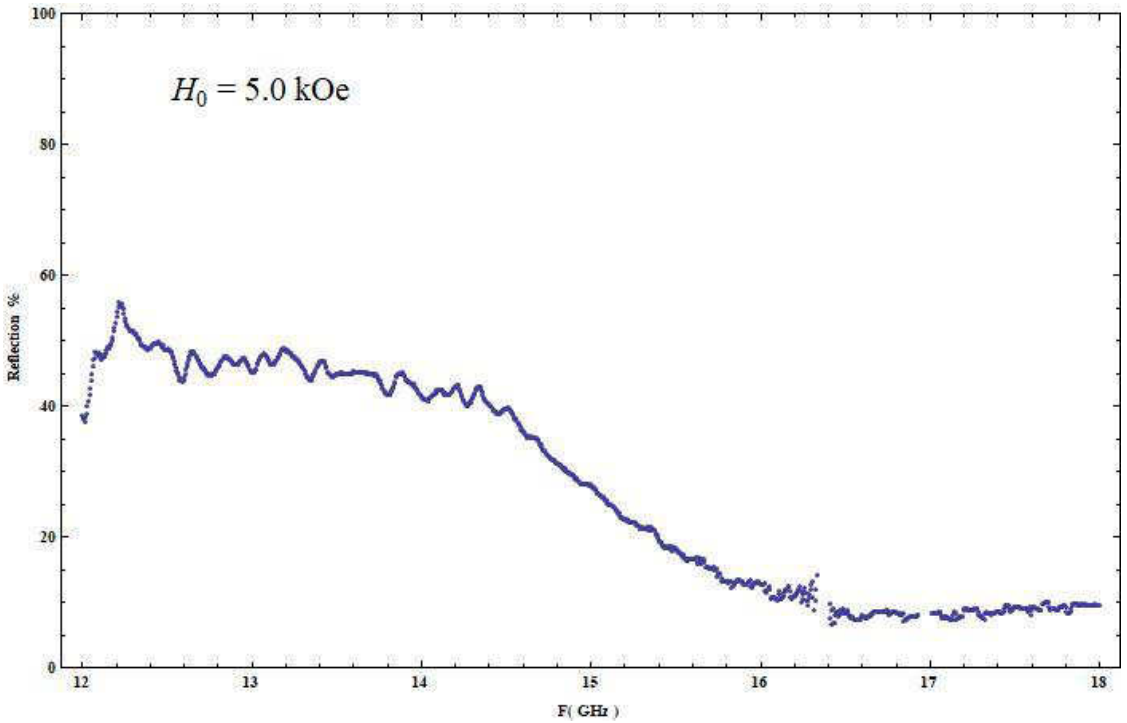

Fig. 4.7.71 Reflection vs. Frequency for $H_0 = 5.0$ kOe

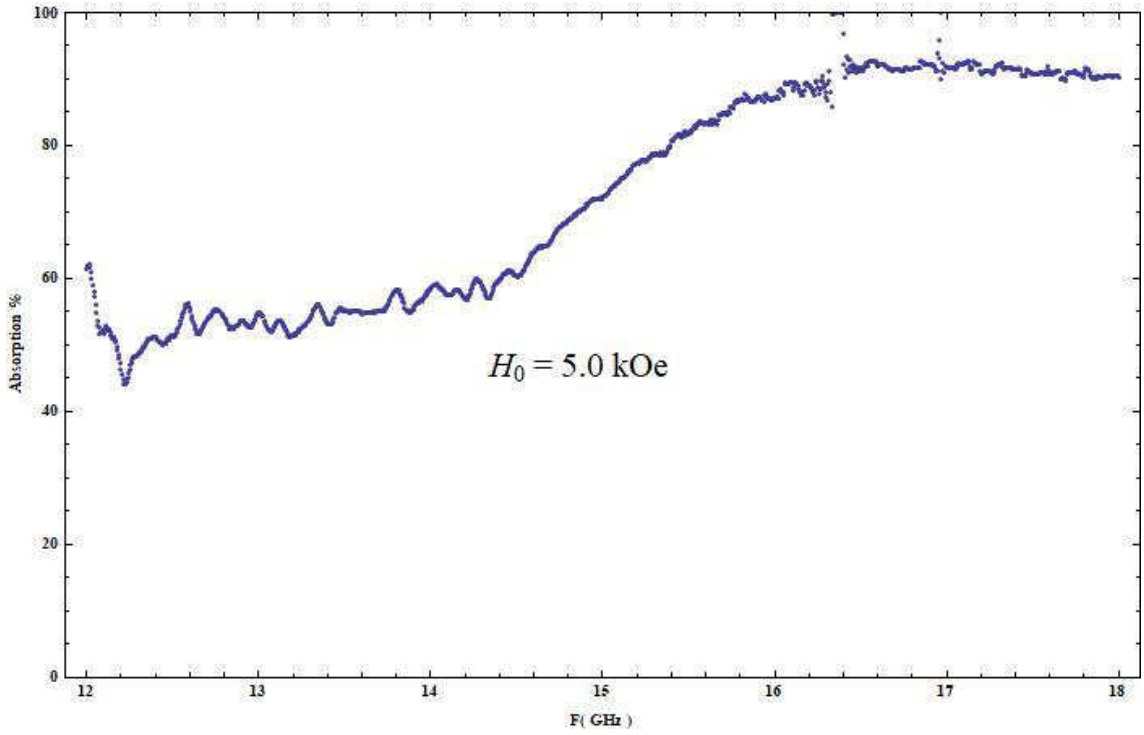

Fig. 4.7.72 Absorption vs. Frequency for $H_0 = 5.0$ kOe

Resonance-Anti-Resonance Frequency: 21.88→29.58 GHz

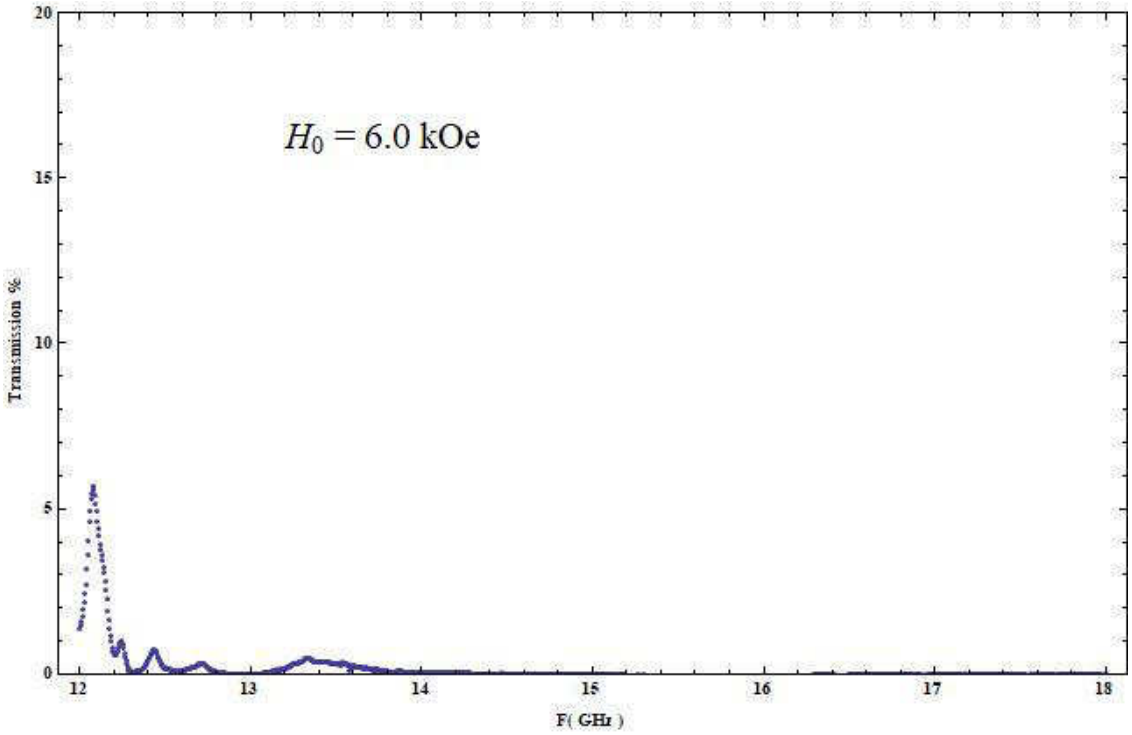

Fig. 4.7.73 Transmission vs. Frequency for $H_0 = 6.0$ kOe

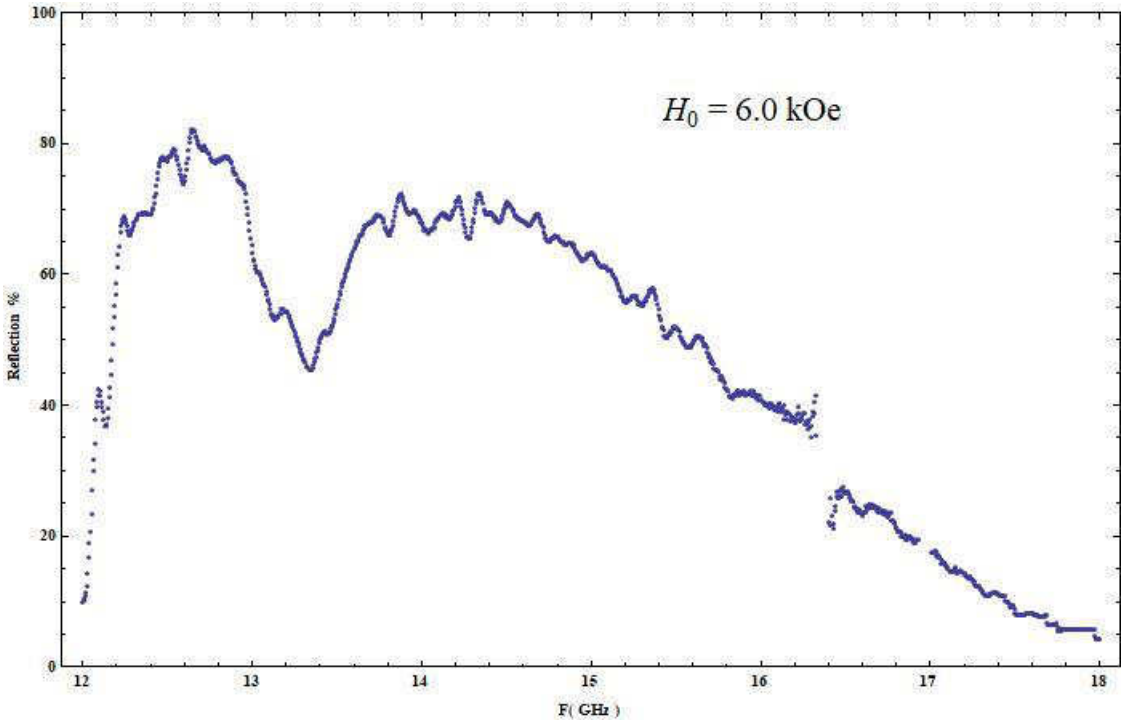

Fig. 4.7.74 Reflection vs. Frequency for $H_0 = 6.0$ kOe

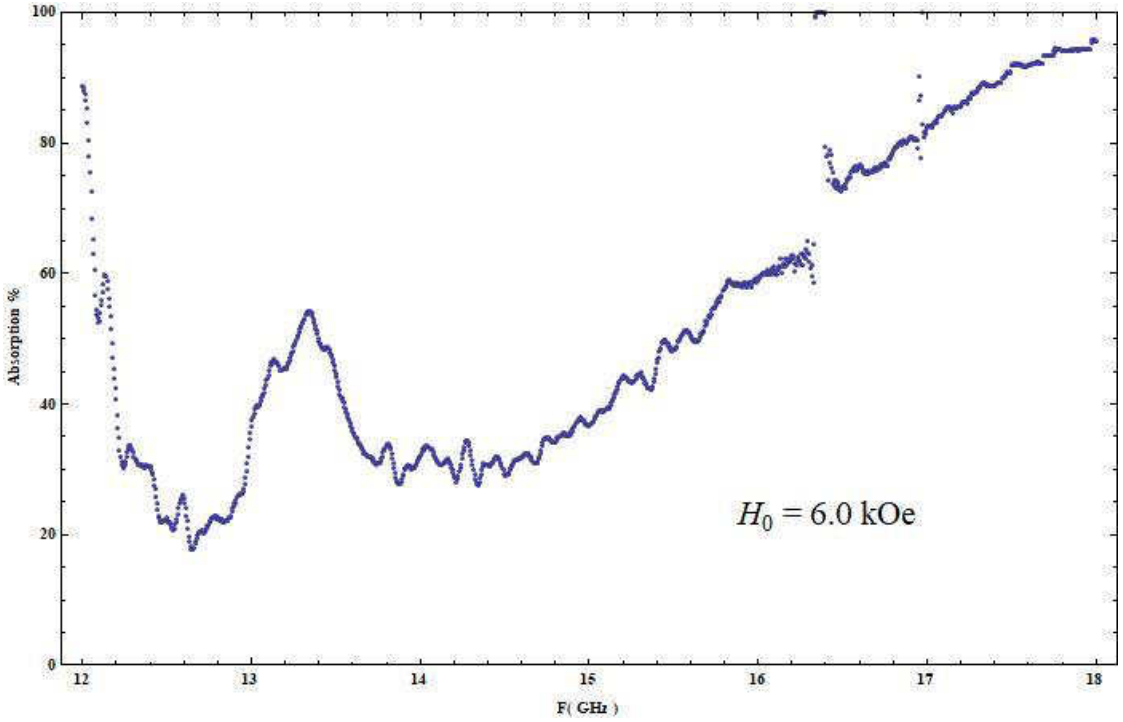

Fig. 4.7.75 Absorption vs. Frequency for $H_0 = 6.0$ kOe

Resonance-Anti-Resonance Frequency: 24.80→32.38 GHz

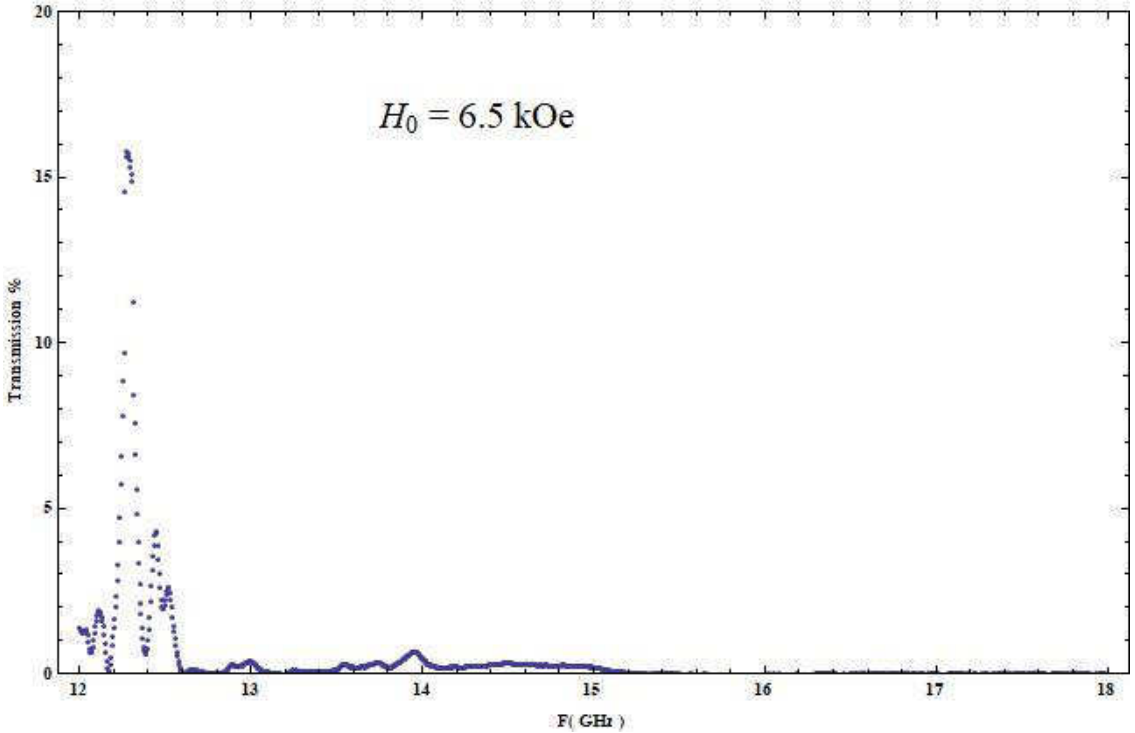

Fig. 4.7.76 Transmission vs. Frequency for $H_0 = 6.5$ kOe

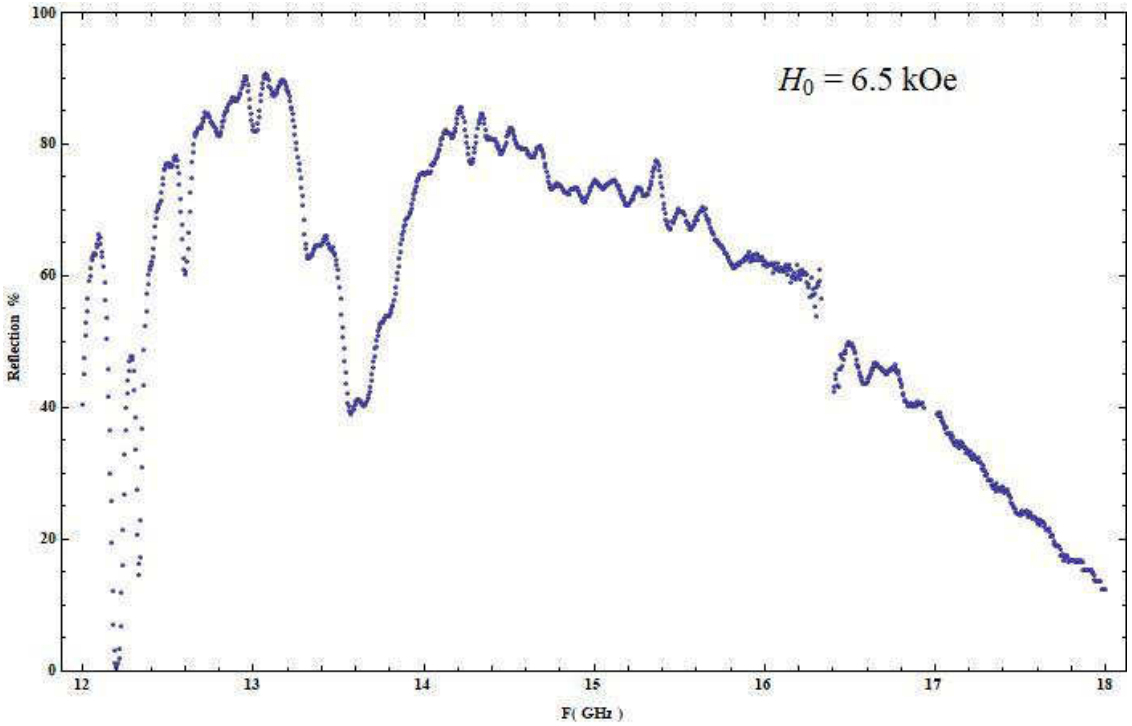

Fig. 4.7.77 Reflection vs. Frequency for $H_0 = 6.5$ kOe

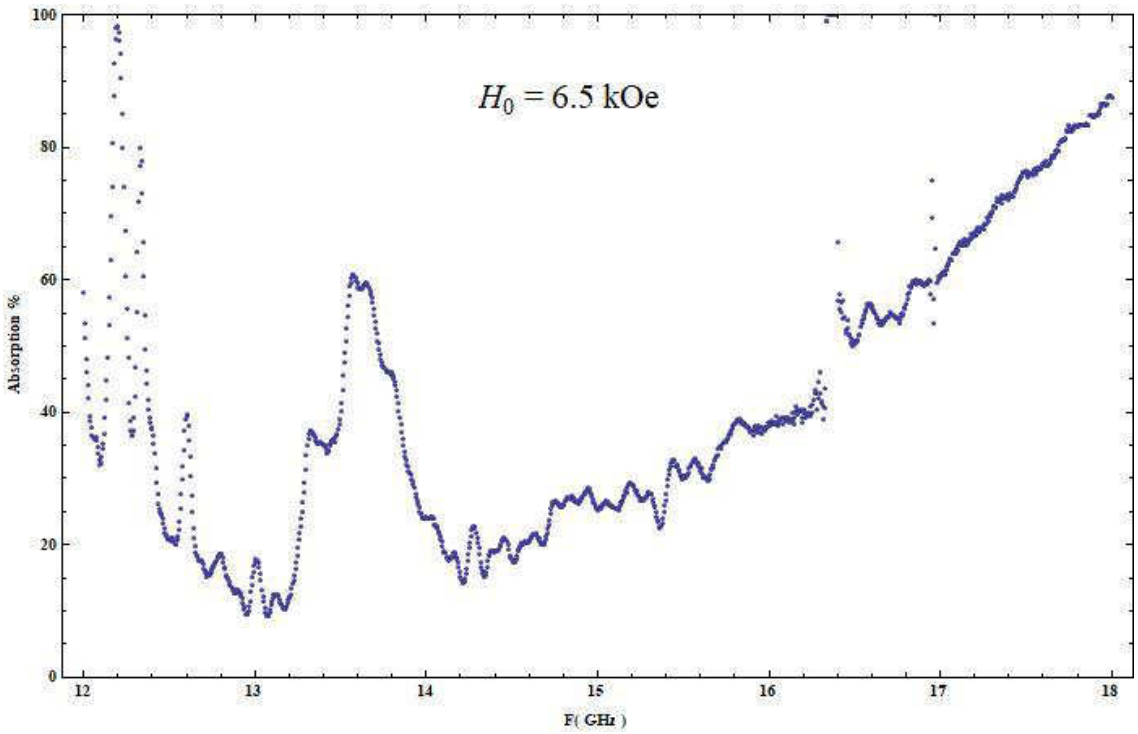

Fig. 4.7.78 Absorption vs. Frequency for $H_0 = 6.5$ kOe

Resonance-Anti-Resonance Frequency: 26.25→33.79 GHz

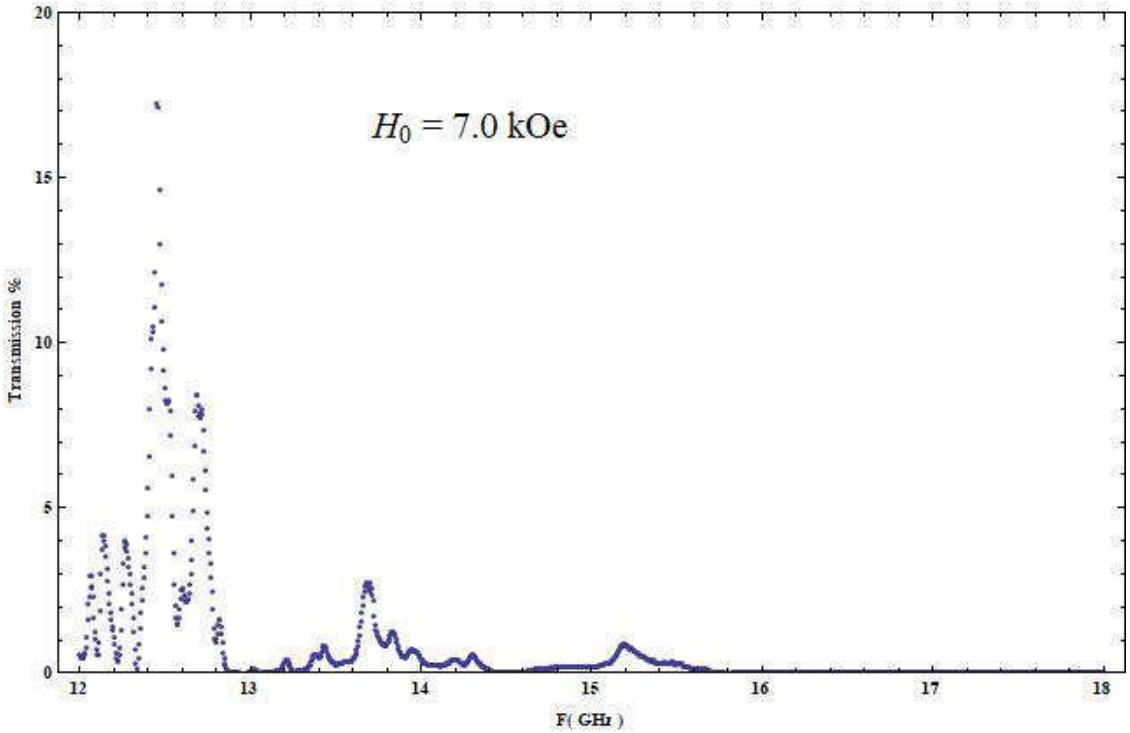

Fig. 4.7.79 Transmission vs. Frequency for $H_0 = 7.0$kOe

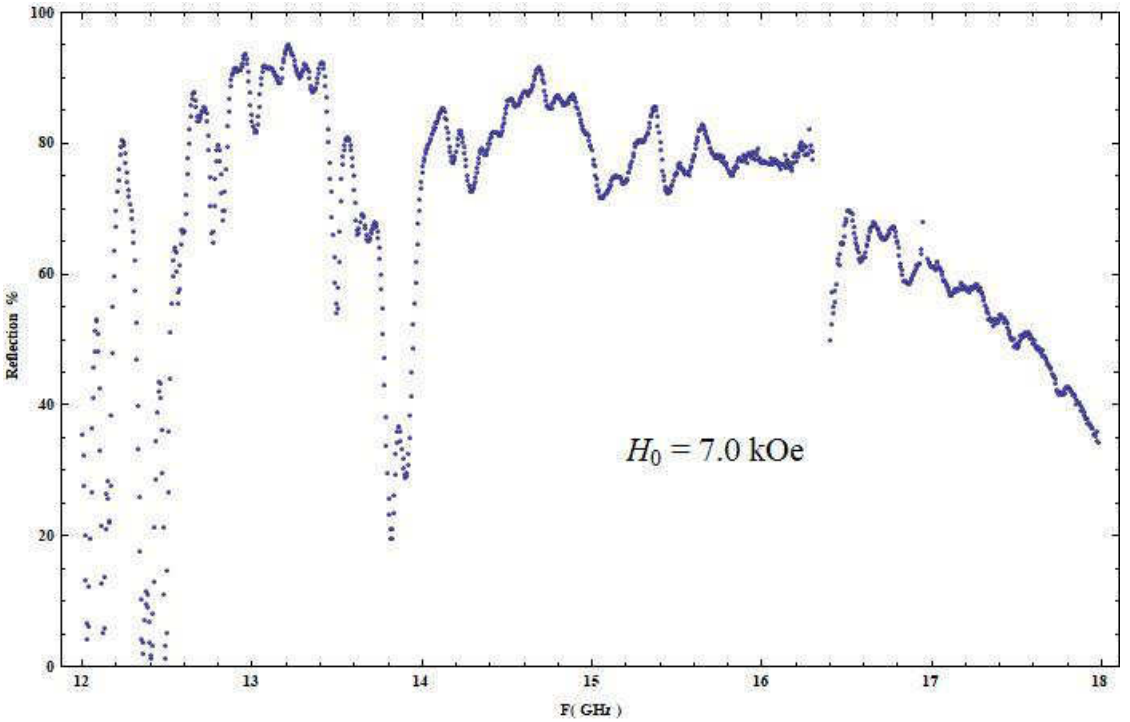

Fig. 4.7.80 Reflection vs. Frequency for $H_0 = 7.0$ kOe

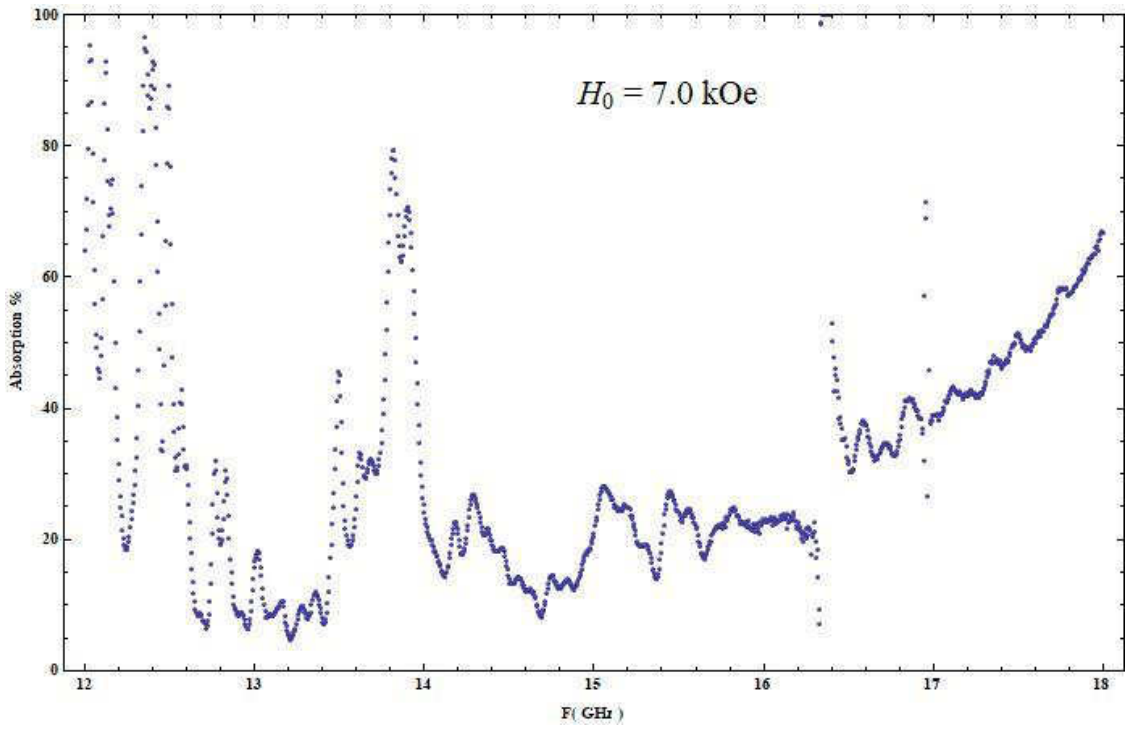

Fig. 4.7.81 Absorption vs. Frequency for $H_0 = 7.0$ kOe

Resonance-Anti-Resonance Frequency: 27.69→35.19 GHz

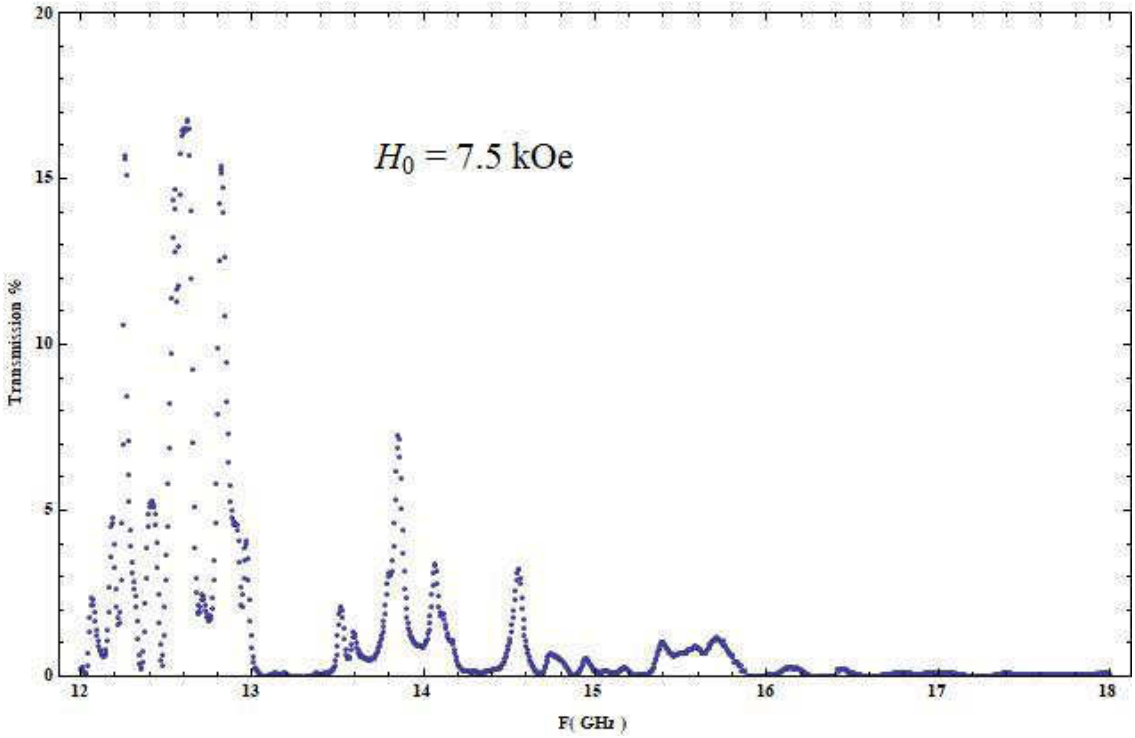

Fig. 4.7.82 Transmission vs. Frequency for $H_0 = 7.5$ kOe

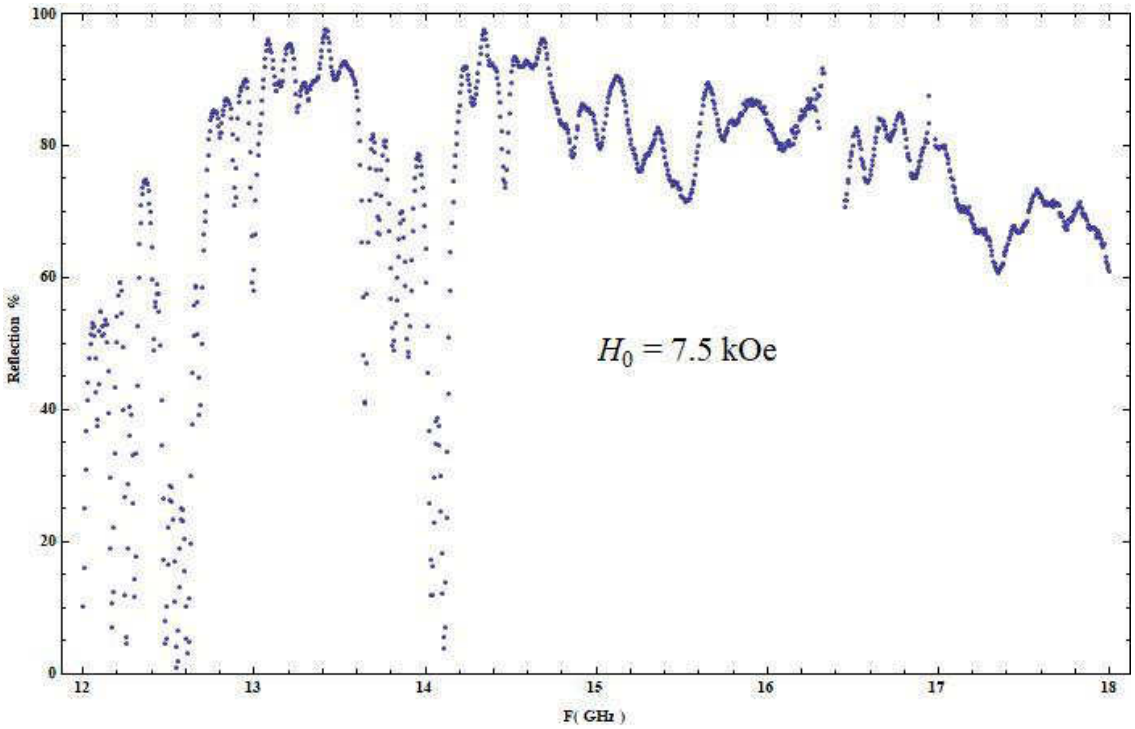

Fig. 4.7.83 Reflection vs. Frequency for $H_0 = 7.5$ kOe

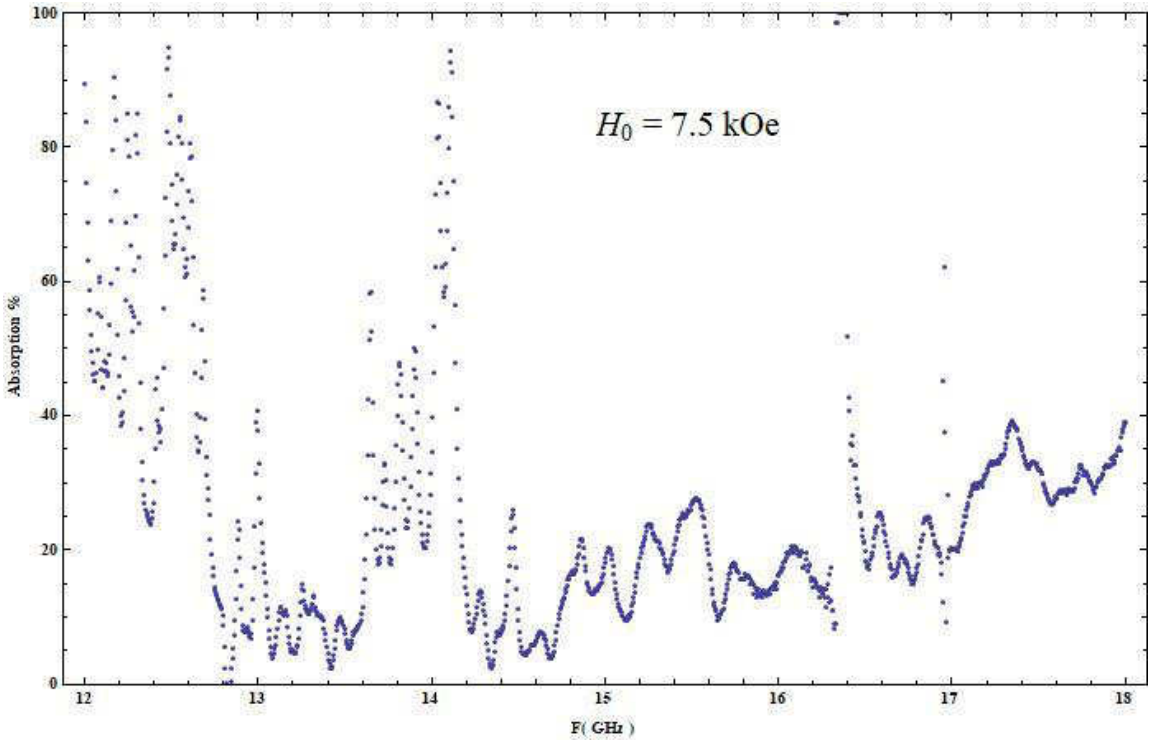

Fig. 4.7.84 Absorption vs. Frequency for $H_0 = 7.5$ kOe

Resonance-Anti-Resonance Frequency: 29.13→36.59 GHz

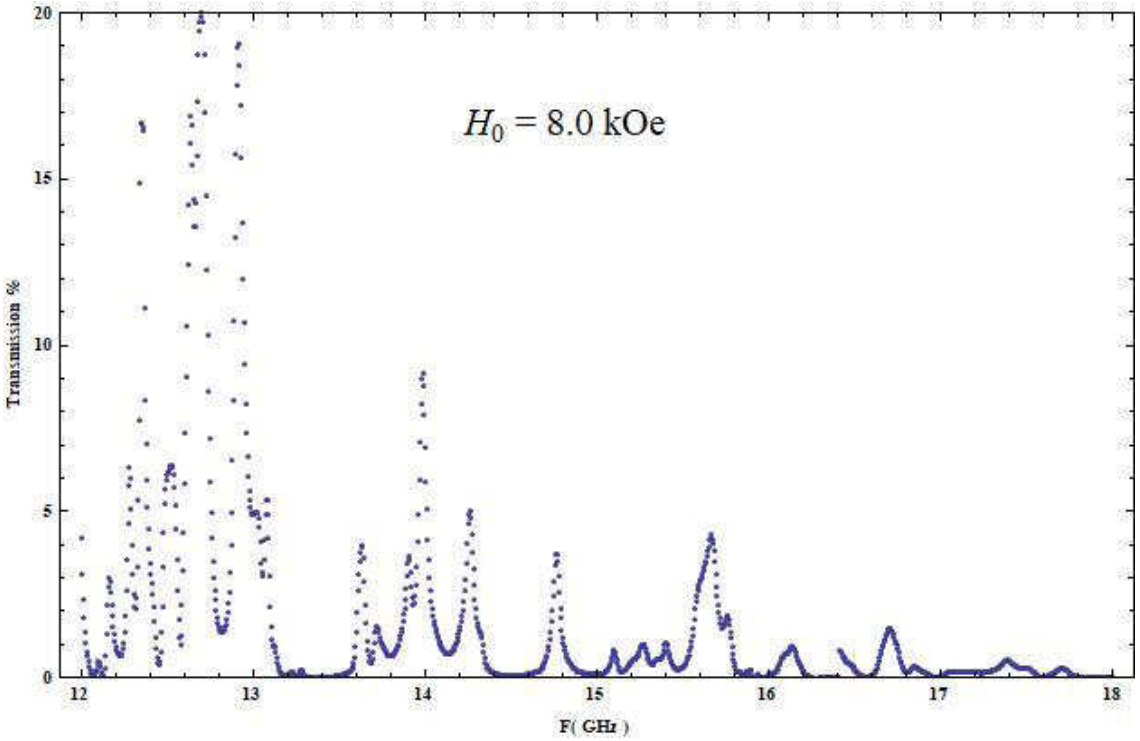

Fig. 4.7.85 Transmission vs. Frequency for $H_0 = 8.0$ kOe

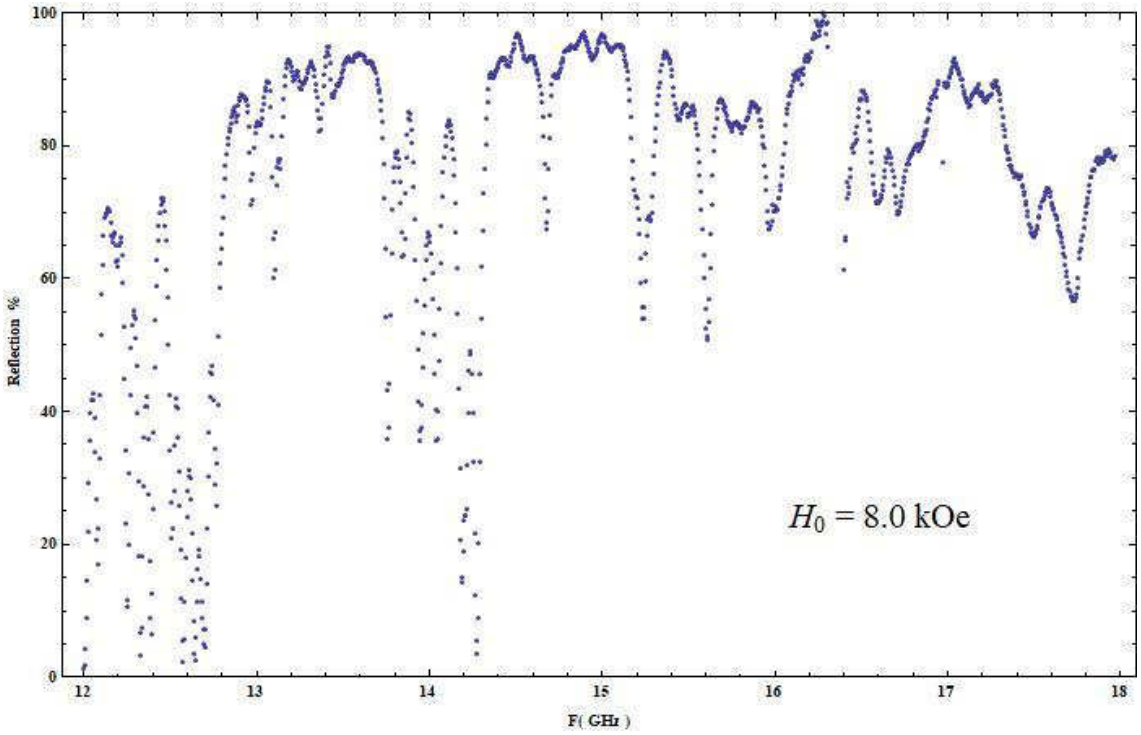

Fig. 4.7.86 Reflection vs. Frequency for $H_0 = 8.0$ kOe

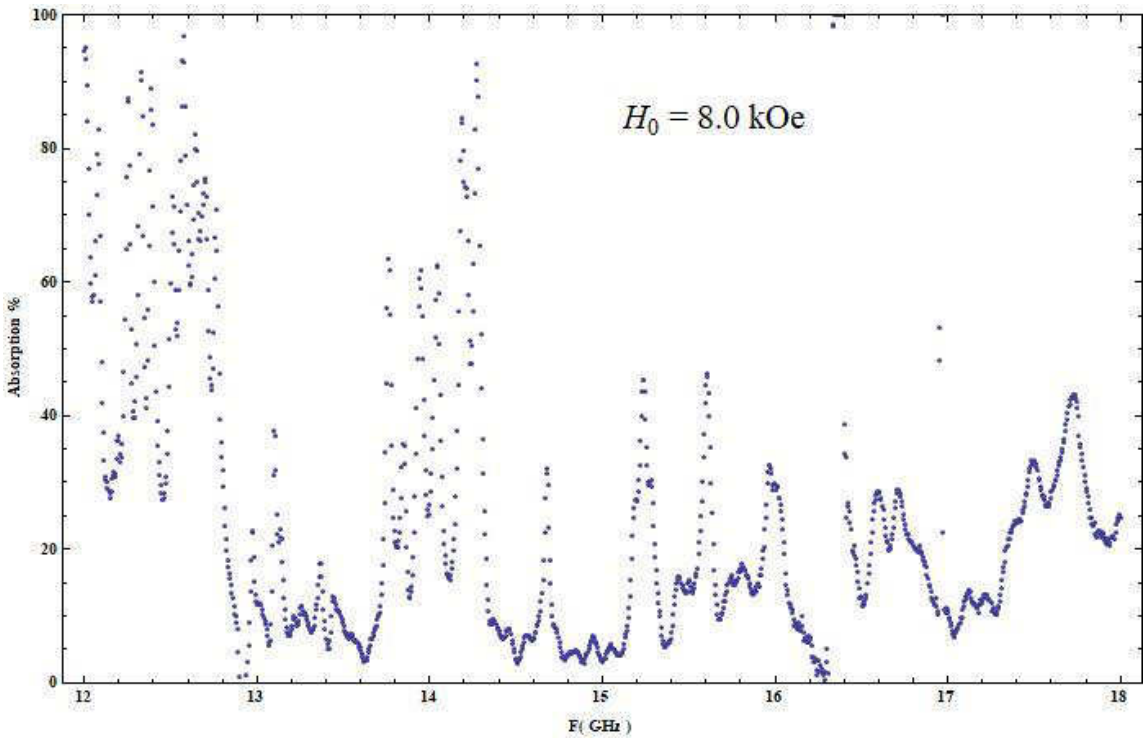

Fig. 4.7.87 Absorption vs. Frequency for $H_0 = 8.0$ kOe

Resonance-Anti-Resonance Frequency: 30.57→38.00 GHz

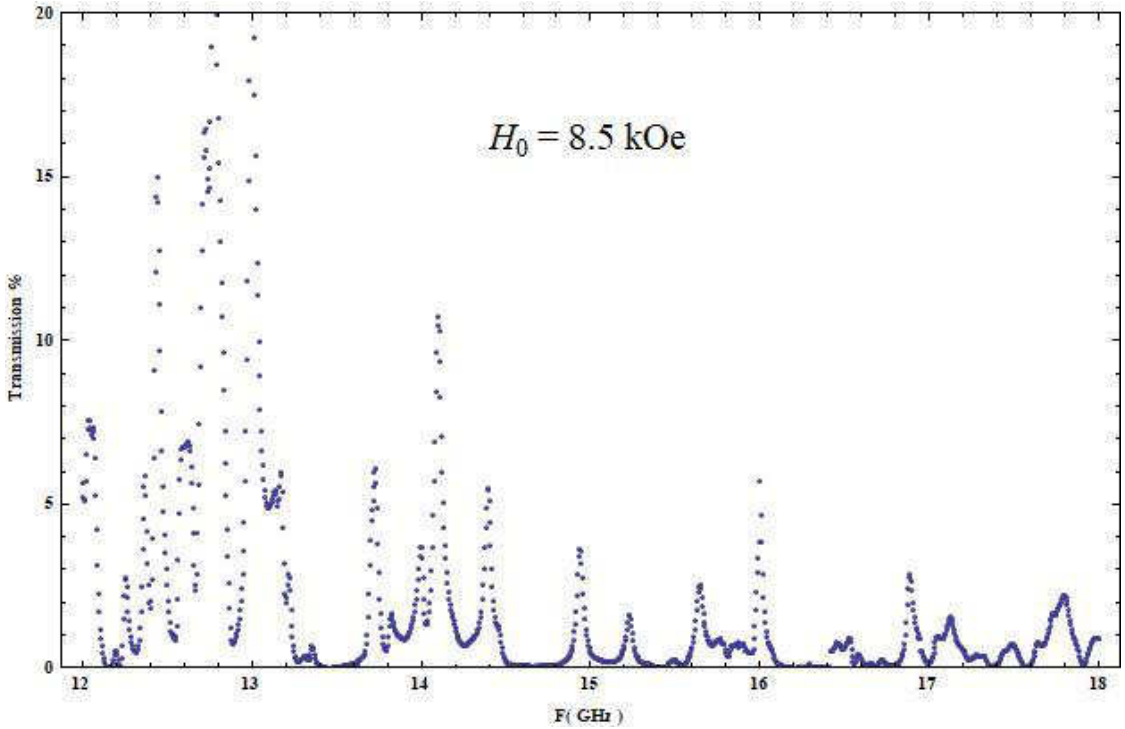

Fig. 4.7.88 Transmission vs. Frequency for $H_0 = 8.5$ kOe

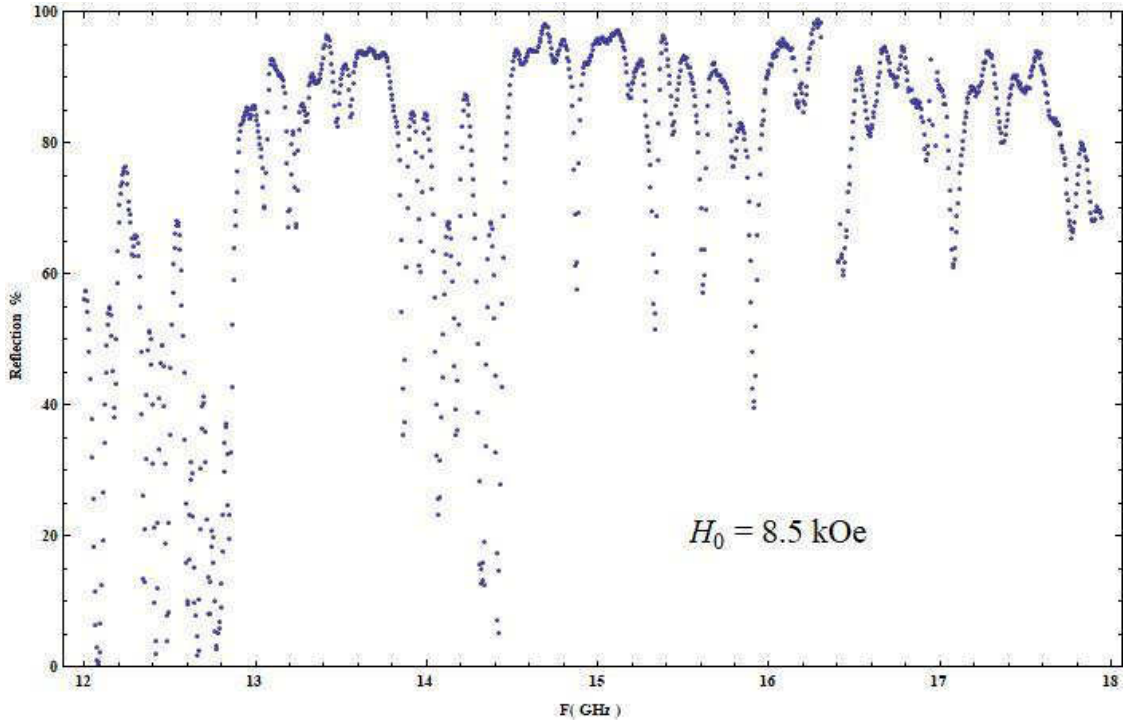

Fig. 4.7.89 Reflection vs. Frequency for $H_0 = 8.5$ kOe

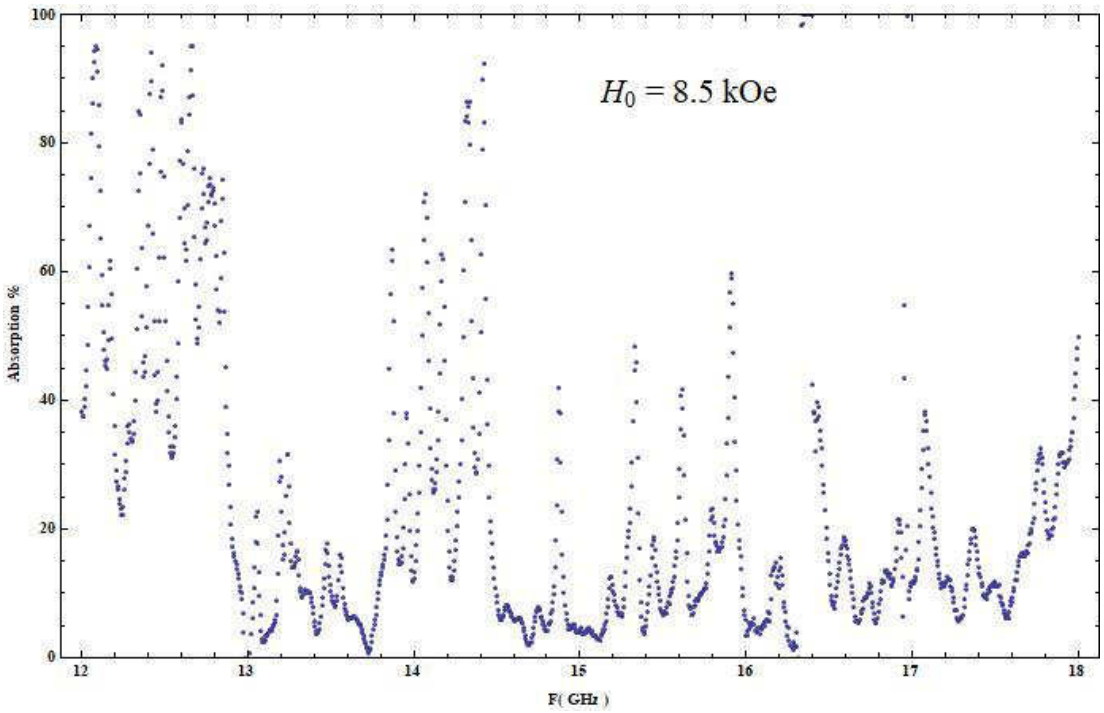

Fig. 4.7.90 Absorption vs. Frequency for $H_0 = 8.5$ kOe

Resonance-Anti-Resonance Frequency: 32.00→39.39 GHz

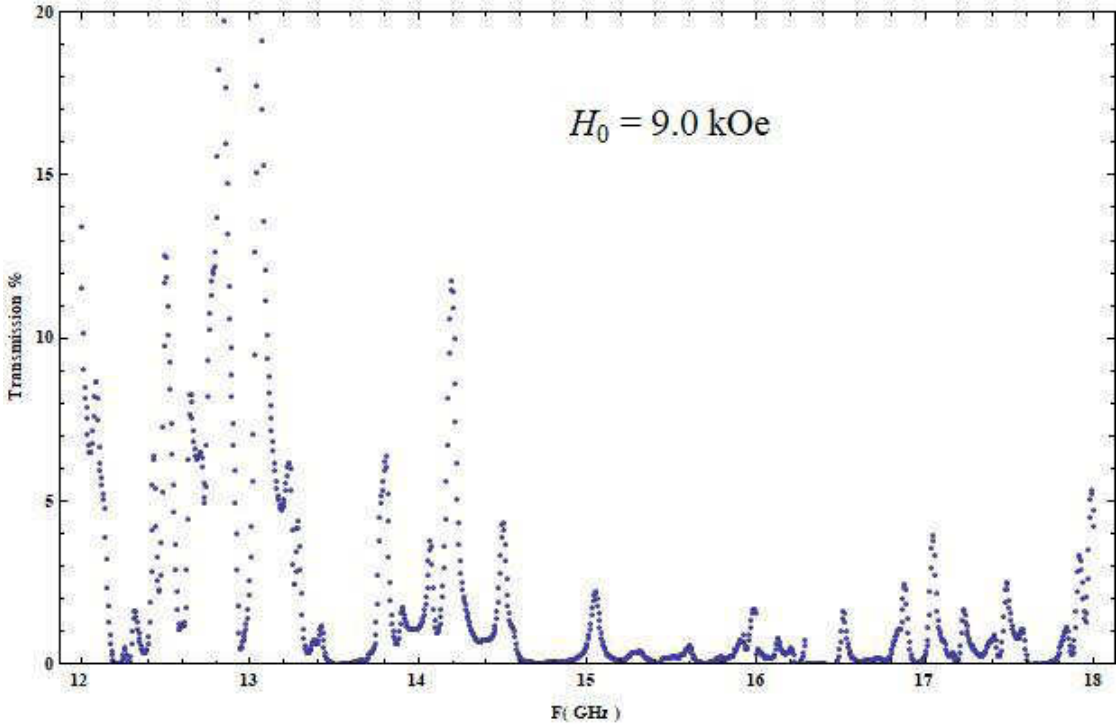

Fig. 4.7.91 Transmission vs. Frequency for $H_0 = 9.0$ kOe

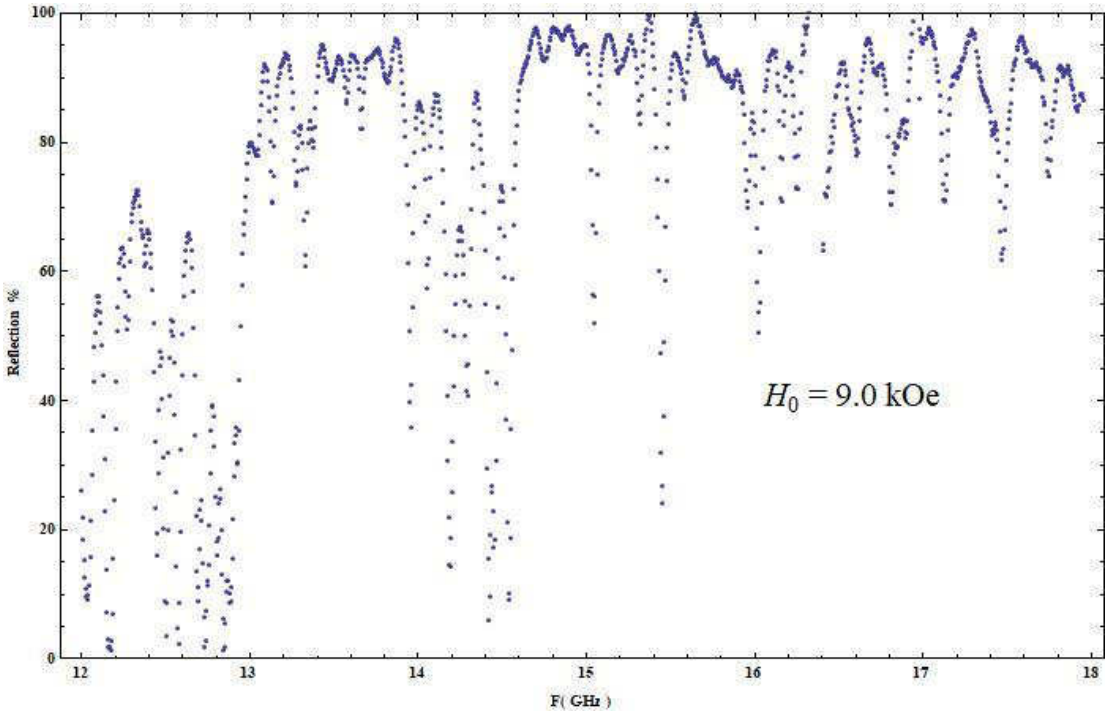

Fig. 4.7.92 Reflection vs. Frequency for $H_0 = 9.0$ kOe

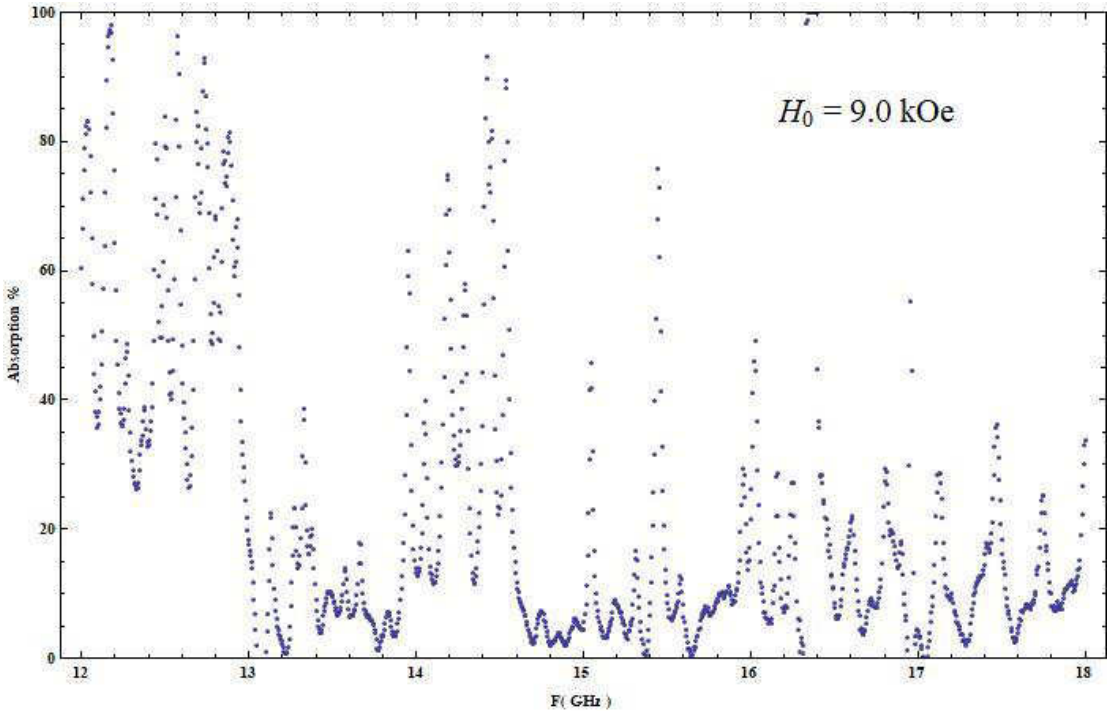

Fig. 4.7.93 Absorption vs. Frequency for $H_0 = 9.0$ kOe

Resonance-Anti-Resonance Frequency: 33.34→40.79 GHz

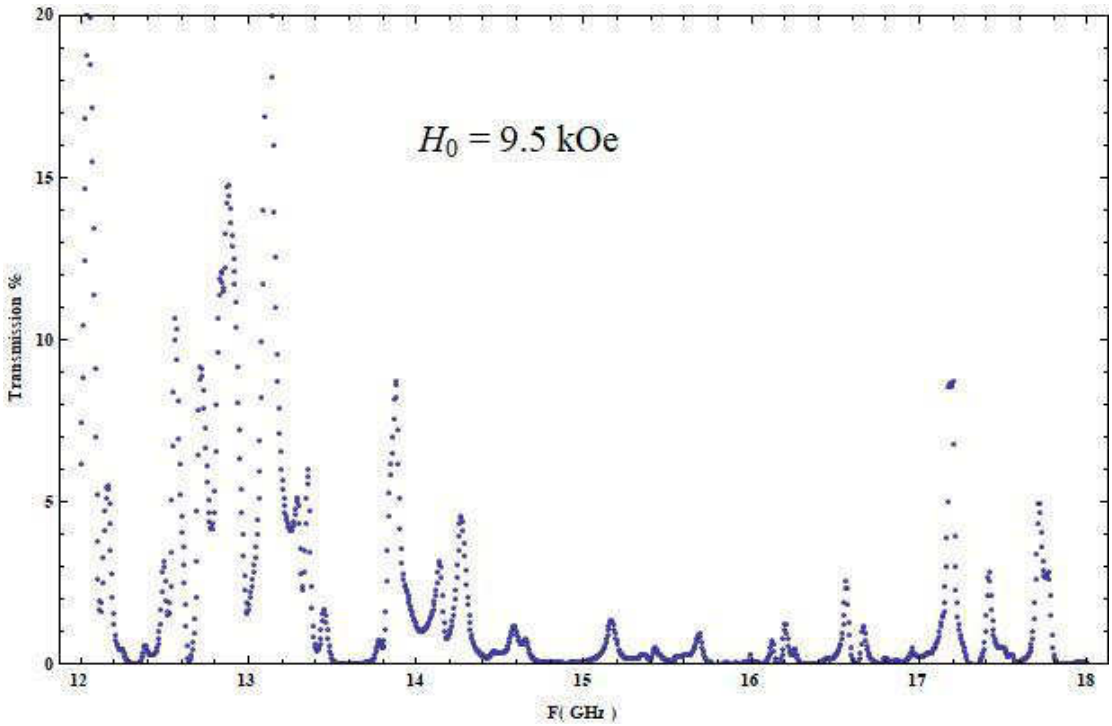

Fig. 4.7.94 Transmission vs. Frequency for $H_0 = 9.5$ kOe

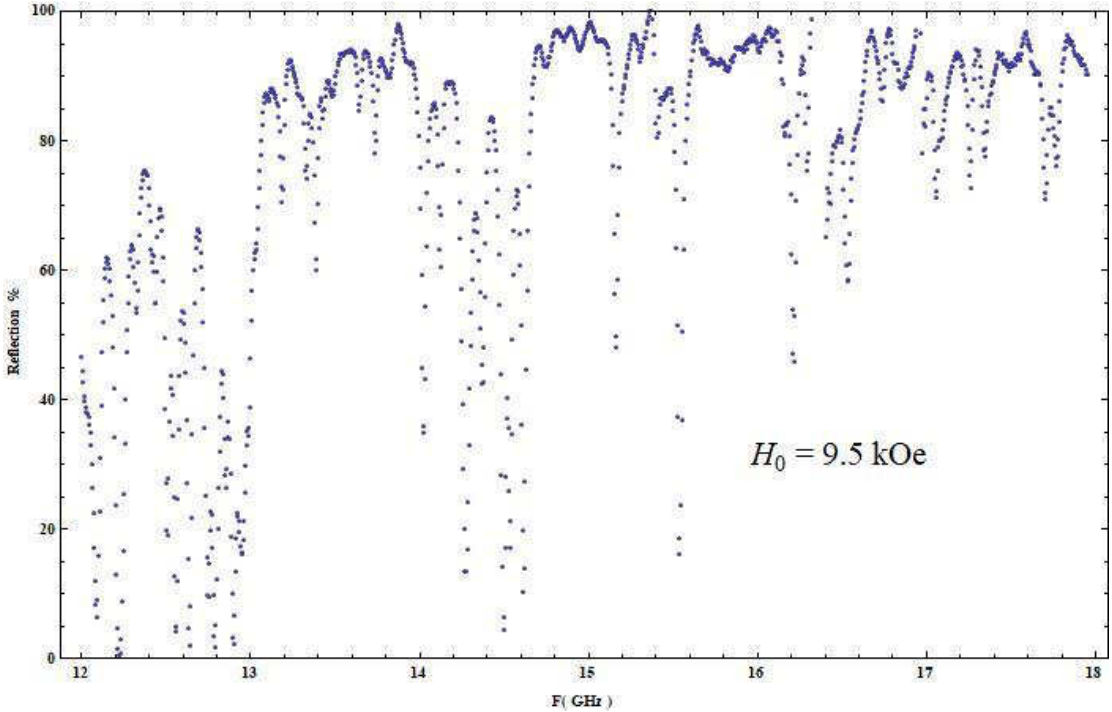

Fig. 4.7.95 Reflection vs. Frequency for $H_0 = 9.5$ kOe

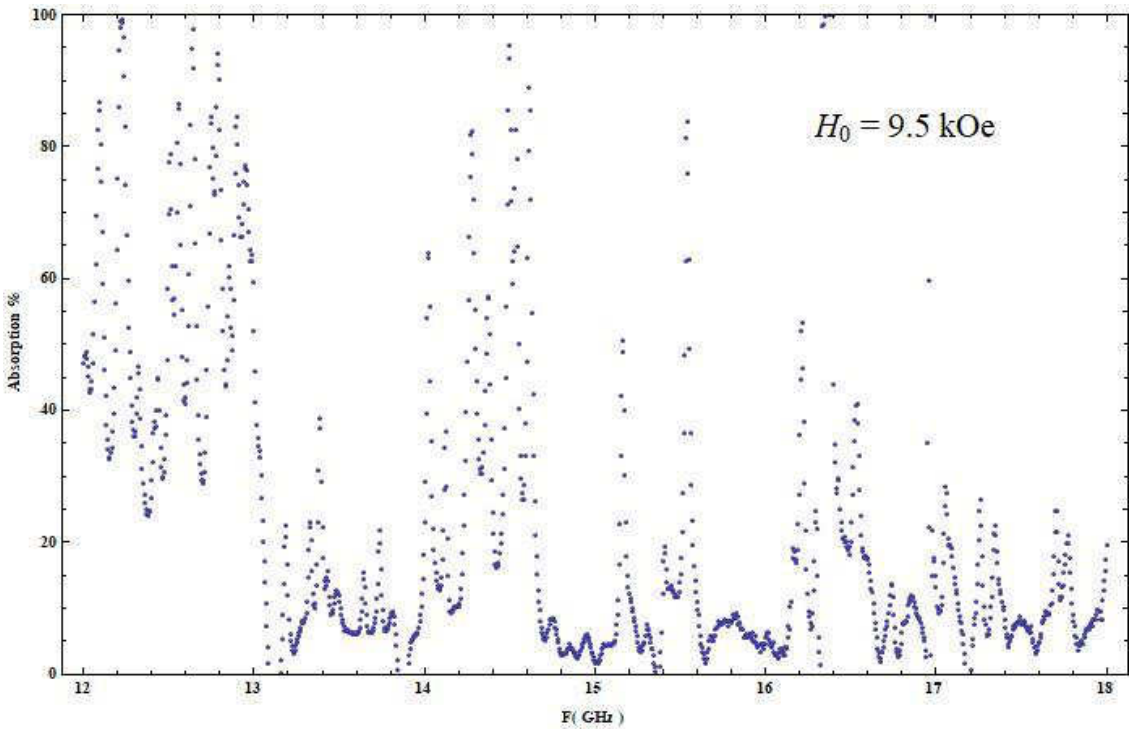

Fig. 4.7.96 Absorption vs. Frequency for $H_0 = 9.5$ kOe

Resonance-Anti-Resonance Frequency: 34.86→42.19 GHz

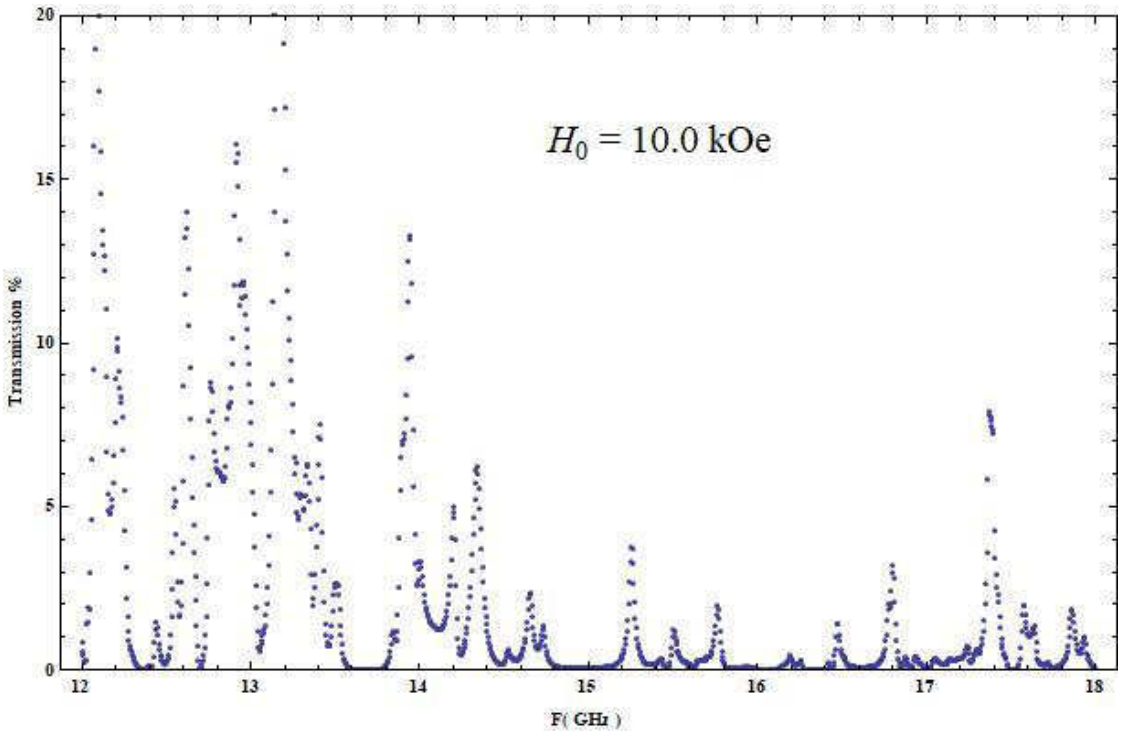

Fig. 4.7.97 Transmission vs. Frequency for $H_0 = 10.0$ kOe

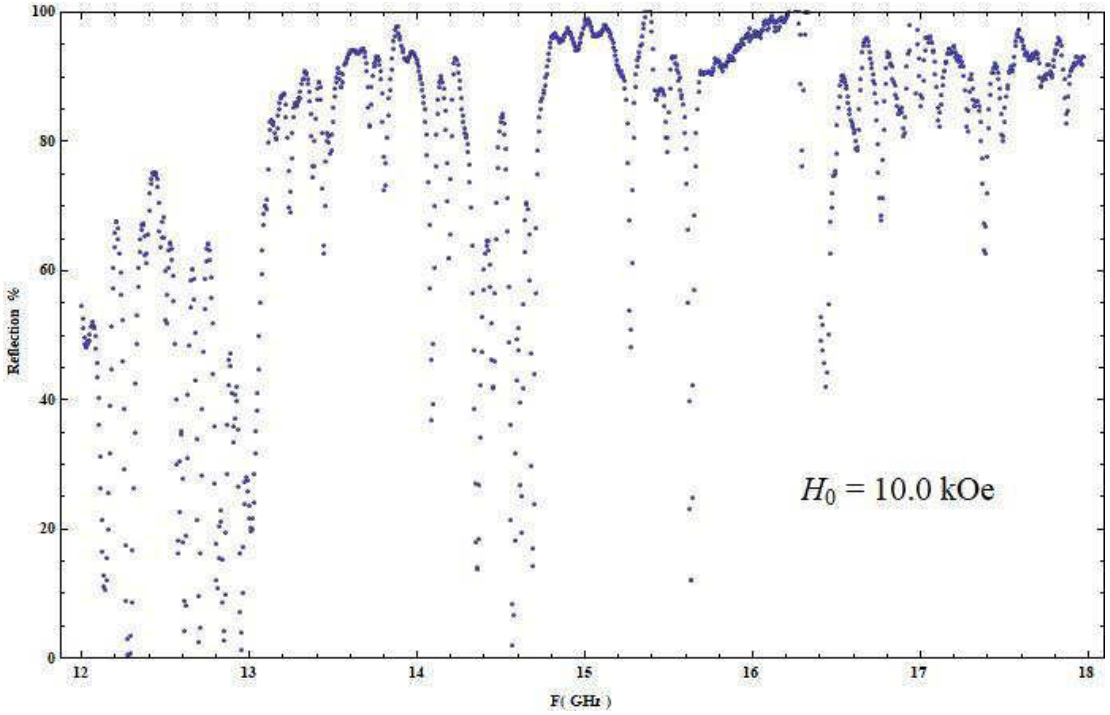

Fig. 4.7.98 Reflection vs. Frequency for $H_0 = 10.0$ kOe

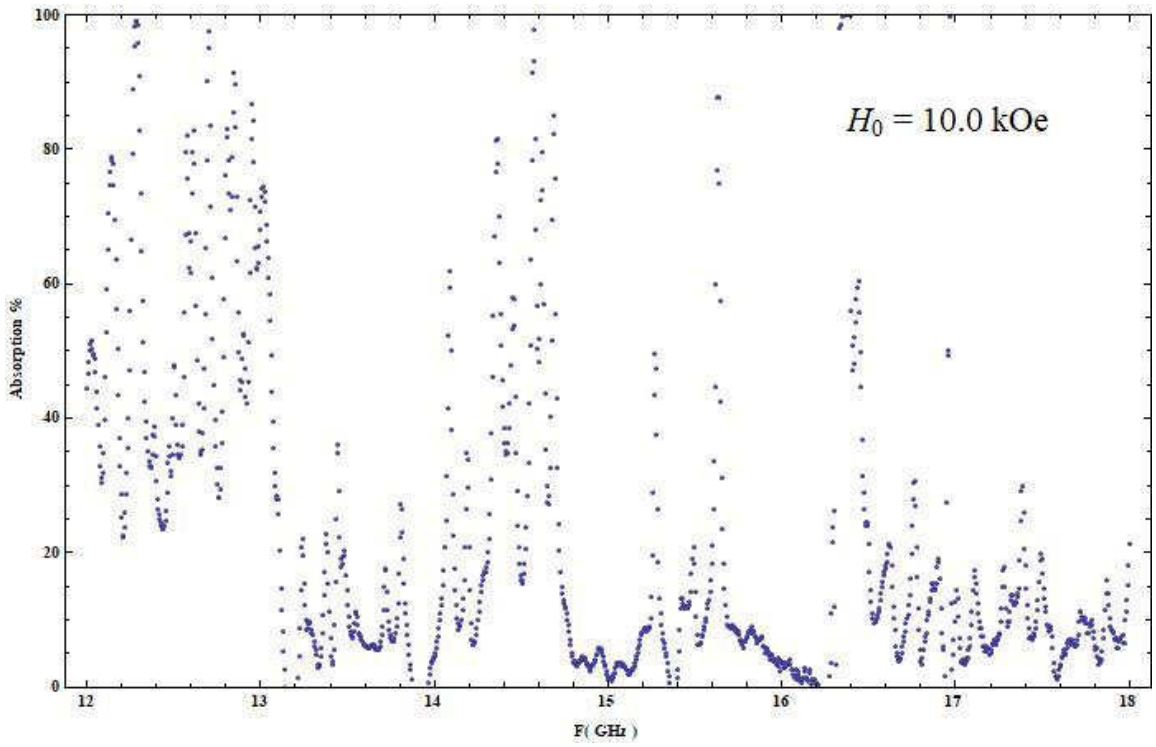

Fig. 4.7.99 Absorption vs. Frequency for $H_0 = 10.0$ kOe

Resonance-Anti-Resonance Frequency: 36.28→43.59 GHz

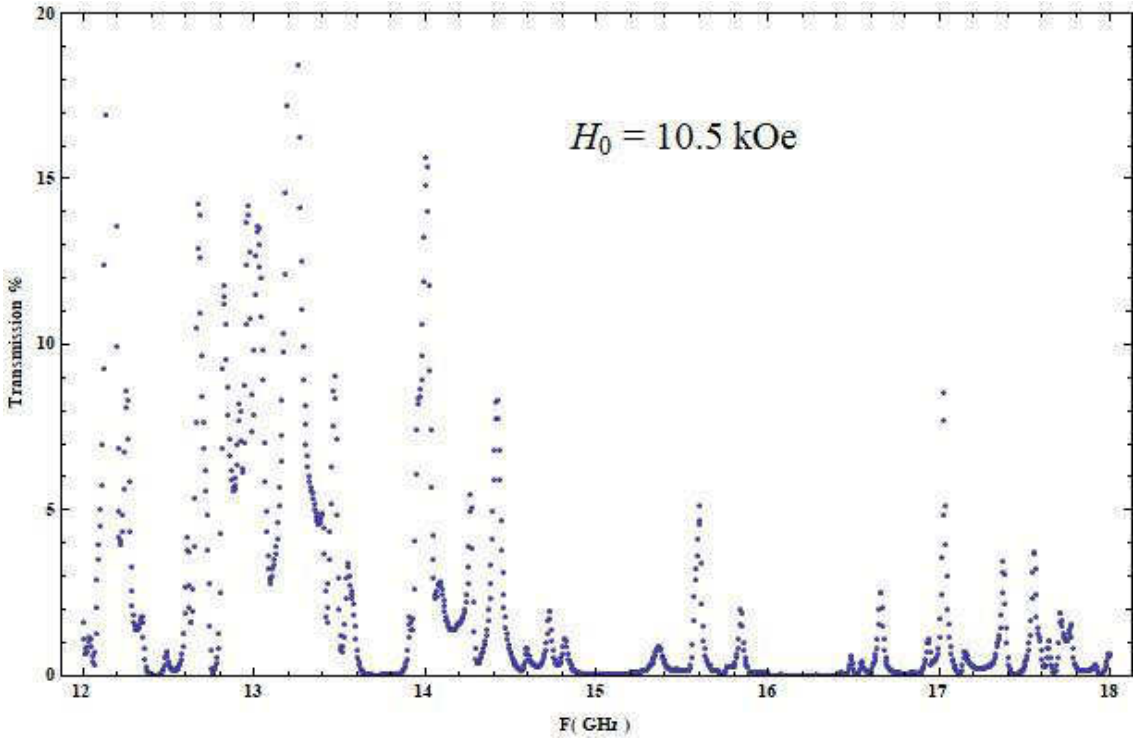

Fig. 4.7.100 Transmission vs. Frequency for $H_0 = 10.5$ kOe

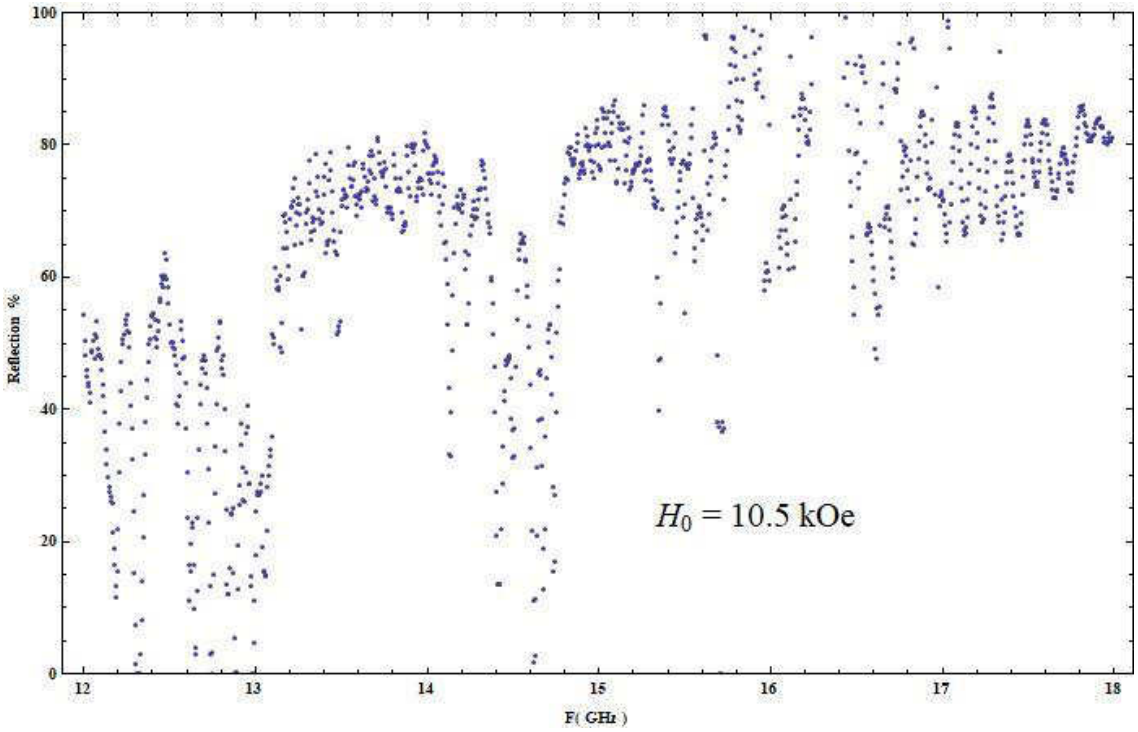

Fig. 4.7.101 Reflection vs. Frequency for $H_0 = 10.5$ kOe

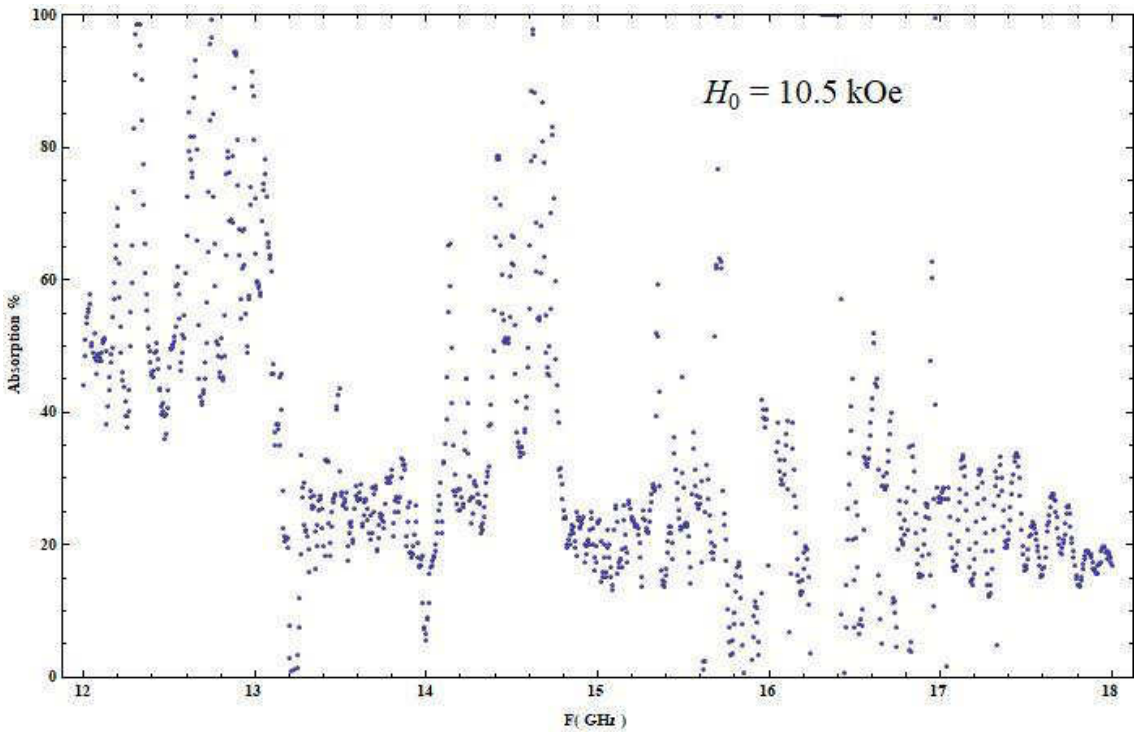

Fig. 4.7.102 Absorption vs. Frequency for $H_0 = 10.5$ kOe

Resonance-Anti-Resonance Frequency: 37.71→45.00 GHz

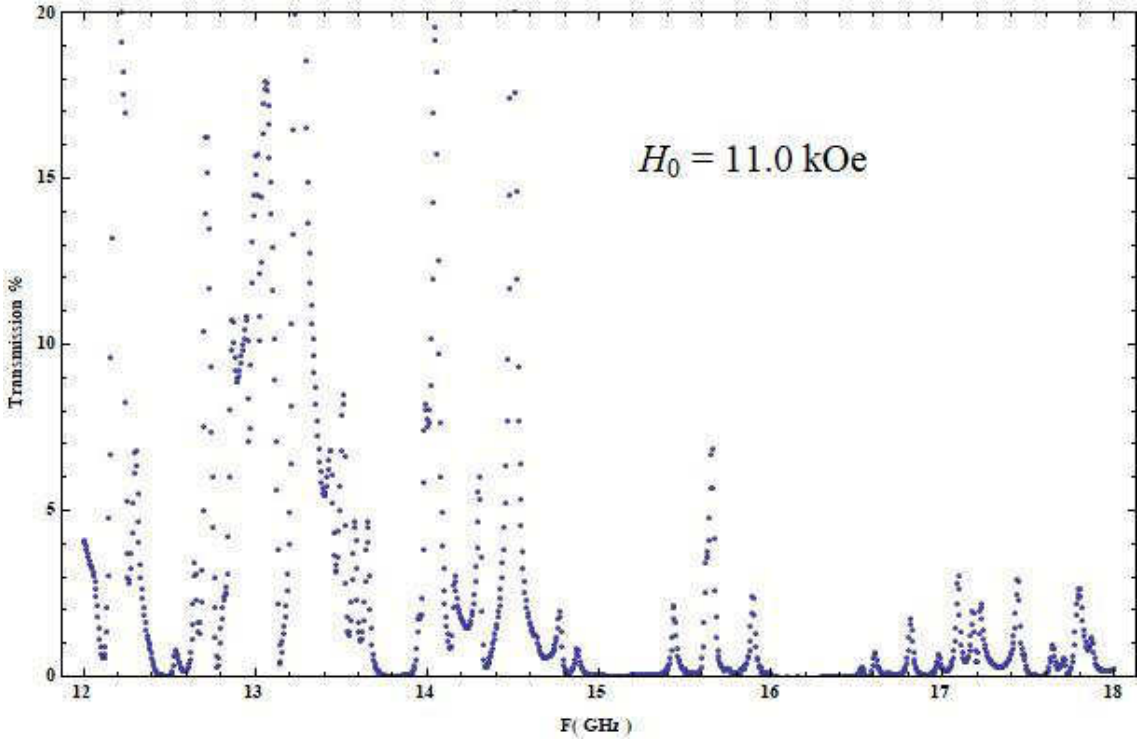

Fig. 4.7.103 Transmission vs. Frequency for $H_0 = 11.0$ kOe

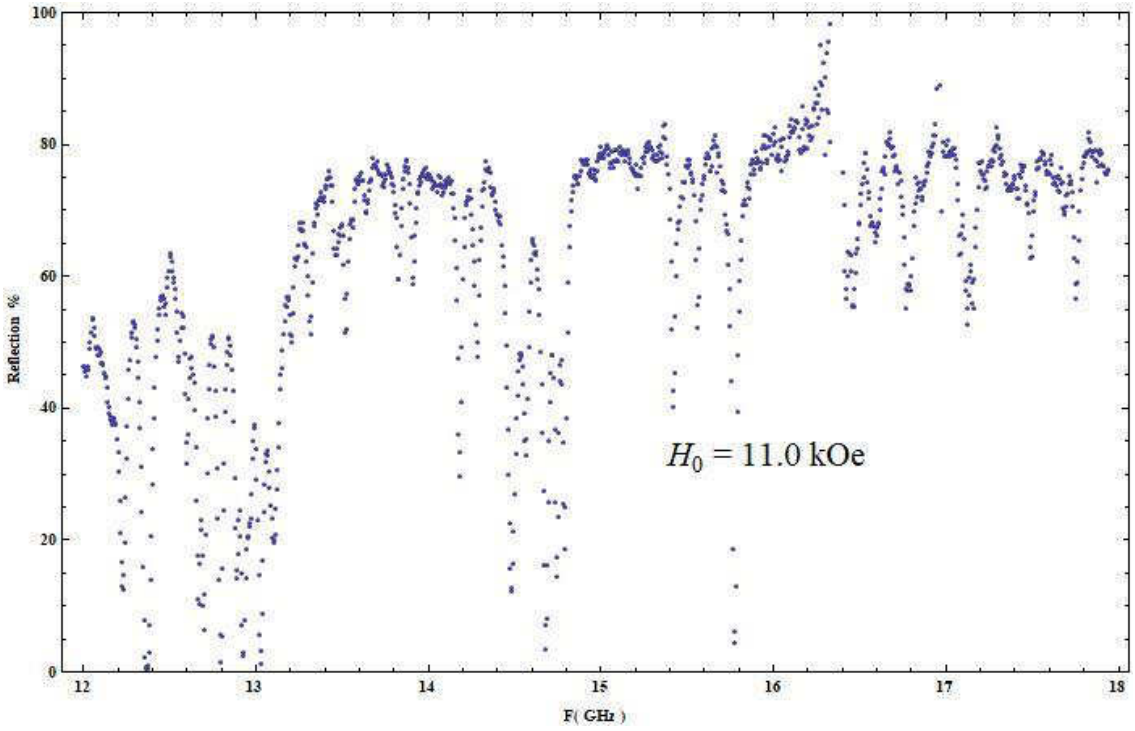

Fig. 4.7.104 Reflection vs. Frequency for $H_0 = 11.0$ kOe

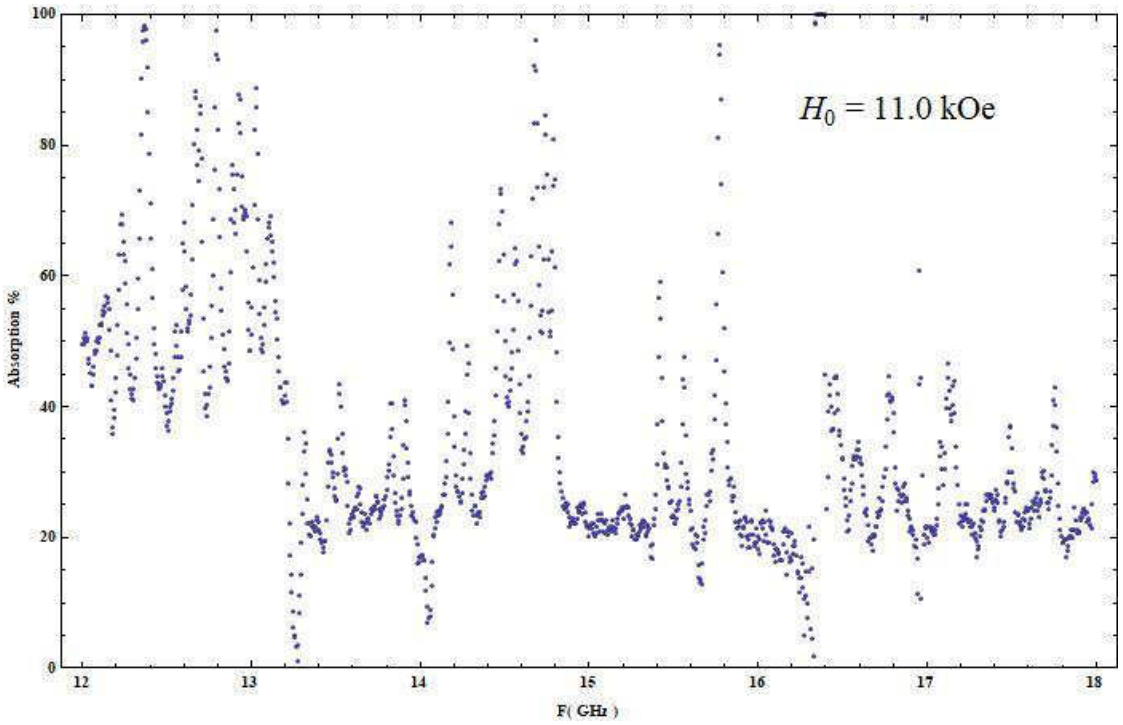

Fig. 4.7.105 Absorption vs. Frequency for $H_0 = 11.0$ kOe

Resonance-Anti-Resonance Frequency: 39.13→46.40 GHz

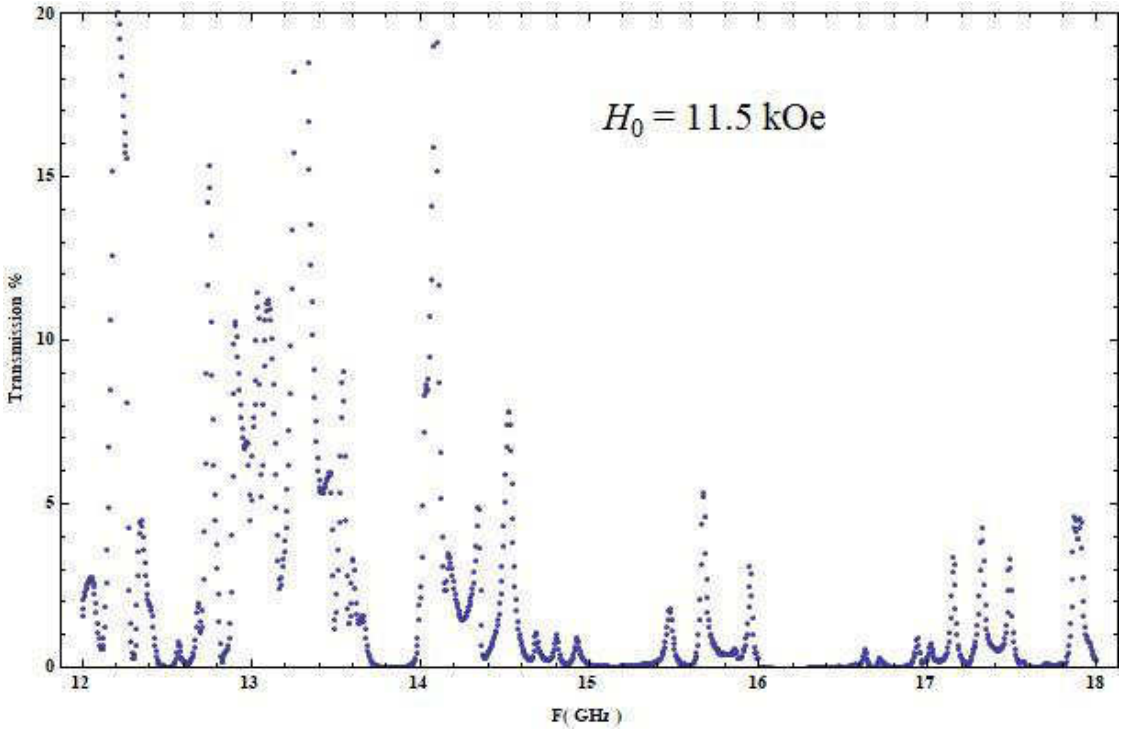

Fig. 4.7.106 Transmission vs. Frequency for $H_0 = 11.5$ kOe

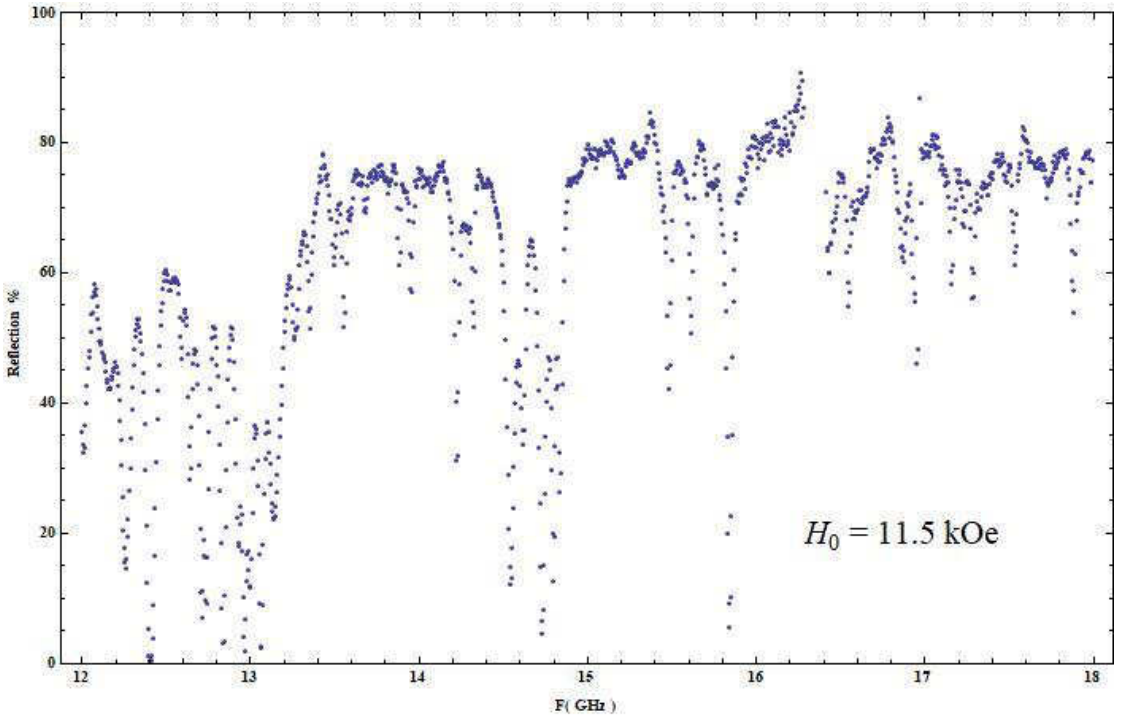

Fig. 4.7.107 Reflection vs. Frequency for $H_0 = 11.5$ kOe

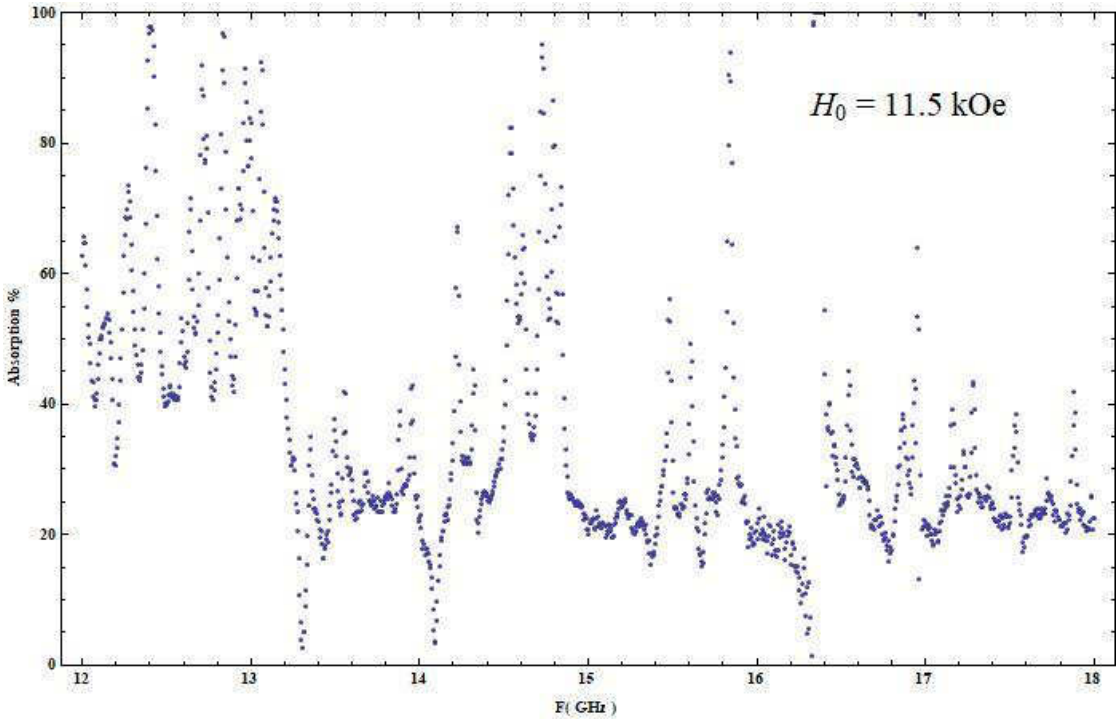

Fig. 4.7.108 Absorption vs. Frequency for $H_0 = 11.5$ kOe

Resonance-Anti-Resonance Frequency: 40.55→47.80 GHz

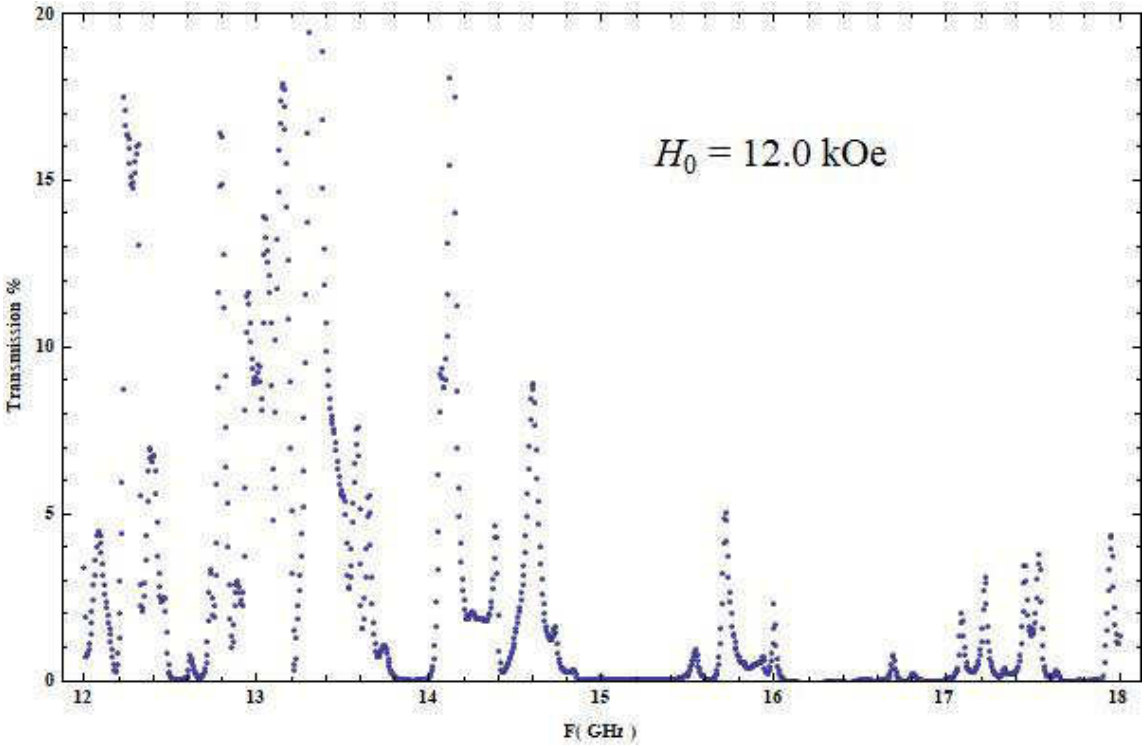

Fig. 4.7.109 Transmission vs. Frequency for $H_0 = 12.0$ kOe

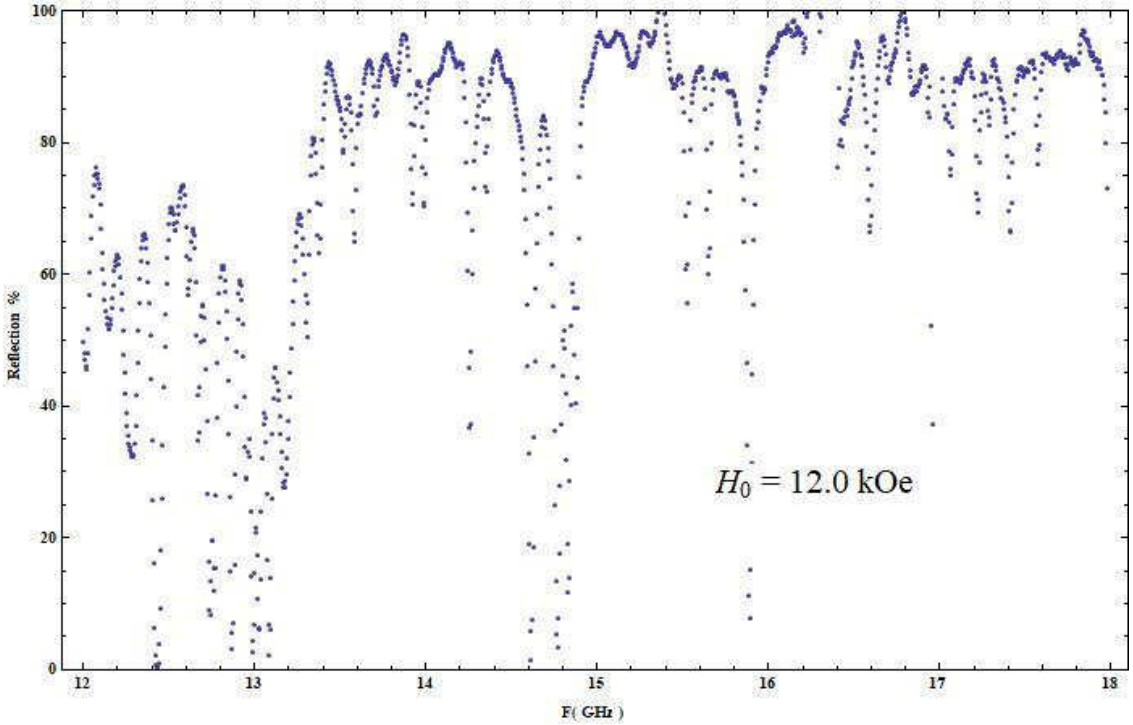

Fig. 4.7.110 Reflection vs. Frequency for $H_0 = 12.0$ kOe

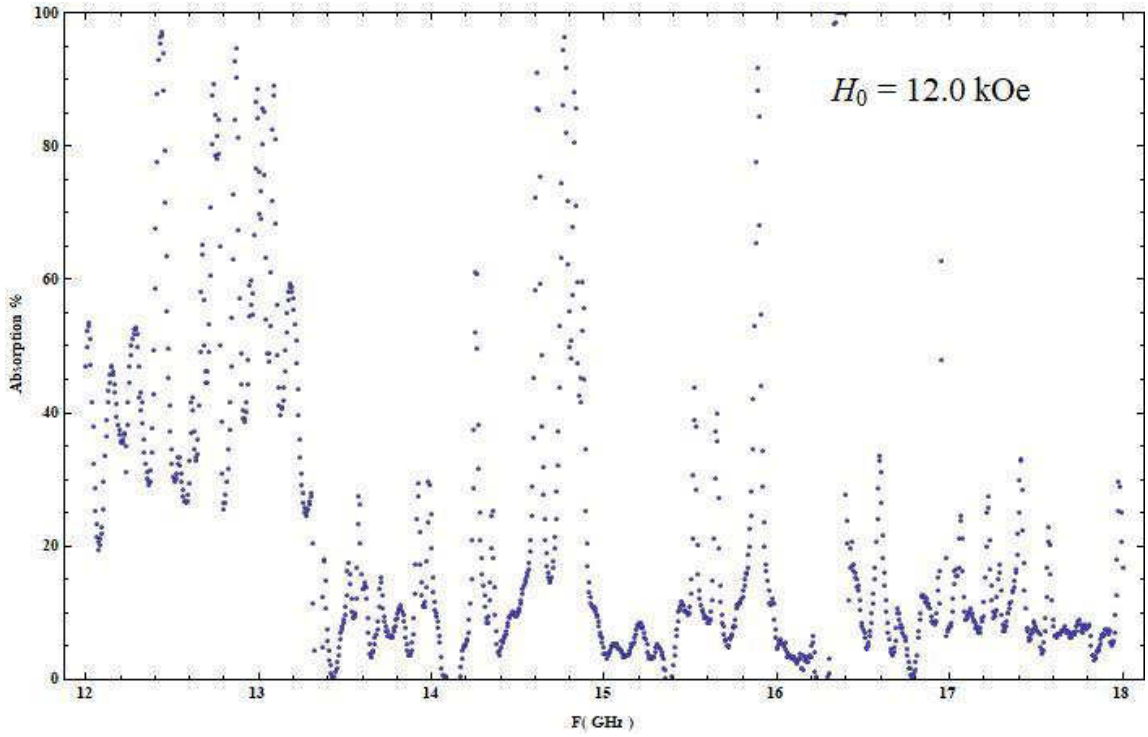

Fig. 4.7.111 Absorption vs. Frequency for $H_0 = 12.0$ kOe

Resonance-Anti-Resonance Frequency: 41.97→49.20 GHz

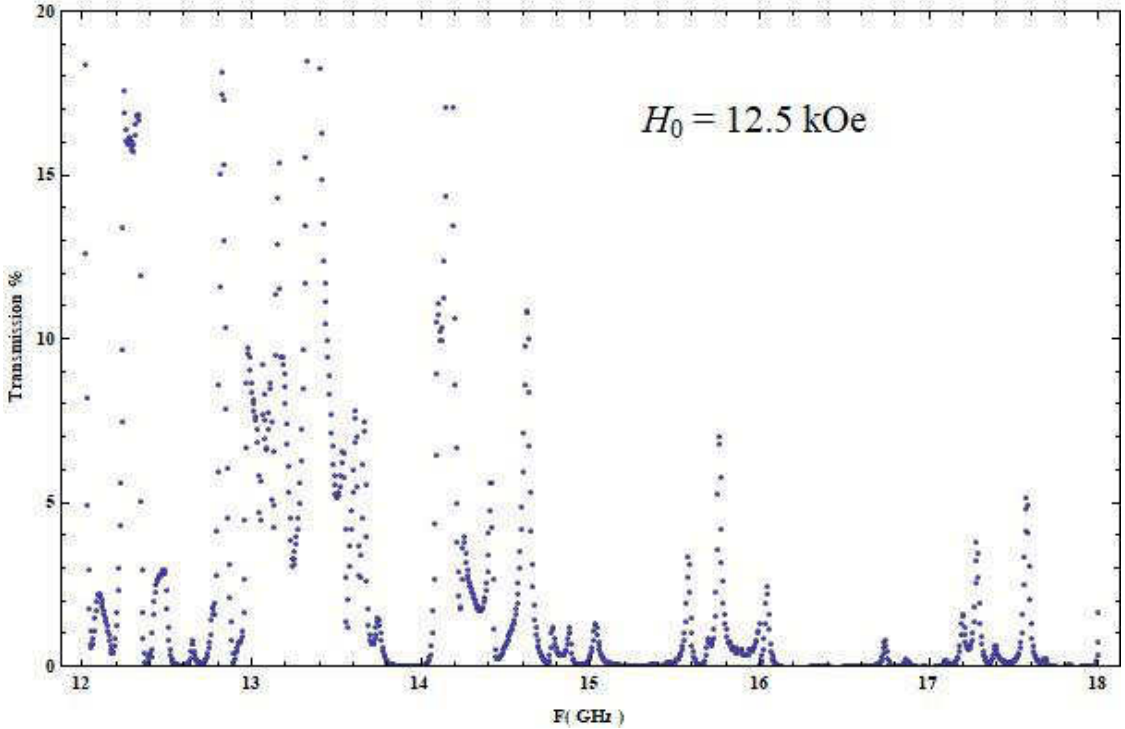

Fig. 4.7.112 Transmission vs. Frequency for $H_0 = 12.5$ kOe

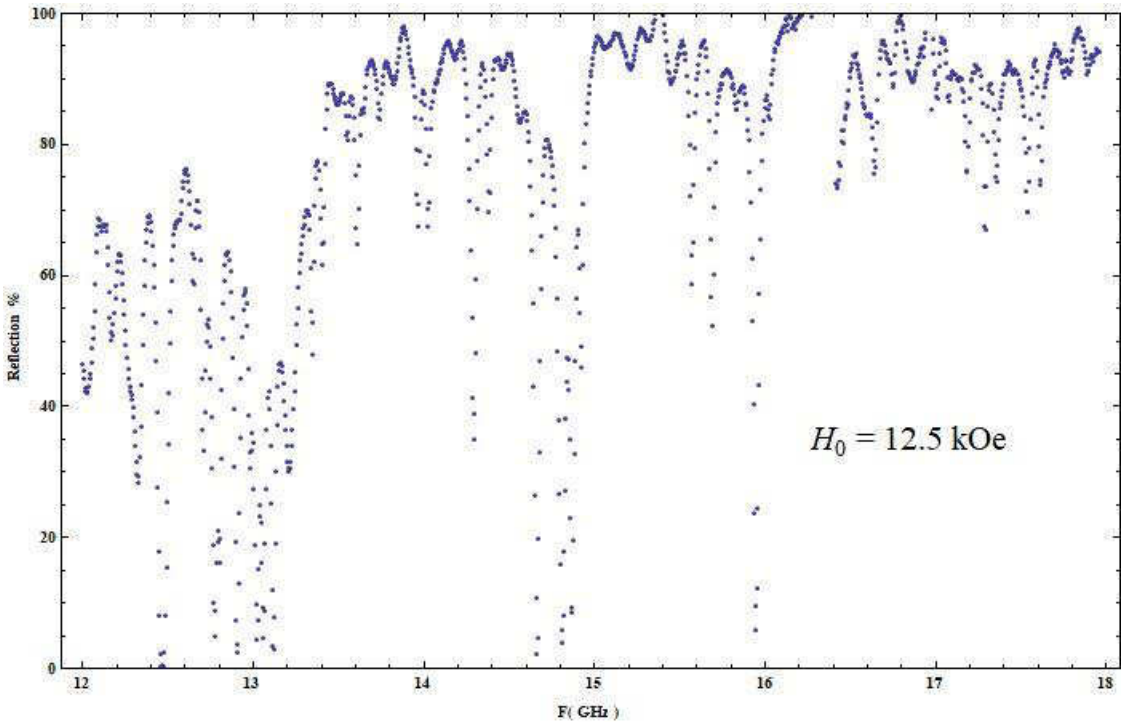

Fig. 4.7.113 Reflection vs. Frequency for $H_0 = 12.5$ kOe

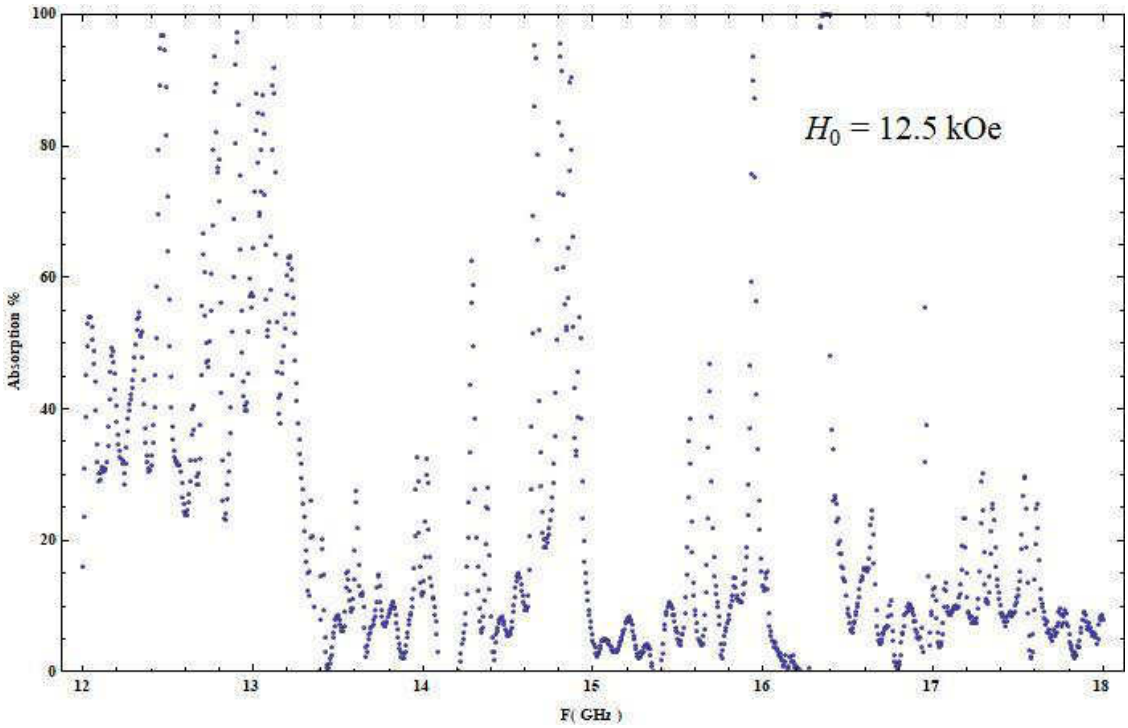

Fig. 4.7.114 Absorption vs. Frequency for $H_0 = 12.5$ kOe

Resonance-Anti-Resonance Frequency: 43.39→50.60 GHz

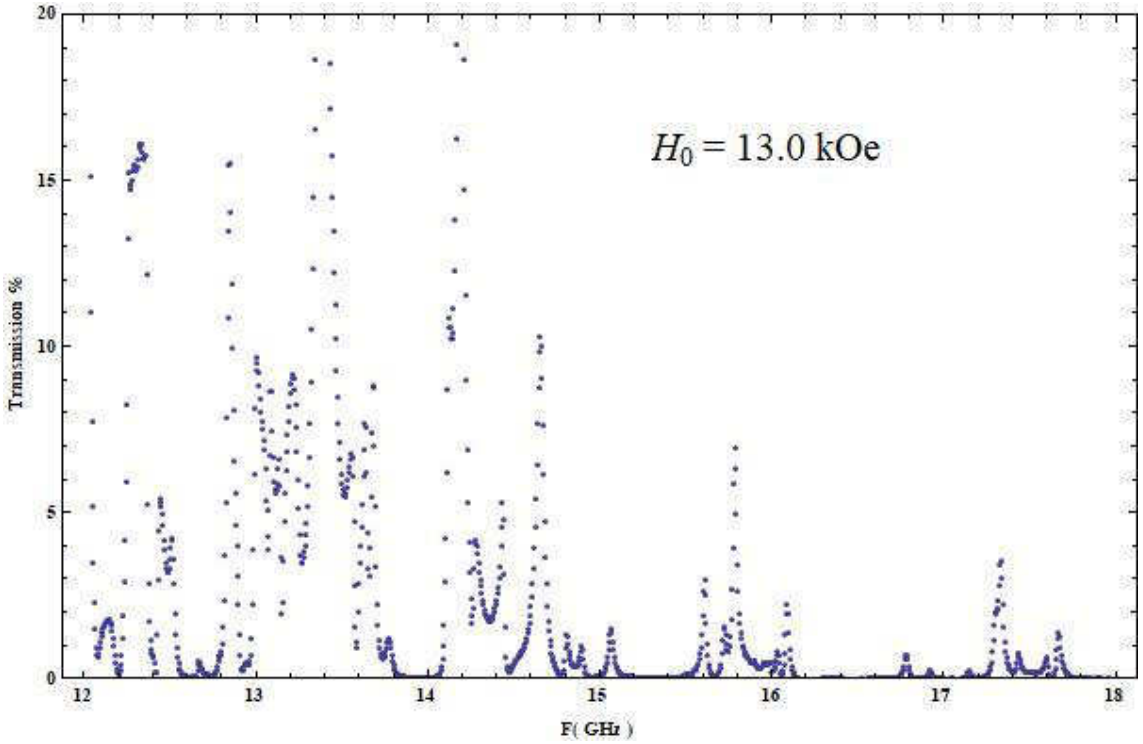

Fig. 4.7.115 Transmission vs. Frequency for $H_0 = 13.0$ kOe

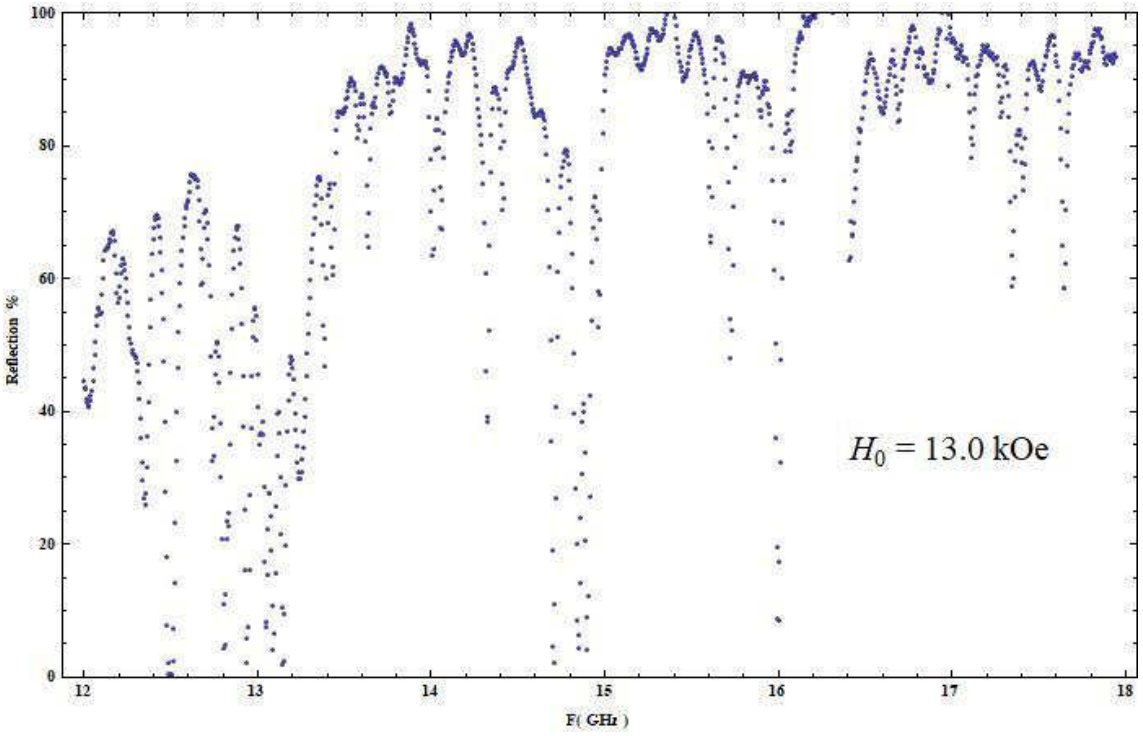

Fig. 4.7.116 Reflection vs. Frequency for $H_0 = 13.0$ kOe

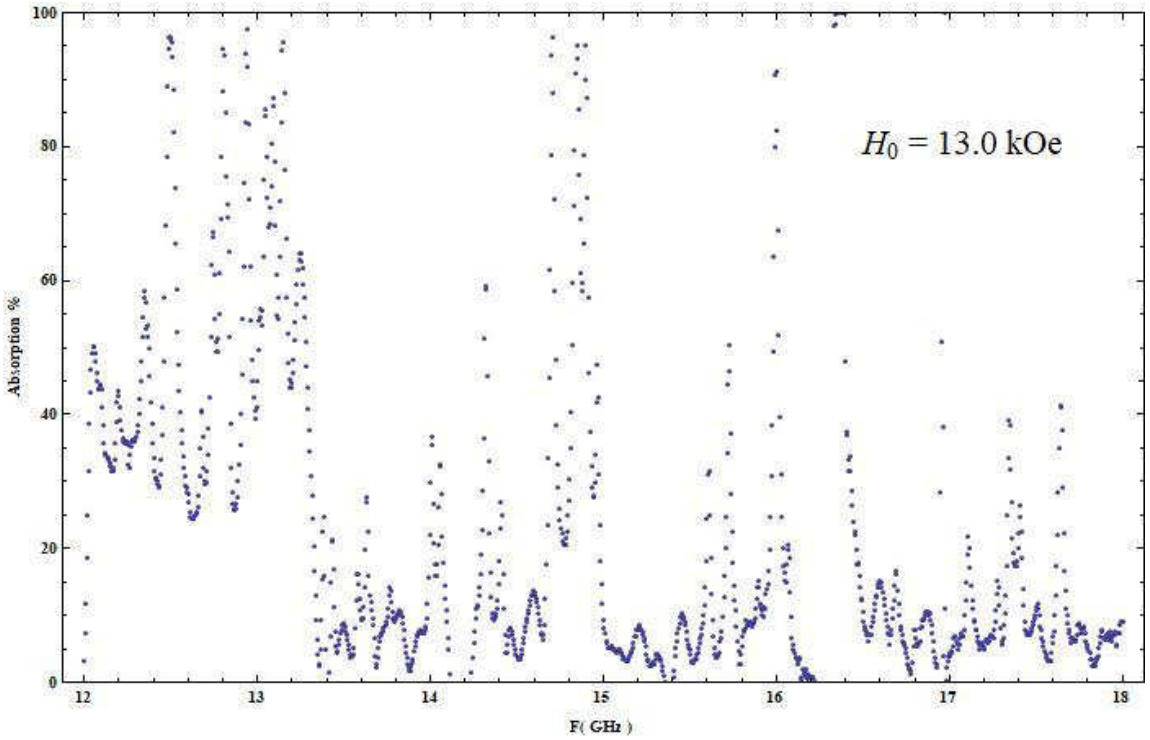

Fig. 4.7.117 Absorption vs. Frequency for $H_0 = 13.0$ kOe

Resonance-Anti-Resonance Frequency: 44.80→52.00 GHz

4.8 Electromagnetic Transmission Modes

After I measured the transmission through the sample and plotted it for different magnetic field values (section 4.7), I tracked the frequency of the electromagnetic transmission modes through different values of magnetic field. I identified 26 different electromagnetic modes in the 39 transmission graphs, the transmission modes appear at (0.042 kOe) and continue shifting up in frequency until (2 kOe), these disappear from (2 kOe) to (6 kOe) due to increased reflection and absorption. These transmission modes reappear at (6 kOe) and continue shifting up in frequency for increasing magnetic field values.

The 26 electromagnetic transmission modes are plotted in frequency-magnetic field space in Fig. 4.8.1

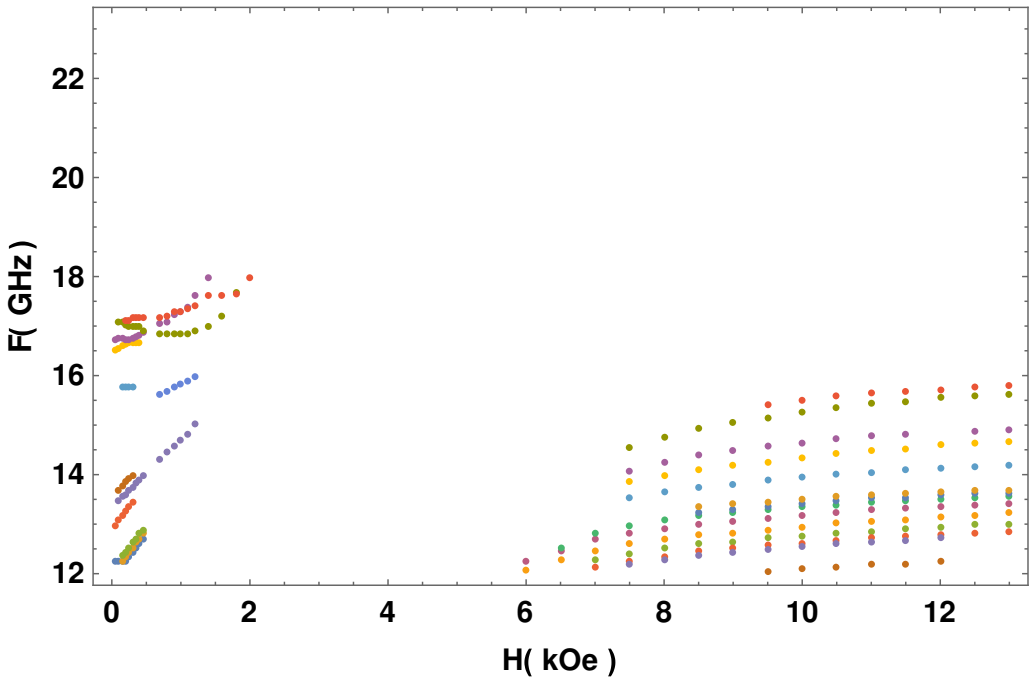

Fig. 4.8.1 Electromagnetic transmission modes

4.9 Resonance Frequency of Wire/Hole as Co-Axial Cavity

The wire-array cladded in Teflon inside the ferrite host represents an array of resonant cavities. Each cavity is a co-axial waveguide terminated by the top and the bottom of the waveguide. The ferrite forms the walls of the cavity. Each hole in this array act as a resonant cavity where the wave inside it can resonate in two directions, radial direction and longitudinal [18]. I calculated the resonance frequency for the two directions to compare to my transmission modes.

The hole in the ferrite host is filled with a central conducting wire cladded by Teflon, air fills reminder of the cavity. Thus, the inhomogeneity of the Teflon-air medium surrounding the wires changes the dielectric constant of the medium depending on the ratio of the cross-section at areas of the different materials. The ratio of inner diameter (which is filled by air-conductor wire) to outer diameter of the Teflon tube is about 1.2 / 1.8 which gives an average electric permittivity for the inhomogeneous medium $\epsilon = 1.50\ \epsilon_0$ using Maxwell-Garnett homogenization theory [15].

The velocity of the wave inside the hole is,

$$v = \frac{1}{\sqrt{\mu_0 \epsilon}} \quad , \tag{4.9.1}$$

$$v = \lambda f \ . \tag{4.9.2}$$

The longest resonant wave length inside the hole is,

$$\lambda = 2d \,, \qquad (4.9.3)$$

where d is the diameter of the hole (for radial direction resonance) or the length of the hole (for longitudinal direction resonance).

I calculated the resonance frequency using Eq. (4.9.1), (4.9.2) and (4.9.3) to obtain the longitudinal direction resonance at 15.3 GHz and the radial direction resonance at 71.3 GHz.

I have observed the longitudinal direction resonance mode as the transmission mode at 15.7 GHz. This resonance mode was almost stationary with respect of changing the magnetic field. This mode appeared at low H_0 where one can expect the magnetic host not to be magnetically saturated in its corners. This inhomogeneity in magnetization allows a small amount of TM polarized microwaves to excite this mode in the holes even though the TM mode cannot propagate freely in the bulk of the ferrite host. This mode is the result of microwave tunneling from hole to hole.

4.10 Electromagnetic Modes in Rectangular Waveguide Filled with Transversely Magnetized Ferrite

Many modes can propagate through the transversely magnetized ferrite slab and they can be divided into two categories: in the limit $\rightarrow \mu_0$, they can be categorized as TE or TM modes. TE modes have the electric field pointing transversely to the wave propagation direction, while TM modes have the magnetic field pointing transversely to the wave propagation direction. The μ for a magnetic material can be expressed as a tensor, and the

propagation modes are not purely TE or TM. However, the modes can be identified with the TE and TM modes one observes for $\mu \to \mu_0$.

I studied the propagation of the quasi-TE and quasi-TM modes through the transversely magnetized ferrite slab of my metamaterial. I used an article [16] to evaluate the parameters of these different modes. This article expressed the wave vectors and the electromagnetic fields as a function of the electric permittivity and magnetic permeability of the ferrite slab.

I evaluated the propagation constants k', of the TE and TM modes in waveguide for different values of μ and ϵ. Determination of the k' allowed an approximate determination (qualitative) of the transmission amplitude for the quasi-TE and quasi TM modes.

The summary of my observation about the transmission amplitude of the two kinds of the modes is listed in table 4.10.1

Table 4.10.1 Transmission power of TE and TM modes for different values of μ and ϵ according to article [16]

Transmission Amplitude	Positive ϵ	Negative ϵ
Positive μ	1-Large amplitude of TE_{10} modes. 2-Small amplitude of the higher TE_{mn} modes. 3-Small amplitude of TM_{mn} modes.	1-Low amplitude of TE_{mn} modes. 2-Low amplitude of TM_{mn} modes.
Negative μ	1-Low amplitude of TE_{mn} modes. 2-Low amplitude of TM_{mn} modes.	1-Large amplitude of TE_{10} modes. 2-Small amplitude of the higher TE_{mn} modes. 3-Small amplitude of TM_{mn} modes.

4.11 Non-Wire Ferrite Transmission Measurements

After I measured the transmission through the wire/ferrite sample, I manufactured a similar ferrite sample without holes to measure the transmission. The reason I manufactured this sample without holes was to identify any resonance modes due to the holes, as I discussed in section 4.9 where the cladded wire-array inside the ferrite host represented an array of resonant cavities which created a transmission mode. The transmission modes observed through the non-hole sample was purely electromagnetic modes.

I measured the transmission through this sample for the magnetic field value $H_0 = 1.0$ kOe which is equivalent to $H_0 = 221.0 \pm 47.0$ Oe in the wire/ferrite medium due to augmentation of the magnetic field created by the holes inside the wire/ferrite sample. The transmission amplitude versus frequency is shown in Fig. 4.11.1.

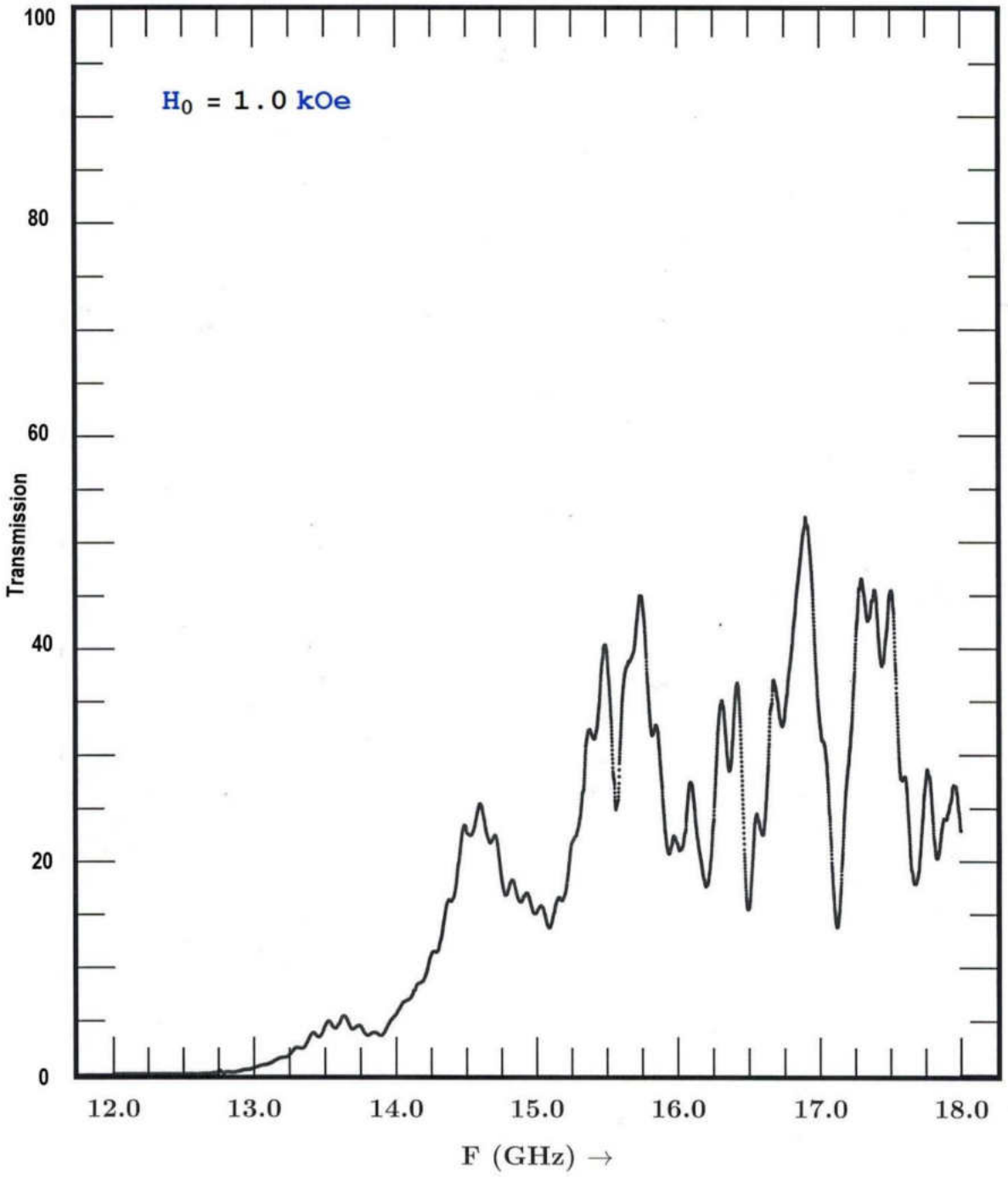

Fig. 4.11.1 Transmission amplitude through non-wire ferrite sample

CHAPTER V
CONCLUSION

I measured the transmission through, and reflection off, a wire-ferrite metamaterial and I conclude that I observed the existence of a negative refractive index for this metamaterial over a limited range of applied magnetic field and microwave frequency. The evidence I depend on to conclude the existence of negative refractive index is the following:

1-Spin wave range:

I showed in section 4.6 that the region of negative magnetic permeability has no overlap with the spin wave frequency range. This means that, for any transmission modes observed in the frequency range for while the magnetic permeability is negative, spin waves cannot account for them, only electromagnetic waves can be involved.

2-TE_{10} modes dominates the other electromagnetic modes:

I showed in section 4.10 that for a ferrite slab placed inside a rectangular waveguide, the TE_{10} modes dominates the transmission when the ferrite slab exhibits a negative

refractive index (negative μ and negative ϵ). There is some transmission due to other modes but they have a low amplitude compared to the TE_{10} mode.

3- Observation of TE modes in negative μ frequency range:

I measured the transmission through the wire-ferrite metamaterial for 39 different values of applied magnetic field within the frequency range 12-18 GHz, some of them showed wholly or partially overlapped the frequency range 12-18 GHz and the frequency region of negative magnetic permeability (0.042 kOe – 3.5 kOe).

Due to the imprecision of the magnetization value I calculated in section 4.2, $M_0 = (3.804 \pm 0.23) \times 10^5\, A/m$, there results or imprecision in determining the negative magnetic permeability region limits by $\pm$0.5 GHz.

I observed 10 TE transmission modes in the range of (0.042 kOe – 1.6 kOe), I call them TE modes because the frequency at which they occur changes with magnetic field (Fig. 4.8.1). 6 out of these 10 TE transmission modes exist in a region of negative magnetic permeability (for example modes of frequencies 12.20,12.30,12.40,13.27,13.6 and 13.84 GHz of H_0 = 0.2 kOe).

Since these TE transmission modes exist in a region of negative magnetic permeability, negative μ must be accompanied by negative ϵ to allow these transmission modes to propagate through the wire-ferrite metamaterial with high amplitude. This demonstrates the existence of negative refraction through this metamaterial.

4- Non-wire ferrite slab has low amplitude TE modes:

To verify that the TE modes I observed in the region of negative magnetic permeability are not the minor (low amplitude) TE or TM modes which can propagate through the ferrite for negative μ and positive ϵ (see Table 4.10.1), I compared the transmission data for the wire/ferrite sample to the transmission data for non-wire ferrite slab at $H_0 = 1.0$ kOe (Fig. 4.11.1).

When I compare Fig. 4.11.1 with transmission through the wire/ferrite metamaterial at $H_0 = 221.0 \pm 47.0$ Oe, I see that the TE Transmission modes at frequencies equal to 12.20,12.30,12.40,13.6 GHz for H_0 = 0.2 kOe disappeared in Fig. 4.11.1 which represents a ferrite medium with negative μ and positive ϵ . This demonstrates that the TE Transmission modes at these frequencies for H_0 = 0.2 kOe observed in the wire/ferrite metamaterial are not the minor (low amplitude) TE or TM modes which can propagate through for a negative μ and positive ϵ**.**

Thus, from all the previous data, I assert that the wire-ferrite metamaterial I manufactured can exhibit negative refraction in specific range of magnetic fields and frequencies.

REFERENCES

[1] V. G. Veselago, "The Electrodynamic of Substance with Simultaneously Negative Value of ϵ and μ " ,Sov. Phys. Usp. Vol.10, pp.509-514 (1968).

[2] R. A. Shelby, D.R. Smith, S. Schultz , "Experimental Verification of a Negative Index of Refraction ",Science Vol.292 , pp.77-79 (Apr. 2001).

[3] R.D. Smith, W.J. Padilla, D. C. Vier, S. C. Nemat-Nasser and S. Schultz, "Composite Medium with Simultaneously Negative Permeability and Permittivity ", Phys. Rev. Lett. Vol.84, pp. 4184-4187 (2000).

[4] https://upload.wikimedia.org/wikipedia/en/7/79/Photo_of_metamaterial_lattice_for_negative_refraction.jpg .

[5] John Franklin, John Biddle, Bohdan Balko, " Double Negative Materials (DNM), Phenomena and Applications", INSTITUTE FOR DEFENSE ANALYSES, IDA Document D-3887.

[6] J. B. Pendry, "Negative Refraction Makes a Perfect Lens", Phys. Rev. Lett. Vol.85, pp. 3966-3969 (2000).

[7] http://www.cmth.ph.ic.ac.uk/photonics/Newphotonics/PerfectLens.html.

[8] C. Kittel. "Ferromagnetic resonance". J. Phys. Radium, 12 (3), pp.291-302 (1951).

[9] C. Kittel, "On the Theory of Ferromagnetic Resonance Absorption ". Phys. Rev. 73, 155 (1948).

[10] Graeme Dewar, "Minimizing of Losses in a Structure having a Negative Index of Refraction", New Journal of Physics, Vol.7, (2005) 161.

[11] Gradsheteyn I S I and Ryshik I M " Tabels of Integrals, Series, and Products 4th ed.", (New York:Acadimic) 1965, pp. 976.

[12] D. S. Jones, " The Theory of Electromagnetism ", (New York: Pergamon) 1964, pp. 450.

[13] Deepak Bhalla, DK. Singh, Swati Singh, Dipti Seth, "Material Processing Technology for Soft Ferrites Manufacturing ", American Journal of Material Science , 2012, 2(6), pp.165-170.

[14] R.W. Damon, J. R. Eshbach, "Magnetostatic Modes of a Ferromagnet Slab", J.Physics Chem. Solids, Pergamon Press, 1961, Vol.19, Nos. ¾, pp. 308-320.

[15] Vadim Markel. Introduction to the Maxwell Garnett approximation: tutorial . Journal of the Optical Society of America A, Optical Society of America, 2016, 33 (7), pp.1244-1256.

[16] G. Barzilai, G. Gerosa, "Modes in Rectangular Guides Filled with Magnetized Ferrite", IL Nuovo Cimento ,Vol. VII, N.5 (1958).

[17] Address: Trans-Tech Ceramic and Advanced Materials ,5520 Adams Town Rd ,MD, 21710 USA.

[18] Emanuel Istrate, Edward H. Sargent, “Photonic crystal heterostructures and interfaces", REVIEWS OF MODERN PHYSICS, VOLUME 78, APRIL–JUNE 2006, pp. 455-481.

[19] J. B. Pendry, A. J. Holden, W. J. Stewart and I. Youngs," Extremely Low Frequency Plasmons in Metallic Mesostructures ", Phys. Rev. Lett. Vol.76, pp. 4773-4776 (1996).

[20] http://www.carverpress.com/products/benchtop-manual/bm-pellet.

[21] https://www.lindbergmph.com/light-industrial/1500-deg-c-heavy-duty-tube-furnace.

[22] https://www.omega.com/pptst/CN3000.html.

[23] http://www.wswells.com/data/drill_press/1963_drillpress_cat_6301E.pdf.

[24] https://www.ietlabs.com/genrad-1621-capaitance-bridge.html.